

**CHEMICALLY MODIFIED THIN ORGANIC FILMS
SUPPORTED ON CHEMOMECHANICALLY
POLISHED INORGANIC SUBSTRATES**

**Thesis submitted to the University of Glasgow in fulfilment
of the requirement of the degree of Doctor of Philosophy.**

by

DAVID SMYTH BOYLE

Department of Chemistry

University of Glasgow

August, 1994.

© D.S. BOYLE, 1994

ProQuest Number: 13834136

All rights reserved

INFORMATION TO ALL USERS

The quality of this reproduction is dependent upon the quality of the copy submitted.

In the unlikely event that the author did not send a complete manuscript and there are missing pages, these will be noted. Also, if material had to be removed, a note will indicate the deletion.



ProQuest 13834136

Published by ProQuest LLC (2019). Copyright of the Dissertation is held by the Author.

All rights reserved.

This work is protected against unauthorized copying under Title 17, United States Code
Microform Edition © ProQuest LLC.

ProQuest LLC.
789 East Eisenhower Parkway
P.O. Box 1346
Ann Arbor, MI 48106 – 1346

Thesis
9901
copy.1



Acknowledgements.

I would like to thank my supervisor Dr. J.M. Winfield for his creative input and for giving me an insight into how academic research is conducted. I would like also to express my gratitude to Dr. T. Baird and Dr. J. Fryer of Electron Microscopy for their practical assistance throughout this work.

Outside the department I would like to thank the following; Dr. A. Hall and Mr. D. Turner of the Department of Geology, Dr. M. Littlewood of Nicolet Instruments, Dr. R. Richardson and Mr. D. Hepburn of Glasgow Caledonia University, Dr. J.A. Chudek and Dr. G. Hunter of the University of Dundee and all those connected with this work at Logitech Ltd., Old Kilpatrick.

Many thanks to my Scottish and Iraqi colleagues for their help, advice and assistance during this study.

I would like to extend my thanks to the Technical Staff, especially Mr. J. Tweedie for the Spectroscopy service, Mrs. K. Wilson for microanalysis, all those concerned in the Mechanical and Glassblowing workshops, Mr. R. Munro for his award-winning poster service and Mr. R. Kennedy and Mr. L. McGhee for some enlightening discussions. I would also like to thank Dr. A. Glidle for his help and expertise in the QCM work.

Thanks to Mrs. E. Hughes for her efficient typing of this thesis and other material.

My very special thanks to my long suffering family for their continual support and encouragement.

I would like to acknowledge SERC for their financial support of this work.

DEDICATION.

I would like to dedicate this work to my parents.

Contents	Page
Chapter 1: Introduction	
A.1. Aims of this work	1
2. Polishing of optical materials	2
3. The lapping process	5
4. Abrasives used in lapping and polishing	8
5. Important parameters in the polishing of optical materials	9
6. Abrasive polishing	13
7. Chemical polishing or etching	14
8. Chemomechanical polishing of silica surfaces	15
B.1. Definition of a glass	18
2. The historical development of optical glass	19
3. Quartz found in nature	22
C. Ultrathin Organic Films	24
D. Polycyclic Aromatic Hydrocarbons	26
E. Charge Transfer Complexes	28
F. High Oxidation State Binary Fluorides	29
G. Charge-transfer complexes and electrical conductivity	31
 Chapter 2: Experimental	
A. Preparation of substrates	
1. The lapping process	34
2. The polishing process	35
3. The polishing reagents	36
B. Etching experiments	37
C. Preparation of thin films	37
D. Preparation of chemically modified films	
1. General high vacuum techniques	39
2. Purification of Molybdenum and Tungsten Hexafluorides	40
3. Purification of Phosphorus and Arsenic Pentafluorides	40
4. Thin film reactions	41

	Page
E. The Quartz Crystal Microbalance (QCM) technique as employed in thin film reactions	42
F. Spectroscopic techniques	
1. Vibrational spectroscopy	44
2. Electronic spectroscopy	48
3. Magic-Angle-Spinning Nuclear Magnetic Resonance (MAS-NMR) spectroscopy	49
G. Powder X-ray diffraction (XRD)	50
H. Characterisation of surface roughness and planarity	
1. The Rank Taylor Hobson Talystep	51
2. Interferometry	52
3. The Nomarski light microscope	53
4. The Scanning Electron Microscope (SEM)	54
I. Radiochemical techniques	
1. Radiochemical counting using Geiger-Müller counters	55
2. Plateau curves	57
3. Background radiation	57
4. Statistical errors	58
5. The direct monitoring Geiger-Müller radiochemical counting technique	58
6. Scintillation counting with solid scintillators	60
7. Radioisotopes	
a. The radioisotope [¹⁸ F]-Fluorine	61
b. The radioisotope [³⁶ Cl]-Chlorine	61
8. Preparation of [¹⁸ F]-radiolabelled CsF	61
9. Preparation and purification of [³⁶ Cl]-radiolabelled anhydrous gaseous hydrogen chloride	62
10. Radiochemical counting of [¹⁸ F]-fluorine on silica and silicon substrates with aqueous [¹⁸ F]-radiolabelled hydrogen difluoride anion	63

Chapter 3: Results	Page
A. Chemomechanical polishing of silica and silicon	
1a. Polishing of silica	64
1b. Polishing of silicon	66
1c. Surface stress introduced in silica by polishing with the Pilkington reagent	66
2. The role of cerium (IV) oxide in the Pilkington reagent	67
2a. The effect of addition of cerium (IV) oxide to aqueous solutions containing the hydrogen difluoride anion over pH range 1-11	68
2b. Gaseous anhydrous [³⁶ Cl]-radiolabelled hydrogen chloride as a probe for surface hydroxyl groups on powdered silica (Spectrosil B) and CeO ₂ (Opaline)	68
2c. Polishing with omission of a lapping process	71
B. Identification of the active species in the Pilkington reagent	
1a. Etching experiments involving silica (1-5)	71
1b. Etching experiments involving silicon	73
2. Radiochemical uptakes of aqueous [¹⁸ F]-labelled hydrogen difluoride anion on silica and silicon	73
2a. Radiochemical uptake of aqueous [¹⁸ F]-labelled [HF ₂] ⁻ on silica over pH=1-9	74
2b. Radiochemical uptake of aqueous [¹⁸ F]-labelled [HF ₂] ⁻ on silicon over pH=1-10	75
2c. Radiochemical uptake of aqueous [¹⁸ F]-labelled [HF ₂] ⁻ on silica and silicon at pH=1	76
2d. Radiochemical uptake of aqueous [¹⁸ F]-labelled [HF ₂] ⁻ on silica at pH=1	78
C. Identification of reaction intermediate formed during polishing and etching	
1. Spectroscopic analysis	
1a. Infrared spectroscopy	79
1b. ²⁹ Si Magic-Angle-Spinning Nuclear Magnetic Resonance spectroscopy	80
2. Powder X-ray diffraction	81

	Page
3. Elemental analysis	81
4. Scanning Electron Microscopy	82
5. Nomarski light microscopy	83
6. Comparison of authentic K_2SiF_6 with reaction intermediate	84
D. Electronic and infrared spectroscopic analysis of supported thin organic films prior to and after chemical modification	
1. Electronic spectra	
a. Perylene	86
b. Bis(ethylenedithio)tetrathiafulvalene (BEDT-TTF)	87
c. Violanthrone	87
d. Pentacene	88
e. Ovalene	88
f. Tetracene	89
g. Rubrene	90
h. Perylene tetracarboxylic dianhydride (PTCDA)	91
i. Coronene tetracarboxylic dianhydride (CTCDA)	91
j. Coronene tetracarboxylic acid (CTA)	92
k. Decacyclene	92
l. Chrysene	93
m. Anthracene	93
n. Fluoranthene	94
o. Pyrene	95
p. 7,7,8,8-tetracyano-p-quinodimethane (TCNQ)	95
2. Attempted chemical modification using PF_3 and BF_3	96
3. Classification of the spectroscopic data	97
4. Infrared spectra	98
E. The Quartz Crystal Microbalance (QCM) technique <i>in vacuo</i> as applied to the reaction of $[Al(Pc)F]_n$ with MoF_6	99

Chapter 4: Discussion	Page
1. Chemomechanical polishing of silica and silicon	103
2. Organic thin films	116
Chapter 5: Conclusions and Future Work	132
References	138

Figures & Tables	After page
Figure 1.	3
Figure 2.	10
Figure 3.	13
Figure 4.	21
Figure 5.	23
Figure 6.	26
Figure 7.	27
Figure 8.	28
Figure 9.	34
Figure 10.	34
Figure 11.	34
Figure 12.	35
Figure 13.	35
Figure 14.	38
Figure 15.	39
Figure 16.	41
Figure 17.	42
Figure 18.	43
Figure 19.	46
Figure 20.	46
Figure 21.	56
Figure 22.	57
Figure 23.	58
Figure 24.	59
Figure 25.	61
Figure 26.	62
Figure 27.	65
Figure 28.	65
Figure 29.	66
Figure 30.	67
Figure 31.	69

	After page
Figure 32.	69
Table 1.	69
Table 2.	69
Table 3.	71
Table 4.	71
Figure 33.	72
Figure 34.	72
Figure 35.	72
Figure 36.	72
Figure 37.	73
Figure 38.	75
Table 5.	75
Figure 39.	75
Table 6.	75
Figure 40.	77
Table 7.	77
Figure 41.	78
Table 8.	78
Figure 42.	78
Table 9.	78
Figure 43.	79
Figure 44.	80
Table 10.	81
Figure 45.	82
Figure 46.	82
Figure 47.	82
Figure 48.	82
Figure 49.	82
Figure 50.	82
Figure 51.	82
Figure 52.	82

	After page
Figure 53.	82
Figure 54.	82
Figure 55.	82
Figure 56.	83
Figure 57.	84
Figure 58.	85
Table 11a.	85
Table 11b.	85
Electronic spectra: a.1-a.2	86
Table A.	86
Electronic spectra: a.3-b.1	87
Table B.	87
Electronic spectra: b.2-c.2	87
Table C.	87
Electronic spectra: d.1-d.3	88
Table D.	88
Electronic spectra: e.1-f.1	89
Table E.	89
Electronic spectra: f.2-g.1	89
Table F.	89
Electronic spectra: g.2-h.2	90
Table G.	90
Table H.	91
Electronic spectra: i.1-j.2	91
Table I.	91
Table J.	92
Electronic spectra: k.1-k.3	92
Table K.	92
Electronic spectra: l.1-m.1	93
Table L.	93
Electronic spectra: m.2-n.1	94

	After page
Table M.	94
Electronic spectra: n.2-o.2	94
Table N.	94
Electronic spectra: o.3-o.5	95
Infrared spectra of thin films of PAHs on silica.	98
Perylene/ Tetracene on silica (ATR-FT-IR)	98
PTCDA/ Chrysene on silica (ATR-FT-IR)	98
Fluoranthene/ Pyrene on silica (ATR-FT-IR)	98
Anthracene on silica (ATR-FT-IR)	98
Figure 59.	100
Figure 60: a-b	101
Figure 60: c-e	102
Table 12.	102
Table 13.	102
Figure 61.	120
Figure 62.	121
Table 14.	129
Table 15.	129

Summary

In this work an investigation of chemomechanical polishing of silica and silicon has been conducted, in order to produce ultrasmooth surfaces (roughness ≤ 1 nm) rapidly and to understand the mechanisms of the chemical processes involved. A comparison of fluoride-based reagents (alkaline colloidal silica sol modified by the addition of potassium hydrogen difluoride and a reagent described in the patent literature (69), comprised of an aqueous suspension of hydrochloric acid, potassium hydrogen difluoride, cerium(IV) oxide and sucrose) with conventional polishing reagents (an aqueous suspension of cerium(IV) oxide and alkaline colloidal silica sol) was made. Fluoride based reagents have been used successfully for the polishing of silica glass and the work developed further and amplified with model studies using fluorine-18 as a radiotracer. Identification of surface and bulk species by FT-IR spectroscopy (diffuse reflectance, photoacoustic, attenuated total reflection and transmission) and FT-IR microspectroscopy coupled with silicon-29 MAS-NMR, SEM and powder XRD techniques has been accomplished. Similar strategies were employed for polishing of silicon. Surface roughness measurements were conducted using a Nomarski light microscope and Talystep stylus profiler, allied with laser interferometry. Work conducted in this part of the study has enabled the positive identification of a reaction intermediate (*the passivating layer*) formed during the chemomechanical polishing of silica for the first time..

By employing highly polished silica and silicon wafers the production of ordered organic films derived from polycyclic aromatic hydrocarbons was achieved by high vacuum sublimation techniques. The compounds chosen in this study were anthracene, tetracene, pentacene, perylene, ovalene, fluoranthene, rubrene, decacyclene, violanthrone, coronene tetracarboxylic acid, coronene tetracarboxylic

dianhydride, perylene tetracarboxylic dianhydride, bis(ethylenedithio) tetrathiafulvalene, pyrene, chrysene and polymeric fluoro-bridged aluminium(III) phthalocyanine. Chemical modification of the films has been achieved by formation of electron donor:acceptor complexes with the volatile high oxidation state main group and transition metal halides arsenic pentafluoride, molybdenum and tungsten hexafluorides and the solid organic electron-acceptor species tetracyano-p-quinodimethane. Films were characterised by UV-vis-NIR and FT-IR spectroscopy. The Quartz Crystal microbalance technique was employed to investigate the oxidative doping of polymeric fluoro-bridged aluminium(III) phthalocyanine, to determine both reaction stoichiometry and mechanism. By comparison of the unmodified organic films with their derived donor:acceptor complexes, films could be placed into one of three categories; those which exhibited both electronic and physical perturbations, those which exhibited physical perturbations only and those for which the electronic spectra were dominated by interference patterns. In all cases there was no conclusive evidence in the electronic spectra for the formation of radical cations derived from donor polycyclic aromatic hydrocarbons.

Chapter 1

Introduction

Introduction.

A1. Aims of this work.

The reactions of organic compounds have been studied traditionally in solution, but there is increasing emphasis on reactions which are carried out under ordered conditions to obtain more information. The aims of this work were to synthesise and characterize, by spectroscopic means, chemically modified epitaxial films derived from polycyclic aromatic hydrocarbons and supported on highly polished silica and silicon wafers. Polycyclic aromatic hydrocarbons were chosen as they are "flat" molecules which are capable of being stacked in arrays. Chemical modification of the organic films, formed by vacuum evaporation on the polished substrates, involved either formation of charge transfer complexes or products of oxidation, with transition metal hexafluorides or high oxidation state halides.

The preponderance of literature on polishing has come from engineers and although the chemistry is often irrational, the majority of ideas and citations in this work were drawn from engineering. It is accepted generally that the production of a plane, specular surface on an optical, electronic or optoelectronic material by chemomechanical polishing requires a chemical reaction which occurs preferentially on the high points on the surface. To understand the mechanisms of the chemical processes involved, the bulk of this work involved chemomechanical polishing of the substrates, using fluorine-18 as a radiotracer and FT-IR spectroscopy (diffuse reflectance, photoacoustic, attenuated total reflection and microscopy) to identify surface species coupled with silicon-29 MAS NMR and X-ray diffraction techniques. Surface

roughness measurements were to be evaluated using a Nomarski light microscope and Talystep stylus instrument.

2. Polishing of optical materials.

The aim of polishing is to produce a specular reflective surface which is free of damage and artifacts (1). The surfaces are required usually to be flat or spherical, although occasionally departures from those shapes are needed, in order to obtain some optical advantage not attainable otherwise. A polished surface differs in both physical and chemical properties from the bulk of the substrate from which it originates. There is often an elevation in mechanical strength and resistance. Polished surfaces may exhibit differing heat and electrical conductivities, electromagnetic characteristics and crystalline structure from single crystal bright faces (2).

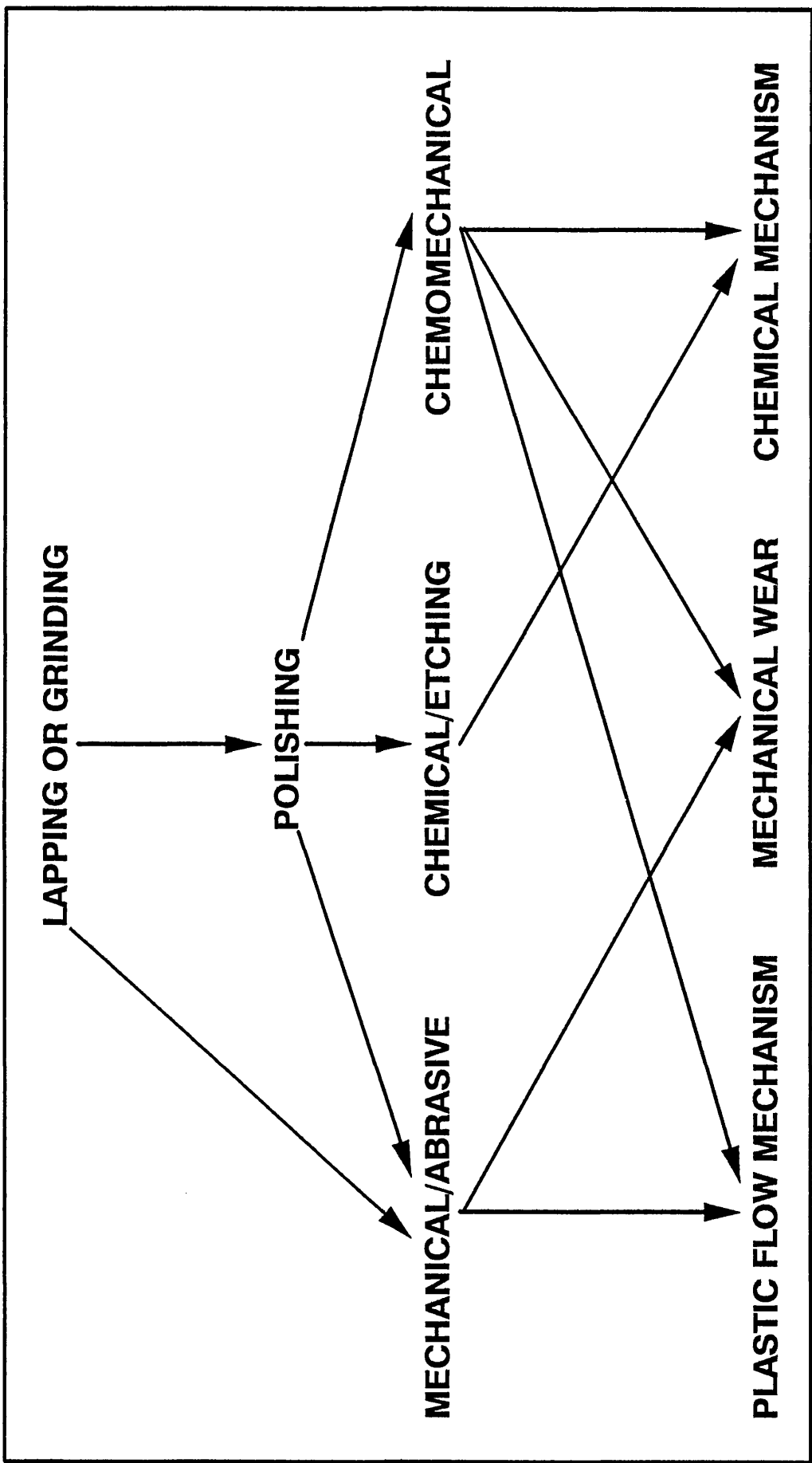
The phenomenon of polishing has been known for many centuries (3). The earliest characterization of optical surfaces was by visual inspection of the surface finish by opticians, who ground lenses to shape then polished the component until the matt finish changed to a shiny surface. A surface finish was considered to be satisfactory when the greyness disappeared. The science of polishing occurs beyond the resolution of the optical microscope. It was only with the advent of the electron microscope (4), phase-contrast techniques (5) the surface profiler (6) and other advances in instrumentation that the significance of the chemical and physical properties of solid surfaces became apparent, producing a great surge of work on the mechanisms of optical polishing (7).

Surface roughness is becoming increasingly important for applications in optics. The production of finishes at the subnanometre level for low scatter lenses, mirrors, filters, beam splitters and other optical components is necessary to reduce light scattering and improve the performance of telescopes, microscopes, binoculars, lasers and other specialised optical systems. Surface roughness has two main attributes; roughness heights or depths and lateral dimensions. A scratch on a glass surface typically will have dimensions of the order of a few microns in width and a depth of a few tenths of a micron; optical films composed of tiny crystallites have heights of a few tens of nanometres and lateral dimensions of a fraction of a micron (8).

Surface roughness values may be reported or measured as the root-mean-square roughness, R_A . The units are nanometres (nm) or Ångströms (Å) for smooth surfaces, microns for rough surfaces and lateral dimensions. Commercially polished glass optics, such as lenses and mirrors, have R_A values in the range of 1.5 to 2.5 nm; superpolished optics have R_A values of less than 0.1 nm. Ground glass surfaces have values ranging from 10 nm to several microns, depending on the type of glass and abrasive particle size.

Polishing is accomplished generally by three distinct polishing processes. Abrasive polishing employs abrasive particles to grind the surface of the material to the required finish. Chemical polishing or etching is accomplished by chemical means, involving the dissolution of the surface of a material. Chemomechanical polishing is a combination of the two processes; a surface is modified chemically and the material formed at the surface is removed by mechanical action. (Fig. 1)

Figure 1.



There has been extensive effort to attempt to explain the mechanisms involved in the polishing of optical glass (7) and as a result of the cross-fertilisation of ideas from various disciplines, the knowledge of the subject has increased considerably. Until recently, the techniques employed for polishing of optical materials had not undergone any considerable change since the beginning of the century, when the standard industrial practices were established (1). There is one major drawback with all "classical" polishing techniques; they are dependent largely on the skill of the craftsmen who develop an intuitive understanding of the process. The efforts of the scientific community have only recently been recognized and developed further within the optical industry (9), because the basic problem for any optical engineer, utilizing a lapping or grinding process, is to control the shape development taking place during the operation. With the realization that glass polishing and glass surface science are related fundamentally by their dependence on an understanding of fracture mechanics and aqueous corrosion chemistry, three main theories to explain the mechanisms underlying glass polishing have been proposed (10).

As reviewed by Izumitani and Holland (7), the mechanisms that have been considered can be categorized as mechanical removal or wear, plastic flow and chemical or chemomechanical. It is accepted widely that the chemo-mechanical mechanism is correct (10), though there is considerable debate at present as to whether mechanical or chemical effects are dominant. There are many factors that have an important influence on what happens during the polishing process, such as the type of glass, the pressure exerted on the sample,

polishing speed, type of polishing compound used and other variables.

The chemical modification of the surface of the material by, for example, hydrolysis of the glass surface, plays an important part of the polishing process (11). There is evidence that it is the hydrolysed layer itself that is removed (12). It is now accepted by most authorities that physical adsorption, with subsequent chemical reaction between the polishing agent and surface in question are intrinsic to many polishing processes (13). It would appear that the physical action of "ploughing off" material cannot be ignored, as it is well known that individual polishing particles leave tracks behind them. These tracks are recorded not only on the surface layer, but also below the surface without appearing visible under the microscope. Polishing tracks may remain hidden by the surface layer, as a consequence of the propagation of strain into the substrate, though it is known that under certain conditions the surface of a glass may be moved by means of plastic flow, the evidence for which comes from studies of single scratch marks made in the absence of water (9). Glass can be polished also in the absence of water and is so, with the use of a polishing lap and reagent only, in many commercial optical workplaces. Under these dry conditions it is likely that plasticity of the surface will play an important role.

3. The lapping process (1).

It is customary to refer to a non-specular surface as "lapped" or "greyed off", that is, produced by a lap and rolling abrasive particles. The lapping or smoothing of the substrate prior to the polishing operation is necessary to

achieve the desired surface shape. A polished surface is produced therefore by a polisher and not a lap. A lapping plate is often referred to as the matrix, whose surface is composed of a material capable of supporting abrasive particles. Grinding with loose abrasives has been, to a large extent, replaced by milling with bonded diamond tools, although for articles too small for diamond grinding tools to be economic, the traditional lapping process is employed. There is some ambiguity in the terms lapping and polishing, which has arisen from the evolution of matrices other than pitch (used traditionally in the optical industry) for polishing. The description "lapping" for polishing in general has been established, so a lap may be a polisher, but a polisher may not be a lap.

In lapping processes, where the abrasives are applied directly to the lapping wheel surface and the substrate to be smoothed is in direct contact with the lapping surface, it is necessary to use a lap which is softer than the substrate. This is necessary to allow the abrasive grains to penetrate and lodge into the lap; the reverse will occur if the lap surface is harder than the substrate material. Laps are composed of materials such as cast iron, copper, tin and composites; all have their own particular characteristics. The lapping plate revolves at a velocity which has an important role in the removal of material in the lapping process. Each material has an optimum wheel speed, where surface removal, subsurface damage and centrifugal forces (which may displace the abrasive slurry on the lapping plate) reach an acceptable compromise. To remove material at a rate which is acceptable, pressure must be applied to the substrate material. The greater the applied pressure, the

deeper the abrasive particle penetrates resulting in deeper scratches in the surface and greater removal rates. Polishing techniques differ from those for lapping as the pressure applied must be distributed uniformly, to avoid altering the shape of the lapped surface. The polishing plate has therefore an elastic surface made of pitch, felt or polymer material.

Lapping or grinding processes can be divided into two forms, depending on the method in which the abrasive is used. Fixed abrasives are termed bonded, while loose abrasive processes are based on a slurry of abrasive particles. For fixed abrasives the grinding particules are anchored, to a cloth or paper backing, with a binder. Fixed abrasives act as single point tools, removing fragments of material of dimensions proportional to the size of the abrasive grain that is employed. The surface produced by bonded abrasives is characterised by a bright finish covered with a mozaic of scratches.

The effectiveness of loose abrasives depends on the control of uniform wear over the whole surface of the substrate. The abrasive grains are applied to a lap where they roll and scour the surface. The abrasives operate in a slurry, often aqueous in nature and the particles are applied frequently to the lapping surface. It is necessary to change the lap periodically as some grains become embedded in the lapping surface, due to the pressure applied in the process. As the abrasive particles roll over the surface, they produce a path of cracks in many directions, the entire area becoming covered with conchoidal fractures at the intersection of the cracks. The small chips that are produced must be removed by the circulating slurry, as they effect damage to the surface. The surface damage or pits have dimensions that are proportional to the

abrasive grains and the surface is dull compared with that produced by fixed abrasives. The problem of controlling wear of the surface is dependent therefore on the speed of rotation, relative displacements of the lapping surface in relation to the substrate to be smoothed, pressure on the surface of the substrate and the application of abrasive particles with an adequate quantity of liquid media, such as water.

4. Abrasives used in lapping and polishing.

A qualitative guide to the type of abrasive for use in any lapping or polishing process can be obtained from the "hardness" of the abrasive, where hardness is described by an extension of Mohs scratch hardness scale (14). A substance will be scratched by any species matching or exceeding it in "hardness". This neglects, however, the crystal orientation and pressure applied and so examples of anomalous behaviour are explained often by the relative melting points of the abrasive and substrates (15).

When a surface is lapped, pressure and heat are important though the entire dynamic picture requires a consideration of all the chemical reactions that may take place. A relatively benign reagent, such as an aqueous suspension of alumina, can become aggressive at the solid-liquid interface where heat evolved by frictional forces may approach activation energies required for chemical reaction to take place.

One of the most successful chemical-mechanical systems employs an alkaline silica sol, pH = 10.5, as a colloidal suspension of silica particles (Mohs hardness of 7) (16). Simple consideration of the relative hardness values, of

the submicron silica particles and a silicon substrate, may explain the success of the reagent in polishing the latter. This mechanical model fails, however, to explain the success of the reagent for the polishing of high alumina ceramics ($\alpha\text{-Al}_2\text{O}_3$); silica alone will not polish sapphire and mild base will not attack sapphire (9).

Abrasives used for polishing are suspended often in non-polar solvents and in these cases their action is unambiguously mechanical. Solvents which are weakly polar such as ethane-1,2-diol are chemically unreactive also; the viscosity of the solvent is useful in preventing abrasive particles settling out of suspension. They can be modified by dilution with water, alcohol or alkyl halide, though this may of course have chemical consequences.

The process of lapping with a range of successively smaller abrasive particles is the traditional method of stock removal prior to polishing. Each grade leaves a damaged and pitted surface which is made smoother in progressive stages. For many semiconductor compounds which are easily damaged by lapping, the critical factor is often not the type of abrasive used but the confidence in the process whereby particles are graded in size, since most particulate size gradings assume spherical species, though the abrasive particles are invariably irregular.

5. Important parameters in the polishing of optical materials.

The polishing of optical materials involves many principles all of which, to some degree, determine the methodology employed. A useful, but potentially dangerous relationship between the size of the abrasive particle and

depth of damage it produces, is invoked often (17) without reference to effective surface areas and the load applied. The greater the loading on the abrasive particles, the greater the rate of removal and so if a surface is acceptably specular and flat, any process which removes a certain amount of material faster merely as a result of increasing load is judged to be economically desirable. However, the depth of damage increases simultaneously, which can be catastrophic for fragile components (18) (Fig:2).

There are six main parameters to consider in any polishing process; the abrasive used, the liquid vehicle employed, the materials used as the lapping/polishing pad, the pressure applied, the rotational velocity of the pad and the work-rotation and sweep.

In choosing an abrasive, it is necessary to consider the material, particle size, shape and density. The material should not break down easily, as agglomeration of smaller particles can occur subsequently, producing surface damage on the substrate. Any tendency to form a mortar with polishing debris should be minimised. With diamond polishing compounds, the rate of removal of material is affected profoundly by the shape of the abrasive particles. The denser the abrasive, the more difficult it is to keep it in suspension.

The choice of liquid vehicle is critical also; the ability to solvate, the viscosity, stability and the liquid-to-abrasive ratio are all factors to be considered. The ability of a solvent to keep a given solute in solution depends considerably on its ability to solvate the dissolved particles, that is, to interact with them in a quasi-chemical way. The ability of a liquid to dissolve ionic

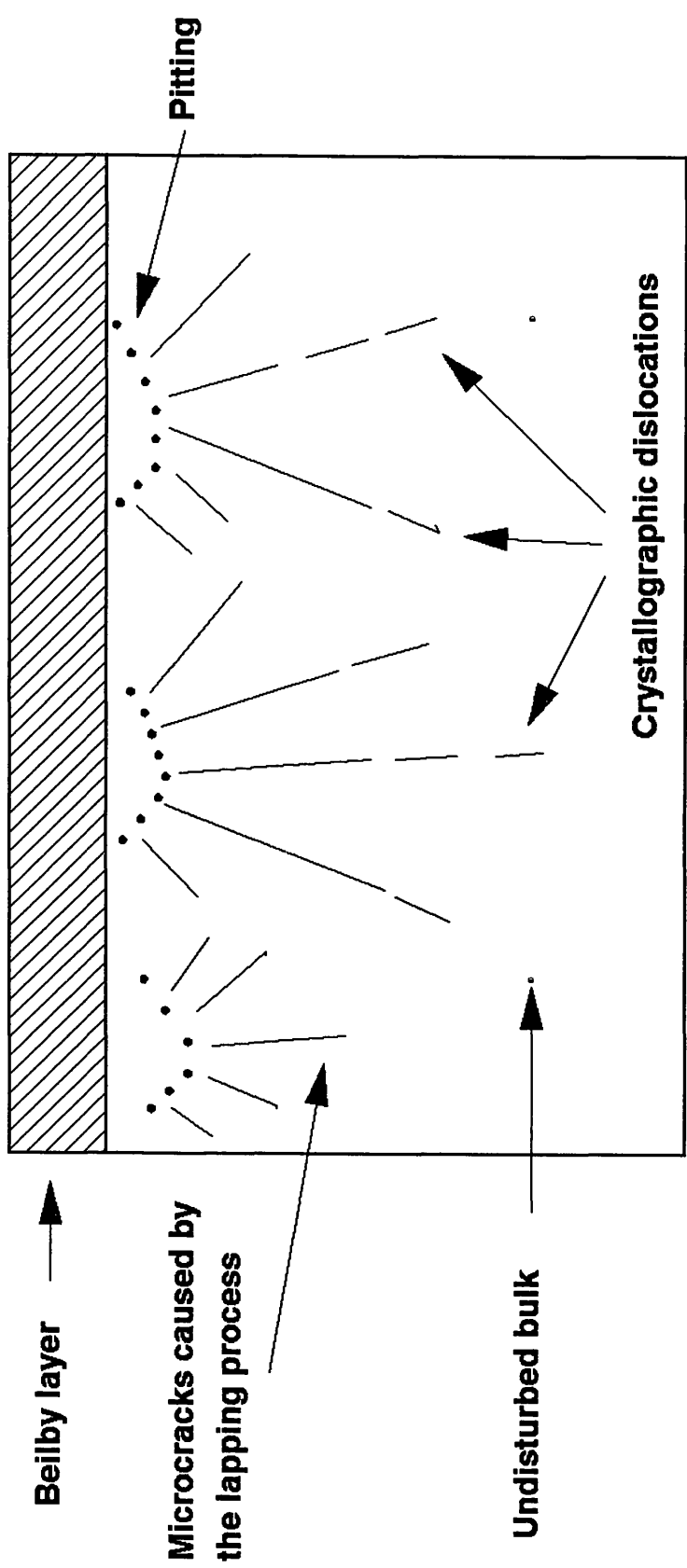


Figure 2: Subsurface damage produced by lapping and polishing

solids (such as alkali halides used for infrared "windows") depends strongly, although not exclusively, on its relative dielectric constant, ϵ (19). The ability to solvate ions and the dielectric constant often increase simultaneously although there is no quantitative correlation; the extent of hydrogen bonding in the solvent plays an important role also. Generally it can be stated that, for ionic species, the more polar the solvent the better able it is to use its negative and positive regions to solvate the cations and anions of the solid.

Solvents can be divided according to whether or not they contain ionizable protons, and are termed protic or aprotic. Protic solvents characteristically react with solutes to give anions and cations by the process of autodissociation, so that solutes encounter both the molecules of the solvent and the cations and anions that form in the autodissociation process. The most common protic solvent is water, though others such as ammonia and sulphuric acid are sometimes employed. Aprotic solvents can be subdivided into those which (a) are nonpolar (or very weakly polar), nondissociated liquids which do not solvate strongly (such as aliphatic hydrocarbons and carbon tetrachloride); (b) those which are nonionized but strongly solvating (generally polar) solvents (such as acetonitrile) and (c) solvents which are highly polar, autoionizing solvents which are extremely sensitive to moisture and of little use in polishing. In general the solvating properties of the chosen liquid media will have consequences for both the substrates and the bonding waxes. The viscosity of the solvent is important too, for if the liquid is too viscous it may promote an aquaplaning effect, thus preventing fine abrasive particles from cutting. The stability of the media under polishing conditions to keep colloidal particles

dispersed is important also. The liquid-abrasive ratio must be adjusted to prevent drag of the substrate on the rotating pad, which will induce damage when the abrasive concentration is too great. If the concentration is too low, however, there may be problems with aquaplaning or wringing (when the substrate adheres to the lapping plate; the solvent is squeezed out at the interface, forcing air out and resulting in a partial vacuum).

The material used for the polishing or lapping plate should be firm enough to stay in shape and stable enough to resist attack from hot polishing slurries, though a softer material will produce less damage to the substrate and support large sized abrasive particles. Any surface interruptions such as grooves on the plate will affect the uniform supply of slurry to the substrate. A continuous surface may reduce removal rates, which can be useful if wringing conditions are not allowed to develop.

The pressure applied to the sample is one of the easiest parameters to control, as well as one of the most important. Increasing the mass/unit area ratio will result in increased removal rate and damage to substrate. The pad/plate may become distorted under increased load and degrade the figure of the surface produced.

The rotation of the substrate with a processing motion helps to maintain flatness, preventing a pattern forming on the substrate surface. Lateral sweep of the sample over the surface of the plate is important as this will prevent a witness forming on the work. The rotational speed of the pad is fixed at a compromise between a low rotational speed which leads to a very flat surface and a high rotation speed which increases stock removal, to minimise any

aquaplaning for the former or wringing with the latter conditions.

6. Abrasive polishing.

The polishing of optical materials using fine abrasive particles can be described by the Preston wear equation (20).

$$\Delta H / \Delta t = K_p (L/A)(\Delta S / \Delta t)$$

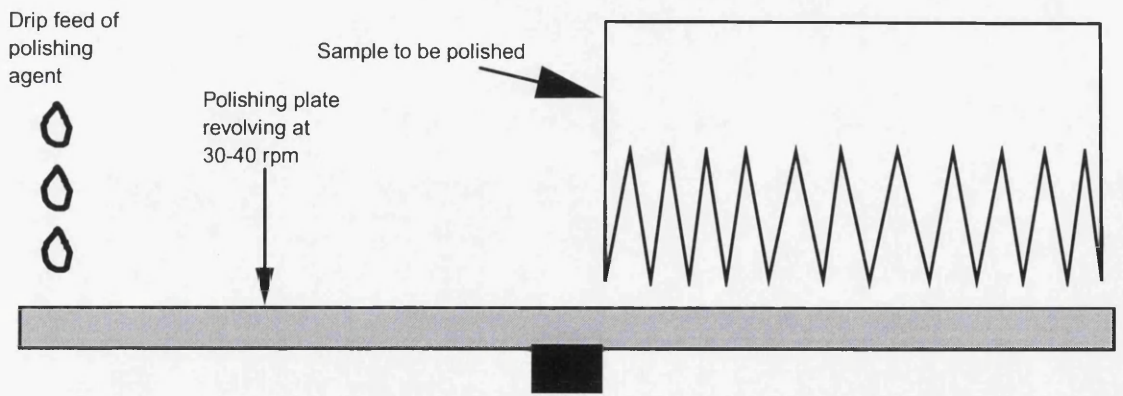
where $\Delta H / \Delta t$ is the change in height $H(\mu\text{m})$ over time $t(\text{s})$, L is the load (g), A is the surface area over which wear occurs (cm^2), ΔS is the relative travel between the surface being polished and the lap over which wear occurs (cm) and K_p is the Preston coefficient which is process dependent ($\text{cm}^2\text{dyne}^{-1}$).

The rate of surface removal is dependent on pressure, which is determined by the contact area between the plate and the substrate in question. As the peaks on the surface are removed, the contact area increases, with the result that the rate of surface removal decreases. It follows that the surface roughness decreases with increasing contact area (Fig:3).

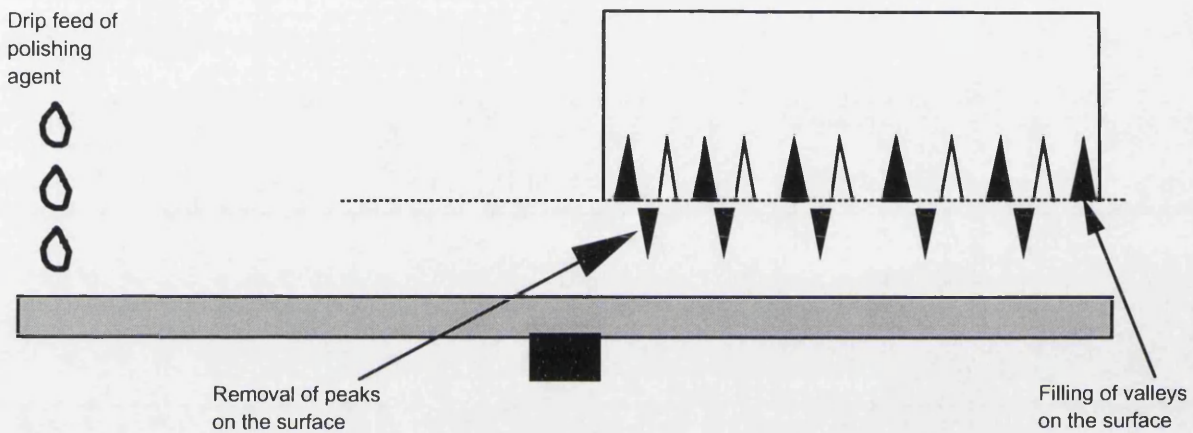
The rate of surface removal increases directly with increasing lap velocity and loading; the greater the applied pressure on the sample, the greater the stock removal. It is known that the rate of surface removal is independent of polishing particle size, but surface roughness is dependent (10). In all models that describe the mechanics of interaction, it is assumed that polishing rates are independent largely of the polishing particle used. Observed rates are proportional to the inverse of the Young's modulus of a given optical glass (21), though they are an order of magnitude lower than is predicted by the mechanical model. For polishing of optical glasses with ceria,

Figure 3: Schematic representation of the polishing process with formation of a passivating layer

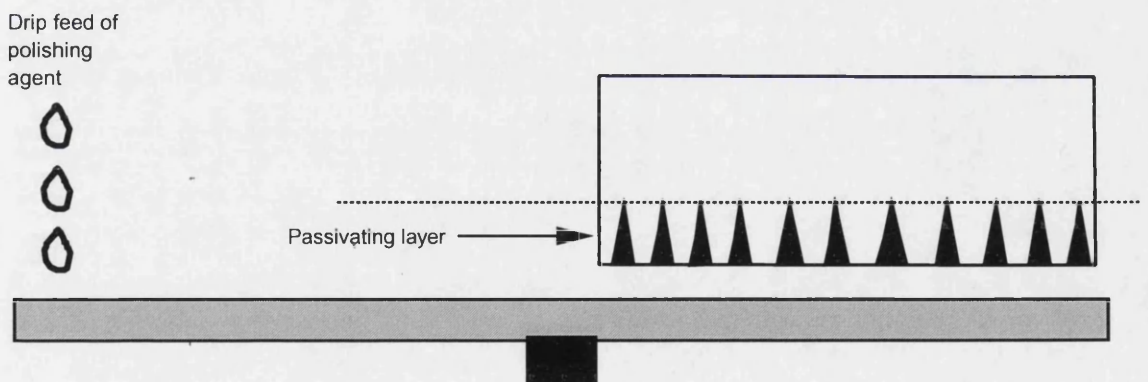
a.



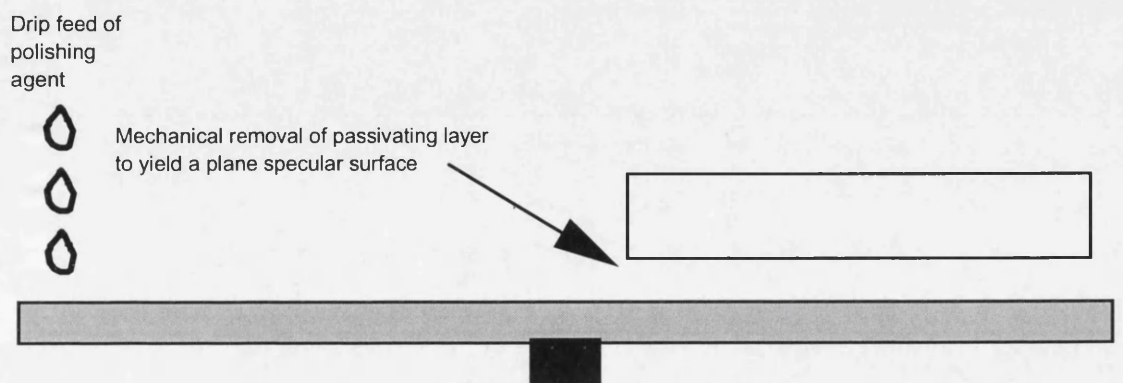
b.



c.



d.



the observed rates are found to be greater than expected and are an indication of the chemical interactions found in glass polishing (10).

7. Chemical polishing or etching.

Etching or chemical polishing is the term given to the process used for polishing and shaping of semiconductors, such as silicon, germanium, gallium arsenide and other technologically important materials. Semiconductors are chemically etched to remove material from the surface, which may be damaged by mechanical cutting or lapping, leaving a polished surface which is free of defects, both at the surface and subsurface.

The fundamental reactions which govern all semiconductor etching processes are electrochemical in nature, where the general reaction pathway involves oxidation-reduction processes with the exchange of one or more electrons between two species, followed by dissolution and/or complexation of reaction products at the surface. The transfer of electrons from reductant to oxidant can be made to take place at a pair of electrodes connected through external circuitry, allowing the redox process to be manipulated by electronic operations on the external portion of the circuit, allowing control of the extent and direction of the reaction. Etching processes are well documented, and are often well understood (22).

The dissolution process is controlled by two factors, the rate of diffusion or transport of the active chemical species to the surface of the substrate and the rate of chemical reaction between the substrate and etchant. Processes which are diffusion controlled have lower energies of activation than those that

are reaction rate controlled, typically $10\text{-}5\text{ kJmol}^{-1}$. It follows that diffusion controlled processes are relatively insensitive to variations in temperature, but sensitive to stirring effects or agitation, as an increased supply of etchant to the surface of the material will lead to higher etch rates. Rate-limiting processes are influenced by other factors, such as variations in etchant composition and initial condition of the substrate to be etched (the type and concentration of doping atoms, lattice defects and crystal orientation for example). The fundamental chemical reactions involved in etching are common to many semiconductor fabrication processes and hence it is often convenient to classify chemical etching studies according to the technique by which the reaction has been conducted. These can be summarized as isotropic and anisotropic (23) liquid etching, electrochemical and selective chemical etching (24), gas and vapour phase etching (25) and sputter and plasma etching (26) all of which have been discussed in detail in the literature (27), although they are of limited relevance to this work.

8. Chemomechanical polishing of silica surfaces.

In this study the technique of chemomechanical polishing was employed. Chemomechanical polishing is the term given to the process where a controlled chemical etch of a substrate is allied with the mechanical action of a polishing lap (and polishing particle were appropriate). An ideal chemical reaction, leading to a plane specular surface, would be one which occurred preferentially at peaks on the surface. In practice, control of a chemical reaction by other means is required, and one way is by the formation of an

insoluble or sparingly soluble species in the valleys on the surface. This is known as the "passivating layer" concept, and is one of several (7) mechanisms whereby a plane specular surface can be achieved (Fig:3).

A model for chemomechanical polishing which has universal applicability is unrealistic, since the nature of the chemical reactions that occur at the solid-liquid interface are a consequence of the nature of the surface to be polished and the reagent used. For silica surfaces however, a model can be described by a series of steps, any of which may be rate-determining or controlling the entire process, occurring at the liquid-solid interface:

- a. Delivery of the reagent to the surface.
- b. Adsorption of the active species on the surface, with or without the prior modification of the surface.
- c. Reaction of the surface layer of the substrate with the adsorbed species.
- d. Removal of the reaction products from the surface.
- e. Redeposition of reaction products from the polishing slurry on to the surface of the substrate material.

For chemically active polishing systems it is important to control the conveyance of the active species to the substrate surface, or an uncontrolled chemical etch may take place. The importance of accumulating reproducible experimental data on polishing conditions makes it necessary to control the reagent delivery. The moderation of an aggressive reagent by use of a supported reagent is one example (28) where the reagent molecule is brought into contact by physical means with the substrate, allowing slower delivery of

reagent and the active species to the surface of the substrate, often with consequential beneficial effects.

It has been accepted generally in the literature that a chemomechanical polishing process requires the prior adsorption of the active species on the substrate surface (10). The reactivity of adsorbates on surfaces is dependent upon the availability of sites suitable for bonding and the degree of chemical interaction between the adsorbate and the bonding site. Silica surfaces have structures terminating in oxygen atoms, either singly bonded to silicon or bridging two silicon atoms. The former terminal oxygen sites are hydrated to some degree to give silanol sites (Si-OH), due to moisture in the atmosphere (29). The silanol sites can form also via breakages in the siloxane (Si-O-Si) network bonds. Reactivity at the silica surface depends therefore upon a potential adsorbate hydrogen bonding to the surface of the silica via the silanol sites, or alternatively undergoing ion-exchange with the proton of the silanol group or the entire hydroxyl group. Surfaces with greater silanol concentrations are more responsive therefore to deposited species (30).

Prior modification may be introduced deliberately to alter the chemistry of the surface of the substrate, before surface adsorbates are interposed. This is a consequence often of the solution pH (10). The silanol groups on a silica surface are protonated or deprotonated depending on the conditions used. The surface silanol concentration can be controlled, by the introduction of fluorine into the silica for example, which affects the surface reactivity. Fluoride doped silica glass is employed in fibre optic waveguides, as the control of the concentration of silanol groups produces specific refractive indices in the

glass (31). The effects of fluorine on the properties of glass are well documented (32). Fluoride ions have been shown to be mobile in silica surfaces (33).

The process whereby products are removed from the surface of the substrate is an important factor in determining the quality of the surface produced in the polishing reaction. Product removal is often the rate-determining step. If reaction products are soluble and removed rapidly, an exposed surface is left which may be attacked further, leading to an uncontrolled etching reaction. If however the products are insoluble or sparingly soluble, the valleys on the surface of the substrate may be filled by this material, leading to a flat surface. This is often called the passivating layer (34). Redeposition of material, produced during the polishing process, may occur when freshly polished surfaces are exposed to the polishing slurry and the mechanical removal of reaction products is inadequate (10).

B.1. Definition of a glass.

A layman's conception of a "glass" is one of an optically transparent, silica-based material and while many amorphous materials produced are indeed of this variety, both traditional (utensils and window materials) and advanced technological (glass fibres for optical communications), very many other materials can be rendered amorphous, many of which have important technical applications. For example, amorphous selenium films formed the photoreceptors initially for the Xerox process and semiconducting amorphous

silicon films are used as large-area solar cells and thin film transistors (35).

An amorphous solid may be regarded as differing from its crystalline counterpart in that it contains an excess of free energy and entropy (36). These are included during the process of preparation, which must be sufficiently rapid to preclude the formation of crystalline material, by not allowing the atoms or molecules enough time to reach the lowest energy state. There are many techniques for producing amorphous materials from crystalline materials, but the most common method is by the rapid quenching of a liquid to form a glass, a method discovered by the Phoenicians to generate glass from a melt of lime, sand and soda (9).

Glasses are distinct from other amorphous materials by virtue of a characteristic transition, the so-called glass transition temperature T_g that they exhibit (37). At T_g the supercooled liquid departs from the equilibrium behaviour, the actual value of T_g depending on the cooling rate. The term glass transition is used generally for positionally disordered material, but other degrees of freedom may be quenched to yield glasses. Disorder in dipole interactions may be frozen to yield dipole glasses, an example being KBr doped with CN^- (38). Thus, the glassy state includes long-range disorder of many types, while the glass transition manifests itself when relaxational and experimental time scales intersect.

2. The historical development of optical glass.

Prehistoric man made implements such as knives and arrowheads from obsidian, a naturally occurring volcanic glass, but it was the discovery around

4000 BC by Egyptian and Mesopotamian potters that glass in the form of a glaze could be produced in an oven that led to the development of glass technology. It was found that a mixture of sand and minerals could cover stone objects with a vitreous glaze and that the glaze could stand by itself and produce glass objects; these were produced about 1500 BC (9).

New methods of glass production replaced the sand-core technique about 100 BC and glassblowing (invented by the Syrians) extended the use of glass by emphasising the need for transparency, which up until then had been opaque. About AD 1550 workers from Venice introduced to England a new product which later became known as English crystal glass. Italian crystal contained "soda" from the ashes of marine plants, but in England the alternative alkali used was "potash" obtained from the ashes of burned trees and bracken. The first glass suitable for hand production, easy to cut and engrave was perfected by George Ravenscroft in 1676. The glass he developed, by replacing some of the potash with lead oxide, was softer, heavier and clearer with a brilliant finish leading to its name "English Crystal". The word "crystal" comes from the Greek "Krystallos" which means "frozen ice", so called because colourless quartz or rock crystal was first discovered on the perpetual snow of the Swiss Alps and was thought to be a form of frozen water. Silica-lead-potash glass is still known as "flint" glass.

Silicate glasses can be divided into four basic types, soda-lime, lead, borosilicate and coloured glasses. Soda-lime glass is the most important type on terms of volume production and variety of use and is made from inexpensive materials, namely sand, soda ash and limestone with small amounts

of other chemicals to achieve specific requirements. Window glass, bottles, light bulbs and volumetric glassware such as burettes are all made from soda glass.

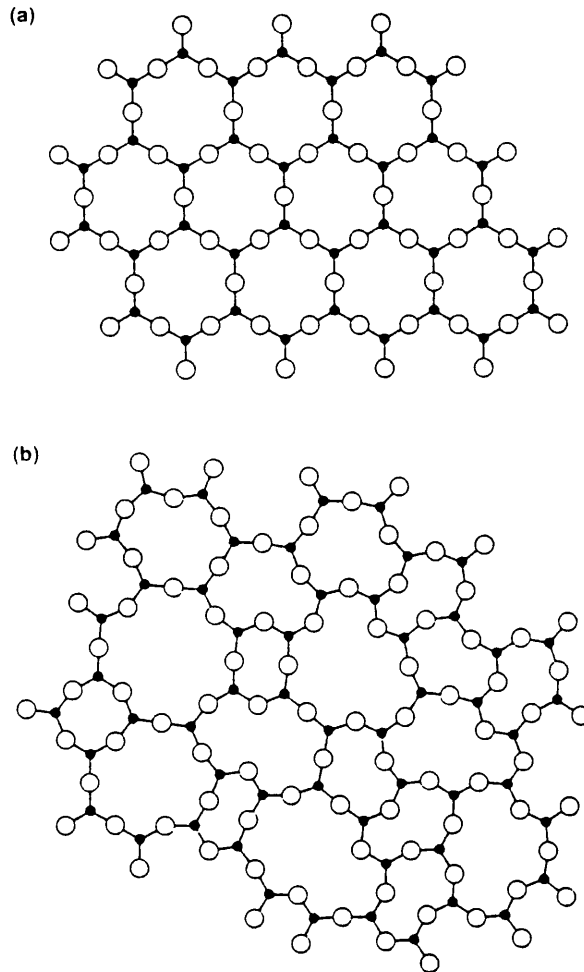
Borosilicate glass known as "Pyrex Brand" was developed by Corning in 1915 and is used widely in the manufacture of scientific glassware. It has a high resistance to chemical attack and greater resistance to thermal shock than soda glass (39).

There are two principal types of optical glass, known as "crown" and "flint" glass. Crown glass is harder, with a lower refractive index, and is so-called because it was used originally to make sheets of glass by applying a centrifugal force to a bulb of glass which would open out in the form of a crown.

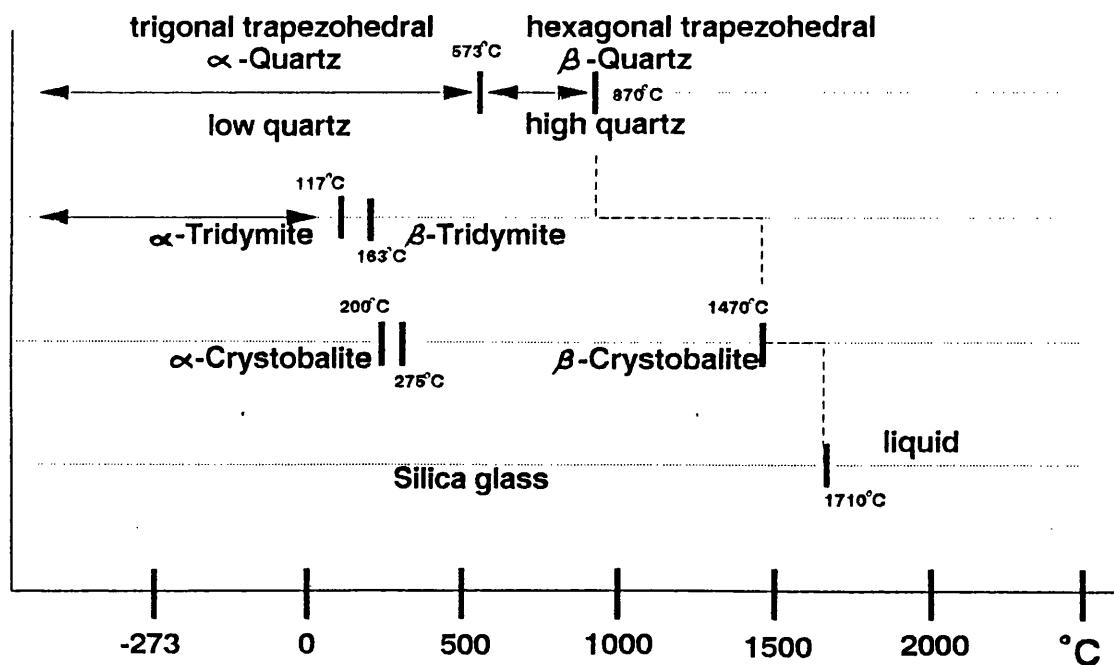
In considering the properties of glasses based on silica with one or more modifiers, it is found that the refractive index and thermal expansion coefficient of a silica glass decrease and the viscosity increases, with increasing silica content. A true silica glass should consist of stoichiometric SiO_2 , each silicon atom co-ordinated tetrahedrally to four oxygen atoms, with every oxygen atom shared between two silicon atoms, in a completely random three dimensional network (Fig:4). Vitreous silica is an ideal optical material; it has a low coefficient of expansion, is capable of resisting thermal shock or scratches and is suitable for imaging systems and microelectronic mask substrates for use with deep UV lithography (9).

Until recently all commercial methods of producing transparent silica were based on melting crystalline quartz. The term "melting" must be

Figure 4: Forms of silica



Schematic representation of crystalline (a) and amorphous (b) silica



qualified with regard to quartz, since the process cannot be compared with processes used for melting conventional glasses. If crystalline quartz is raised to a sufficiently high enough temperature, the bonds which hold the tetrahedra in an ordered structure are weakened. Given adequate time at that temperature, the network would form a random structure. In practice there is little difference between the energy required to weaken these bonds and rupture them completely to produce vapourised silica, therefore a compromise is met whereby the particles of quartz crystal are heated to just below the temperature at which the silica will evaporate from the crystal surfaces. At this temperature the viscosity of the material is still too high to allow complete randomisation of the silica network, so a small residue of the original crystal structure remains.

To maintain both chemical purity and low water content, vitreous silica has been developed by reacting silicon tetrachloride with dioxygen in a hydrogen free atmosphere, the product having a totally random structure free of any impurities. The most important optical application for synthetic vitreous silica is for use in the ultraviolet and visible spectral regions. UV absorption and transmission are controlled largely by the presence or otherwise of metallic impurities, thus pure forms of vitreous silica such as Spectrosil and synthetic crystalline quartz are virtually free from absorption effects due to metallic impurities.

3. Quartz found in nature.

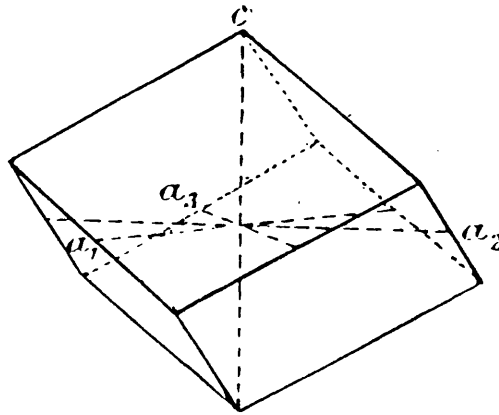
Natural rock quartz crystals are the product of weathering of silicates.

Silica produced by weathering is precipitated as quartz in cavities and crevices in all types of rock. Volcanic magma contains vast amounts of silica, which form both rock silicates and crystallites of quartz upon cooling. Quartz crystals grown without disturbance are bounded by plane faces which possess a brilliant polish. The angles between the faces are constant, though the individual faces may be of different sizes for each crystal. Quartz crystals grow in six-sided prisms bounded by six-sided pyramids and belong to the hexagonal crystal system, in which there are three equivalent horizontal axes of symmetry at 120° to each other (Fig:5a) and a single vertical axis (40). Quartz has the property of rotating polarised light transmitted along the optical axis, in a clockwise or anticlockwise manner (termed "right handed" or "left handed" rotation respectively) when the observer faces the source of light. Quartz may be either "right handed" or "left handed" (Fig:5b).

Quartz is used for optical work, for example as prisms, though the material must be colourless and free of defects. Quartz crystals are used widely as oscillators in many electronic components, such as radios, by utilizing the piezoelectric effect (41). A crystal is said to be piezoelectric if it develops a dipole when subjected to an applied stress or, conversely, if it changes its shape when placed in an electric field. Compression of a crystal of quartz can generate an electrostatic voltage across it and application of an electric field may cause the crystal to expand or contract, in certain directions. Piezoelectricity is only possible in crystal classes which do not contain a centre of symmetry. When a piezoelectric quartz crystal is exposed to an oscillating electric current, it resonates with a frequency dependent on the thickness and

Figure 5: Natural rock quartz

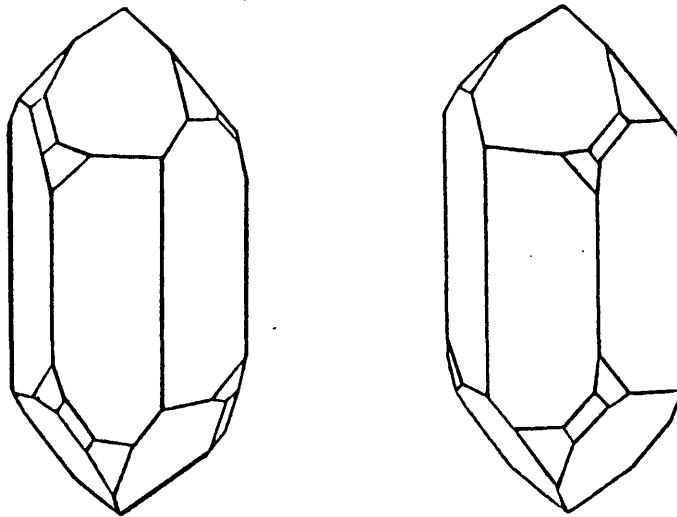
Trigonal system



a. A rhombohedron and trigonal axes

Three equivalent horizontal axes at 120° to each other and a vertical axis of different length.

Enantiomorphous quartz crystals



b. Left and right handed quartz

temperature of the crystal (42). Homogeneity of the quartz is critical for this purpose and great care is necessary in the cutting operation, in order to achieve the desired thickness and required oscillation frequency, for the electrical axis of the quartz. Oscillating quartz crystals are used for monitoring thin film depositions, in high vacuum coating units (43).

A quartz crystal is as sensitive as a microbalance and was employed as such in this work. A quartz crystal microbalance is practically unaffected by vibration and mechanical shock (44). A thin quartz crystal is contacted on its two surfaces and made part of an oscillating circuit; the alternating current induces sheer oscillations in the crystal, whose resonance frequency is inversely proportional to wafer thickness. The temperature coefficient of frequency (TCF) is related to the elastic constants of the crystal. As a result, temperature fluctuations may affect the frequency, which in turn would affect the accuracy of mass determinations. To counter this problem, the crystal is cut at an orientation of 35° to the vertical axis so the TCF terms can be made to compensate each other, allowing precise measurement to be made.

When quartz crystals are used as film thickness monitors, one crystal is exposed to the evaporating material while another is shielded from the vapour and the difference in oscillation between the two crystals can be used to calculate the rate of deposition; calibration of the system allows mass or thickness of the material to be determined.

C. Ultrathin Organic Films.

Ultrathin ordered organic films with thicknesses ranging from a few

nanometres to about a tenth of a micron show considerable technological potential as a new class of materials, where the term "material" is used to describe a substance which is synthesised or developed for a specific purpose.

Of particular interest are their tailor-made electrical and optical properties, which are related to their structure which itself can be controlled on a molecular scale. However, synthetic anisotropic organic films, such as those prepared by the Langmuir-Blodgett (LB) technique (45) have the problem of long term instability in the presence of mechanical, chemical and thermal stresses. A Langmuir-Blodgett film is the term given to a monomolecular assembly on a substrate surface, so called after the pioneering work of Irving Langmuir and Katherine Blodgett in the late 1930s.

Ordered organic thin films can be prepared in a number of ways. The self-assembly technique (46) involves chemisorption and physisorption of dissolved polar compounds, vapour deposition (PVD and CVD) (47) is common and the Langmuir-Blodgett (LB) technique (45) is the most widely used of all techniques for thin film preparation. Thermal evaporation *in vacuo* is a less popular method of preparation, as the structure exhibited by materials in thin film form depends on many factors, such as pressure and nature of residual gas in the deposition chamber, the temperatures of the evaporation source and substrate, nature of the substrate (amorphous, monocrystalline or polycrystalline), presence of electric or magnetic fields at the substrate surface, mobility of deposited species at the surface and chemical reaction between deposited material and substrate (48). When films are formed by thermal evaporation, on a heated substrate, a thermal stress will

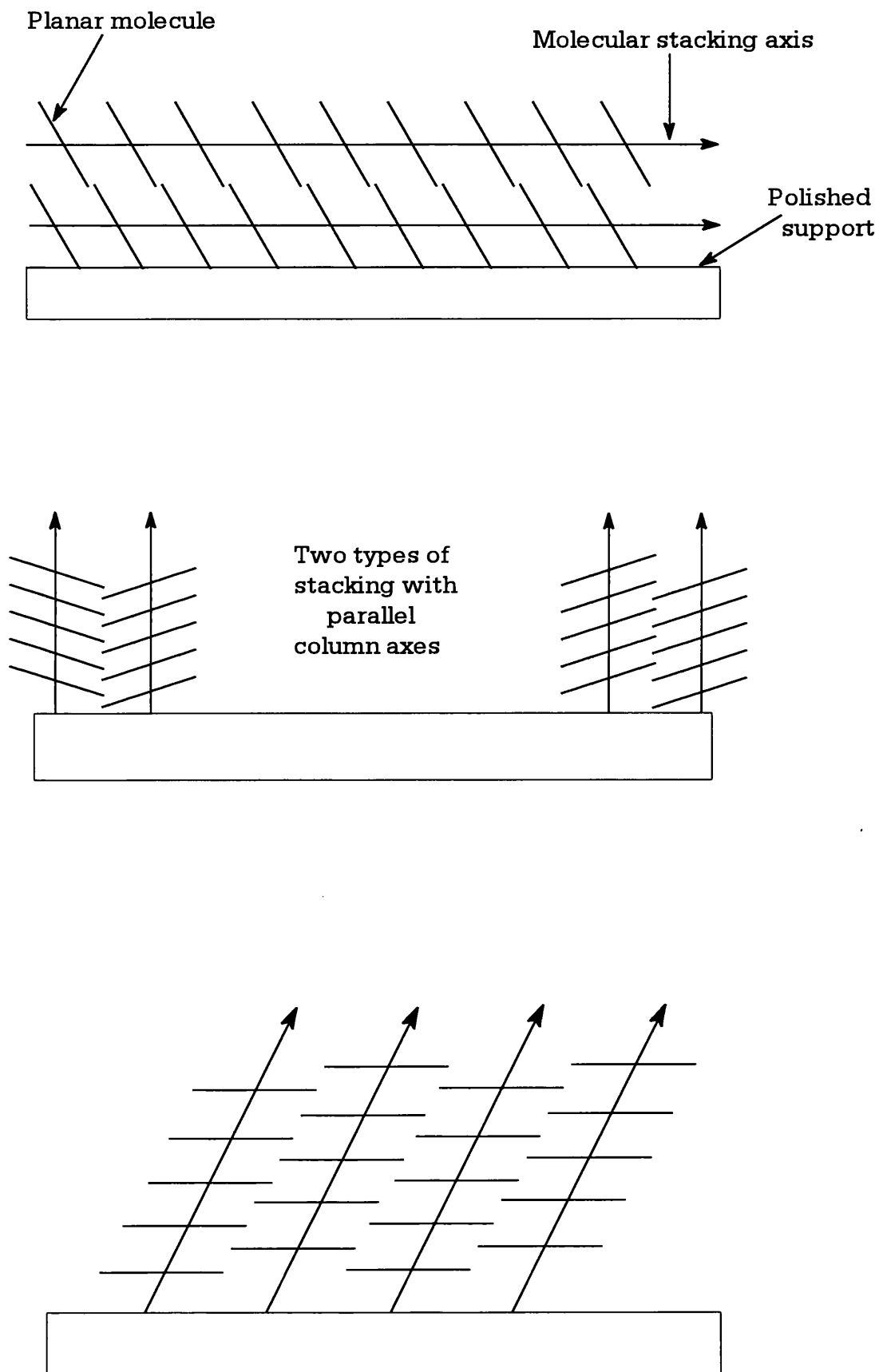
develop when the system cools to room temperature unless the film and substrate material have identical expansion coefficients. This may result in detachment of the film from the surface. Thermal stress effects exist even in films deposited on room temperature substrates. Condensing film molecules arrive with very high thermal velocities, the thermal energy of the condensed material is governed by many factors all of which determine the "temperature" of the material. The temperature of the substrate surface is only partly determined by the radiation received by the source, as there is a contribution from the latent heat given out by the condensing film. It is difficult therefore to determine the effective parameters for thin film deposition.

Preparation of thin films *in vacuo* is achieved by the following method (49). The substrate is cleaned by heating under vacuum (10^{-5} - 10^{-6} Torr), and allowed to reach the requisite temperature for thin film formation. Optimum conditions can be determined only by experimental investigation, but as a general rule this temperature is one third of the boiling point of the material. The organic material is evaporated from a shaped boat of refractory metal, such as tungsten or molybdenum, by resistance heating and the molecules allowed to orientate themselves (under as close to equilibrium conditions as possible) on the substrate surface (Fig:6).

D. Polycyclic Aromatic Hydrocarbons.

Benzene is the simplest and most important aromatic compound, as its chemistry has been investigated extensively and the concept of aromaticity based on the properties of benzene (50). More complex benzenoid

Figure 6: Some orientations of planar molecules such as polycyclic aromatic hydrocarbons on polished supports

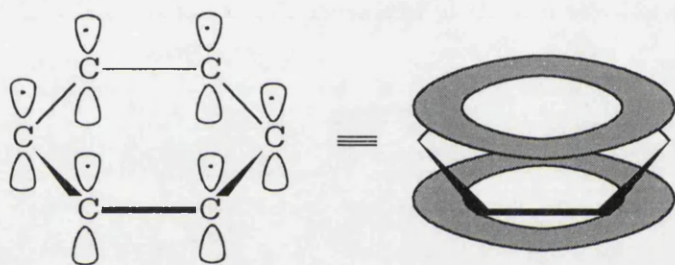
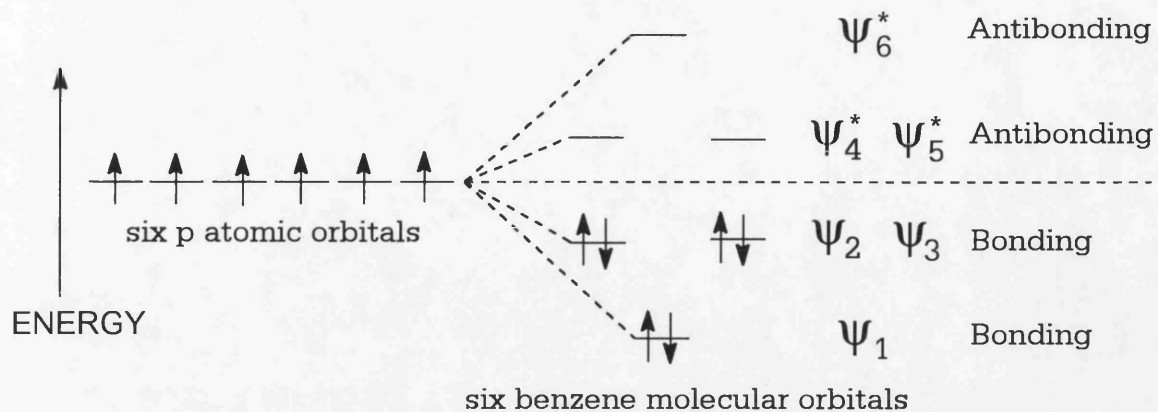


hydrocarbons, such as anthracene, pyrene and perylene (Fig:58) show aromatic character in different degrees. There are many definitions for "aromatic compounds", but the simplest would derive from a combination of the predictions of molecular orbital (MO) theory and the observable phenomenon of diamagnetic anisotropy; aromatic systems are planar, cyclic and exhibit a diamagnetic ring current, where each atom of the ring or rings must have a p-orbital perpendicular to the plane of the ring which is involved in a single conjugated system (Fig:7).

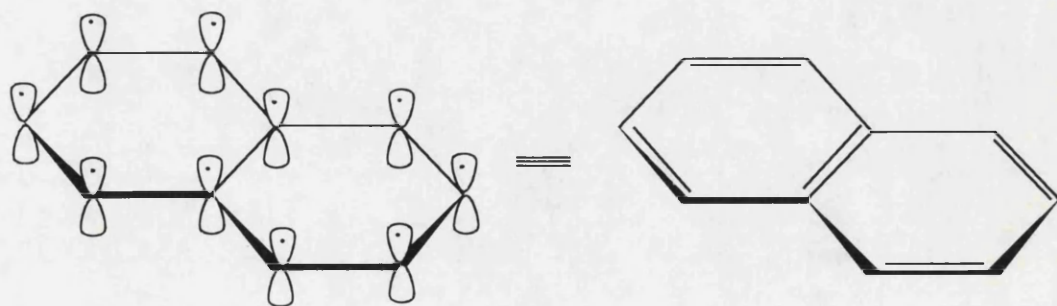
Polycyclic systems present a number of problems which are not found for monocyclic systems. In monocyclic aromatic compounds the conjugation of π -electrons occurs over the entire system, but for polycyclic species the conjugation may behave as if composed of individual discrete cycles, rather than a concerted unit. Counting the number of π -electrons and applying Hückel rules (51) does not in general supply any meaningful predictions of the properties of polycyclic systems. The classification of polycyclic systems presents another problem. Various classification schemes are possible, all of which have their own advantages and drawbacks (52).

The fusion of benzene rings to form polycyclic systems has been considered in detail by Clar (53). He has developed the theory of the effect of annelation (54) on the physical and chemical properties of a system, which state that these properties depend on the number of aromatic sextets that can be formed. The changes in the electronic spectra of these systems were correlated by Clar, and he established that the electronic absorption bands arose from the same transitions as those in benzene. The electronic spectra

Figure 7: Aromaticity



An orbital picture of benzene; the six pi electrons are delocalized over the entire ring



An orbital picture of naphthalene; the ten pi electrons are delocalized throughout both rings.

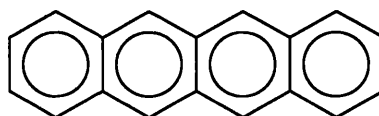
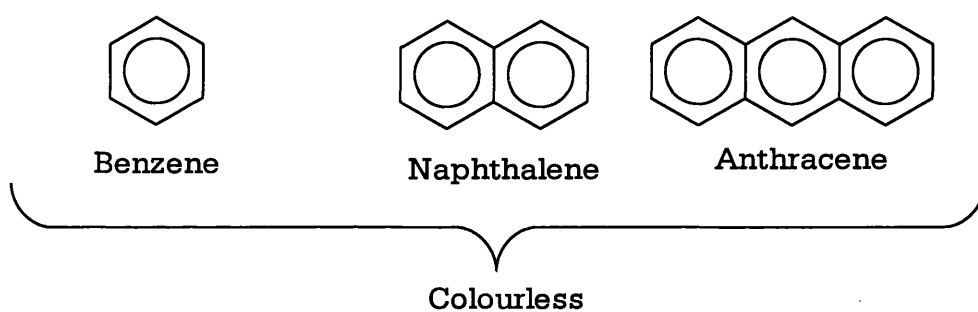
of benzene, naphthalene, anthracene and tetracene have three main absorption bands, and annelation in this series produces a progressive shift to longer wavelength in those bands; benzene is colourless, while tetracene is yellow in colour. The large polycyclic aromatic hydrocarbons are all coloured, ranging from yellow through red to blue with increasing annelation (Fig:8).

E. Charge Transfer Complexes.

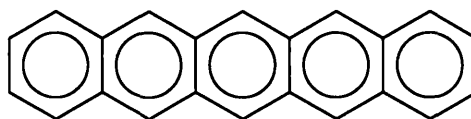
All molecules interact with other molecules, but for the most part the intermolecular forces involved are small compared with the interatomic forces within molecules. There is a gradation from the extremes of classical ionic or covalent bonding to the weakest van der Waals interactions, dipole-dipole, dipole-induced dipole or dispersion forces. The term "charge-transfer" complex has been used to describe weak interactions between electron donors and electron acceptors, where the intermolecular charge transfer transition results in an electronic absorption additional to the absorption bands of the components. It is important to realise that the terminology cannot be taken to imply that transfer of charge is the major mode of binding in these complexes, although Mulliken's (55) now widely accepted description of charge transfer complexes represents the evolutionary results of earlier conflicting studies (56).

Mulliken divided electron donor species and electron acceptor species into increvalent and sacrificial types. The Mulliken description avoids the restriction of the Lewis acid-base (57) concept of donation of pairs of electrons. Increvalent donors are lone-pair donors such as alcohols and

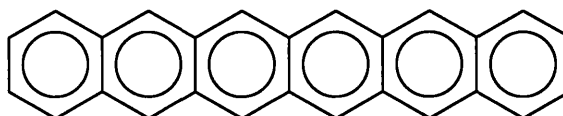
Figure 8: Polycyclic aromatic hydrocarbons and the effect of increasing annelation.



Tetracene (yellow/orange)



Pentacene (blue/violet)



Hexacene (green/black)

phosphines. Sacrificial donors are compounds which donate a single electron from a sigma (σ) or pi (π) orbital. The σ -donors (such as small cyclic hydrocarbons) are weak electron donors, while the π -donors (such as polycyclic aromatic hydrocarbons) are often strong donors. Some donors (for example, aromatic amines) may act as increvalent lone-pair donors or sacrificial π -donors, depending on the acceptor moiety (58).

Increvalent acceptors have a vacant orbital, and may form strong covalent bonds with electron acceptors; weak acceptors such as Ag^+ can produce charge transfer complexation however. Sacrificial acceptors may be of the σ or π type. The former include strongly accepting halogens and pseudo-halogens (such as Br_2 and ICl). The π -acceptors include aromatic systems containing electron withdrawing substituents, such as picric acid (2,4,6-trinitrophenol) and chloranil (tetrachloro-p-benzoquinone) which are well known complexing agents (59).

The division of electron donor and acceptor species is relative, as a species may behave in both senses, for example the self complexes of benzene. Large polycyclic aromatic hydrocarbons such as anthanthracene, perylene and pyrene may act as good acceptors from evidence obtained with the powerful donor tetrakis (dimethylamino) ethylene (I) (60).

F. High Oxidation State Binary Fluorides.

Binary fluorides of second and third row transition metals span oxidation states VII to I, but the most important and extensively studied fluorides are those in oxidation states VI and V. The hexafluorides form a

well defined group of compounds, which display a systematic variation in physical and chemical properties. The hexafluorides of second row elements are more reactive and less stable in the thermodynamic sense than the corresponding third row element compounds, the differences becoming more obvious to the right of the Periodic Table. It follows that molybdenum and tungsten hexafluorides (which were used in this work) are readily prepared, while platinum hexafluoride is thermally unstable, decomposing to difluorine and platinum tetrafluoride (61).

It is now known that there is a marked difference between the reactivities of molybdenum and tungsten hexafluorides, contradictory to earlier work and in fact the only reaction in which the chemical reactivities of the pair are similar is in their reaction with moisture. Some years ago O'Donnell and Stewart (62) examined the relative reactivities of molybdenum and tungsten hexafluorides in detail towards a range of reagents and concluded that either reduction to lower fluorides, or halogen exchange, occurs more rapidly with molybdenum hexafluoride than with tungsten hexafluoride.

The hexafluorides are all volatile compounds, monomeric in the vapour phase, having an octahedral arrangement in which six fluorine atoms surround the central metal atom. They possess extremely short liquid ranges and undergo a solid-phase transition from low temperature orthorhombic form to a high temperature cubic form. The volume change associated with the transition is large enough to warrant care when allowing solid hexafluorides to warm up from low temperatures in glass vessels. An interesting feature of the compounds is the increased volatility of the third row hexafluoride in

comparison to the corresponding second row species. The average metal-fluorine bond distances are 1.820Å for MoF₆ and 1.832Å for WF₆ (63).

The oxidising properties of the hexafluorides were exploited in this work, so the value of the electron affinity (EA) of each hexafluoride was of importance. The electron affinity of a molecule, or atom, is defined as the difference in energy between the neutral molecule or atom in its ground state (E^o) and the ion in its ground state (E⁻) (64). The measurement of an electron affinity is difficult due to the complexity of molecular negative ions, and although there is some disagreement among the exact values of electron affinities, it is accepted that the EA value for MoF₆ is greater than that for WF₆ (65). The low electron affinity of the latter is demonstrated in its inability to intercalate oxidatively with graphite, unlike MoF₆ (66).

G. Charge-transfer complexes and electrical conductivity.

The majority of solid charge-transfer complexes, formed from non-radical electron donor and acceptor species, are poor electrical conductors and are diamagnetic. There are however solid complexes formed from strong electron donors and acceptors where there is ionic character in the ground state, paramagnetism and high electrical conductivity. Studies have been made on the change in conductivity of an electron donor or acceptor when a thin layer of a second component was deposited on the surface; in the anthracene-iodine and phthalocyanine-*o*-chloranil systems large increases in conductivity have been observed (67).

The degree of band filling determines the electronic properties.

Conduction cannot take place in an empty band (because it lacks electrons) or in a full band (because the total population of electrons cannot have any net motion). A metal has a partially filled band while an insulator has only filled and empty bands separated by a large energy gap. A semiconductor is similar to an insulator with one important difference in that it has a smaller gap and mobile charge carriers. These charge carriers are introduced by impurities, defects, deviations from stoichiometry or the excitation of electrons from the highest filled valence band to the lowest empty conduction band.

It was not until 1973 (68) that single crystals of the salt TTF-TCNQ were shown to exhibit metal-like electrical conductivity; the magnitude and the temperature dependence of the conductivity indicated that the first "organic metal" had been discovered. The area of organic metals has drawn the attention of many researchers in subsequent years. The basis for the electrical properties of TTF-TCNQ (and other TCNQ salts) lies in the structure of the crystalline material; both TTF and TCNQ are planar molecules and so can approach closely in the direction perpendicular to their molecular plane.

There are many factors to be considered in designing organic metals.

These include:

- (a) Stable free radical species to form a partially filled conduction band.
- (b) Radical species must form segregated stacks (regardless of charge-transfer a mixed stack will always have a completely filled band).
- (c) Molecules must be planar with π -molecular orbitals to allow electronic states to mix as so to form bands, each band consisting of electronic states whose energies form a continuous range (called the bandwidth). If the

highest filled band is partially filled, empty states will exist infinitesimally close to the Fermi level (the highest occupied state) and those electrons nearby can participate in electronic conduction.

(d) Reduction in the energy gap between the HOMO and LUMO, with increased bandwidths to allow overlap of the two bands.

(e) No periodic distortion that opens up a gap at the Fermi level, with little or no structural disorder.

In short, we can state that molecules must be located in a close spatial proximity and in similar crystallographic and electronic/Coulombic environments so that a uniform extended pathway (devoid of charge carrier traps such as hills and valleys) exists for electronic charge diffusion, with the further requirement that in the molecular stack the highest energy band must be incompletely filled.

In all the molecular metals to date the molecular subunits are in formal fractional oxidation states (partial oxidation, incomplete charge transfer or mixed valence systems). It was of interest therefore to study in some detail the oxidation/partial oxidation of the polymeric fluoro-bridged phthalocyanine $[\text{Al}(\text{Pc})\text{F}]_n$ with MoF_6 (Results:E).

Chapter 2

Experimental

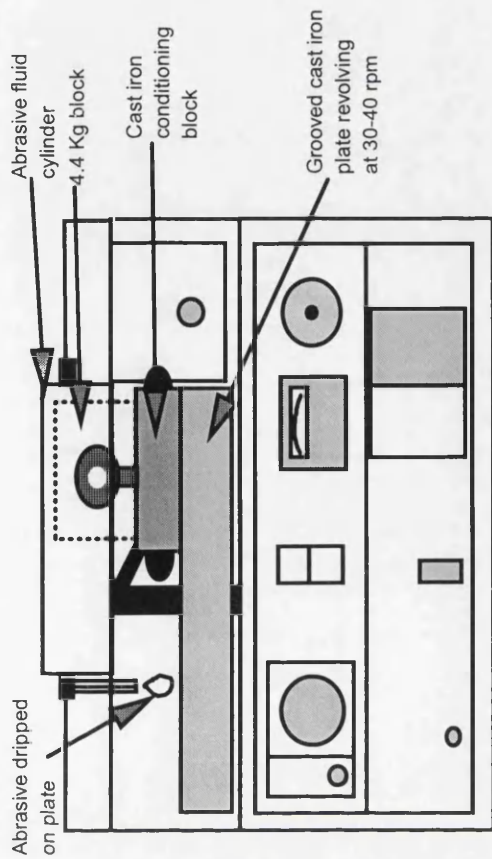
Experimental

A. Preparation of substrates.

1. The lapping process (Fig:9)

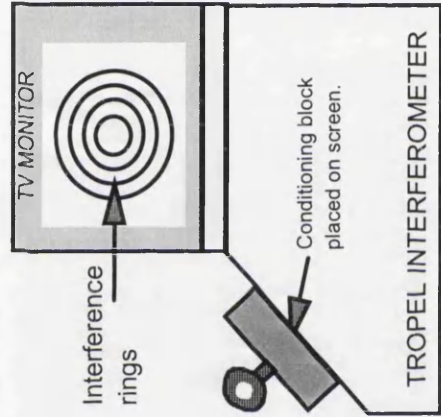
A grooved cast iron plate was conditioned on a PM2A precision lapping/polishing machine, using an aqueous suspension of 12 micron alumina as the abrasive fluid at 30-40 rpm (Fig:10) and a cast iron conditioning block (with an additional loading of 4.4 kg). At regular intervals (ca. 15 min) the surface flatness of the conditioning block was checked by a Tropel interferometer (see Experimental.G.2) and when the block was found to be 2 micron convex in shape, the plate was examined by a single dial gauge (zeroed previously on a flat test block) to ensure the plate was 2 micron concave. The plate was removed and thoroughly washed and cleaned under running water, then refitted to the PM2A.

Silica wafers (ca. 2x1x0.5cm; Spectrosil B, Multilab Ltd) were wax bonded to a glass puck (flatness ≤ 2 micron), of diameter 83mm and thickness 12mm, with quartz wax (m.p. 70°C) and the sample attached to a bonding jig in order to expel air bubbles in the wax bond. The wax was allowed to cool, then any excess wax was removed using a razor blade before the puck was attached to a PP5 polishing jig (Fig:11) by means of a vacuum chuck. The jig ensured that samples were held parallel to the plate. The silica wafers were lapped on the conditioned cast iron plate at 30-40 rpm using 3 micron alumina under full jig loading (≈ 2.3 kg). The duration of the lapping stage was dependent upon the original condition and height of the sample. The surface flatness was checked by a Tropel interferometer periodically until a 2 micron

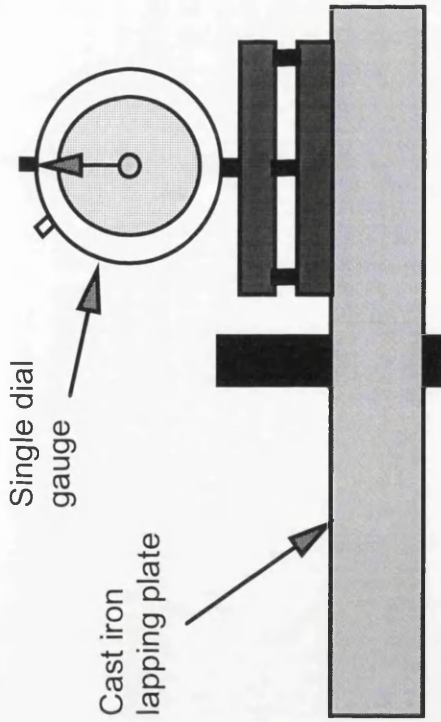


PM2A precision lapping/polishing machine

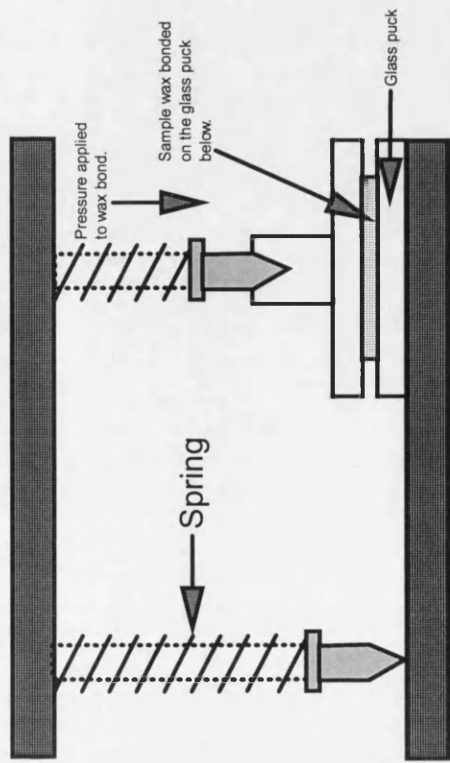
a. Conditioning of cast iron lapping plate



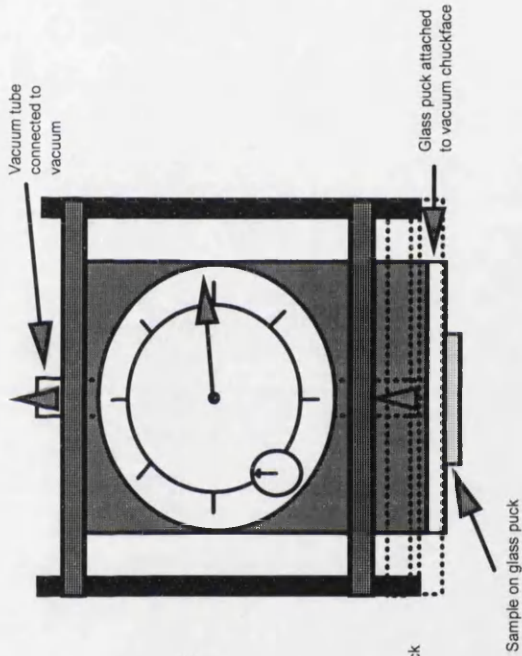
b. Measuring the flatness of conditioning block



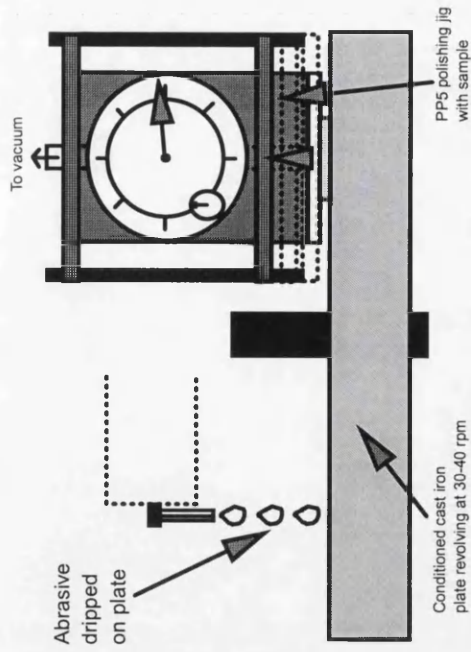
c. Measuring the flatness of lapping plate



d. Samples wax bonded to glass puck



e. Attaching sample puck to PP5 polishing jig



f. Lapping of samples on PM2A

Figure 9: The lapping process

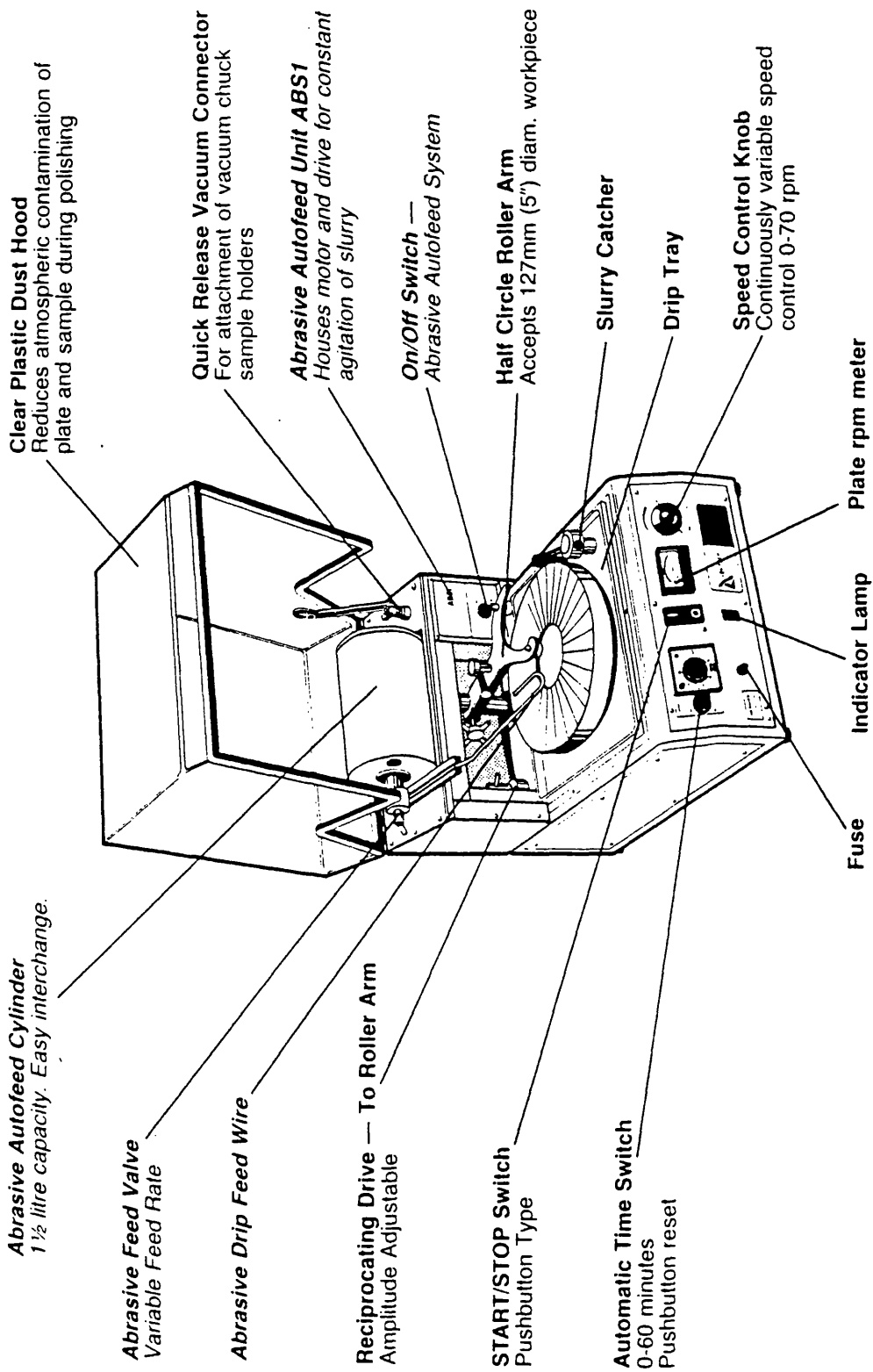


Figure 10:PM2A precision lapping and polishing unit

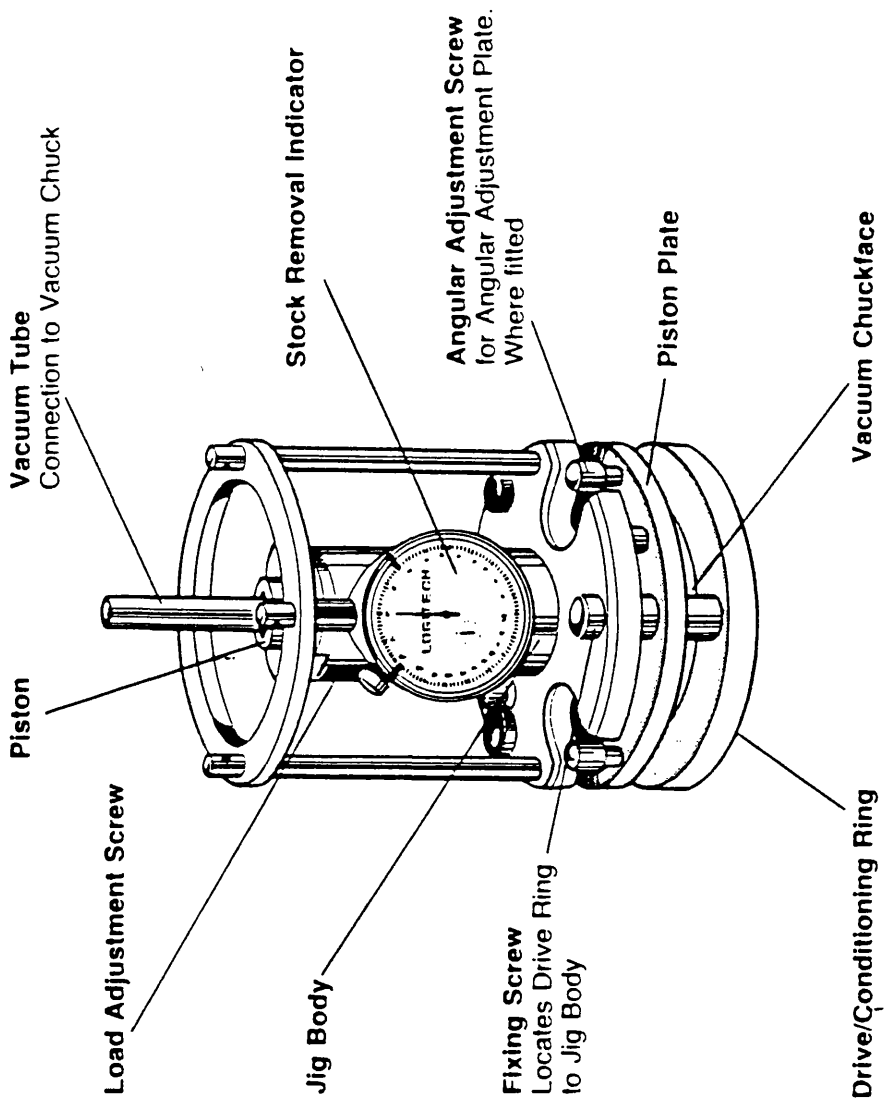


Figure 11:PP5 polishing jig

convex surface was achieved. The sample was removed, then washed and cleaned under running water.

2. The polishing process (Fig:12).

An expanded polyurethane plate (grade LP87) was conditioned using a weighted conditioning block with bronze studs, embedded with 40 micron diamond particles. The conditioning process was essential to remove debris from the surface, as well as determining the overall shape of the plate. A hacksaw blade, held with the serrated edge pressed flat against the plate surface, was used also to score the plate if it had become very smooth, generally after 30 min of polishing. The plate was conditioned to 2 micron convex, checked using a single dial gauge on the plate surface. The lapped sample was reattached to the PP5 jig (in exactly the same position as before for the lapping stage) by means of a vacuum chuck and polished on a PM2A precision polishing unit, using a selective reagent (delivered by means of a drip feed) for a specific period of time.

Where chemically aggressive reagents were used a CP2000 chemical polishing unit was employed (Fig:13). The CP2000 is constructed of materials resistant to corrosion such as PTFE. The polishing process was similar to that for the PM2A, except for the omission of the jig assembly and hence the glass puck was held in a plastic holder (with additional loading of 440g) face down on the polishing pad.

When the surface finish was acceptable by visual inspection, the glass puck was removed and washed and cleaned thoroughly under running water,

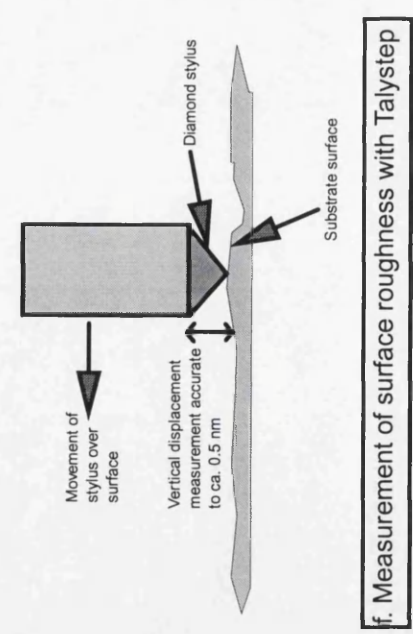
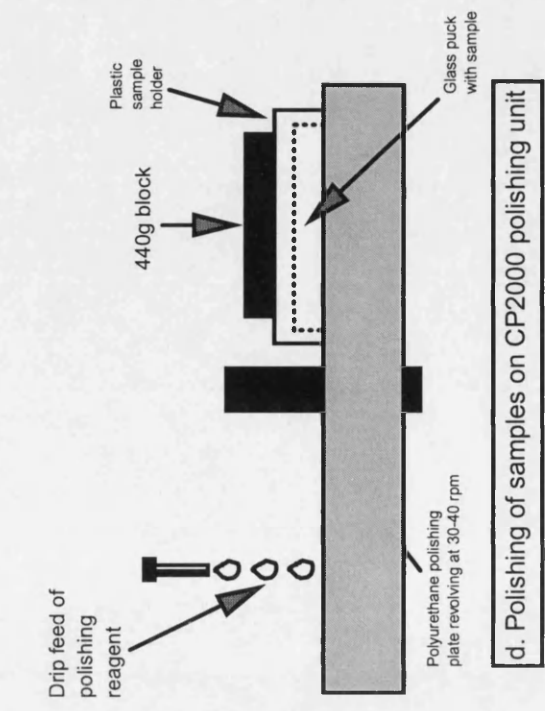
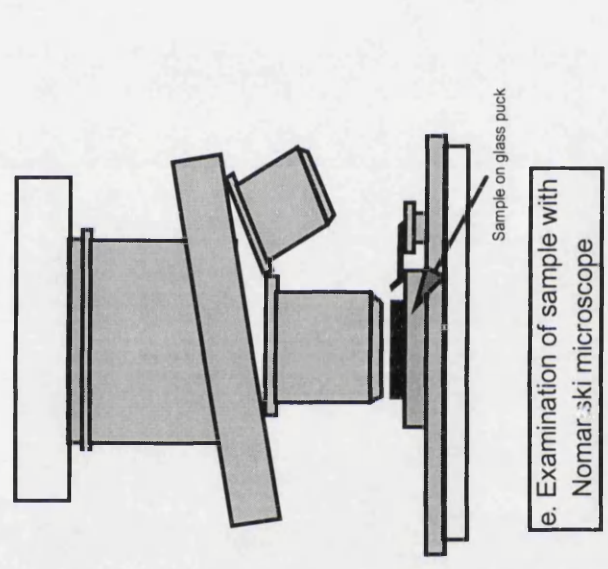
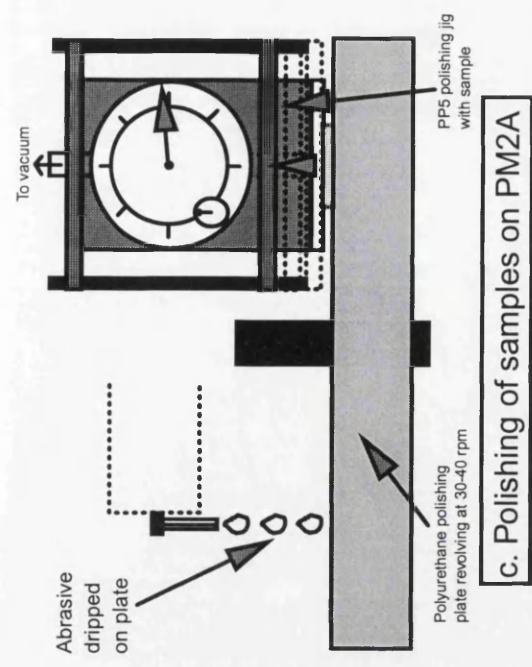
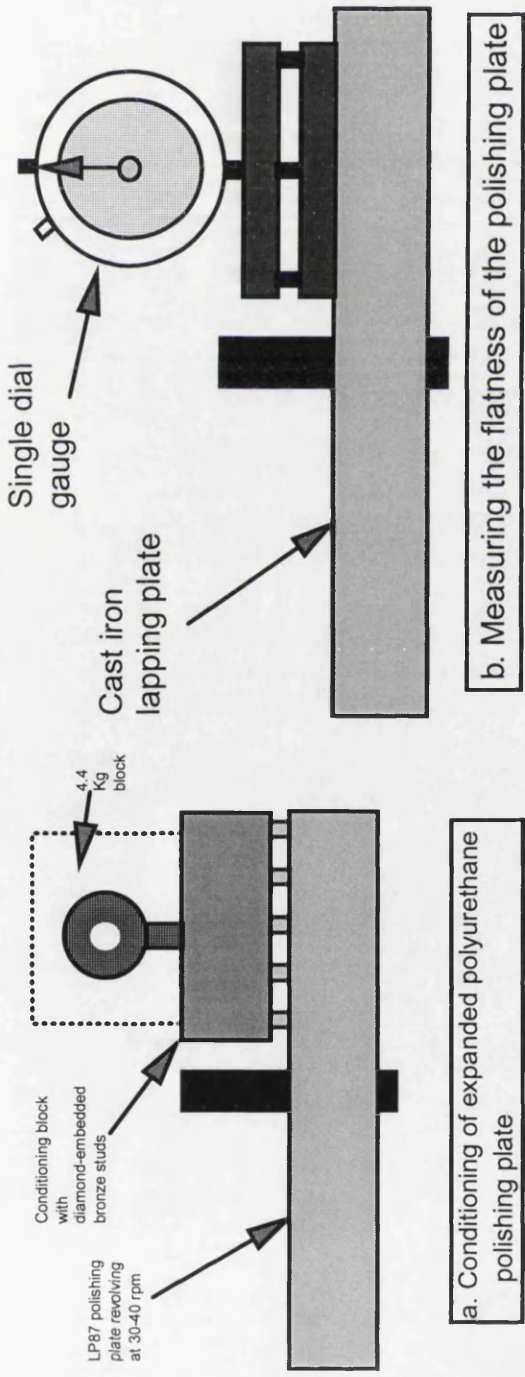


Figure 12: The polishing process

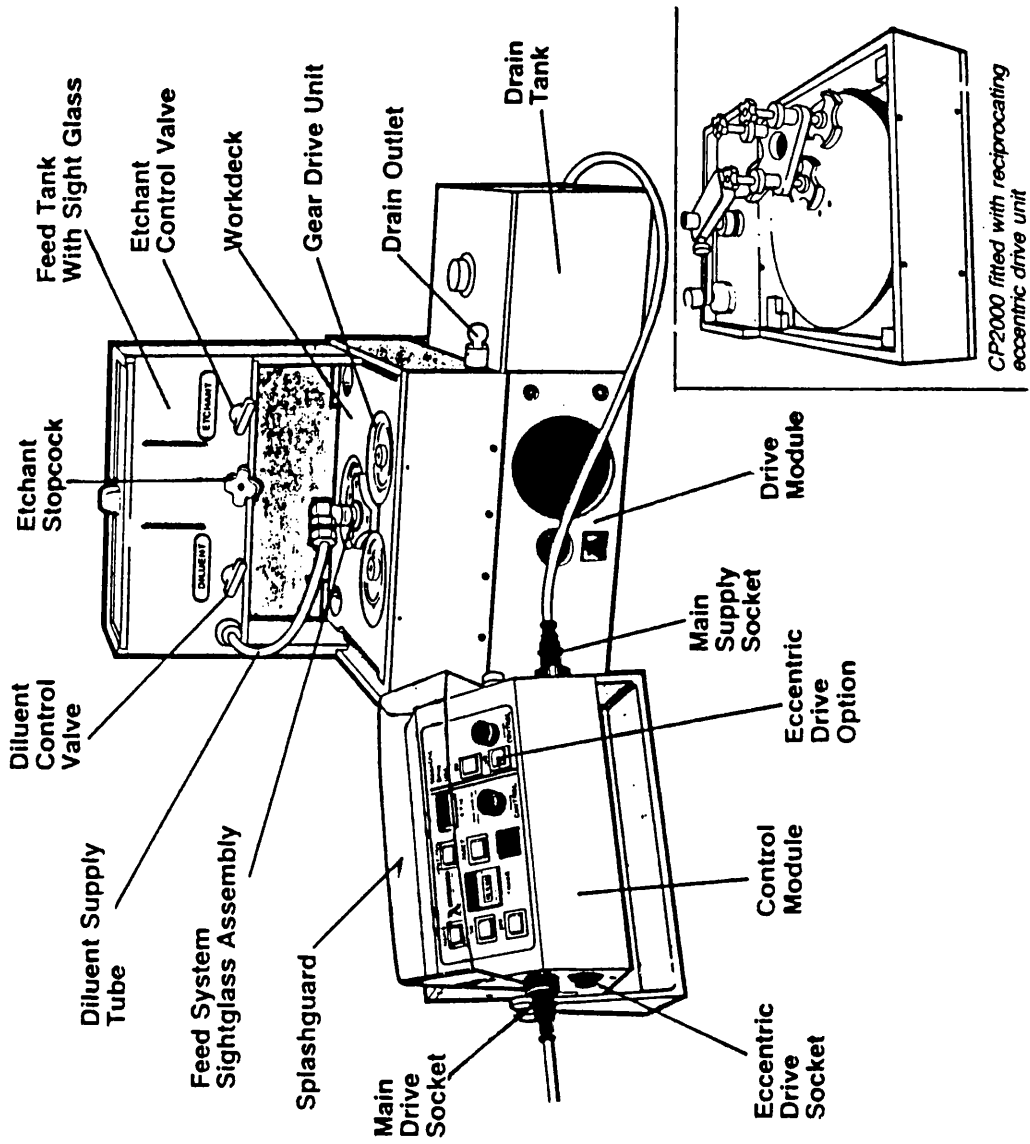


Figure 13:CP2000 chemical polishing unit

then examined using a Nomarski light microscope. If the surface was devoid of lapping damage, the surface roughness was determined using a Rank Taylor Hobson Talystep profiler, which was capable of detecting vertical displacements of less than 1nm over horizontal displacements of 500 micron. Where lapping damage was evident still under the Nomarski, the polishing process was repeated until all surface damage was removed.

3. The polishing reagents.

The polishing reagents used were an alkaline silica sol (Syton; Monsanto Ltd, London), fluoride-modified silica sol, cerium(IV) oxide (Opaline, particle size 0.5 micron; Rhône Poulenc) and a reagent specified by Pilkington (69) for finishing glass surfaces. The composition of fluoride-modified Syton (28) was 1.00g potassium hydrogen difluoride (GPR, 95% acidimetric assay; BDH) to 125 cm³ Syton. Due to the corrosive nature of the fluoride-based reagents, all polishing reagents were prepared using plastic apparatus.

The Pilkington reagent was prepared as follows. Sucrose (450g, GPR; BDH) was added slowly, with stirring, to a solution of dilute hydrochloric acid (120 cm³ HCl; 36% w/w; M & B Ltd in 400 cm³ of distilled water). Potassium hydrogen difluoride (270g, GPR; 95% acidimetric assay; BDH) was added to the solution, stirring until dissolution was complete. Cerium(IV) oxide (50g, particle size 0.5 micron; Opaline; Rhône Poulenc) was added to produce a thick suspension. The neutraliser solution, as specified in the patent, was an aqueous solution of sodium carbonate (100g dm⁻³, GPR; M & B Ltd) with cerium(IV) oxide (10g dm⁻³; Opaline; Rhône Poulenc). The neutraliser

solution was applied immediately at the end of a polishing run to the sample and the polishing plate until all effervescence (due to the evolution of CO₂) had ceased, whereupon the sample and polishing plate were washed with distilled water.

B. Etching experiments.

The identification of the active species in the Pilkington reagent (69) was determined by a series of etching reactions. The behaviour of each component towards silica and silicon was examined. Solutions of each component were prepared using concentrations appropriate to those used in the polishing reagent. A polished silica wafer (2x1cm; Spectrosil B, Multilab Ltd) or silicon wafer (2x1cm; p-type [100]; MCP Wafer Technology Ltd), cleaned previously, dried and weighed, was added to each solution (*ca.* 100 cm³) contained in a plastic beaker. The solution was agitated by magnetic stirring, over various periods of time at room temperature. The wafers were removed using plastic forceps, rinsed under running water and distilled water, oven dried and allowed to cool in a desiccator. The wafers were reweighed (precision $\pm 0.0001\text{g}$; the handling and weighing procedures were standardised as far as possible to ensure reproducibility) and any changes in mass recorded. These experiments, although simple in design, proved significant in this work.

C. Preparation of thin films.

Chemomechanically polished silica wafers (2x1cm; surface roughness $\leq 1\text{nm}$ over 250 micron) were degreased and cleaned carefully by ultrasonic

agitation for 5 min in concentrated nitric acid (GPR, 68% w/w Rhône Poulenc), Genklene (ICI) and isopropyl alcohol (GPR, M & B) to ensure clean surfaces on the wafers before use.

The thermal evaporation technique *in vacuo* was employed as the method of thin film preparation, using an Edwards high vacuum coating unit (Fig:14). A measured quantity of material to be evaporated (*ca.* 10mg) was placed in a molybdenum or stainless steel boat at a measured height. The system was evacuated and pumped until a pressure of 10^{-5} - 10^{-6} Torr was achieved, as determined by a Pirani gauge. The furnace was heated to a temperature of 493 K to obtain clean and dry wafer surfaces and the temperature maintained for 30 min, to allow the system to reach thermal equilibrium. The furnace was allowed to cool to a temperature appropriate for thin film growth of a given material, generally $\frac{2}{3}$ of the melting point of the material. The boat was heated to evaporate the material and after cooling to ambient temperature, the wafers were removed for examination by electronic spectroscopy. The film thicknesses were calculated to an order of magnitude using the following equation (47)

$$\text{Thickness (nm)} = \frac{3M \times 10^7}{16\pi r^2 d}$$

where r = boat to substrate distance (cm), M = mass of material (g) and d = density of material (g cm^{-3}).

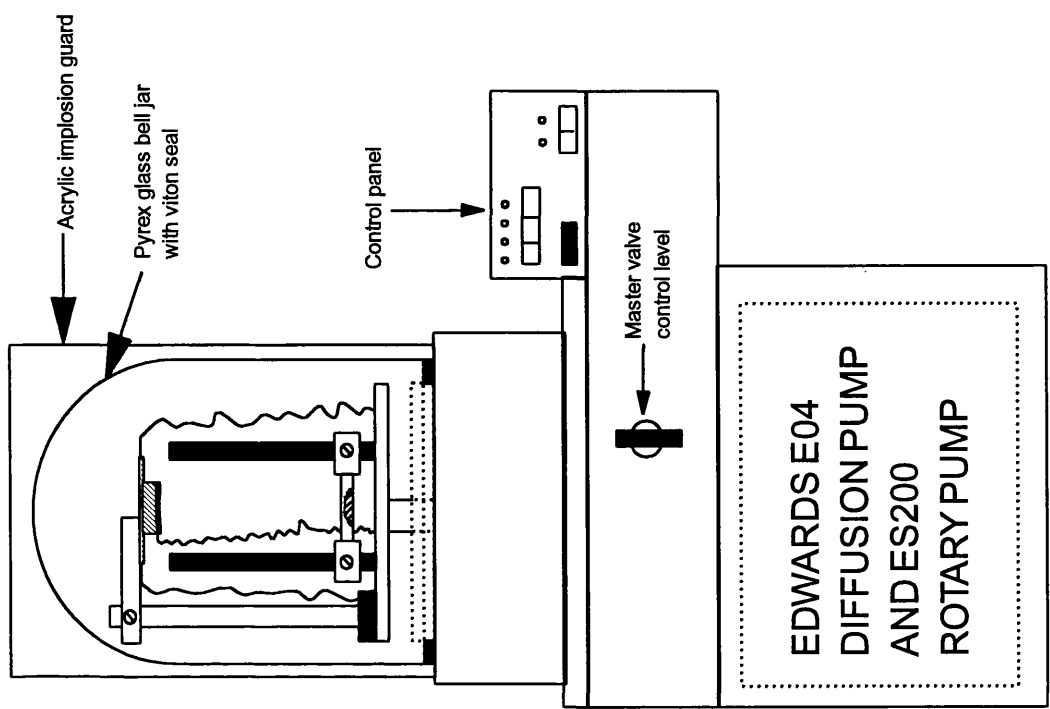
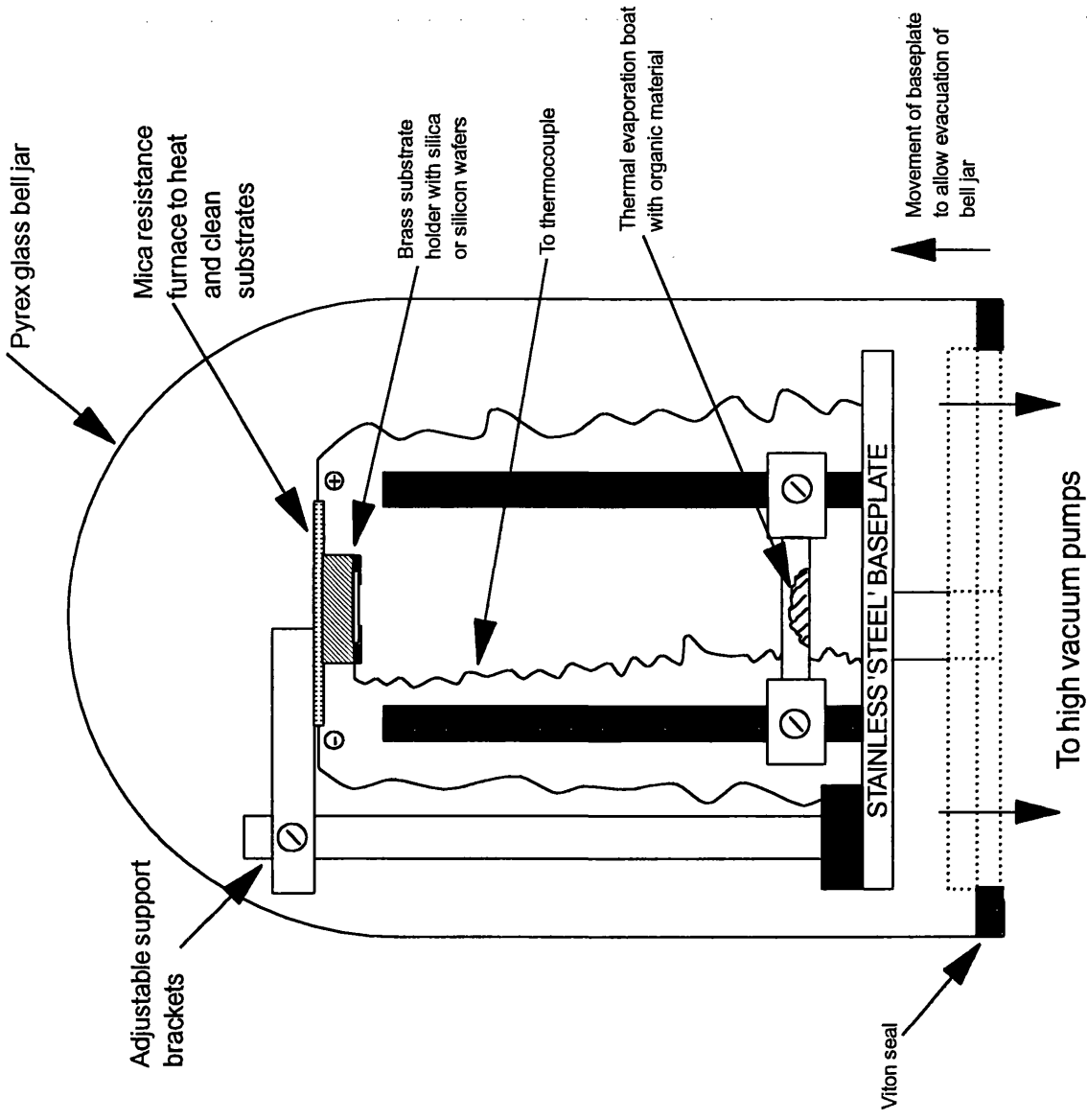


Figure 14: Edwards high vacuum coating unit

D. Preparation of chemically modified films.

1. General high vacuum techniques.

In this part of the work, it was important to ensure that moisture and air were excluded from the reactions examined due to the hygroscopic nature of many of the materials. All the reactions were studied therefore *in vacuo* (10^{-4} Torr) using a Pyrex glass vacuum system.

The vacuum line (Fig:15) was an enclosed Pyrex glass structure which consisted of a manifold, a constant volume manometer and vacustat, all of which were individually isolable. The vacuum was achieved using an oil-sealed rotary pump (Edwards high vacuum) and mercury diffusion pump (Jencons) to achieve a pressure of 10^{-4} Torr as measured by a mercury vacustat (Edwards high vacuum) which allowed manipulation of materials such as MoF_6 with no evidence of hydrolysis occurring over the timescale of an experiment. The pumps were protected from volatile material in the line by a series of three cold traps at 77 K, directly before the pumps. The standard glass joints were greased with Apiezon N or Voltalef Kel-F high vacuum greases. Apiezon black wax was used for sealing the semi-permanent joints. Polytetrafluoroethylene (PTFE) Pyrex stopcocks (Rotoflo or J. Young) were used to isolate various components on the manifold. All the glassware and reaction vessels were flamed out under vacuum using a gas-oxygen torch flame, as this process results in a substantial reduction in the amount of moisture on the glass surface (70).

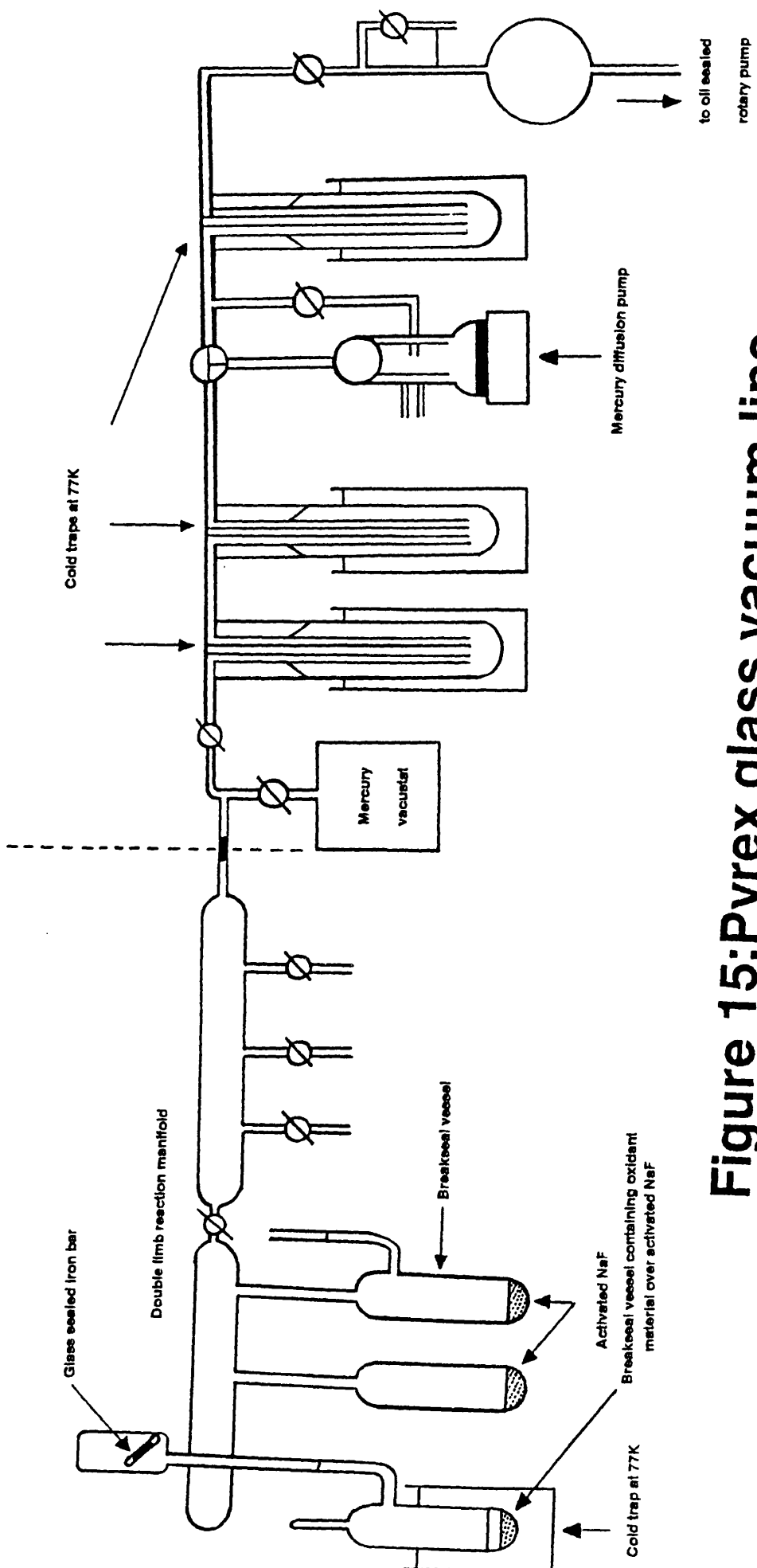


Figure 15: Pyrex glass vacuum line

2. Purification of Molybdenum and Tungsten Hexafluorides.

Like most transition metal hexafluorides, molybdenum hexafluoride (m.p. = 17.4°C , b.p. = 35°C) and tungsten hexafluoride (m.p. = 2°C , b.p. = 17.1°C) are toxic and highly hygroscopic materials and thus must be manipulated in a clean and dry high vacuum system.

Molybdenum hexafluoride (Fluorochem) or tungsten hexafluoride (Fluorochem) were vacuum condensed from the metal cylinder to a cold trap at 77 K containing activated NaF (heated overnight at 200°C *in vacuo*), to reduce any HF impurity, in a Pyrex glass manifold (flamed out and allowed to cool; this sequence was repeated three times). The material was purified by trap to trap distillation at 77 K to remove MoOF_4 the main impurity and any residual HF. The purified material was transferred finally to a break-seal vessel containing activated NaF at 77 K and stored at that temperature until required.

3. Purification of Phosphorus and Arsenic Pentafluorides.

Phosphorus pentafluoride (b.p. = -84.5°C ; Fluorochem) or arsenic pentafluoride (b.p. = -52.8°C ; Matheson) were vacuum condensed from the metal cylinder to a cold trap at 77 K containing activated NaF, in a Pyrex glass manifold (flamed out and allowed to cool; this sequence was repeated three times). The condensed material was pumped out for 5 min, then the material was purified by trap to trap vacuum distillation over activated NaF at 77 K. The material was transferred finally to a break-seal vessel containing activated NaF at 77 K and stored at that temperature until required.

4. Thin film reactions.

Thin films on silica substrates were loaded into an evacuable reaction gas cell fitted with Spectrosil B windows, by means of a PTFE holder (Fig:16). The cell was attached to the reaction manifold on a vacuum line and evacuated. The manifold and cell were pumped out for 24 hr to remove moisture and then flamed out and allowed to cool; this sequence was repeated three times. The breakseal vessel was cracked open, by use of a glass sealed iron bar and the vessel containing the oxidant material (MoF_6 , WF_6 , PF_5 or AsF_5) at 77 K pumped out for 5 min. The manifold was isolated from the vacuum pumps and the oxidant purified by trap to trap distillation over activated NaF at 77 K. The oxidant material was allowed to warm to ambient temperature and the reaction cell filled with oxidant vapour. The cell was closed to the manifold and the vapour phase in the manifold transferred back to the cold trap, then the manifold pumped out for 5 min to remove any volatile material. The cell was then pumped out for 5 min to remove any unreacted oxidant adsorbed on the film or hydrolysis products. The remaining oxidant material was transferred finally to a break-seal vessel, containing activated NaF at 77 K by vacuum distillation.

In all reactions, except those experiments involving the quartz crystal microbalance (see Experimental : E), a mole ratio of film material : oxidant far in excess of that required to react completely with the film was used. The electronic spectrum of the chemically modified film was recorded and compared with that of the unreacted material.

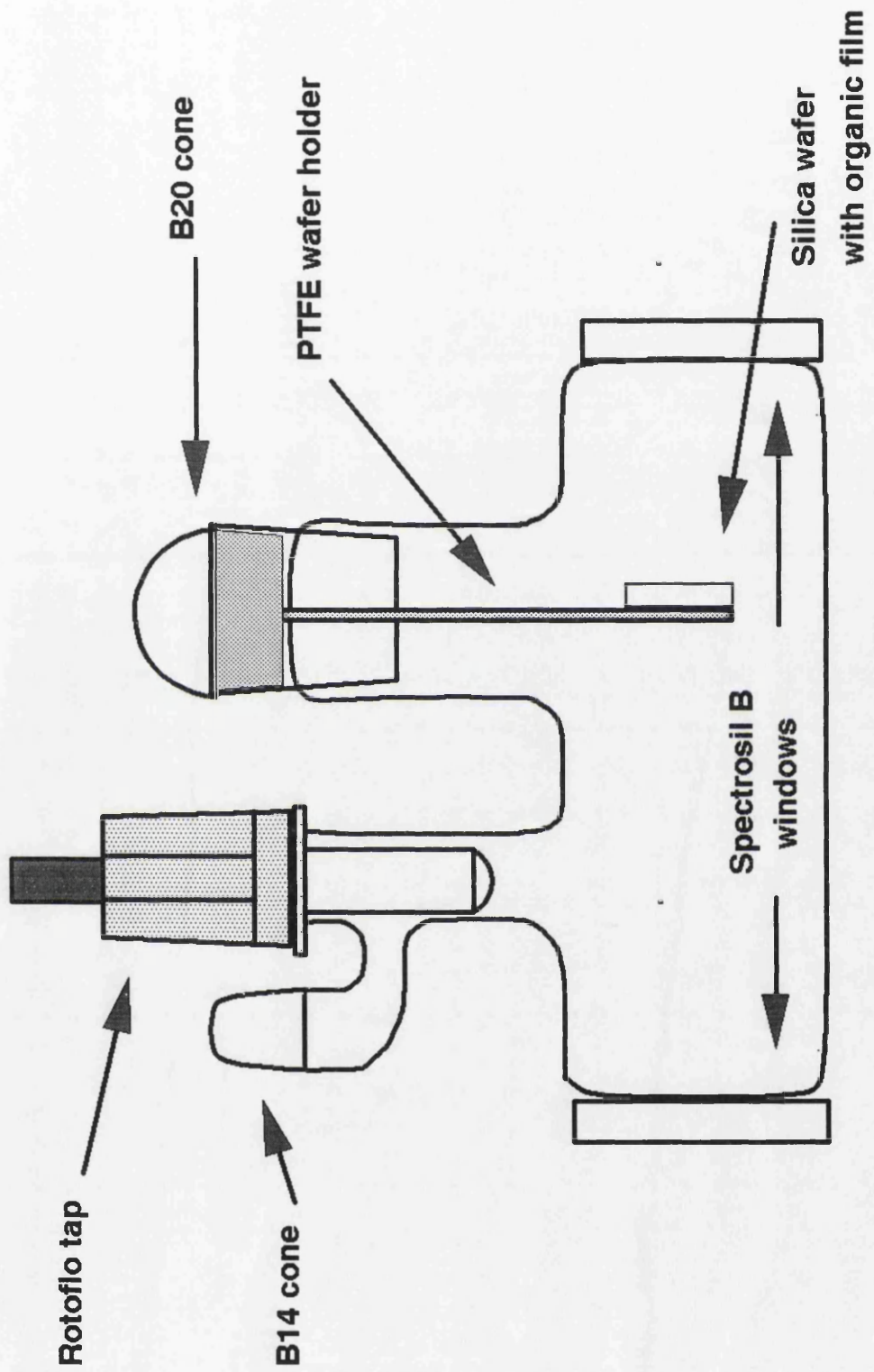


Figure 16: Evacuatable reaction gas cell

E. The Quartz Crystal Microbalance (QCM) technique as employed in thin film reactions.

The quartz crystal microbalance (QCM) is composed of a piezoelectric quartz crystal wafer, with metal film electrodes deposited on both sides of a wafer and an appropriately designed oscillator circuit (42). One electrode on the crystal is exposed to the species to be deposited and serves as the working electrode. Sauerbrey (43) developed quantitative relationships between frequency changes of piezoelectric quartz crystals and deposited species under various conditions. The results may be summarised as

$$\Delta F = -2.3 \times 10^6 F^2 (\Delta Ms/A)$$

where ΔF = the change in frequency due to the coating (Hz), F = the frequency of the quartz crystal (MHz), ΔMs = the mass of material deposited on the quartz crystal (g) and A = area of the quartz crystal that is coated (cm^2). The microbalance is capable of detecting changes in mass of the order of nanograms.

In this part of the work (developed with Dr. A. Glidle) the microbalance apparatus was housed in a specially adapted B20 cone, fitted to an evacuable gas cell with Spectrosil B windows (Fig:17). The working electrode was one of a pair of electrodes on opposite sides of the quartz crystal. The opposing electrodes were necessary to bring the quartz crystal to resonance in the electrical oscillator circuit, allowing simultaneous measurement of frequency, conductivity and accompanying spectroscopic changes on a silica substrate *in vacuo*. The working quartz crystal was of an operating frequency of 10 MHz. A reference crystal oscillating at a slightly

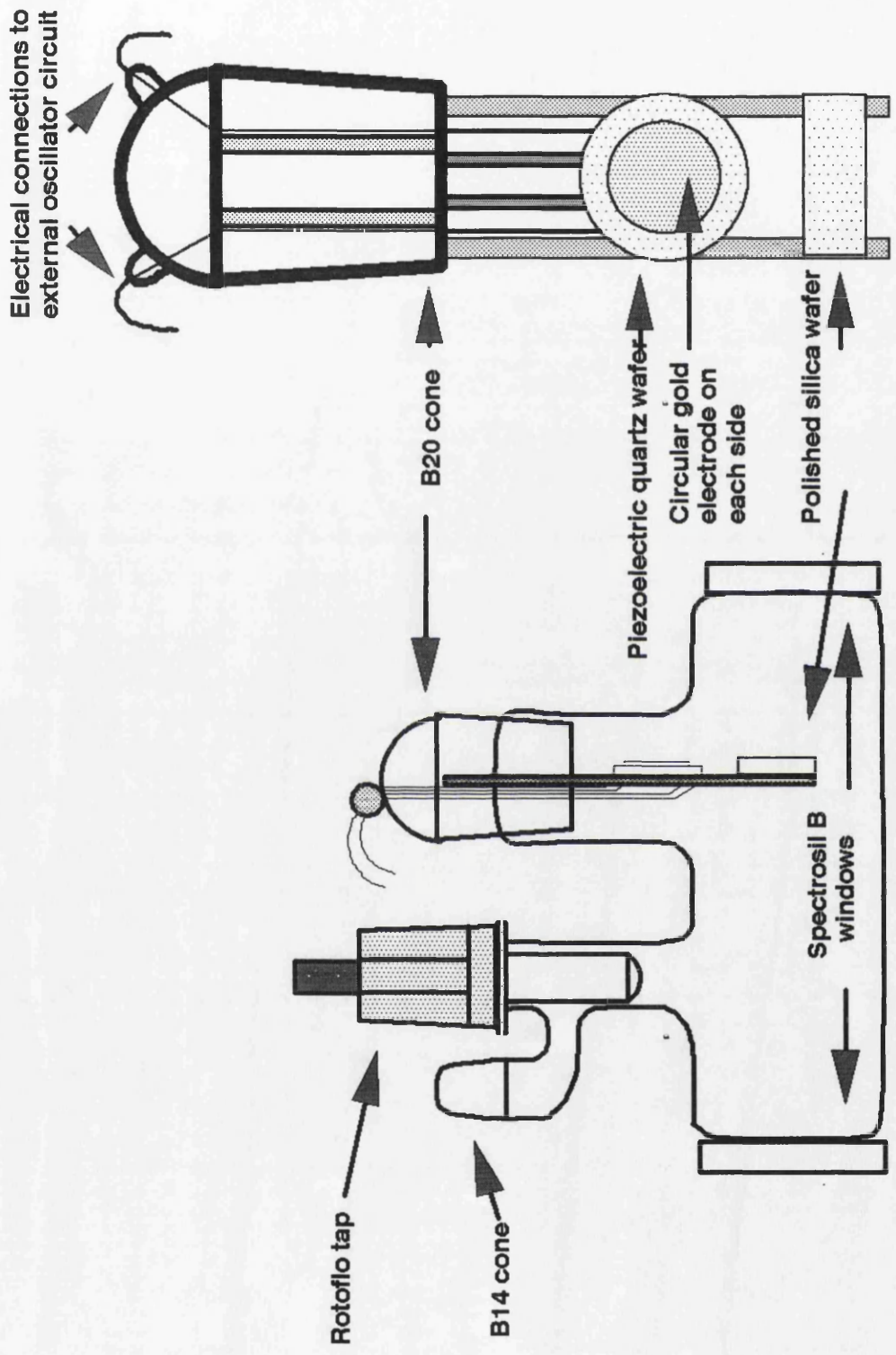


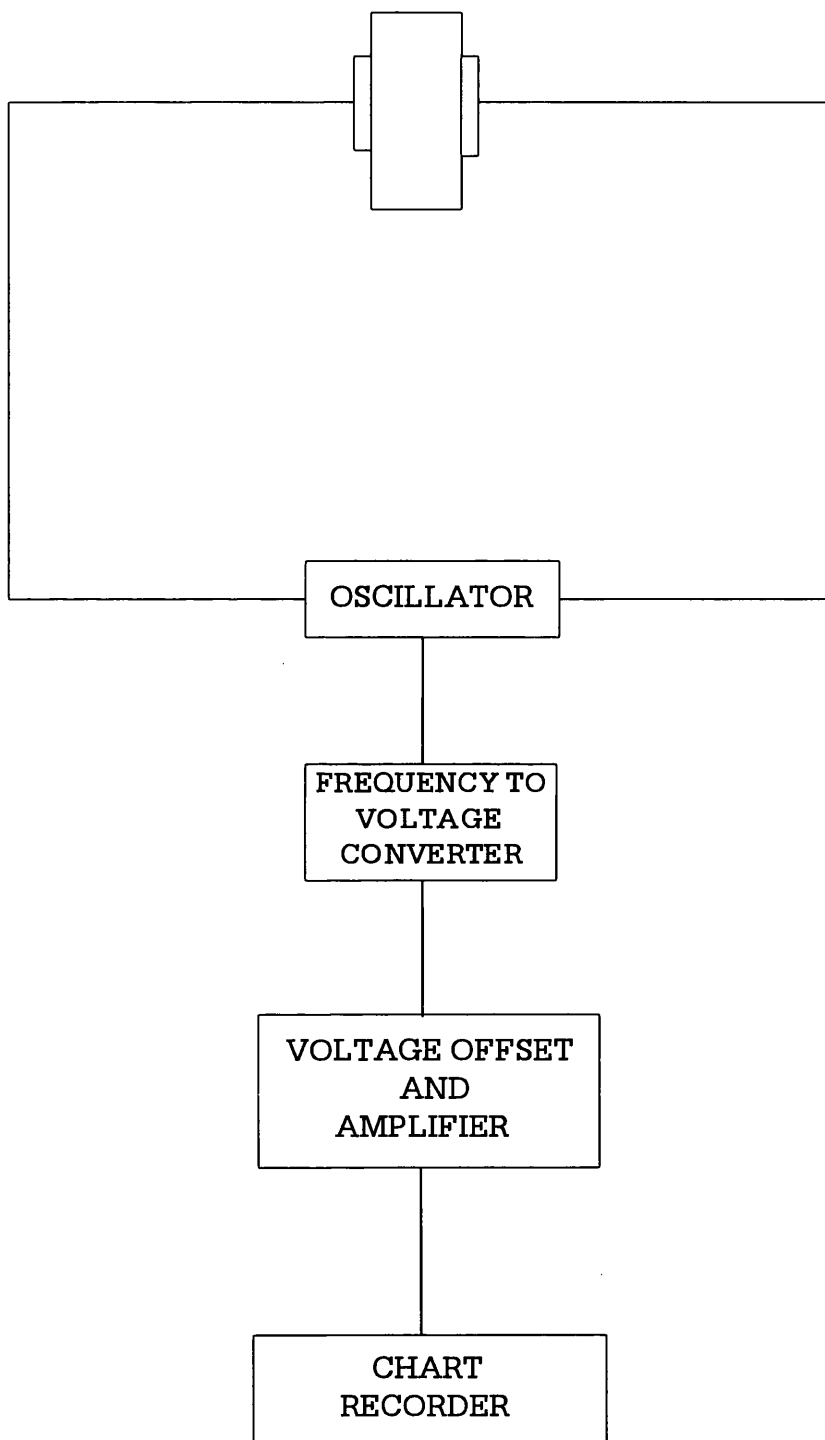
Figure 17: Quartz Crystal Microbalance (QCM) cell

greater frequency was used to "beat" the frequency of the working crystal down to ca. 10 KHz (Fig:18), to enable more accurate measurement of the frequency changes in the crystal.

The experimental procedure was as follows. The specially adapted B20 cone with the microbalance apparatus was fitted to the evacuable gas cell. The cell was attached to the reaction manifold on the vacuum line and evacuated. The cell was pumped out for 30 min then the microbalance apparatus was connected to the external oscillator circuit. A measurement of the base frequency of the quartz crystal was taken. The cell was detached from the reaction manifold and the B20 cone removed. A thin film of material was prepared as described in Experimental : C, with omission of the heating of the substrate prior to and after film deposition. The B20 cone was fitted to the evacuable gas cell and attached to the reaction manifold on the vacuum line and evacuated. The manifold and cell were pumped out for 24 hr to remove moisture.

The manifold and cell were flamed out and allowed to cool; this sequence was repeated three times. The microbalance apparatus was connected to the electrical oscillator circuit and a measurement of the new frequency of the quartz crystal made. The breakseal vessel was cracked open, by use of a glass sealed iron bar and the vessel containing the oxidant at 77 K pumped out for 5 min. The manifold was isolated from the vacuum pumps and the oxidant purified by trap to trap distillation over activated NaF at 77 K. The oxidant material was allowed to warm to ambient temperature. The reaction cell was fitted with a measured quantity of oxidant vapour by

Figure 18: Schematic representation of QCM instrumentation



monitoring the change in frequency of the quartz crystal on a chart recorder. Calibration of the system allowed precise aliquots of oxidant to be dispensed (ca. mole ratio of film material : oxidant of 10 : 1). The cell was closed, the vapour phase in the manifold transferred back to the cold trap and the left hand limb of the reaction manifold isolated. The cell and manifold was pumped out for 5 min to remove any volatile material. The frequency reading on the chart recorder was allowed to stabilize over 15 min and the new value noted. The cell was closed and the electronic spectrum recorded over 190-3200 nm.

The gas cell was attached to the reaction manifold as before and evacuated. The manifold and cell were pumped out, then the right hand limb of the manifold and the cell were flamed out and allowed to cool; this sequence was repeated three times. The oxidant material was allowed to warm to ambient temperature and the reaction cell was filled with a measured quantity of oxidant vapour as before. The entire process was repeated in order to obtain a series of electronic spectra corresponding to specific levels of doping with the oxidant material. A simple modification of the external oscillator circuitry allowed simultaneous mass change and conductivity measurements to be recorded. The oxidant material was pumped out finally into the cold traps before the pumps.

F. Spectroscopic techniques.

1. Vibrational spectroscopy (71).

Vibrational spectroscopy is the title which embraces emission and

absorption of infrared radiation of wavelengths between 10^{-4} - 10^{-1} cm, including the scattering phenomenon known as the Raman effect (72) which is of no concern in this work. Infrared spectroscopy is concerned with absorptions in the region 10^{-2} - 2×10^{-4} cm which arise from the quantization of vibrational energy within molecules. Absorption in this region implies the occurrence of vibrational transitions in a molecule while it remains in its ground electronic state, or more simply, the molecule absorbs energy and its bonds vibrate with greater amplitude. Vibrations which cause no transient change in the dipole moment of a bond cannot produce an infrared absorption.

Experimental techniques and equipment for measuring infrared spectra have developed considerably from the early prism or grating instruments (73). Modern Fourier Transform (FT) spectrometers, which employ the multiplex or Fellgett advantage of interferometry (74), allow high speed multiple scans to be made in a few seconds without any loss in sensitivity or resolution.

Conventional transmission infrared spectroscopy with the radiation normal to the sample under investigation is often unsuitable for many materials. Weakly absorbing, high light scattering and optically opaque materials are not readily amenable to the transmission mode and in these circumstances a variety of other infrared techniques are available (71). As the materials in this work were intractable by transmission spectroscopy, diffuse reflectance (DRIFTS) (75), photoacoustic (FT-IR-PAS) (76), attenuated total reflection (FT-IR-ATR) (77) FT infrared techniques and FT-IR Microspectroscopy (78) were employed.

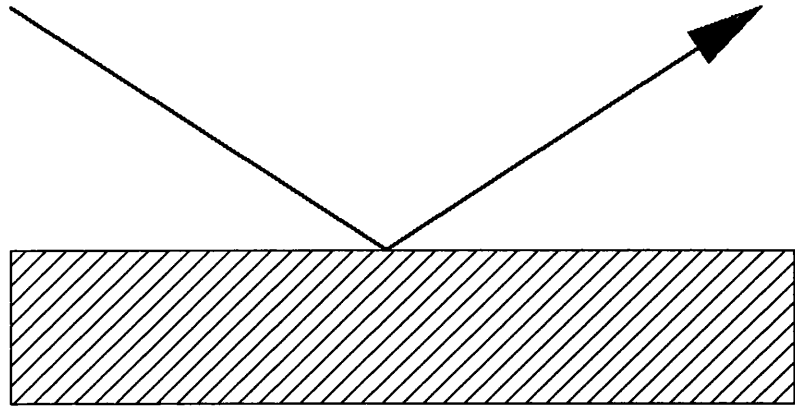
In the DRIFTS process the diffusely reflected light from the sample is

used to produce an absorption spectrum by means of a Kubelka-Monk transform (79). The direction of the reflected light is random with respect to the incoming beam, unlike regular or specular reflectance (Fig:19). The depth of penetration of the radiation is a function of the internal scattering of the material; a simple analogy would be a clear lake where one can see the bottom many metres below the surface, in contrast to a muddy river where the total reflectance spectrum is composed of the surface reflection plus the scattering and absorption of the medium.

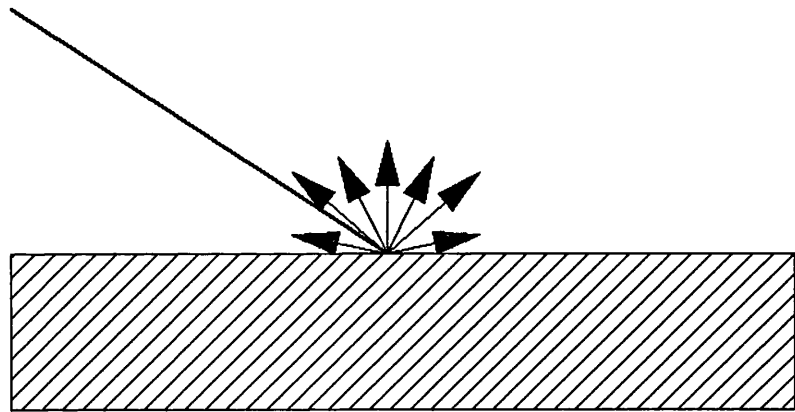
Another technique known as attenuated total reflection (ATR) employs the principle that radiation, transmitted at certain angles through a transparent block, can undergo total internal reflection to emerge diminished slightly in intensity or "attenuated" by sample absorption (Fig:19). The block is made of material which is transparent to infrared radiation and must necessarily have a refractive index greater than the material being examined, otherwise internal reflection will not occur. Germanium and silver chloride are therefore often employed as ATR crystals.

Photoacoustic (FT-IR-PAS) spectroscopy does not depend on the direction of transmitted or scattered radiation; rather the absorption of modulated radiation causes periodic heating of a solid sample, which in turn effects a periodic variation in the ambient gas in a confined volume (Fig:20). As absorption of electromagnetic radiation is required before a photoacoustic signal can be generated, problems associated with light scattering are avoided. A unique aspect of photoacoustic spectroscopy is its relative insensitivity to surface morphology (80). Transmission samples must be uniform in thickness,

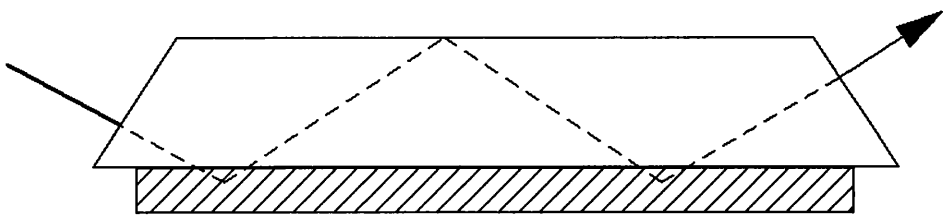
Figure 19:Types of reflectance



SPECULAR REFLECTANCE



DIFFUSE REFLECTANCE



ATTENUATED TOTAL REFLECTION

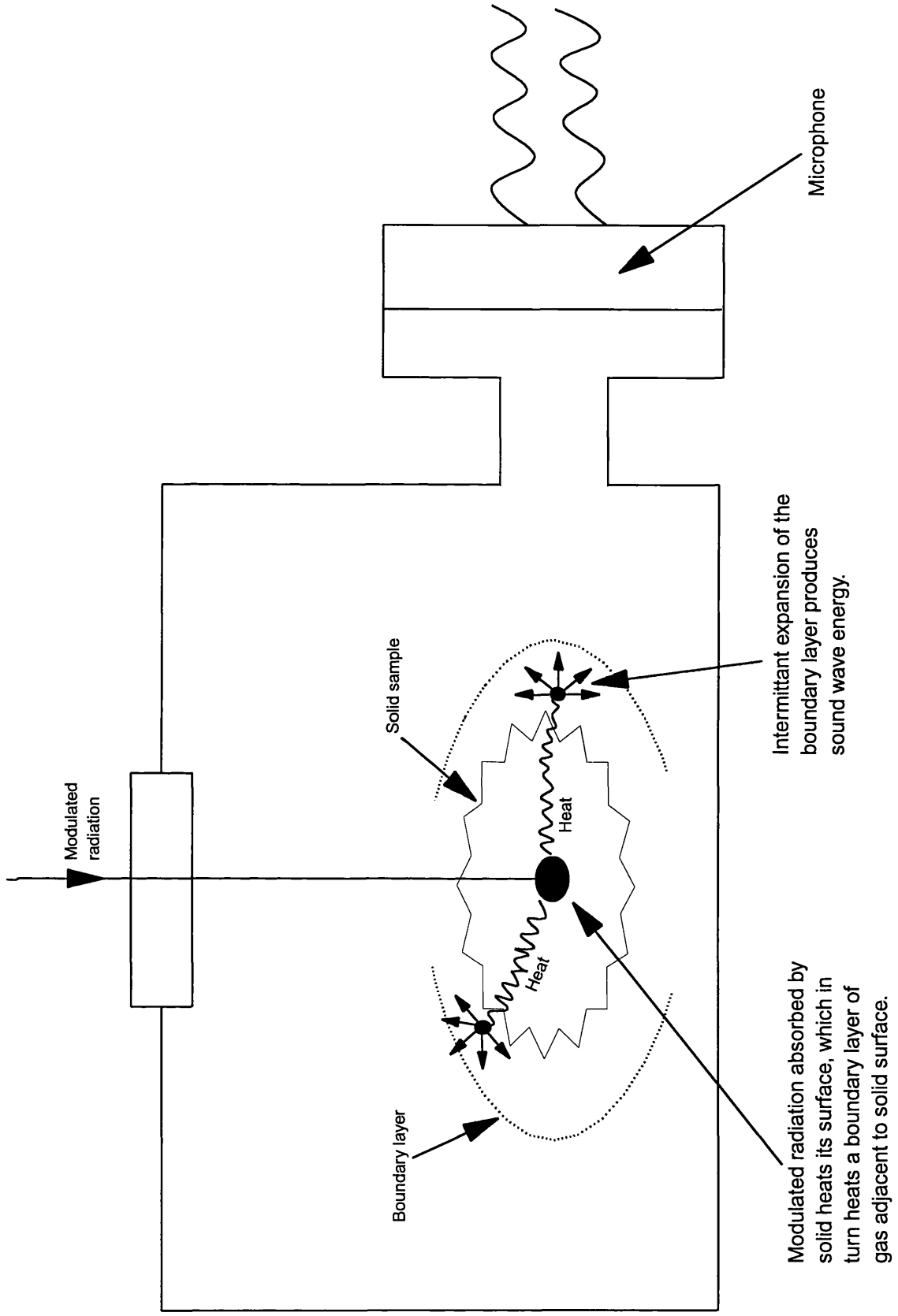


Figure 20: Photoacoustic cell for solid samples

optically thin and free of scattering, diffuse reflectance samples must be highly scattering and attenuated total reflectance requires the material to be flat and easily deformable, or very finely powdered (81).

FT-IR Microspectroscopy incorporates a specially designed optical microscope coupled with a FT-IR spectrometer. This enables viewing of the sample while aperturing to the area of interest for infrared analysis. The FT-IR microscope can be operated in reflectance or transmission mode. The infrared radiation is focussed on the spot to be analysed and either reflects or transmits through the sample allowing collection of the infrared spectrum without losing sight of the relationship of the sample with respect to the surrounding area.

In this work IR spectra were recorded using a Nicolet 5DX C spectrometer, with a SpectraTech collector for diffuse reflectance and a MTEC 100 photoacoustic cell for photoacoustic analysis. Samples for diffuse reflectance were prepared by grinding the material in question (with or without KBr or diamond dust) in an agate pestle and mortar and placing in a stainless steel sample holder. Photoacoustic samples were placed without pretreatment in specially designed sample holders. A Nicolet Nic-Plan microscope with an ATR (ZnSe crystal) accessory was used to obtain microspectroscopic and ATR data. This work was conducted with Dr. Bob Richardson and Donald Hepburn of Glasgow Caledonia University. Samples examined by this method required no prior treatment.

2. Electronic spectroscopy (82).

Photons from the ultraviolet and visible regions of the electromagnetic spectrum have sufficient energy to promote electrons from their ground states to excited states. The difference in energy is quantized between any two of these states and so a photon of only a precise energy may be absorbed. The wavelength of the absorption is thus a measure of the separation of the energy levels of the orbitals concerned.

The highest energy separation is found when electrons in σ -bonds are excited, giving rise to absorption below 200 nm. Known as the vacuum ultraviolet, it is both difficult to measure and relatively uninformative. Above 200 nm however the excitation of electrons from σ or π bonding orbitals and non-bonding orbitals may give rise to absorption spectra which are both informative and readily measured. Whether or not a particular absorption band is observed is dependent on the symmetry of the molecule being irradiated as well as the energy of the incident radiation, which induces further selectivity as to which wavelengths of radiation may be absorbed. Molecular vibrations often distort molecular symmetry so that theoretically forbidden transitions are sometimes exhibited, a common example being the d-d transitions observed in transition metal complexes. Such bands are described often as "forbidden transitions" (83).

In this work polycyclic aromatic hydrocarbons and their derivatives were examined by electronic spectroscopy. Samples were supported on silica substrates as thin films. Spectra were recorded using a Perkin Elmer Lambda 9 UV-vis-NIR spectrometer over the spectral region 190-3200 nm.

3. Magic-Angle-Spinning Nuclear Magnetic Resonance (MAS-NMR) Spectroscopy (84).

It is accepted today that solids are almost as amenable to NMR spectroscopy as solutions. The advent of magic-angle-spinning (85) in the 1950's coupled with cross polarization (CP) (86) and high power proton decoupling (HPPD) techniques in 1976 stimulated an explosion of interest in the NMR of solids. The complexity of solid state NMR arises from the fact that all important NMR interactions, leading to the chemical information, vary with the angles linking the local nuclear environment to the applied magnetic field. In solution, molecules have sufficient degrees of freedom to allow these anisotropic effects to be "averaged out"; in solids this is not the case. The magic-angle-spinning technique allows all anisotropic effects to be removed, by spinning the bulk sample coherently about an axis, at an angle of $54^{\circ}44'$ to the magnetic field, which essentially replicates the tumbling of molecules in liquids or solutions.

It is now well established that high resolution MAS-NMR can probe the nature of short-range order in both non-crystalline and crystalline solids (85,87). For example, information on the distribution of Si-O-Si angles in silicate glasses may be obtained from ^{29}Si -MAS-NMR, where the crystallinity of the materials range from zero to 100% (88). In recording ^{29}Si -MAS-NMR spectra it is important to realise the spin-lattice relaxation times T_1 of the nuclei are very different in the microcrystalline and non-crystalline states; in the former case this is order of seconds while in the latter of the order of hours.

This large difference in relaxation times allows the possibility of distinguishing between regions of crystallinity and non-crystallinity and their relative abundance in a given silicate. Whereas the spectrum of the crystalline part of the material can be obtained relatively easily, a spectrum comprising signals of both the amorphous and crystalline regions can be measured only if short pulses and long pulse delays are used.

The total range of ^{29}Si -NMR chemical shifts in silicates lies between $\delta = -60$ and -120 ppm for Si(IV) split up into five intervals (89), whereas chemical shifts for Si(VI) lie between $\delta = -179$ and -220 ppm (90). The large difference in chemical shifts for tetrahedral and octahedrally coordinated ^{29}Si nuclei was exploited in this work.

Spectra were recorded, using a Bruker AM 300 Hz/WB spectrometer equipped with a 7 Tesla superconducting magnet and 9cm bore, by Dr. J.A. Chudek and Dr. G. Hunter at the University of Dundee.

G. Powder X-ray diffraction (XRD)

In 1912 von Laue and his assistants discovered that crystals can act as diffraction gratings to X-rays (91). As a result of the knowledge of the way atoms are arranged geometrically in crystals, a revolution has taken place in modern science particularly in solid state physics and chemistry. Although much information is lost or degraded, the powder (in particular the Debye-Scherrer) method (92) has proved to be exceedingly useful in those cases where one would wish to examine a crystalline material which was not composed of single discrete crystals. The widest application of the powder

method is in the identification of the constituents of a given material, since the X-ray diffraction pattern of a crystalline substance is characteristic of the atomic arrangement in that substance and as such is a "fingerprint" of that material. However, diffraction techniques as described generally only produce an average structure in a disordered material. In addition, light atoms are difficult to locate due to their low scattering power.

In this work, powder XRD measurements were made using a Philips PW 1050-35 diffractometer with a vertical goniometer and Co-K α radiation. This work was conducted by Douglas Turner of the Department of Geology, University of Glasgow. Samples were prepared either as an acetone slurry or mounted on adhesive tape.

H. Characterisation of surface roughness and planarity (work conducted at Logitech Ltd, Old Kilpatrick with Mr. Gordon Graham, Jim McAnemy and Crawford Scott).

Several methods are available for measuring surface roughness and the light scattering the roughness produces, but they can be grouped into those that give pictures of surfaces such as optical and scanning electron microscopes, or those that give quantitative statistical information about the surfaces such as mechanical profilers. Surface planarity is measured often by interferometry and is so on a routine basis by the optical industry.

1. The Rank Taylor Hobson Talystep (93).

The Talystep is an instrument that takes profiles along a line on a

surface, by measuring the vertical displacement of a diamond stylus probe as it translates the surface of a material. The height sensitivity of the Talystep is in the subnanometre range, or in other words the instrument is capable of detecting peak-to-trough heights of the order of a few Å (10^{-10}m). The Talystep utilises a contact method for measuring surface roughness and therefore the loading on the stylus must be controlled carefully to prevent leaving a track on the surface being examined.

In this work, a standard conical (STD) diamond stylus (0.125mm radius) was employed with a loading of 10-30 μN . A magnification of $\times 10^6$ was used which allowed reproducible measurements to be taken over an ambient temperature range of 278-313 K. Surface roughness values were measured for 2000 data points over a horizontal displacement of 500 micron and the root-mean-square (RMS) value calculated and reported in units of nanometres.

2. Interferometry (5).

The principle of interferometry is simple. Two coherent beams of light, usually from a laser source, are reflected or transmitted through a test piece and a reference surface. The combination of the two beams forms an interference pattern known as fringes. The shape of the fringes indicates the optical path difference between the two wavefronts. The fringes are observed as alternate dark and light bands of destructive and constructive interference respectively.

The planarity of the lapped silica or silicon substrates was determined by use of a Tropel 9000 surface flatness analyser. The glass puck (with the

lapped sample face down) was placed on the screen to produce a series of circular interference fringes on a TV monitor. Convex surfaces were characterised by fringes which would appear to dilate when the puck was pressed into the screen, while concave surfaces were seen to have fringes which contracted. Each fringe observed on the monitor represented a deviation from planarity of 2 micron. Photographic copies of the Fizeau interferograms were produced using a Logitech interferometry and fringe analysis system, coupled with a L125 Fizeau optical tester.

3. The Nomarski light microscope (94).

The differential interference contrast or Nomarski microscope was used to observe the lapping damage or pitting of the surface during the polishing process. A simple compound microscope provides a magnified image of an object so that it can be seen in focus by an observer, whereas a Nomarski microscope allows incident light to be polarised linearly to allow the polarisation of light transmitted by the specimen to be analysed.

The most important additional features of the polarizing microscope are the two polars capable of insertion into the light path before and after it passes through the specimen. The feature that separates the Nomarski microscope from other polarising microscopes is the ability to accentuate surface morphology. Two beams of light, sheared laterally from a single beam by a Wollaston prism, strike the surface to be inspected. Surface features that produce phase differences between the two beams reflected by the surface become visible as shades of light and dark contrast. A low magnification (x80)

was employed in this study as surface damage and pitting were easier to observe under such conditions. Some of this work was conducted in the Department of Geology with the help of Dr. Alan Hall.

4. The Scanning Electron Microscope (SEM) (95).

The scanning electron microscope (SEM) produces a vivid, seemingly three-dimensional picture of a specimen surface with a depth of focus *ca.* 500 times that for a light microscope at equivalent magnifications. A narrow beam of electrons is produced in an electric gun at one end of the vacuum column and then focussed, on as small a spot as possible, on the surface of a specimen placed at the far end of the column. Focussing and scanning of the electron beam is achieved by a series of deflector coils and electromagnetic lenses, designed to produce an extremely small electron beam (typically less than 10 nm). The beam scans the specimen surface repeatedly and forms a raster as is seen in a television set.

While scanning, the electron beam ejects electrons from the specimen surface; these are collected and conveyed to an amplifier, which determines the potential of the modulating electrode of a cathode ray tube. The generator that operates the scanning coils is also connected to the deflector plates of a cathode ray tube. The current reaching the collector determines therefore the voltage signal used to modulate the brightness of the spot on the cathode ray tube. The voltage signal is synchronised also with the movements of the electron beam.

As the secondary electrons are characteristic of the surface at that point,

the current from any point is determined by the composition, texture and topology at the point; electron current reaching the collector is dependent therefore on all three factors. The brightness of the cathode ray spot is used therefore to build up an image of the specimen surface, point-by-point from signals received in their correct relative positions. The size of the raster scanned on the specimen surface is considerably smaller than the size of the surface of the cathode ray tube. Thus the final picture is a magnified image of the surface of the specimen.

In the SEM, specimens must be capable of enduring very low pressures (10^{-5} - 10^{-6} Torr) and the surface should not charge up when exposed to the electron beam. Irregular charging of the specimen surface would seriously and unpredictably affect incident and secondary electrons. To circumvent the problem, specimens are coated with conductive materials such as gold. Any excess incident electrons are thus effectively removed.

This part of the work was conducted with Dr. Tom Baird of the Department of Chemistry. A Philips 500 SEM was employed, with a Polaron SC 515 SEM coating unit to cover specimens with a thin layer of gold. Samples were mounted to the specimen stub by using double-sided sticky cellophane tape. A small quantity of conductive silver paint was applied to connect electrically the specimen to the metal of the stub.

I. Radiochemical techniques (96)

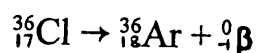
1. Radiochemical counting using Geiger-Müller counters.

The detection of particles and rays emitted by radioactive isotopes

depends upon their energy, type and the nature of the material into which they pass. Radioactive decay energies are considerably larger than chemical bond energies and the ionisation energies of atoms, often by a factor of 10^3 - 10^6 (Fig:21). As a consequence, the electrons liberated by ionisation may be collected and the information used to quantitate the amount of incident radiation.

Geiger-Müller counters are a form of ionisation detector. A Geiger-Müller (GM) counter is an earthed cylindrical metal tube with a thin mica "end-window". The cylindrical casing is designed to act as the cathode, with a central metal wire as the anode. The central wire is held at a high positive potential with respect to the wall cathode. Electrons formed move rapidly towards the wire, whereas positive ions formed drift slowly towards the wall. The applied voltage is increased until ionisation, induced by the acceleration of the initially produced electrons from the Ar/CH₄ filler gas, produces ion multiplication. At this point the number of electrons collected at the central wire becomes greater than the number of electrons created by the passage of radiation through the detector gas. This is known as the "avalanche effect". The proportionality of the incident energy-voltage pulse relationship no longer applies at this point. To prevent secondary electron emission from the cathode walls the fill gas contains methane, to react by electron transfer with positive ions formed by ion multiplication in a process called quenching.

In this work the radioisotope chlorine-36 was used, which decays by beta particle emission according to



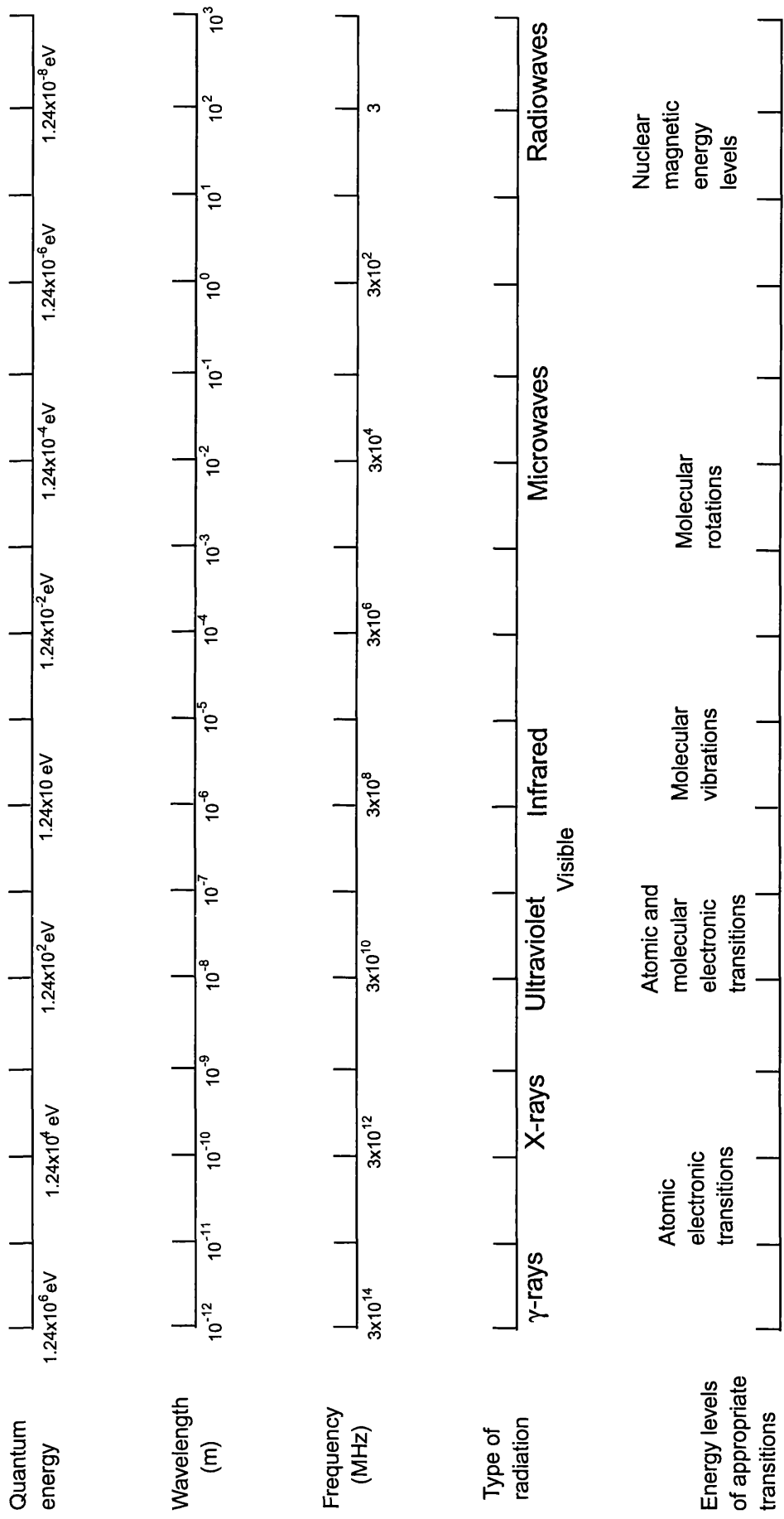


Figure 21: Types of electromagnetic radiation

As the half-life of the isotope is large (3×10^5 yr (97)) no decay correction was required for the radiochemical counting experiments. The maximum energies of the beta particles for the isotope are 0.714 MeV (98).

2. Plateau curves.

In a GM counter no counts are recorded until the applied potential is large enough to attract the free electrons to the anode. At the Geiger threshold V_0 , the count begins to rise rapidly reaching a plateau where increasing voltage has little effect on count. Beyond the plateau voltage, the quench gas is unable to cope with the number of spurious discharges and the count rises rapidly. It is desirable therefore to operate in the middle of the plateau region at the appropriate voltage.

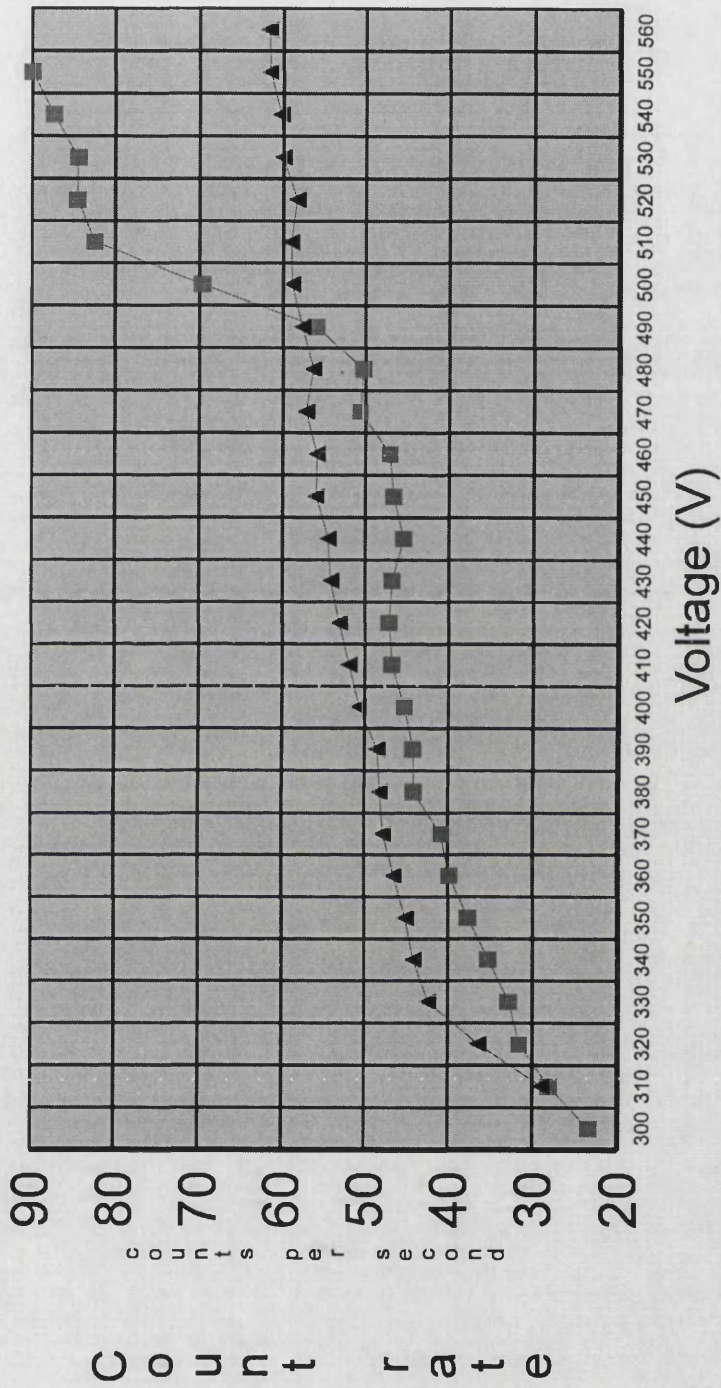
The plateau region was determined for each GM counter, by constructing a plot of counts obtained from a solid ^{137}Cs source against applied voltage. The plateau was never completely flat due to the generation of spurious discharges inside the counter, caused by a small number of secondary electron emissions. The working voltage was set in the middle of the plateau region (Fig:22).

3. Background radiation.

A GM counter will register counts in the absence of a radioactive source, due primarily to cosmic radiation and radiation from materials used in the construction of the laboratory. A count of background radiation was taken over 300s at the beginning and end of each experiment and the average

Figure 22

Counts of Cs-137 source against voltage for GM1 and GM2



■ Tube 1 ▲ Tube 2

Geiger-Muller Tubes to be Calibrated

background reading subtracted from all counts in radiochemical experiments.

4. Statistical errors.

The decay of a radioisotope is a random process. It is subject therefore to fluctuations due to its statistical nature. The expression for the expected standard deviation for radioactive disintegration n is given by

$$n = (me^{-\lambda t})^{1/2}$$

where m = number of counts, λ = half life of the radioisotope and t = observation time. In practice, for observation times very much less than the half-life of the radioisotope the equation reduces to

$$n = \sqrt{m}$$

with the result that 10,000 counts were required for good counting statistics (i.e. where $n \leq \pm 1\%$ of m) with each radiochemical measurement.

5. The direct monitoring Geiger-Müller radiochemical counting technique.

This technique was developed by Thomson and developed further by Thomson, Webb and their colleagues (99), to determine radioactivity on the surface of solids exposed to radiolabelled gases. A Pyrex glass reaction vessel (Fig:23) containing two GM counters was connected via a Pyrex glass manifold, to a constant volume manometer and gas handling facilities. A Pyrex glass boat, divided into two sections capable of being loaded with solid, was placed inside the reaction vessel. The boat could be traversed the length of the vessel by means of a magnet. The system was calibrated before use.

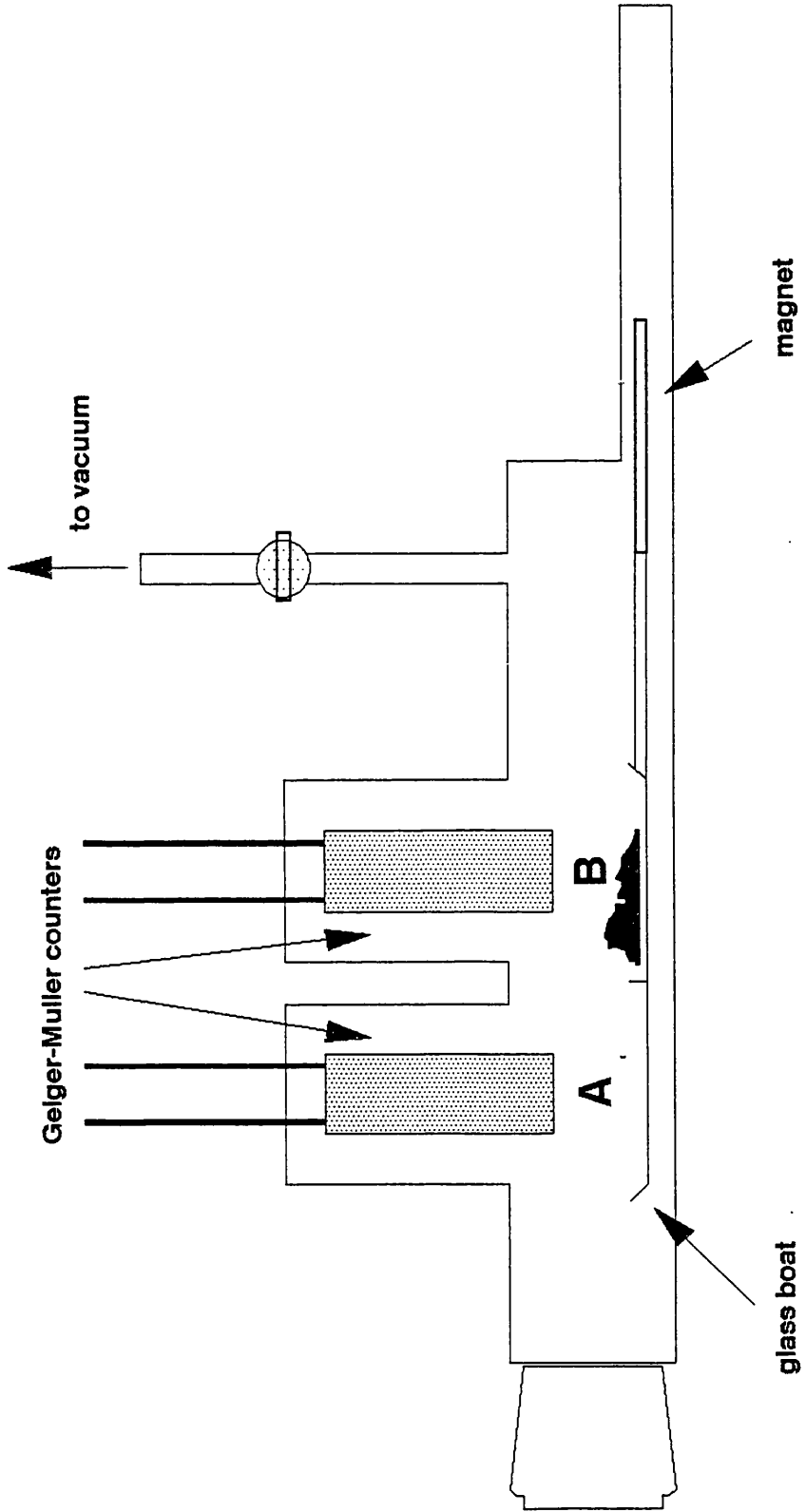
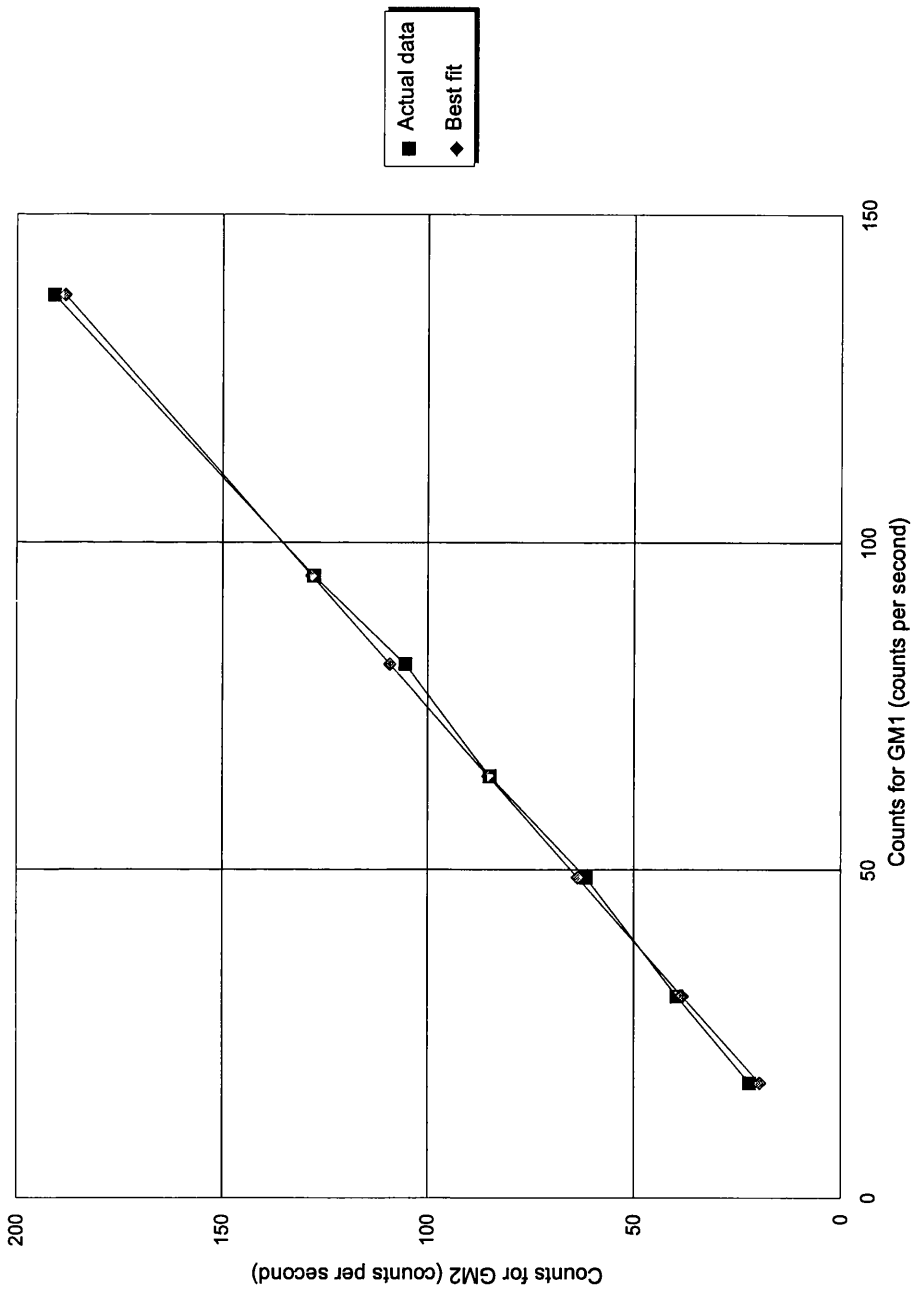


Figure 23: Pyrex glass Geiger-Muller counting vessel

The GM counters were intercalibrated by taking counts of gaseous anhydrous [^{36}Cl]-labelled HCl at various pressures in a flamed-out system. Plotting a graph of pressure against counts gave a straight line passing through the origin. The counts from each GM counter were plotted against one another and the gradient of the straight line produced was equal to the counting ratio of the pair (Fig:24). In using end-window GM counters it was necessary to consider factors such as distance of the end-window from the source, absorption of the radiation by the window and scattering of the radiation as well as the efficiency of the counter ($< 5\%$ for low energy beta emitters). The geometry of a GM counter was therefore maintained as similar to each other as possible.

The procedure for the application of the technique to solid-gas systems was as follows. A weighed sample of solid was placed into the right hand portion of the boat. The boat was manouvred so the left hand portion was directly below GM counter A. The reaction vessel was evacuated and pumped for 24 hr, flamed out and allowed to cool; this sequence was repeated three times. A measured pressure of gaseous anhydrous [^{36}Cl]-labelled HCl was admitted to the reaction vessel and the vessel isolated from the manifold. Counts of each GM counter with respect to time were taken. Counts from GM counter A corresponded to the gas alone, while counts from GM counter B corresponded to counts from gas + solid. Measurements were corrected for background and intercalibration and the counts for solid alone calculated.

Figure 24
Intercalibration of Geiger-Muller counters with chlorine-36-radiolabelled HCl



Gradient=1.40

6. Scintillation counting with solid scintillators.

The most significant penetration of ionising radiation into solid materials is achieved by gamma (γ) radiation. The low efficiency of ionisation of gases by gamma radiation prevents the use of Geiger-Müller techniques. An alternative method of counting, using solid scintillators such as sodium iodide containing traces of thallium iodide, is employed necessarily for gamma radiation.

A gamma ray photon interacting with a sodium or iodine atom in the crystal produces a Compton effect electron or a photoelectron. This electron produces ionisation as it traverses the crystal lattice and around 1% of the energy dissipated is converted to photons of visible light. The scintillation counter is constructed to allow a large proportion of photons emitted to arrive at the photomultiplier, by virtue of the reflecting surface of the casing surrounding the scintillator crystal. The photomultiplier produces a voltage pulse at its output proportional to the intensity of the incident light, or more correctly, the photon energy dissipation in the crystal. Where the initial interaction is via the photoelectric effect, the voltage pulse is proportional to the energy of the photon initiating the process.

The advantage of the NaI scintillation counter over the Geiger-Müller counter is its much higher efficiency for the detection of gamma radiation, due to the increased mass of the detector material and the relatively high atomic number of iodine which enhances the photoelectric interaction. In this work the radioisotope fluorine-18 was employed, whose decay leads to gamma emission of 0.51 MeV. It was very suitable therefore for detection by the NaI

scintillation counter (Fig:25).

7. Radioisotopes.

(a) The Radioisotope [^{18}F]-Fluorine.

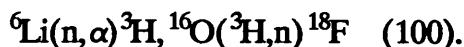
The [^{18}F]-fluorine radioisotope is a positron emitter and annihilation of positron particles with negative electrons releases energy in the form of gamma radiation. As the half-life of the radioisotope is relatively short (109.72 ± 0.06 min (97)) all experimental work was completed necessarily in one day; after six half-lives (11 hr) only 1.6% of the original activity remains.

(b) The Radioisotope [^{36}Cl]-Chlorine.

The [^{36}Cl]-chlorine radioisotope decays by beta emission with a half-life of 3×10^5 yr (97). The isotope was supplied as an aqueous solution of [^{36}Cl]-NaCl (Amersham International plc) and was diluted with concentrated hydrochloric acid to give a solution of specific activity *ca.* $25 \mu\text{Ci cm}^{-3}$.

8. Preparation of [^{18}F]-radiolabelled CsF.

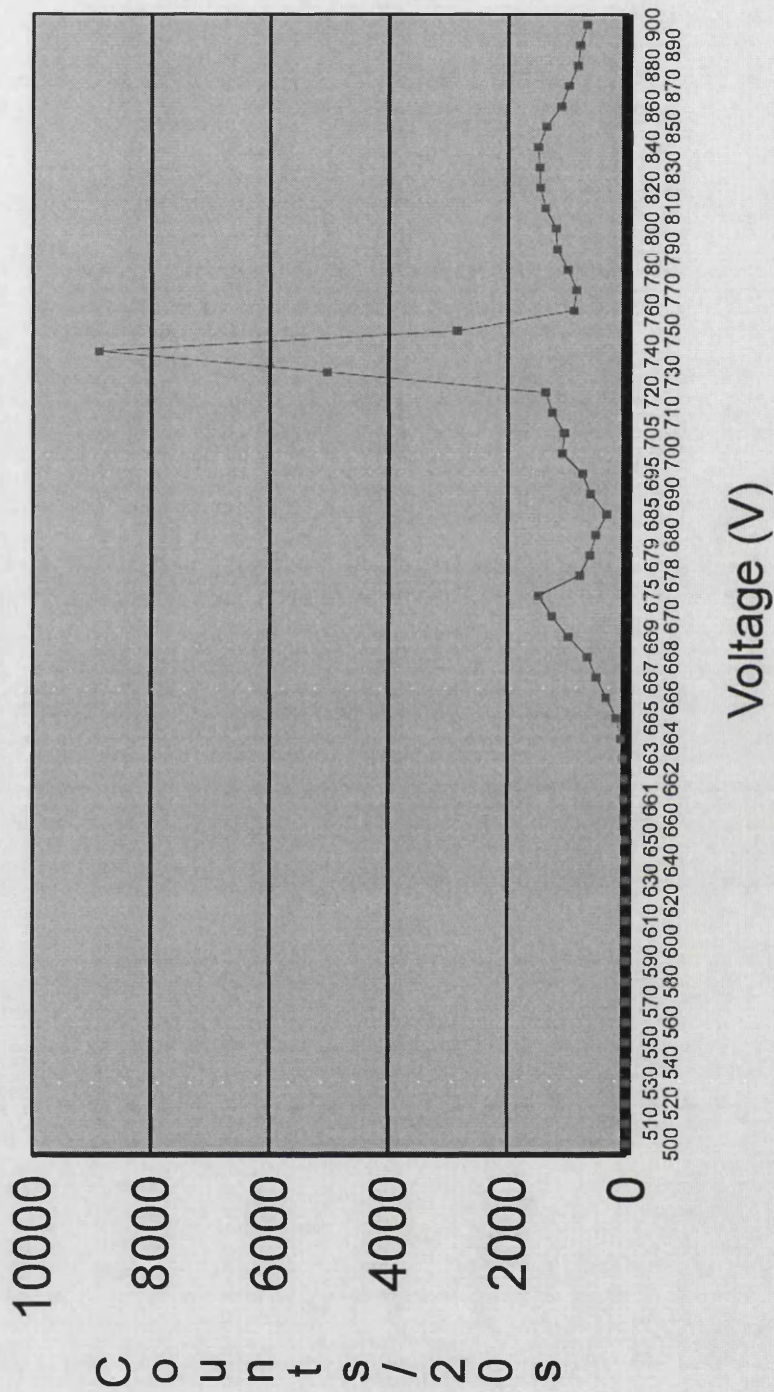
[^{18}F]-fluorine was prepared by irradiation of lithium carbonate (*ca.* 2g; GPR; BDH) in the central core of the Scottish Universities Research Reactor at East Kilbride using the sequence



The lithium carbonate was pressed in the form of pellets and placed in a sealed plastic sachet. The sachet was inserted in a "rabbit" and irradiated for

Figure 25

Gamma ray spectrum of Fluorine-18



50 min at a flux of 3.6×10^{12} neutrons $\text{cm}^{-2} \text{s}^{-1}$. The [^{18}F]-LiF produced by the irradiation process was converted to [^{18}F]-HF by reaction with sulphuric acid (conc. H_2SO_4 : H_2O , 1:1 by volume). The [^{18}F]-HF was distilled into a solution of caesium hydroxide at 273 K. The solution was neutralised by addition of aqueous hydrogen fluoride, followed by evaporation to dryness to yield [^{18}F]-CsF as a grey powder. This process was necessary to remove ^3H which due to its nature is a potential biological hazard (101).

9. Preparation and purification of [^{36}Cl]-radiolabelled anhydrous gaseous HCl (102).

The preparation of anhydrous [^{36}Cl]-radiolabelled HCl of high specific activity was achieved as follows. Concentrated sulphuric acid (13cm^3 ; 98% w/w; M & B Ltd) was added to a reaction vessel with a dropping funnel and pressure equilibrating arm, to which a series of cooled traps were attached (Fig:26). Concentrated hydrochloric acid (11cm^3 ; 36% w/w; M & B Ltd) was added to the thistle funnel and [^{36}Cl]-NaCl solution (2cm^3 ; 50 μCi ; Amersham International plc) was added. The mixture was added dropwise to the sulphuric acid, mixing the solution by agitation of a glass sealed iron bar with a magnet. The U-shaped traps at A and B were cooled to 193 K by dichloromethane/dry ice baths. Phosphorus pentoxide (*ca.* 2g; GPR, BDH) was present at the bottom of each trap to dry the hydrogen chloride gas. The [^{36}Cl]-radiolabelled HCl gas was condensed into the collecting vessel, cooled to 153 K using an isopentane/liquid nitrogen bath, then transferred to a Pyrex glass vacuum line (flamed out and allowed to cool; this sequence was repeated

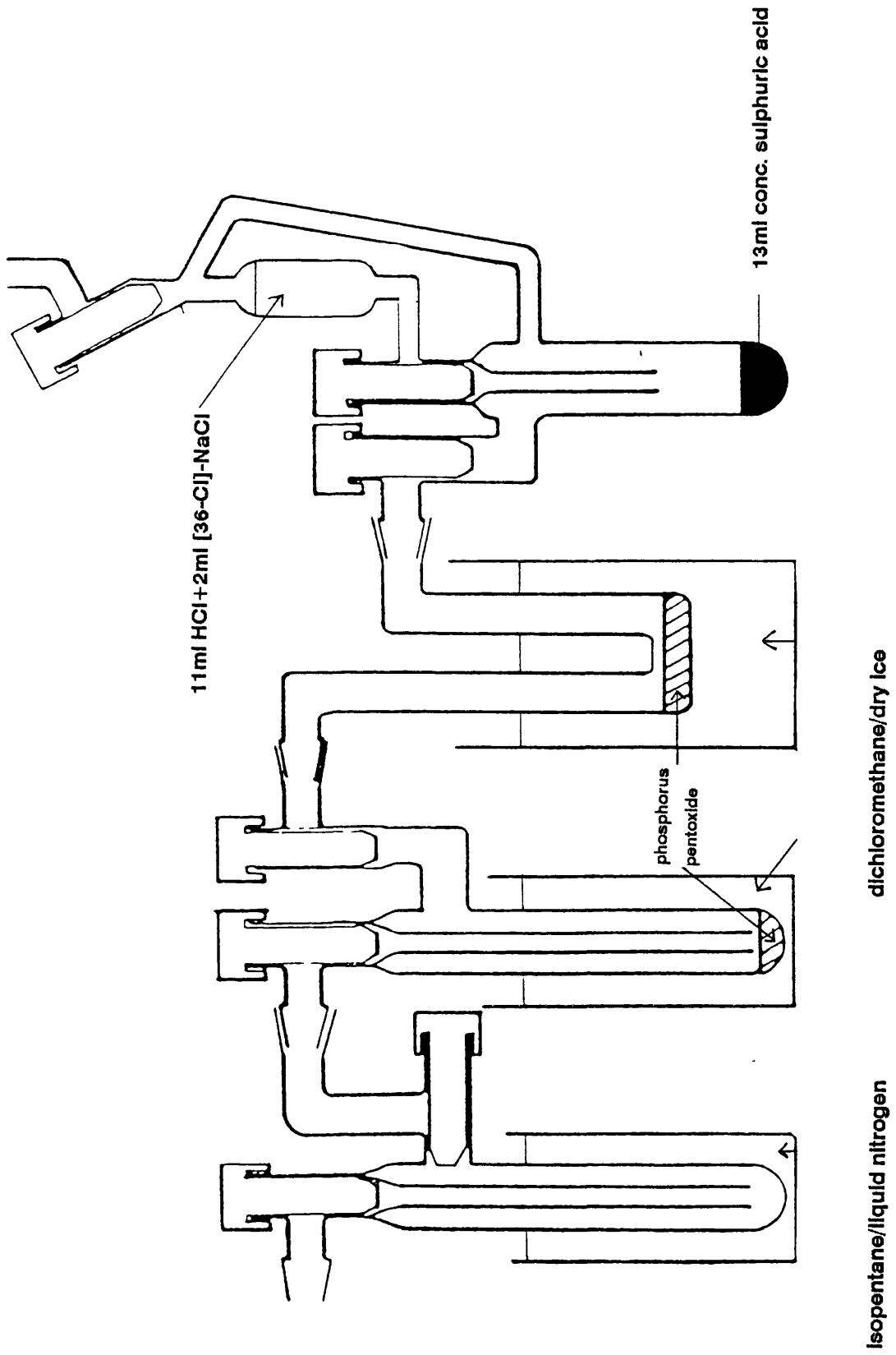


Figure 26: Preparation of chlorine-36 radiolabelled HCl

three times). The [^{36}Cl]-radiolabelled HCl was degassed by cooling to 77 K then vacuum distilled into a stainless steel bomb.

10. Radiochemical counting of [^{18}F]-fluorine on silica and silicon substrates with aqueous [^{18}F]-radiolabelled hydrogen difluoride anion.

A measured quantity (*ca.* 2g) of [^{18}F]-radiolabelled CsF was added to a FEP radiochemical counting vessel, containing an aqueous solution (2cm^3) of $[\text{HF}_2]^-$ (of known concentration and solution pH, as described for etching experiments in Experimental : B) and allowed to equilibrate for 15 min. To each vessel a silica (*ca.* 0.17g, $0.5 \times 0.5 \times 0.2\text{cm}$; Spectrosil B, Multilab Ltd) or silicon (*ca.* 0.01g, $0.5 \times 0.5 \times 0.05\text{cm}$; [100] p-type, MCP Wafer Technology Ltd) substrate was added. A series of counts were taken for each vessel over a specific period. The substrates were removed and dried under an infrared lamp (with or without a prior rinse in distilled water depending on the experiment) and counted in clean FEP vessels. The counts were background and decay corrected and expressed as count rates in units of count s^{-1} . The mass of [^{18}F]-radiolabelled CsF in each FEP was different and hence [^{18}F] retained on the substrate was expressed as a percentage of the solution activity at the beginning of the experiment (i.e. at T_0). This enabled results from different experiments to be compared. Errors due to differing surface areas were assumed to be negligible.

Chapter 3

Results

Results.

A. Chemomechanical polishing of silica and silicon.

The objective of the work was to synthesise and characterize chemically modified ordered films derived from polycyclic aromatic hydrocarbons (PAHs) and supported on highly polished silica and silicon wafers. It was anticipated that by employing "flat" surfaces the production of ordered organic films (PAHs are planar molecules capable of being "stacked" in arrays) would allow for example, the study of cooperative effects among molecules and selectivity in the degree or position of chemical modification. The "Pilkington reagent" (69) was one of a number of fluoride-based reagents used successfully for silica glass polishing. Fluoride-modified silica sols have been employed as reagents for the production of subnanometre finishes on LiNbO_3 with encouraging results for silica glass also, in work done at Glasgow (34). Chemical modification of the surface occurs during polishing. An investigation of chemomechanical polishing of silica was conducted therefore, in order to understand the mechanisms of the chemical processes involved in the production of smooth (surface roughness $< 1\text{nm}$) surfaces rapidly. Polishing of silicon was investigated also to determine the applicability of fluoride-based reagents, for example, was it necessary to include an oxidizing agent in order to remove Si efficiently and what was the role (if any) of the oxide layer on silicon.

1a. Polishing of silica (see Experimental:A.2).

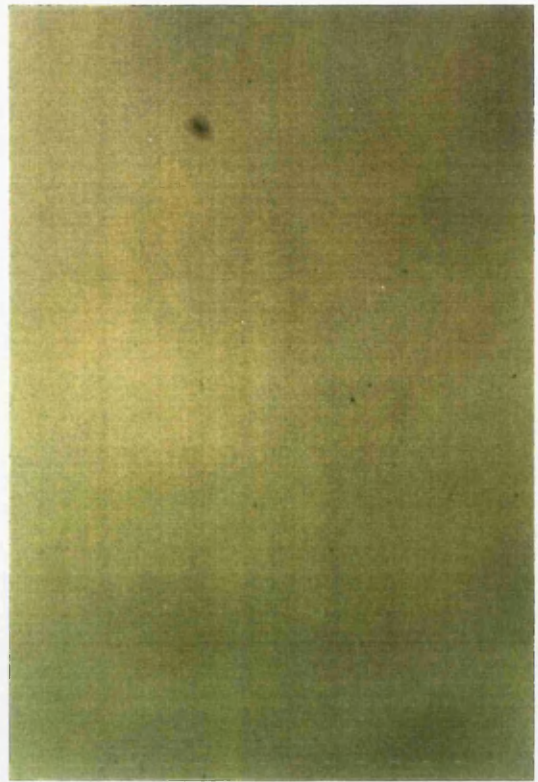
Samples of silica (lapped previously as described in Experimental:A.1)

were polished using the Pilkington reagent, (a mixture of potassium hydrogen difluoride, cerium(IV) oxide and sucrose in aqueous hydrochloric acid (69)), Syton (an aqueous alkaline silica sol), fluoride-modified Syton (1g potassium hydrogen difluoride in 125 cm³ Syton) and an aqueous suspension of Opaline, a commercial cerium(IV) oxide polishing reagent (see Experimental:A.3). Wafers were polished until lapping damage was visible no longer under a Nomarski light microscope (Fig. 27). Talystep profiles of surface roughness were obtained and the results plotted (Fig. 28) using *ca.* 10-12 data points for each reagent. All four reagents were capable of producing surfaces which approached the subnanometre level. As seen clearly in Figure 28, the Pilkington and Opaline reagents achieved satisfactory finishes most rapidly. The Pilkington reagent was characterised by its inconsistency, the spread of results is large in contrast to the narrow range of values obtained with the Opaline reagent. The pattern of results obtained for Syton and fluoride-modified Syton suggested that there was no obvious advantage in employing the latter over Syton alone, as both reagents were capable of producing surfaces which approached the subnanometre level in no less than one hour of polishing; in contrast, both Opaline and the Pilkington reagents produced satisfactory finishes often within 20 min. It was concluded therefore that under polishing conditions the [HF₂]⁻ anion was effective only at low pH as in the Pilkington reagent. During the course of polishing experiments employing the Pilkington reagent, a surface layer developed often on the silica which, with omission of the neutralisation step as specified in the patent (69), was removed easily after washing with distilled water and drying.

**Figure 27:Lapping damage as seen under a
Nomarski light microscope**



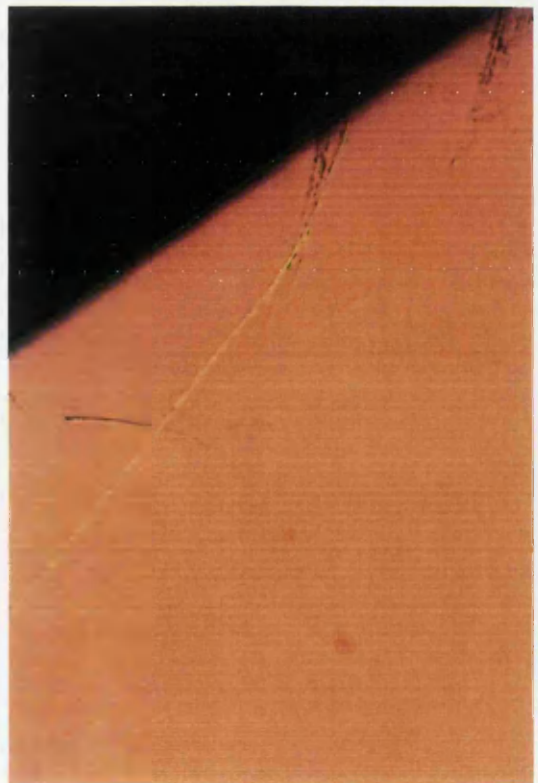
a.Silica after lapping



b.Silica after polishing



c.Silicon after lapping

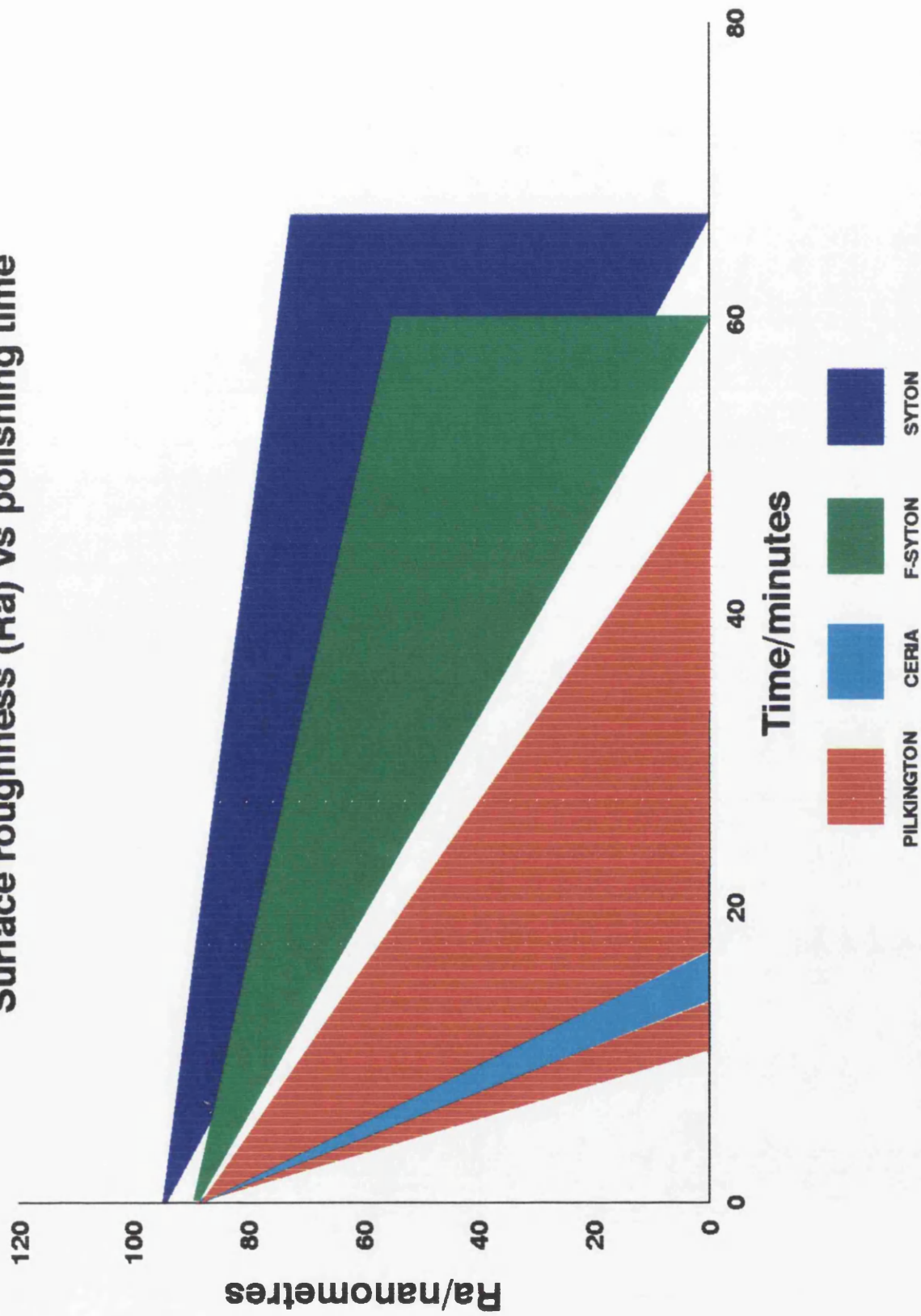


d.Silicon after polishing

Magnification x80

Figure 28

Surface roughness (Ra) vs polishing time



1b. Polishing of silicon (see Experimental:A.2).

Samples of silicon (lapped previously as described in Experimental:A.1) were polished using the Pilkington reagent, Syton, fluoride-modified Syton and Opaline as described previously for silica substrates. Wafers were polished until lapping damage was visible no longer under a Nomarski light microscope (Fig. 27). Talystep profiles of surface roughness were recorded and the results plotted (Fig. 29) using *ca.* 8-10 data points for each reagent. It was found that Syton, fluoride-modified Syton and Opaline would polish silicon, although only a binary combination of Opaline and Syton would remove lapping damage within 1 hr. The Pilkington reagent was unsuccessful for the removal of lapping damage and so no Talystep measurements were made for this reagent. As seen clearly in Figure 29 the addition of $[\text{HF}_2]^-$ anion to Syton had a detrimental effect on the polishing of silicon. Opaline and Syton produced a similar pattern of results. A binary combination of Syton and Opaline was capable of producing surfaces that approached the subnanometre level within 1 hr although the results were not reproducible, as seen from the spread of values in Figure 29.

1c. Surface stress introduced in silica by polishing with the Pilkington reagent.

Samples of silica were lapped on both sides (see Experimental:A.1) and immersed in 48% aqueous hydrogen fluoride for 1 min to remove stress produced by the lapping process. The wafers were polished with Opaline (see Experimental:A.2) on one side then demounted, cleaned and rebonded to the glass puck with the etched side of the wafer face up. Baseline

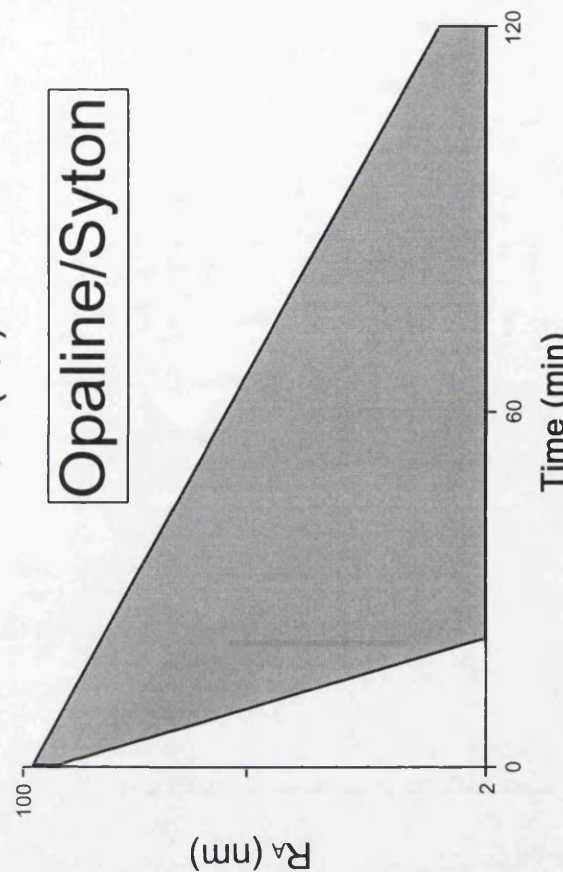
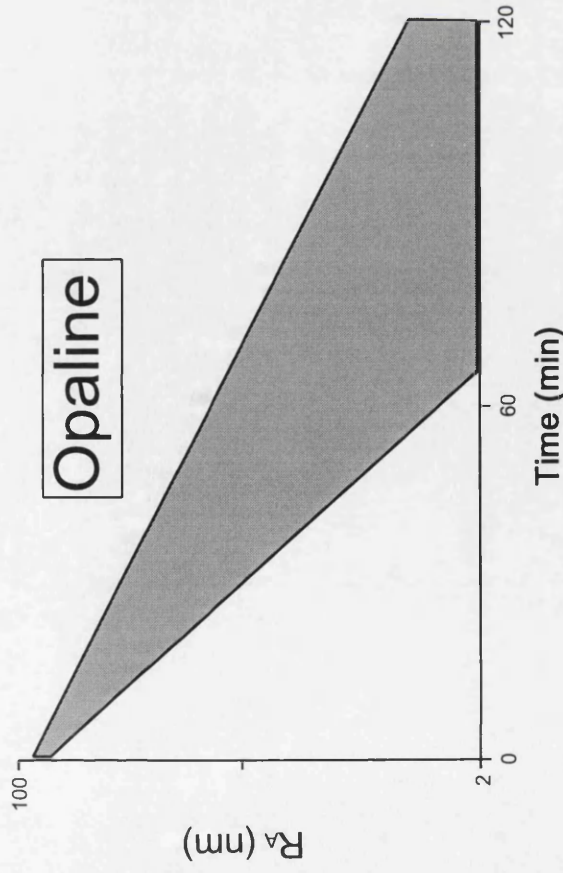
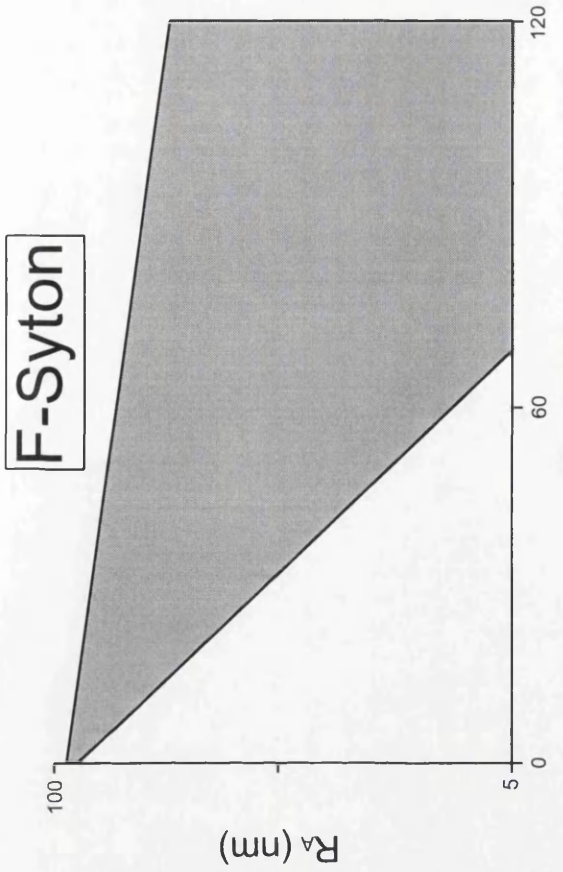
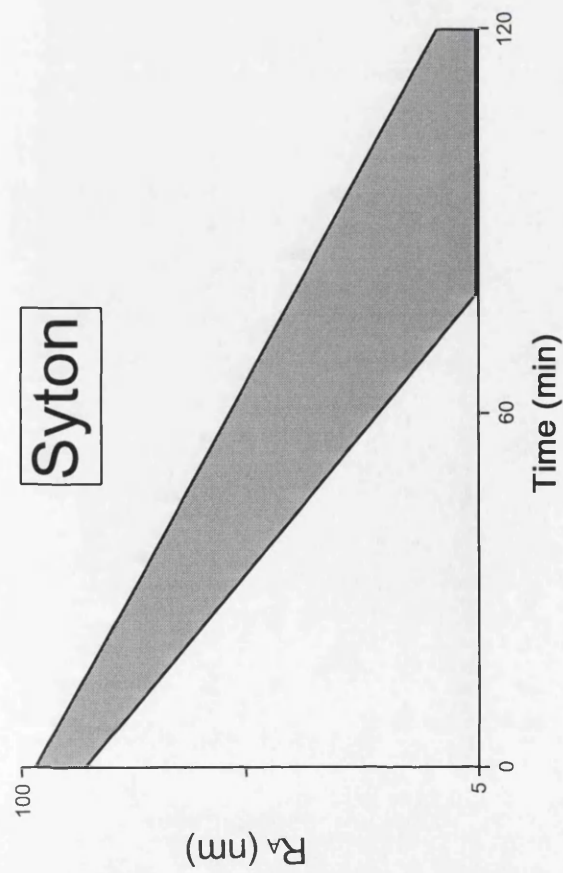


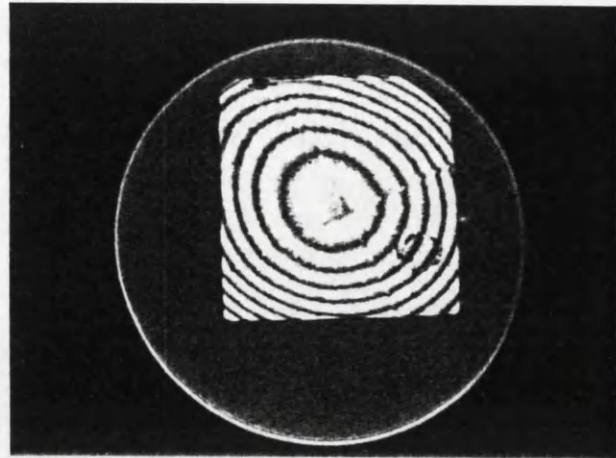
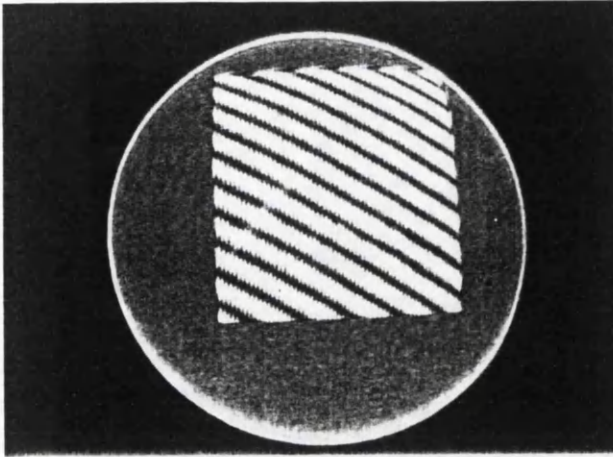
Figure 29: Surface roughness (Ra) vs polishing time for silicon

interferograms (see Experimental:H.2) were taken of the substrate before polishing with the Pilkington reagent and compared with interferograms after polishing. Surface stress introduced by polishing would manifest itself as a circularly symmetric distortion on the polished side, detected easily by interferometry. Figure 30 shows clearly the effect of polishing silica with the Pilkington reagent. Fizeau interferograms taken after 15, 30 and 60 min of polishing for three separate silica wafers indicated that a surface stress was established, as a series of concentric interference fringes described as a Twyman effect (103) were produced. The results were surprising as the Pilkington reagent employs both CeO_2 and $[\text{HF}_2]^-$ anion and both CeO_2 and aqueous hydrogen fluoride (where a significant concentration of $[\text{HF}_2]^-$ anion exists (104)) are known to remove stress produced by the lapping process (105).

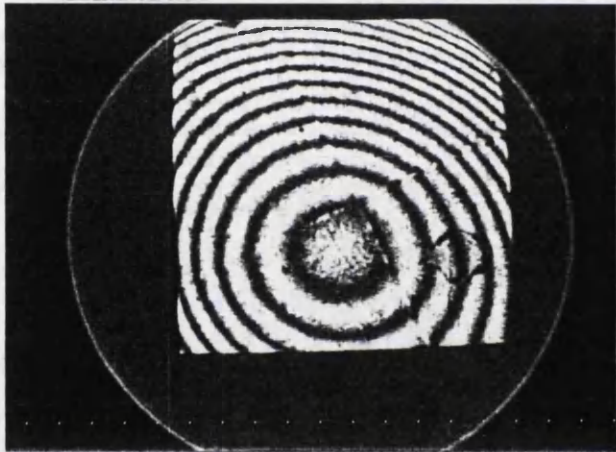
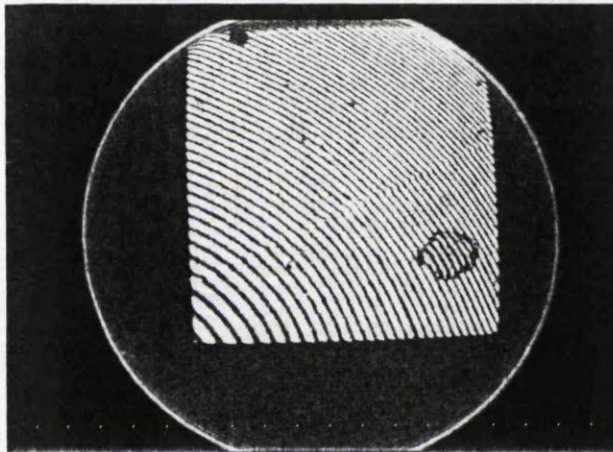
2. The role of cerium(IV) oxide in the Pilkington reagent.

Cerium(IV) oxide (CeO_2) is used widely as a polishing reagent for glass and its unique properties are well documented (10). Its inclusion in the Pilkington reagent was of interest as it was one of many compounds (eg. BaSO_4 , CeO_2 , Cr_2O_3 , ZrO_2 and SnO_2) described in the patent (69) as inert abrasive particles, whose role is believed to be to remove reaction products from high portions on the workpiece. Abrasive particles were included also in the aqueous alkaline neutraliser solution. In order to ascertain the role of CeO_2 in the Pilkington reagent (ie. mechanical, chemical or chemomechanical) several experiments were conducted.

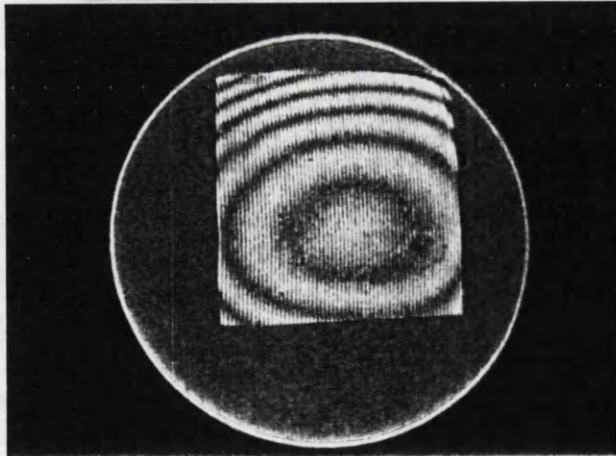
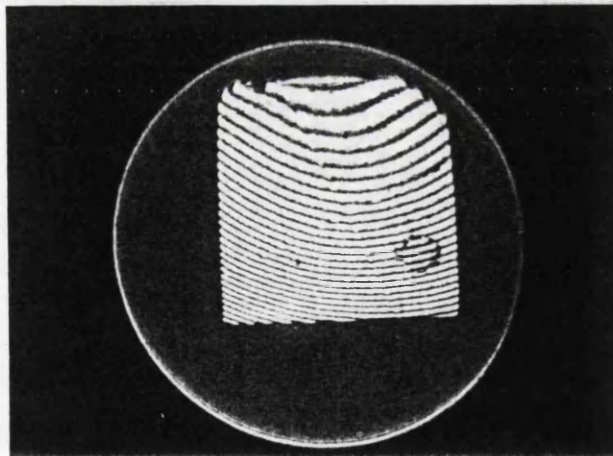
**Figure 30: Surface stress introduced by polishing
with Pilkington reagent**



A: Fizeau interferogram before polishing B: After polishing for 15min



C: Fizeau interferogram before polishing D: After polishing for 30min



E: Fizeau interferogram before polishing F: After polishing for 60min

2a. The effect of addition of cerium(IV) oxide to aqueous solutions containing the hydrogen difluoride anion over pH range 1-11.

CeO_2 and $[\text{HF}_2]^-$ are known to undergo a slow reaction at room temperature (106). It would be expected that any reaction would moderate the aggressive nature of the Pilkington reagent. A series of experiments was conducted in which CeO_2 was added to aqueous solutions of $[\text{HF}_2]^-$ (agitated by magnetic stirring) at pH 1-11 (as prepared in Results:B1.a4) and the effect on solution pH noted. Under all conditions there was no disturbance in solution pH upon addition of CeO_2 . In particular there was no effect for a solution 6.6 mol dm^{-3} in $[\text{HF}_2]^-$ of pH = 1, comparable with the Pilkington reagent. It was concluded therefore that the interaction of CeO_2 with $[\text{HF}_2]^-$ in the Pilkington mixture had a negligible effect on solution pH.

2b. Gaseous anhydrous $[\text{}^{36}\text{Cl}]$ -radiolabelled hydrogen chloride as a probe for surface hydroxyl groups on powdered silica (Spectrosil B) and CeO_2 (Opaline).

Preliminary results from model etching experiments (see Results:B.1) suggested the active species in the Pilkington reagent to be hydrogen difluoride anion employed at low solution pH. The presence of hydroxyl groups, on the surface of both silica and cerium(IV) oxide, was of interest therefore as they would be sites suitable for adsorption and subsequent reaction with the active species. In order to establish the extent and relative chemical reactivity of hydroxyl groups on the surface of both powdered Spectrosil B and Opaline, the two materials were exposed to gaseous anhydrous $[\text{}^{36}\text{Cl}]$ -radiolabelled HCl as described in Experimental:I.5. The specific count rate of the HCl used in each

case was identical and therefore it was possible to compare quantitatively silica and CeO_2 . The results were plotted (Fig. 31 and 32) and tabulated (Table 1 and 2).

The nature of the interaction between HCl and the solid was important. Where there is a strong chemical interaction between the adsorbed molecule and the atoms on the surface, a complete monomolecular layer is formed even at a relatively low concentration of gas phase adsorbate. Adsorption of a second layer can occur only through the interaction of weaker secondary forces between adsorbate molecules. In these systems the first layer is described by the process of chemisorption and follows a Langmuir adsorption isotherm (107) while the second layer is described by the process of physical adsorption. Where there is a weak interaction between the adsorbate molecules and the atoms on the surface a second layer may begin to form before the first is completed. In these systems all adsorption is termed physical adsorption.

It is important to recognise that unlike crystalline stoichiometric CeO_2 atoms on the surface of amorphous silica are by definition not in a regular geometric arrangement and hydroxyl groups on the surface are not therefore equidistant from each other, leading potentially to hydrogen bonding between neighbouring hydroxyl groups in close proximity. It follows that many surface hydroxyls are not equivalent either in their behaviour to adsorbates or in chemical reactions. Determination of the number of surface hydroxyls by chemical means has previously given inconsistent results (108) with various probe molecules. It has been suggested that large substituent groups (e.g. chlorine or ethoxy) are too large to be accommodated at every surface hydroxyl

Table 1

[³⁶Cl]-HCl uptakes by powdered Spectrosil B

Pressure (Torr)	GM1 count/ 300s	GM2 count/ 300s	GM1-GM2
	Gas+solid	Gas	Solid (count s ⁻¹)
147.1	21056	21858	
134.14	19414	21054	
92.79	14286	14332	
48.74	8789	7963	2.75±1.7
19.18	4352	3216	3.79±1.94
15.37	3722	2589	3.78±1.94
9.62	3106	2003	3.68±1.92
8.6	2823	1529	4.31±2.08
4.3	2145	950	3.98±2.00
0	382	0	0.06±0.25
104.72	15022	15411	
78.8	10172	10266	
52.11	8998	8296	2.34±1.53
34.88	6425	5327	3.66±1.91
21.42	4977	3866	3.70±1.92
15.46	3817	2625	3.97±1.99
10.90	3402	2159	4.14±2.04
5.62	2944	1708	4.12±2.03
2.47	1626	564	3.54±1.88
0	406	0	1.35±1.16

Figure 31

Chlorine-36 uptake by powdered Spectrosil B

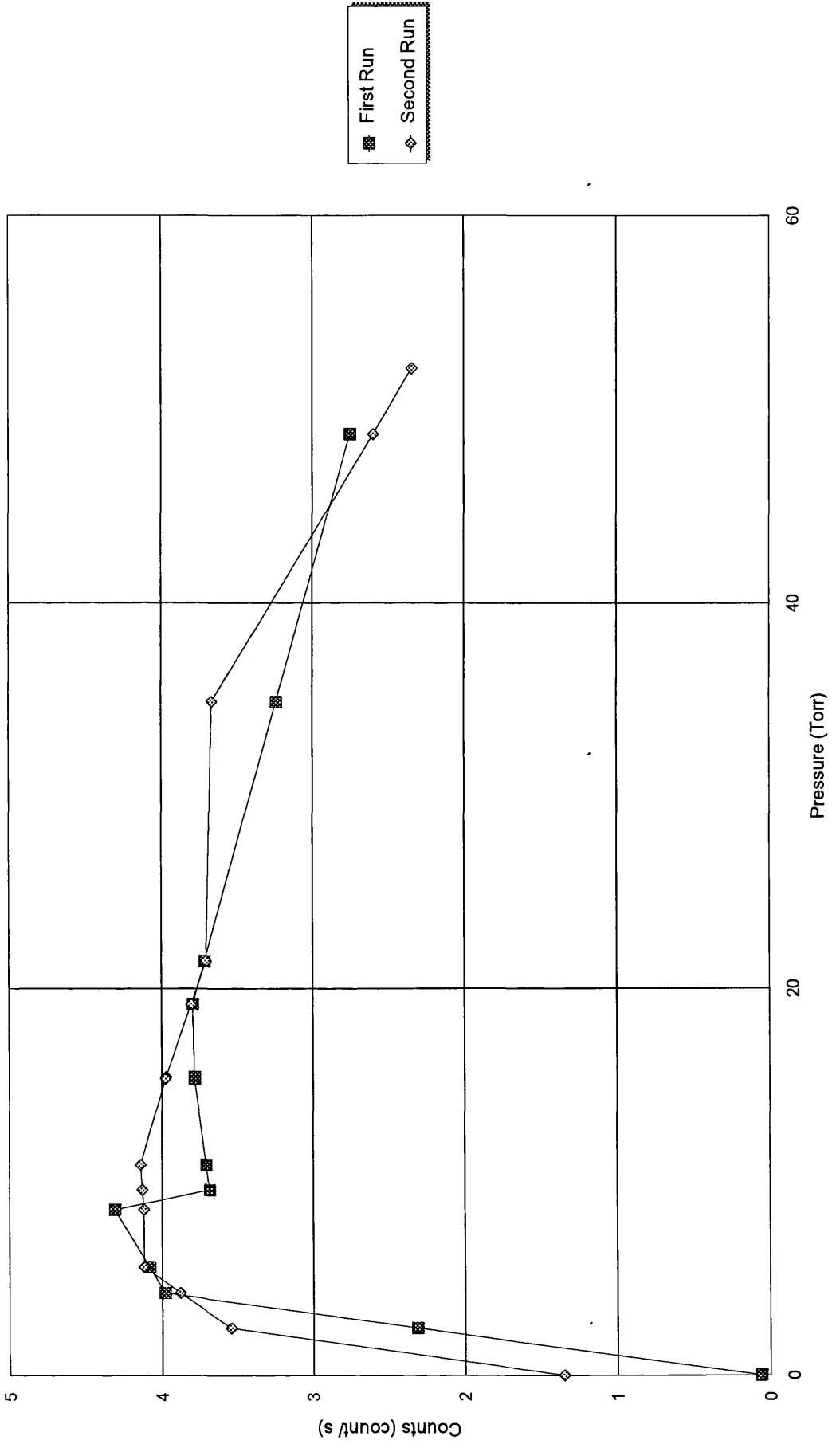


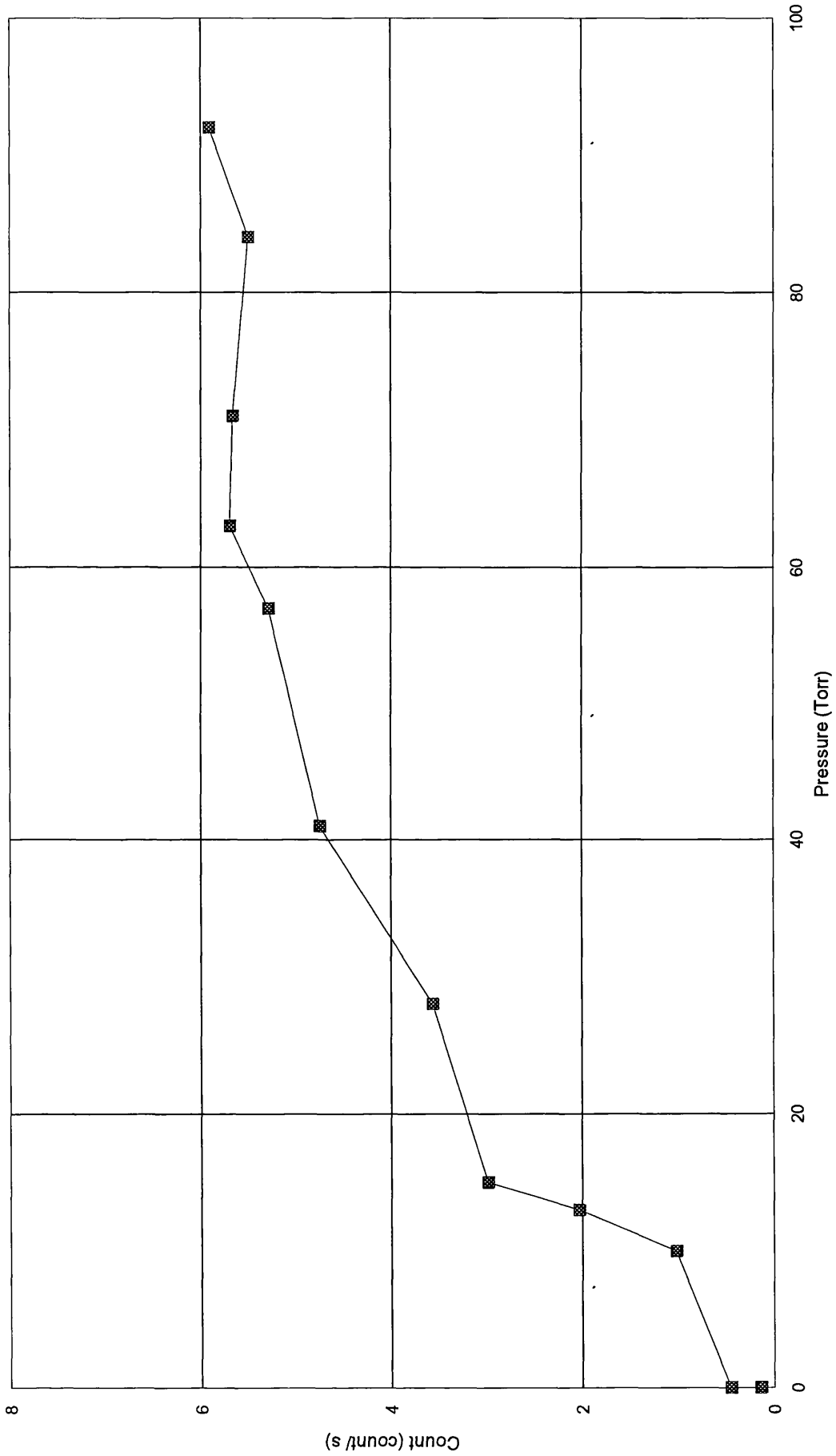
Table 2

[³⁶Cl]-HCl uptake by Opaline

Pressure (Torr)	GM1 count/ 33s	GM2 count/ 300s	GM1-GM2
	Gas+solid	Gas	Solid (count s ⁻¹)
92	29844/ 300s	28072/ 300s	5.91± 2.43
84	27325/ 300s	25677/ 300s	5.49± 2.34
71	24799/ 300s	23102/ 300s	5.66± 2.38
63	22140/ 300s	20433/ 300s	5.69± 2.38
57	18208/ 300s	16624/ 300s	5.28± 2.3
41	15538/ 300s	14116/ 300s	6.74± 2.18
28	11770/ 300s	10702/ 300s	3.56± 1.89
15	14699/ 900s	12021/ 900s	2.98± 1.72
13	10356/ 900s	8532/ 900s	2.03± 1.42
10	11260/ 1500s	9730/ 1500s	1.02 ±1.01
0	13010/ 7200s	9741/ 7200s	0.45± 0.67
0 ^a	4932/ 36000s	0/ 36000s	0.14± 0.37

^aPumped under vacuum overnight

Figure 32
Chlorine-36 - HCl uptake by Opaline



site (109). This would have consequences for a process involving the dissociative adsorption of HCl on silica.

No attempts were made to determine the effective surface areas of both silica and CeO₂ although it was an important factor to consider. It was assumed that the surface areas were approximately equal. Dinitrogen is the adsorbate used most commonly to measure the surface area of a solid, where the surface is understood to mean the boundary of the nonporous solid phase that is impervious to N₂. Micropores exist however into which water but not N₂ may penetrate. It follows that by the BET method (110) the hydroxylated surface would therefore exhibit a concentration of surface hydroxyls which would appear to be abnormally high.

Figure 31 shows clearly there was a small but rapid uptake of [³⁶Cl]-radiolabelled HCl on powdered Spectrosil B at low pressures which decreased gradually at higher pressures. The uptake of [³⁶Cl]-radiolabelled HCl on Opaline is shown in Figure 32. In contrast to silica, the surface count increased with increasing pressure of the gaseous phase. There was a small quantity of permanently retained species that could not be removed by pumping under vacuum overnight. If the assumption is made that HCl behaved similarly towards both silica and CeO₂ (e.g. dissociative adsorption, non-dissociative adsorption etc) and that all hydroxyl groups on the surface were potential sites for the adsorption of HCl, the results suggest there was a stronger interaction between surface hydroxyl groups on CeO₂ and the probe molecules than was the case for Spectrosil B. In view of all the experimental uncertainties and assumptions made there could be no firm conclusions drawn

from the data.

2c. Polishing with omission of a lapping process.

The physical (viscous liquid with suspended abrasive particles) and chemical (highly acidic and corrosive) nature of the Pilkington reagent suggested that it would be possible to omit the lapping process prior to polishing. Samples of silica, not lapped previously were polished using the Pilkington reagent as described in Experimental:A.2. It was found that for all conditions (different loading on sample puck, polishing time etc) an etched surface was produced on the silica wafers.

B. Identification of active species in the Pilkington reagent.

1a. Etching experiments involving silica.

1. Solutions of each component of the Pilkington reagent were prepared in concentrations appropriate to the patent specifications (see Experimental:A.3). Wafers were exposed to each component for 1 hr, under conditions described in Experimental:B. The results were tabulated (Table 3) and it was concluded that no single component had a dominant effect, as determined by mass loss.

2. Binary combinations of components of the Pilkington reagent were prepared in concentrations appropriate to the patent specifications. Wafers were exposed to the mixtures overnight and the results tabulated (Table 4). It was found that a KHF_2/HCl combination produced significant etching and mass loss. CeO_2 appeared to interact with KHF_2 , silica or KHF_2 : silica in

Table 3

The effect of single components of Pilkington reagent on silica

Reagent	Conc/ mol dm ⁻³	Wafer no.	Change in mass/ g
CeO ₂	58.1 mmol in 102cm ³ H ₂ O as a suspension	1	+0.0028
		5	+0.0003
		9	+0.0008
		13	-0.0121
HCl	2.7	2	+0.0027
		6	+0.0013
		10	+0.0001
		14	-0.0004
KHF ₂	6.4	3	+0.0022
		7	+0.0001
		11	-0.0007
		15	+0.0038
Sucrose (C ₁₂ H ₂₂ O ₁₁)	0.26	4	+0.0028
		8	+0.0004
		12	+0.0003
		16	+0.0004

Table 4

The effect of binary combinations of components in Pilkington reagent on silica

Reagent	Conc/ mol dm ⁻³	Wafer no.	Change in mass/ g
		1	0.0000
HCl	2.7	2	-0.0008
+		3	-0.0010
CeO ₂	58.1 mmol in	4	-0.0002
	104 cm ³	5	-0.0001
KHF ₂	6.3	6	-0.0092
+		7	-0.0131
HCl	2.7	8	-0.0111
KHF ₂	1.0	9	(-0.0022) -0.0190*
+ HCl	2.7	10	(-0.0034) -0.0219*
KHF ₂	6.4	11	-0.0027
+	58.1 mmol in	12	-0.0015
CeO ₂	102 cm ³	13	-0.0022
KHF ₂	1.0	14	(+0.0017) -0.0012*
+ CeO ₂	As above	15	(+0.0019) +0.0009*

Conditions overnight at room temperature ; figures in parentheses are mass changes

determined after 1hr reactions, prior to overnight* reactions

an irreproducible manner.

3. In order to establish an optimum $[\text{HF}_2]^-$ concentration for etching with binary combinations of KHF_2/HCl , a series of solutions was prepared by varying $[\text{HF}_2]^-$ concentration in aqueous HCl (2.6 mol dm^{-3}). Wafers were exposed to the solutions overnight and the results plotted (Fig. 33). In all cases the mass of the wafers decreased. For concentrations of $[\text{HF}_2]^-$ in the range $3-1 \text{ mol dm}^{-3}$ a surface layer developed on the silica. Upon drying the layer fractured and was removed easily. Maximum mass loss occurred at $2-2.5 \text{ mol dm}^{-3}$.

4. In order to establish an optimum solution pH for etching in binary combinations of KHF_2/HCl , solutions of $\text{pH} = 1-11$ were prepared by the dropwise addition of concentrated aqueous ammonia solution (0.88 sp.gr) to solutions of KHF_2 (1.0 or 2.0 mol dm^{-3}) in aqueous HCl (1.04 mol dm^{-3}). Solution pH values were determined to a precision of ± 0.1 pH units. Solutions were made up to 250 cm^3 with distilled water to maintain constant volume and molarity. The wafers were exposed to the solutions overnight. Mass changes in the silica wafers at different pH values and concentration of $[\text{HF}_2]^-$ were plotted (Fig. 34). The pattern of results appeared to suggest that mass loss occurred preferentially at low pH. The mass changes were small however and subject to experimental artifacts, the most significant of which were collisions involving the magnetic stirring bar with the silica wafers.

5. In order to eliminate mechanical effects (produced by collisions with the magnetic stirring bar) wafers were supported in Perspex boats (Fig. 35) and the preceding experiment repeated. The results were plotted (Fig. 36) and

Figure 33

Mass loss from silica wafers stirred in HCl/KHF₄ solutions of varying [HF₂⁻] concentration

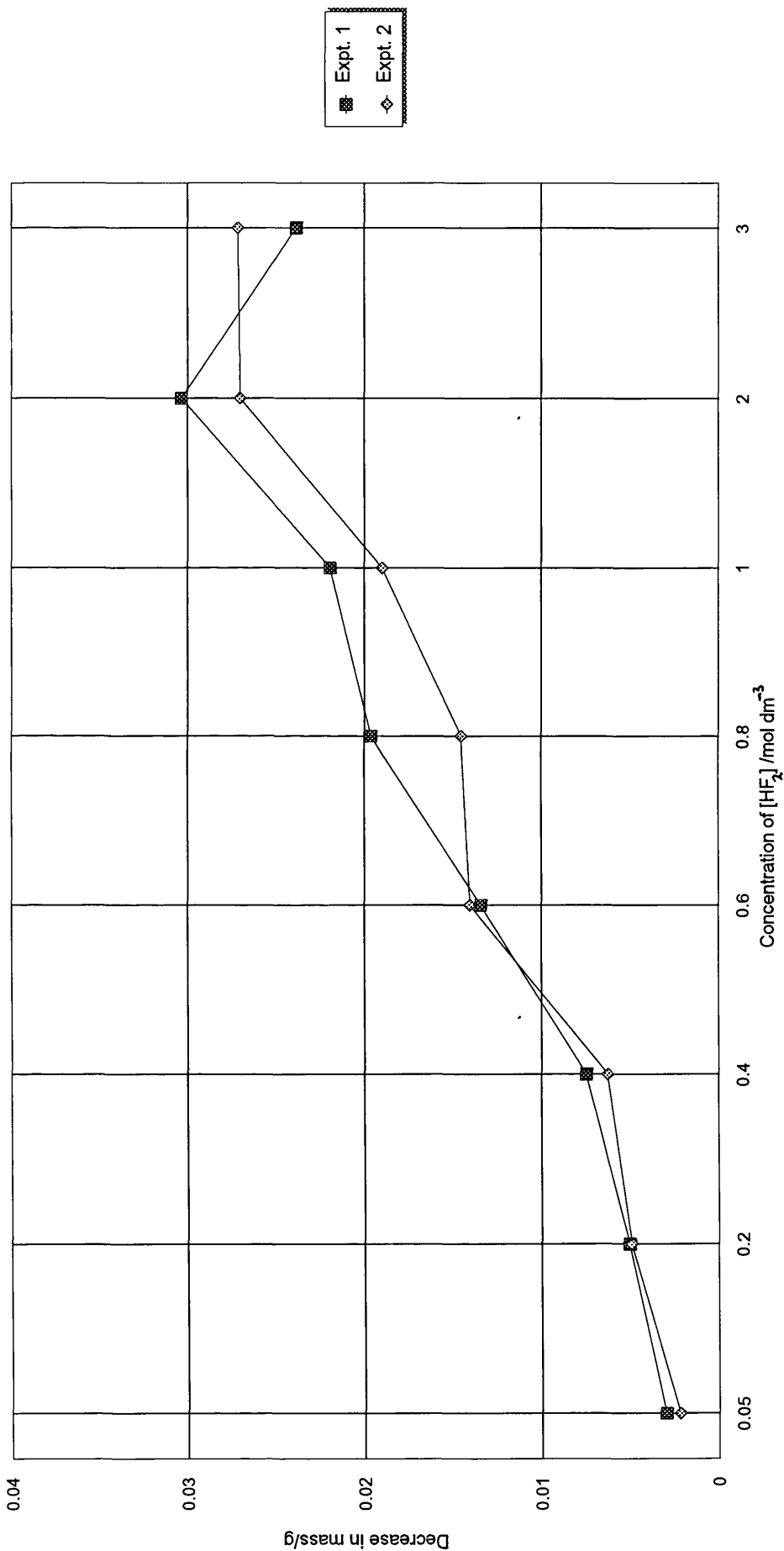
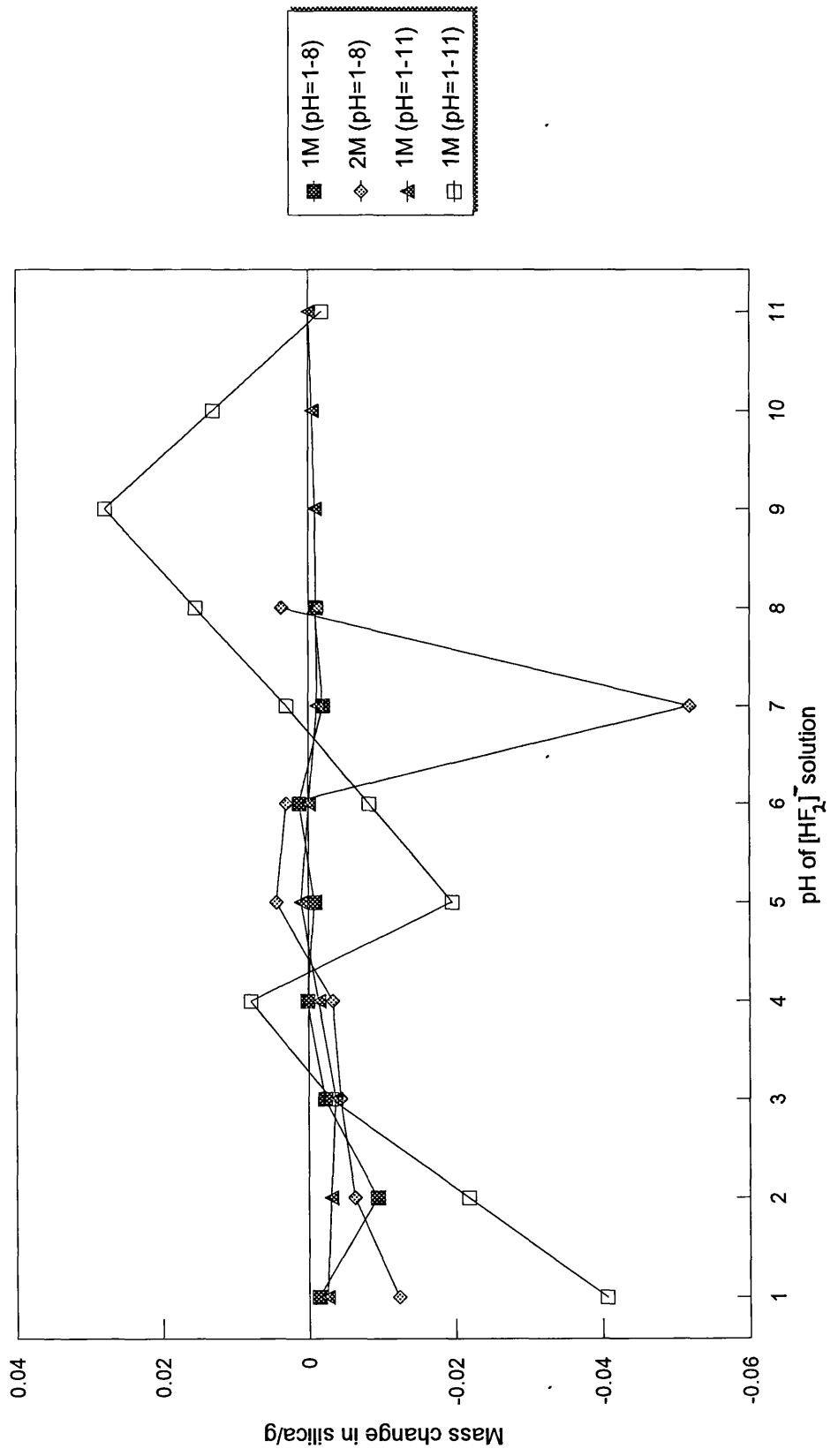


Figure 34
 Mass loss from silica wafers in HCl/KHF₂ solutions of varying pH



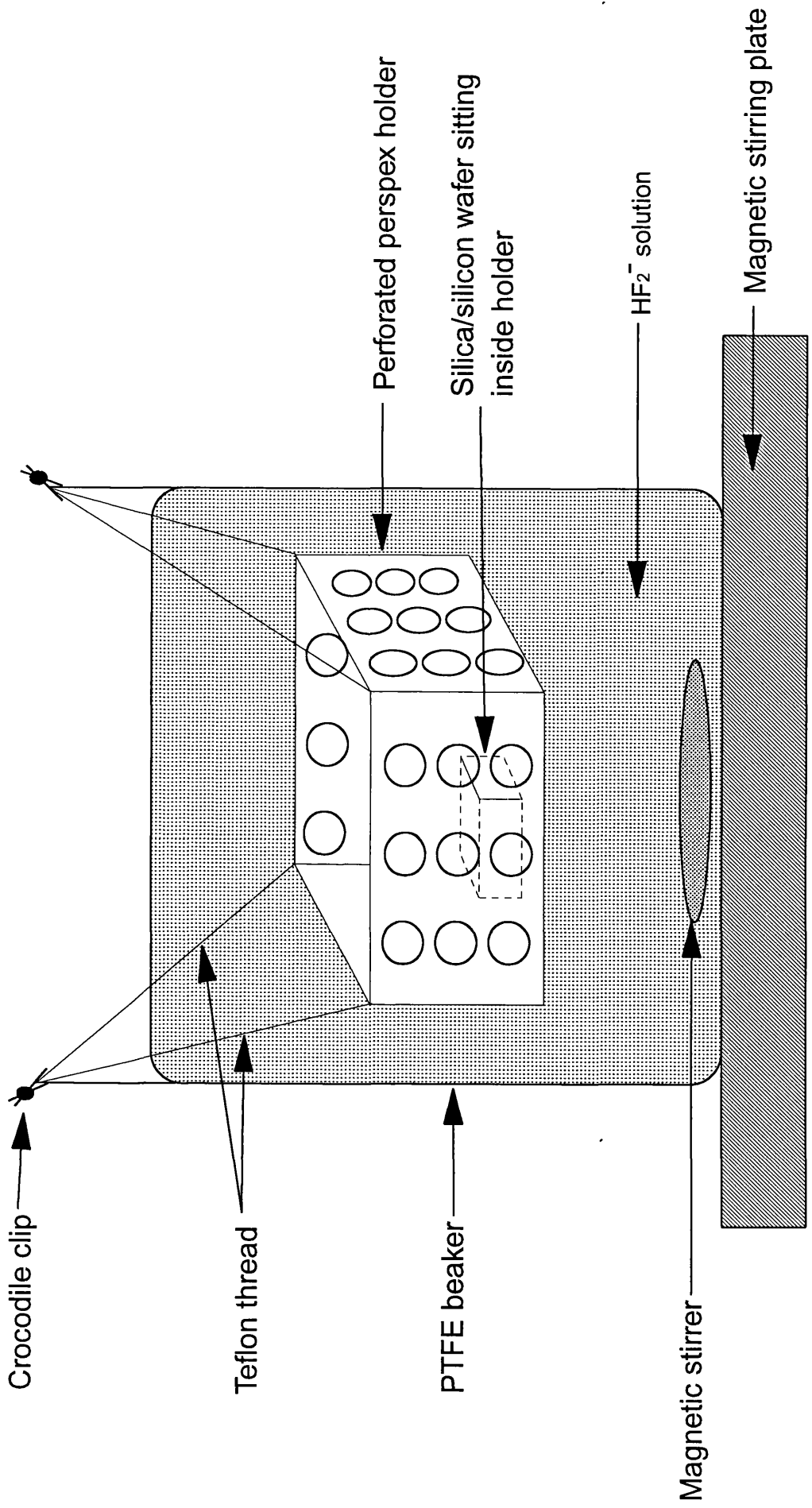
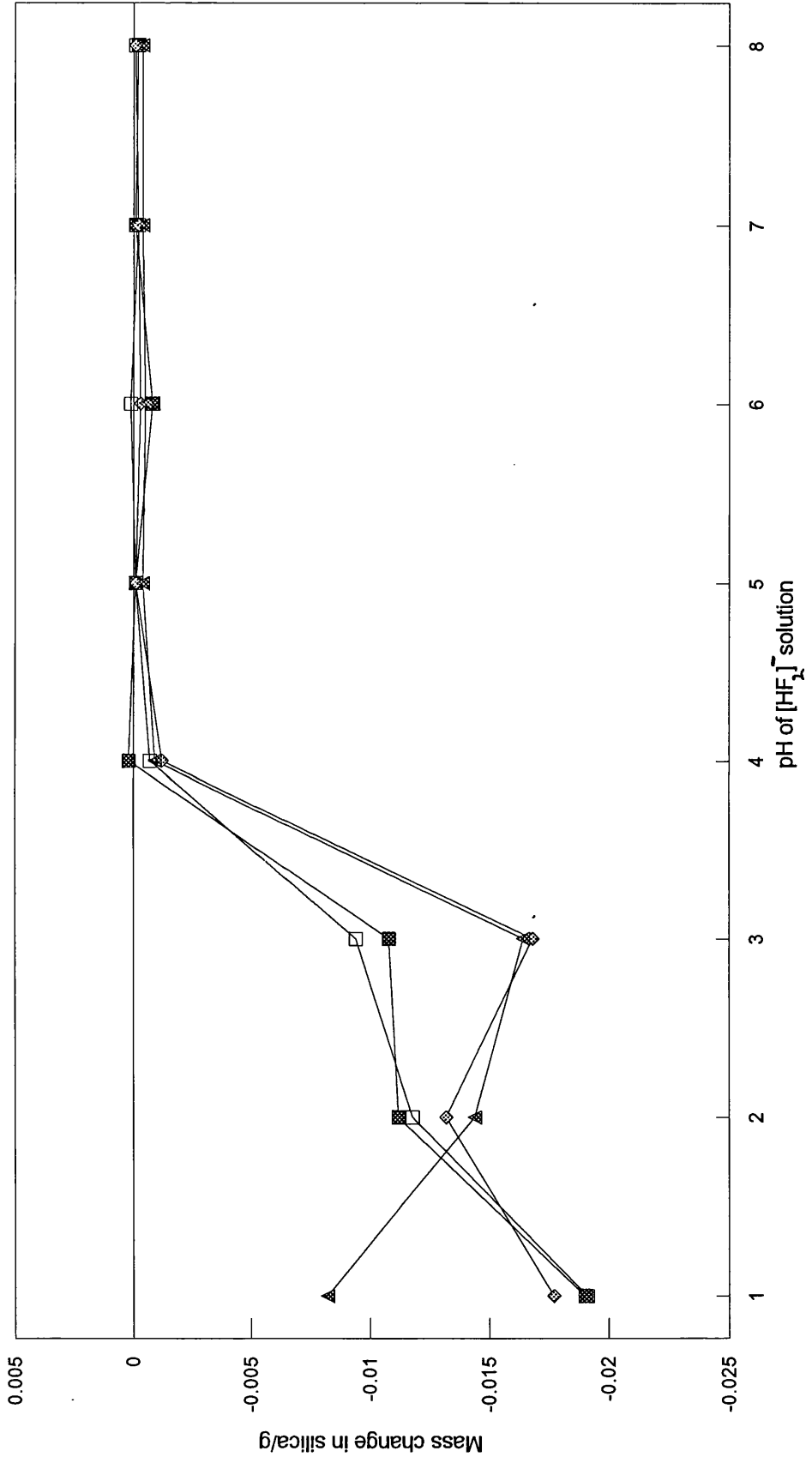


Figure 35: Perspex wafer holders for etching experiments

Figure 36
Mass loss from silica wafers in HCl/KHF₂ solutions of varying pH



compared with previous data. Better control of experimental conditions produced a more defined pattern of results, similar to those in Figure 34 and confirmed that mass loss occurred preferentially at low pH. The formation of "layer material" was more pronounced especially at pH=3.

1b. Etching experiments involving silicon.

Under typical experimental conditions (i.e. in the open atmosphere or in aqueous solution containing dissolved oxygen) a silicon substrate is covered with an oxide layer (111). As a consequence any polishing process for silicon must involve the removal of the oxide layer in the initial stages.

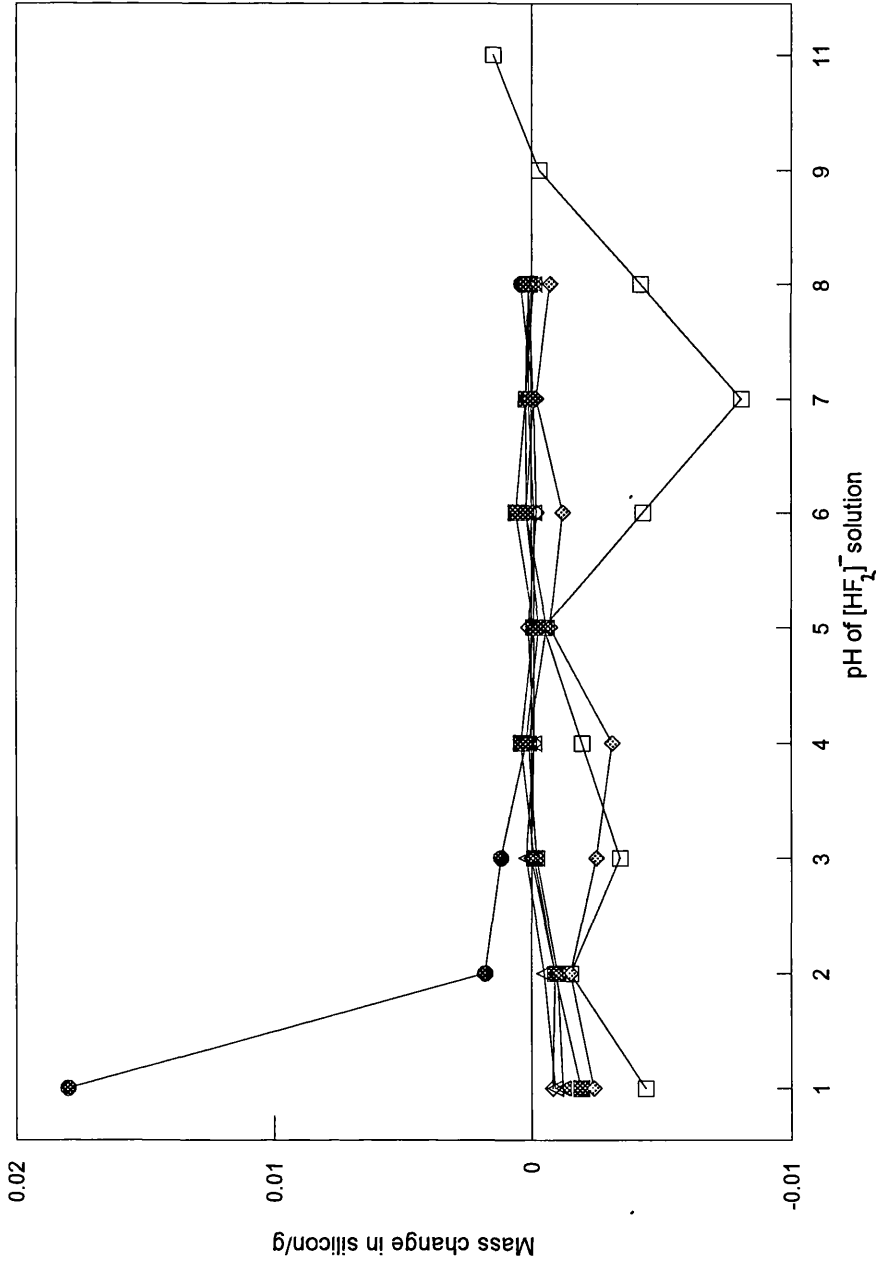
To establish whether a mass change vs solution pH relationship existed for silicon, parallel to that for silica, a series of experiments was conducted (under conditions identical to those described for silica in 1a. 5) over 15 min, 1 hr and overnight. The results were plotted (Fig. 37) and it was concluded that in the absence of mechanical effects, the early stages of etching reactions involving silicon in binary combinations of KHF_2/HCl resembled those for silica, although the mass changes were of an order of magnitude smaller than those for silica. Wafers exposed to solutions overnight exhibited mass gains, in contrast to silica under identical conditions.

2. Radiochemical uptakes of aqueous [^{18}F]-labelled hydrogen difluoride anion on silica and silicon.

During the course of both polishing and etching experiments a surface layer developed often on the wafer for which there was evidence for the

Figure 37

Mass loss from silicon wafers in HCl/KHF_2 solutions of varying pH



- without perspex holders for 60 min
- with perspex holders for 15 min
- with perspex holders for 60 min
- with perspex holders overnight

incorporation of fluorine, from spectroscopic and other methods (see Results:C). Experiments employing the radiotracer fluorine-18 were conducted to amplify previous work and determine both the degree of fluorine incorporation (over a range of pH values) and whether the fluorine was inert or labile to exchange.

A number of attempts were made to label the hydrogen difluoride anion before a technique was found which ensured a high specific activity and good counting statistics (see Experimental:I.10). From early experiments it was established that any fluorine incorporated was water soluble, as there was no measurable activity on wafers after washing with distilled water.

2a. Radiochemical uptake of aqueous [^{18}F]-labelled $[\text{HF}_2]^-$ on silica over pH=1-9.

In order to establish a relationship or otherwise for the incorporation of fluorine over a wide pH range, silica substrates were exposed to $[\text{HF}_2]^-$ solutions of pH = 1-9 (see Results:B1.a4) under conditions described in Experimental:I.10. For all experiments, in order to minimise effects due to physical differences in each sample (e.g. surface areas), silica and silicon of similar mass and geometry were employed. The physical nature of the "passive layer" material made it possible only to make comparisons with silica of similar mass. Fresh silica, silica which was etched prior and layer material isolated from earlier experiments was investigated. Results were expressed as count-rates in units of count s^{-1} (background and decay corrected to time T_0 when the first radiochemical count was initiated) and as a percentage of the

solution activity at time T_0 in Table 5 and Figure 38. In Table 5 the numbers in the vertical columns before the bold horizontal line (i.e. between 113 and 121 min) refer to counts for FEP vessels containing the substrate and [^{18}F]-labelled solution, beyond which the counts are for FEP vessels containing the dry substrate only, plotted in Figure 38.

The pattern of results indicated that fluorine was incorporated preferentially at low pH on fresh silica. Under comparable conditions, etched silica displayed significantly less incorporation of fluorine. There was evidence from earlier experiments that etched silica and layer material contained Si-F species on the surface, as detected by DRIFTS and PAS (see Results:C.1). This suggested that fluorine incorporated was inert to radiochemical exchange. Counts for the "passive layer" could not be ascertained with any precision as the bulk of the material was water soluble.

2b. Radiochemical uptake of aqueous [^{18}F]-labelled $[\text{HF}_2]^-$ on silicon over pH = 1-10.

In order to establish whether a relationship similar to that for silica existed for silicon, an experiment was conducted where silicon wafers were exposed to $[\text{HF}_2]^-$ solutions under conditions described in Experimental:I.10 over pH = 1-10. Samples of fresh silicon and silicon that had been etched from earlier experiments were employed. Results were expressed and presented as described for the preceding experiment in Table 6 and Figure 39.

The pattern of results for silicon was similar to that found for silica, with incorporation of fluorine occurring preferentially at low pH. The degree

Figure 38
Radiochemical uptake of ^{18}F on silica with aqueous $[\text{F}^-]$ -labelled $[\text{HF}_2^-]$

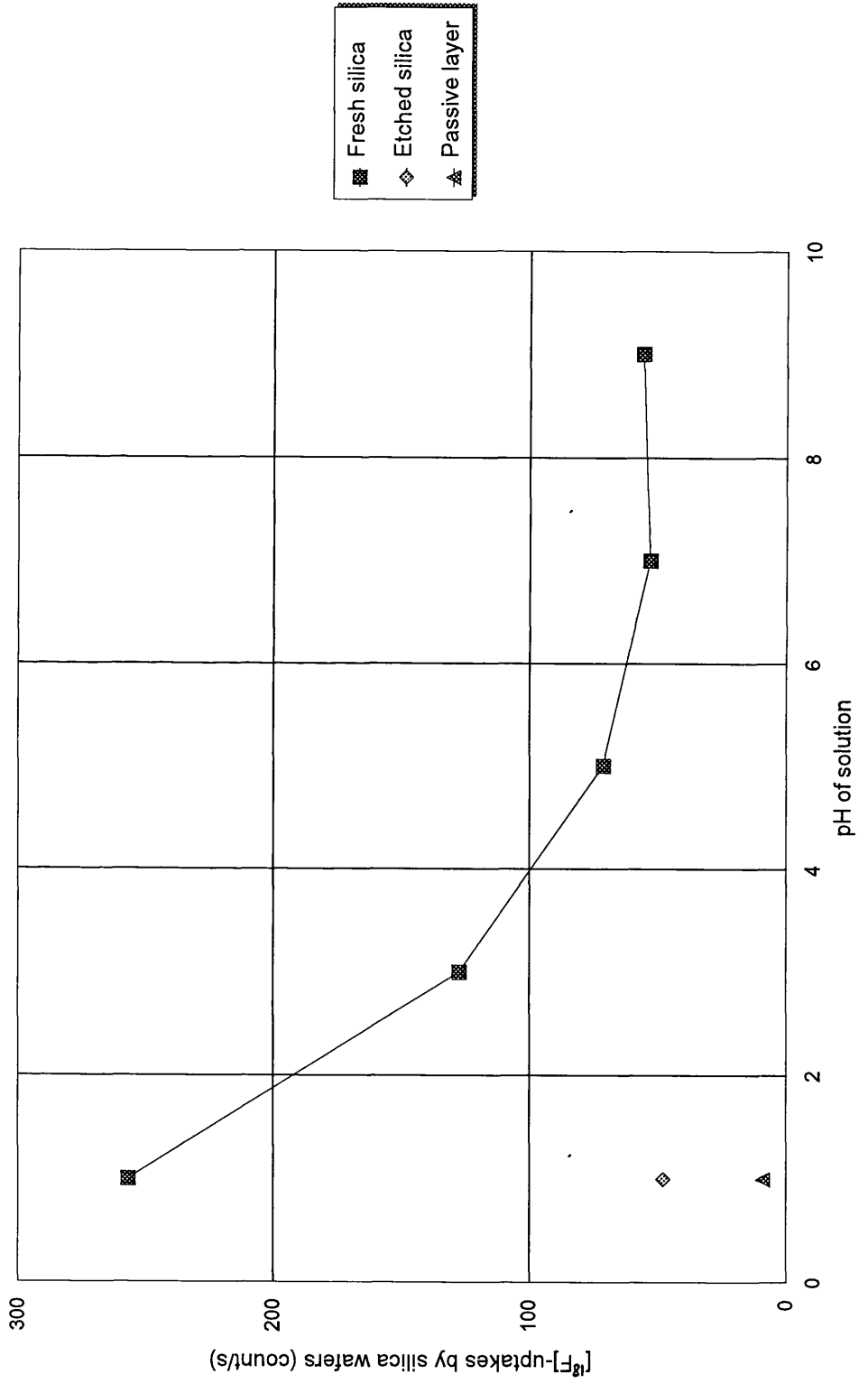


Table 5

Radiochemical uptake (count s⁻¹) of ¹⁸F on silica with aqueous [¹⁸F]-labelled [HF₂]

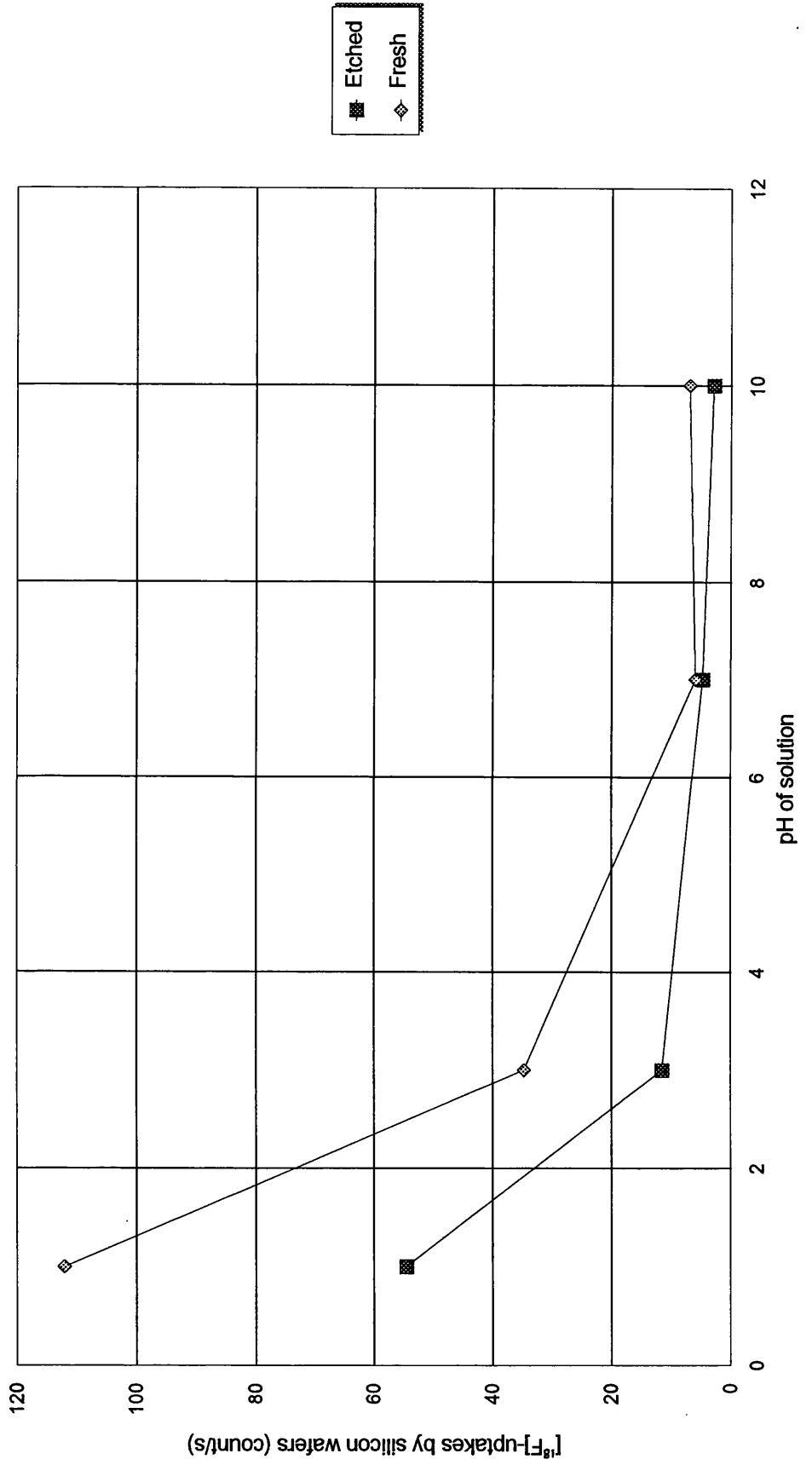
Time (min)	pH=1 Etched	pH=1 Fresh	pH=1 Passive Layer	pH=3 Fresh	pH=5 Fresh	pH=7 Fresh	pH=9 Fresh
0	1849.05±43						
1			1557.58±39				
2							
24		2321.17±48		2722.28±52			
25					2359.03±49		
26						2804.87±53	
27							2765.93±53
28	1689.89±41	2802.38±53					
30			2141.22±46				
60				3286.96±57	2727.91±52		
61						3275.06±57	
62							3627.65±60
63	2340.38±48						
64		3566.34±60					
65			1824.98±43				

Time (min)	pH=1 Etched	pH=1 Fresh	pH=1 Passive Layer	pH=3 Fresh	pH=5 Fresh	pH=7 Fresh	pH=9 Fresh
73				3604.86±60	2784.55±53		
74						3473.74±59	
75							3911.34±63
76			1850.55±43				
77	2382.80±49						
78		3825.61±62					
79				3653.96±60	2718.95±52		
80						3494.69±59	4025.27±63
81	2273.63±48						
82		3789.39±62					
83			1760.30±42				
84				3613.68±60	2675.16±52		
85						3415.96±58	
86							4103.09±64
91		4099.22±64	1735.64±42				
92	2348.34±48						
93				3697.51±61			

Time (min)	pH=1 Etched	pH=1 Fresh	pH=1 Passive Layer	pH=3 Fresh	pH=5 Fresh	pH=7 Fresh	pH=9 Fresh
94					2727.47±52		
100						3506.71±59	
102							4538.34±67
103	2143.53±46	4060.29±64					
104			1732.92±42				
105				3720.12±61			
106					2798.75±53		
107						3528.84±59	
108							4509.80±67
109	2266.07±48	4283.70±65					
110			1706.50±41				
111				3833.67±62			
112					2879.35±54		
113						3796.85±62	4667.90±68
121			8.79±3				
124	47.51±7						
126		256.76±16					

Time (min)	pH=1 Etched	pH=1 Fresh	pH=1 Passive Layer	pH=3 Fresh	pH=5 Fresh	pH=7 Fresh	pH=9 Fresh
142				127.06±11			
147					71.08±8		
153						52.74±7	
163							55.50±7
% uptake of original solution activity	2.57%	11.06%	0.56%	4.67%	3.01%	1.88%	2.01%

Figure 39
Radiochemical uptake of ^{18}F on silicon with aqueous $[\text{F}^-]$ - labelled $[\text{HF}_2^-]$



Time (min)	pH=1 Etched Si	pH=1 Fresh Si	pH=3 Etched Si	pH=3 Fresh Si	pH=7 Etched Si	pH=7 Fresh Si	pH=10 Etched Si	pH=10 Fresh Si
129							10580.50±103	
131	54.56±7							
135		112.03±11						
139			11.48±3					
144				34.69±6				
147						5.98±2		
149					4.78±2			
153								6.95±2
157							2.90±2	
% of original solution activity	0.82%	1.22%	0.097%	0.36%	0.051%	0.067%	0.052%	0.049%

of incorporation (measured as a percentage of the original solution activity) was of an order of magnitude less than that for silica under comparable conditions. In common with silica, fluorine deposited on the surface of silicon appeared to be inert to radiochemical exchange at low pH. At pH > 3, the counts were too small to obtain reliable data.

2c. Radiochemical uptake of aqueous [^{18}F]-labelled $[\text{HF}_2]^-$ on silica and silicon at pH=1.

In order to quantify the incorporation of [^{18}F]-fluorine on silica and silicon surfaces, experiments were conducted to determine the number of fluorine atoms corresponding to a given degree of incorporation, for silica and silicon substrates exposed to aqueous [^{18}F]-labelled $[\text{HF}_2]^-$ at pH=1. Experimental conditions were similar to those described in Experimental:I.10 with one important exception. To ensure silica and silicon wafers were exposed to similar [^{18}F] activities a standard solution containing [^{18}F]-labelled $[\text{HF}_2]^-$ was prepared, by dissolving [^{18}F]-labelled CsF in the appropriate volume of KHF_2 (1 mol dm^{-3})/HCl (1.04 mol dm^{-3}) solution (i.e. 12 cm^3 for 6 FEP vessels, 8 cm^3 for 4 FEP vessels etc). The resulting combination (pH=1) was dispensed in 2 cm^3 (\pm 0.05 cm^3) aliquots to each FEP vessel. A "blank" FEP vessel, containing the labelled solution only, was counted in order to establish the specific count rate of the solution. The mass of [^{18}F]-labelled CsF (i.e. $\text{Cs}^{18}\text{F} + \text{Cs}^{19}\text{F}$) was known and hence the number of fluorine atoms could be related directly to the specific count rate as follows, assuming the efficiency of counting the solid equals that of the solution:

Each 2 cm³ aliquot contains x mol CsF (i.e. ¹⁸F + ¹⁹F) and y mol KHF₂ (which in each is 2x10⁻⁴ mol). Total "F" is therefore x + 2y mol.

¹⁸F count rate for 2 cm³ "blank" = z count s⁻¹

Therefore specific ¹⁸F count rate = $\frac{z}{x + 2y}$ count s⁻¹ (mol F)⁻¹

or $\frac{z}{(x+2y)N}$ count s⁻¹ (atom F)⁻¹,

where N is the Avogadro constant.

For a wafer exposed to aqueous [¹⁸F]-labelled [HF₂]⁻, removed and dried, where count rate of the wafer is W

"F" atoms on surface of wafer = $W \left[\frac{z}{(x+2y)N} \right]^{-1}$

Fresh silica and silicon, silica and silicon etched prior, silica exposed overnight to an aqueous suspension of cerium(IV) oxide (and so developing a thin film of CeO₂) and layer material isolated from earlier experiments was investigated. Results were expressed and presented as described for the earlier experiments, in Table 7 and Figure 40.

As seen clearly in Figure 40 levels of radiochemical incorporation of fluorine-18 on fresh silica and CeO₂-treated silica were similar and approximately twice those found for etched silica. Fresh and etched silicon displayed incorporation levels of an order of magnitude less than those found for silica under comparable conditions. Figures calculated for fluorine atom coverage, reported at the foot of Table 7, were of the order *ca.* 10¹⁹ - 10²⁰ and

Figure 40

Radiochemical uptake of fluorine-18 on silica and silicon with aqueous [^{18}F]-labelled [HF_2^-] at pH=1

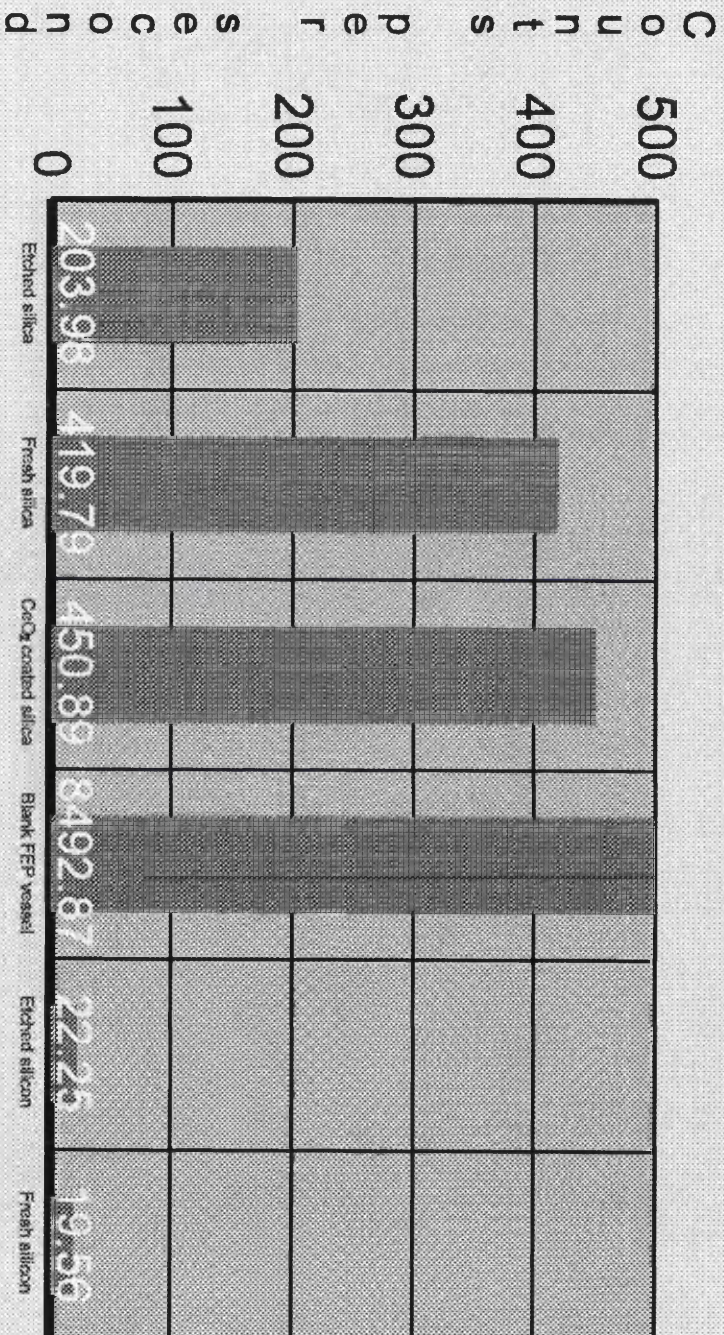


Table 7

Radiochemical uptake (count s⁻¹) of ¹⁸F on silica and silicon with aqueous [¹⁸F]-labelled [HF₂] at pH=1

Time (min)	Etched silica	Fresh silica	CeO ₂ coated silica	Blank FEP tube	Silicon etched	Silicon fresh
0				8507.45±92		
5	8499.5±92					
7		8233.75±91	8507.45±92			
8					10600.95±103	12226.25±111
10	8206.41±91					
11		8927.12±94				
12			6437.82±80			
14				7961.29±89		
65	8541.78±92					
66		8317.10±91			10612.12±103	12795.59±113
67			6515.22±81			
68				8814.40±94		
90	8557.70±92					
91		8326.55±91			10638.94±103	12764.14±113
92			6530.53±81			

Time (min)	Etched silica	Fresh silica	CeO ₂ coated silica	Blank FEP tube	Silicon etched	Silicon fresh
93				8866.80±94		
94	8514.75±92					
99		8572.60±93			10944.55±105	12314.33±11
100			6453.64±80			
101				9222.40±96		
102	8462.26±92					
103		8526.85±92			11567.52±108	12383.52±11
107			6564.80±81			
108				9494.86±97		
109	8579.95±93					
192		419.79±20				
193			450.89±21			
194				8492.87±92		
195	203.98±14					
199					22.25±5	
204						19.56±4
% of original solution activity	2.4%	5.1%	5.3%		0.21%	0.16%
F atoms on surface	5.99x10 ¹⁹	1.23x10 ²⁰	1.32x10 ²⁰		6.54x10 ¹⁸	5.74x10 ¹⁸

10^{18} F atoms for silica and silicon respectively. The pattern of results was in good agreement with previous experiments.

2d. Radiochemical uptake of aqueous [^{18}F]-labelled $[\text{HF}_2]^-$ on silica at pH=1.

In order to substantiate results obtained for silica exposed to aqueous [^{18}F]-labelled $[\text{HF}_2]^-$ at low pH, the preceding experiment was repeated twice for fresh silica, etched silica and CeO_2 -treated silica. The results were tabulated (Tables 8 and 9) and plotted (Figures 41 and 42). It was established that under comparable conditions, levels of incorporation of fluorine on fresh and CeO_2 -treated silica were similar and approximately twice those found for etched silica. Figures calculated for fluorine atom coverage (reported at the foot of Tables 8 and 9) were of the order *ca.* 10^{19} - 10^{20} F atoms in agreement with earlier radiochemical experiments.

C. Identification of reaction intermediate formed during polishing and etching.

During the course of both polishing and etching experiments, a surface layer developed often on silica substrates when the hydrogen difluoride anion was employed at low pH. The material fractured and so was removed easily after washing and drying. In order to identify the chemical components the material was examined by a variety of techniques. The material was a reaction intermediate formed during the polishing process, as described by the "passivating layer" concept (34) which has been invoked in mechanistic explanations for chemomechanical polishing, particularly for silica. Identification of the material has provided the first direct evidence for the

Table 8

Radiochemical uptake (count s⁻¹) of ¹⁸F on silica with aqueous [¹⁸F]-labelled [HF₂]
at pH=1

Time (min)	Fresh silica	CeO ₂ coated	Etched silica	Blank FEP tube
0				310.3±18
4			377.4 ±19	
6		334.10±18		
7	333.3±18			
9				304.28±17
10			398.22±20	
11		332.68±18		
13	348.07±19			
62				311.26±18
64			449.17±21	
66		379.53±19		
68	338.76±18			
70				308.39±18
74			468.18±22	
76		380.49±19		
78	366.68±19			
118				316.77±18
122			419.77±20	
124		363.93±19		
125	401.18±20			
130				308.76±18
150				335.30±18
155			2.90±2	
157		6.99±3		
159	6.50 ±2			
% of original solution activity	6.12%	7.78%	2.4%	
Number of F atoms on surface	5.15x10 ¹⁹	5.54x10 ¹⁹	2.30x10 ¹⁹	

Figure 41

Radiochemical uptake of fluorene-18 on silica with aqueous [^{18}F]-labelled [HF_2^-] at pH=1

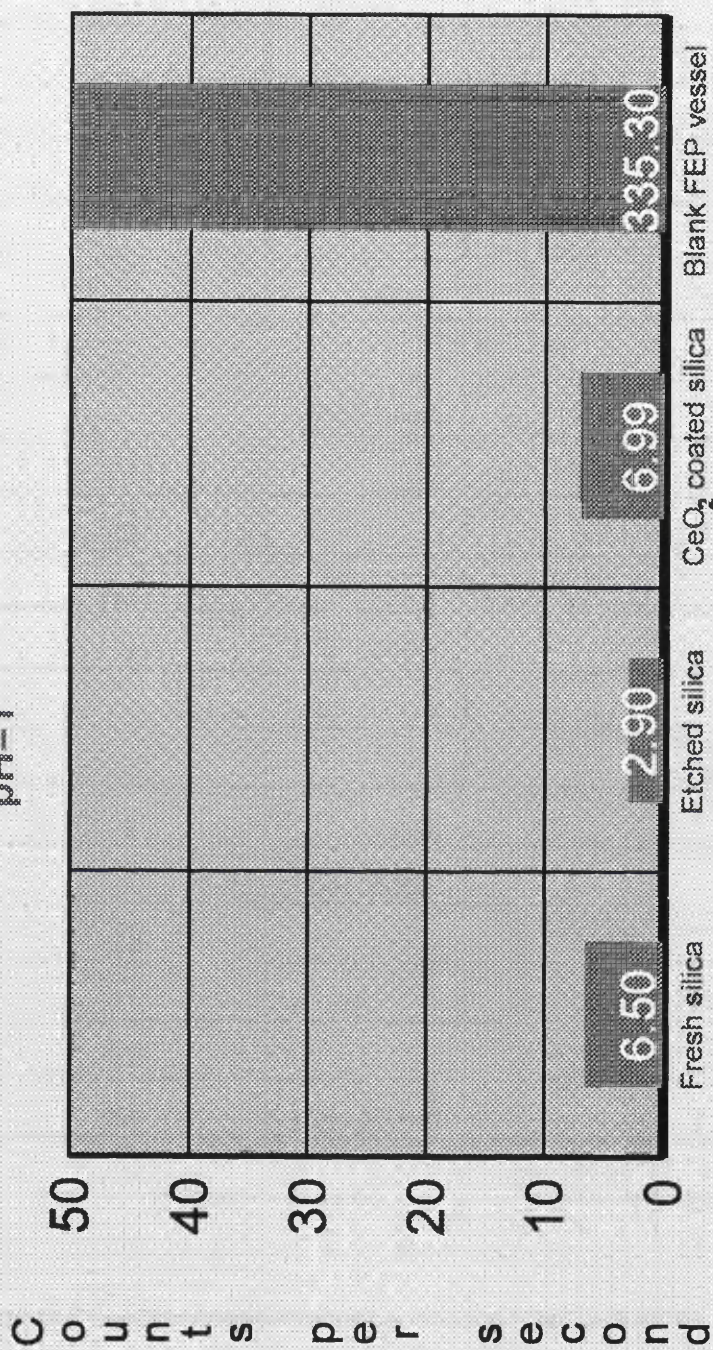


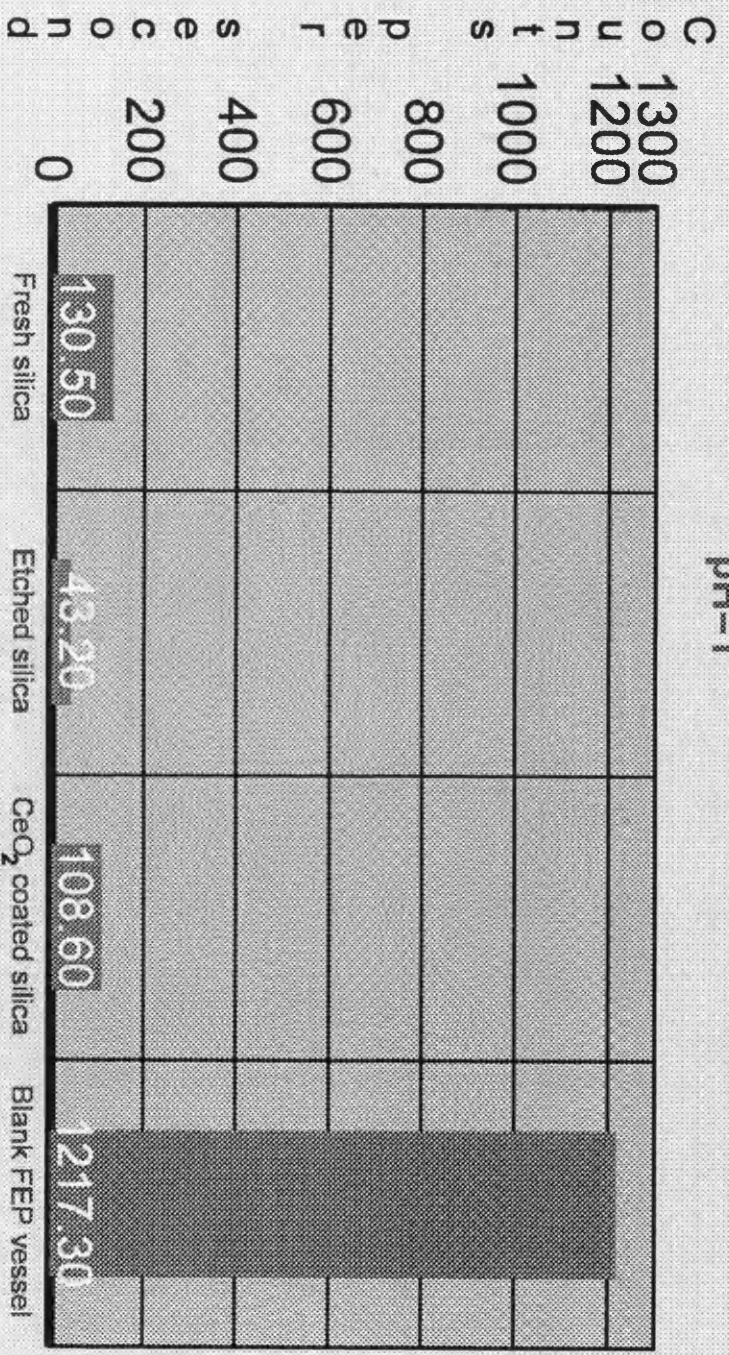
Table 9

Radiochemical uptake (count s⁻¹) of ¹⁸F on silica with aqueous [¹⁸F]-labelled [HF₂]⁻ at pH=1

Time (min)	CeO ₂ coated	Fresh silica	Etched silica	Blank FEP tube
0	1289.45±36			1115.8±33
3		1352.4±37	1002.40±32	
6			1031.47±32	
7	1489.71±39			1125.05±33
11		1497.40±39		
12			1005.04±32	
15				1121.67±33
77	1959.72±44			
78		1446.12±38		
79			1001.87±32	
84				1188.26±34
86	1448.59±38			
88		1384.35±37		
90			1488.83±39	
91				1157.30±34
147	1506.74±39			
148		1585.14±40		
150			1145.90±34	
154				1257.75±35
156	1594.66±40			
158		1378.62±37		
160			1175.76±34	
165				1200.80±35
189	108.6±10			
195		130.5±11		
198			43.2±6	
200				1217.3±35
% of original solution activity	8.42	9.65	4.23	
Number of fluorine atoms on surface	2.40x10 ²⁰	2.89x10 ²⁰	9.53x10 ¹⁹	

Figure 42

Radiochemical uptake of fluorine-18 on silica with aqueous [^{18}F]-labelled [HF_2^-] at pH=1



existence of a passive layer formed on silica.

1. Spectroscopic analysis.

1a. Infrared spectroscopy.

The transmission IR spectra of the material prepared as KBr discs displayed two bands at 740 cm^{-1} and 482 cm^{-1} . Material prepared as a Nujol mull exhibited bands at 742 cm^{-1} , 660 cm^{-1} , and 482 cm^{-1} (Figure 43:a and b). Comparison with literature values led to the initial conclusion that the material contained the $[\text{SiF}_6]^{2-}$ anion (112). It was found however that diffuse reflectance spectra with raw material, or material mixed with KBr or diamond dust, differed significantly from those obtained in transmission mode (Figure 43:c). There was no obvious evidence for K_2SiF_6 under all conditions. Features from $980\text{-}1450\text{ cm}^{-1}$ were consistent with a surface covered with a silica-like species, similar to those for powdered Spectrosil B (Figure 43:d).

The photoacoustic spectra were similar to those obtained by diffuse reflectance although $\nu_3(740\text{ cm}^{-1})$ and $\nu_4(485\text{ cm}^{-1})$ of $[\text{SiF}_6]^{2-}$ were observed. The $1000\text{-}1200\text{ cm}^{-1}$ region was consistent with features associated with a silica-like species, with a sharp peak at 1225 cm^{-1} (Figure 43:e).

IR Microspectroscopy of the material confirmed the presence of ν_3 of $[\text{SiF}_6]^{2-}$, albeit the ν_4 band was obscured (Figure 43:f). Features observed between $1100\text{-}1120\text{ cm}^{-1}$ and 1255 cm^{-1} were similar to those observed in the photoacoustic spectra associated with a silica-like species (113).

Figure 43: Infrared spectra of passive layer material

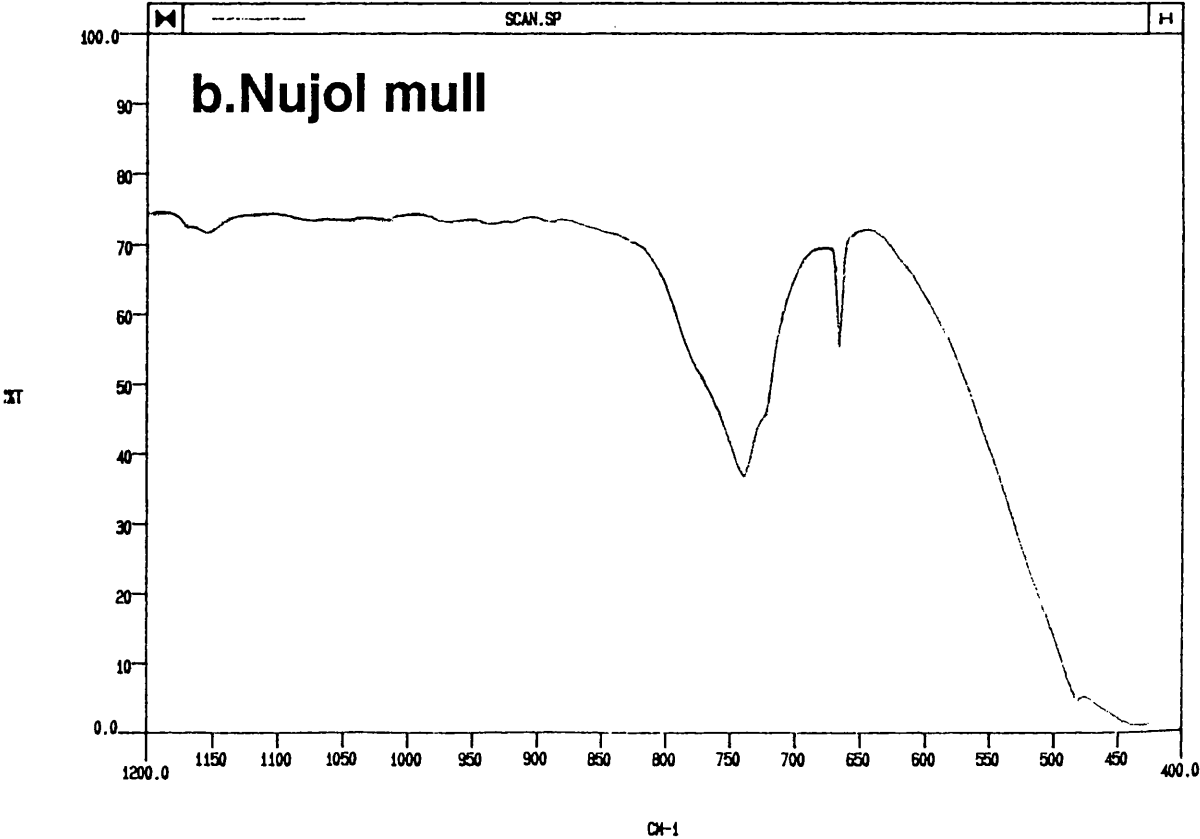
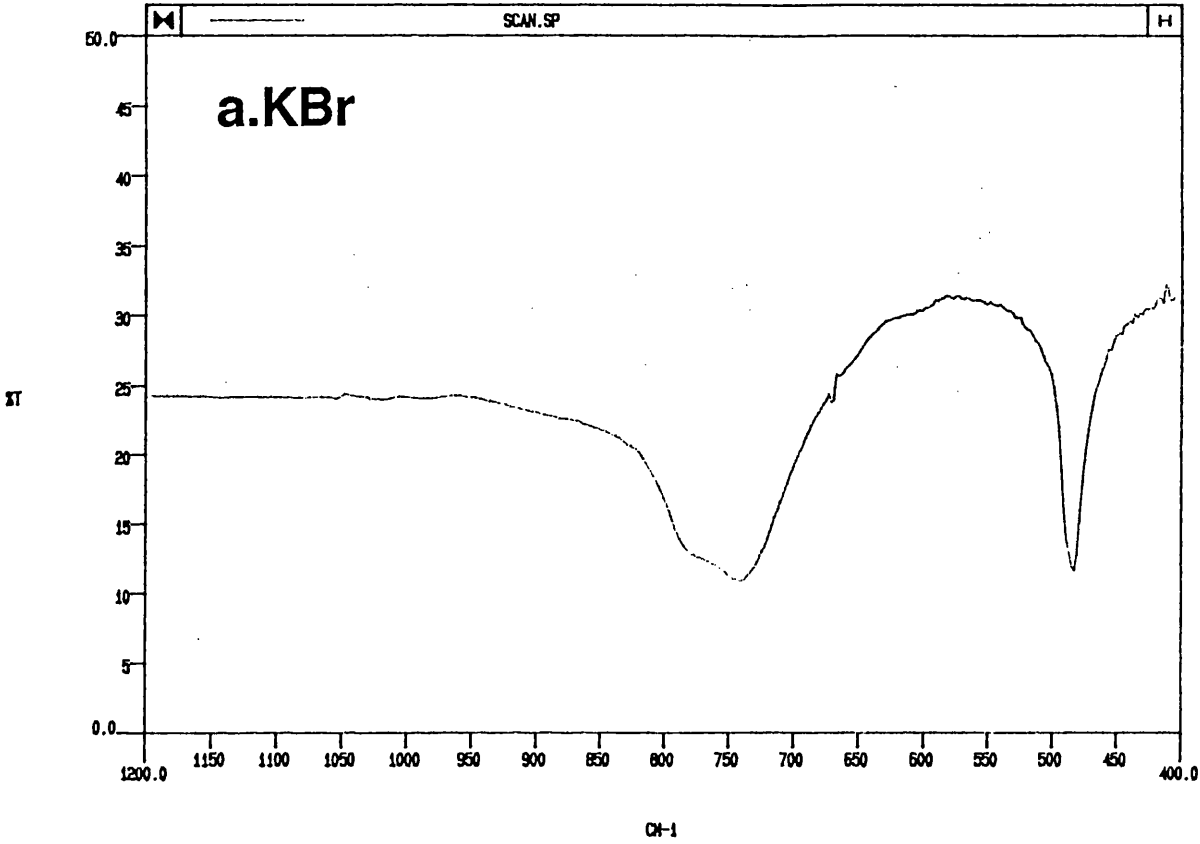


Figure 43: Infrared spectra of passive layer material

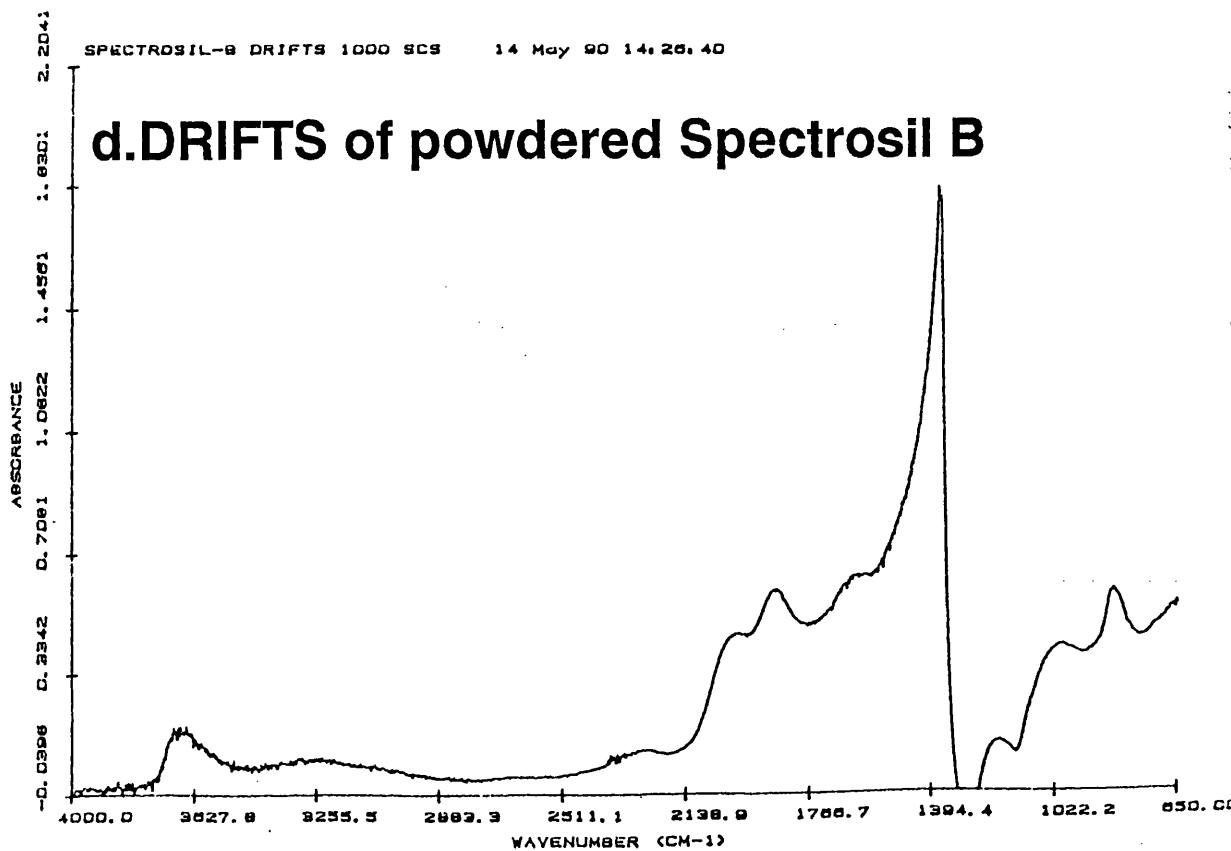
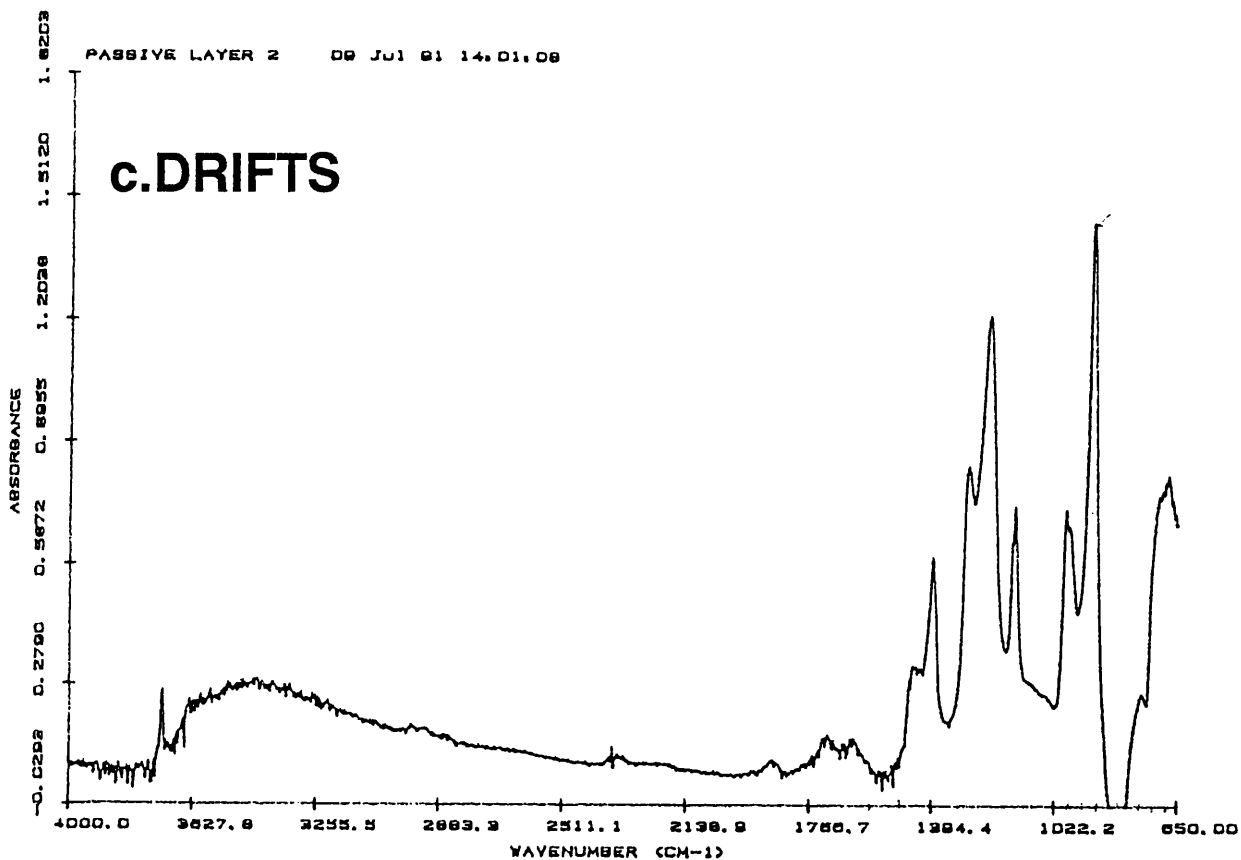
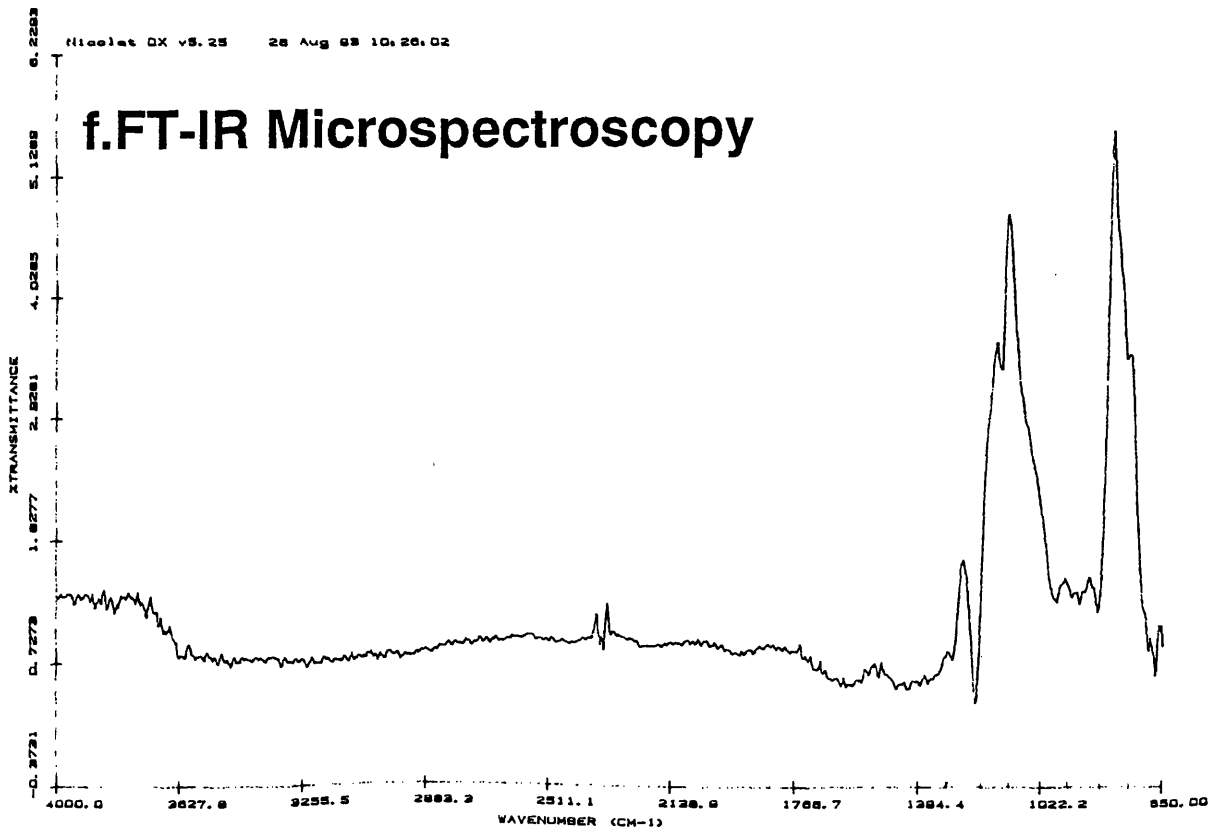
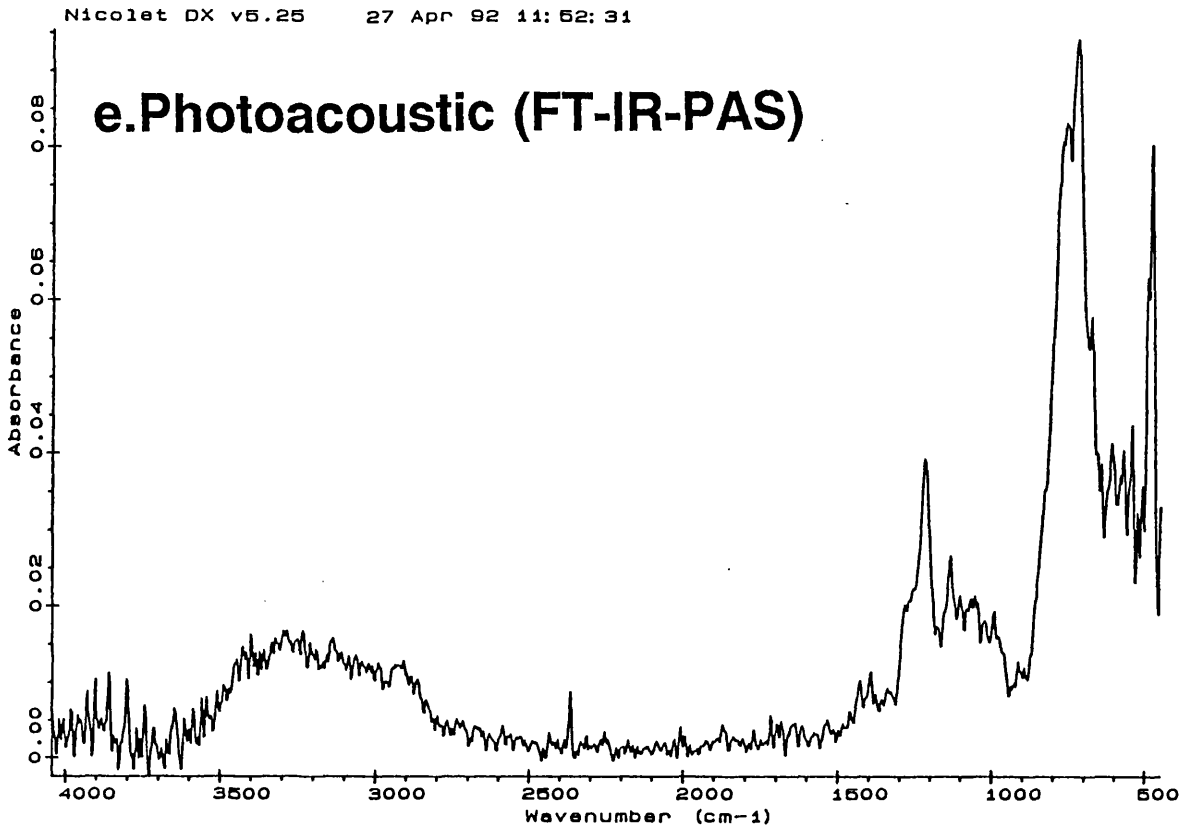


Figure 43: Infrared spectra of passive layer material

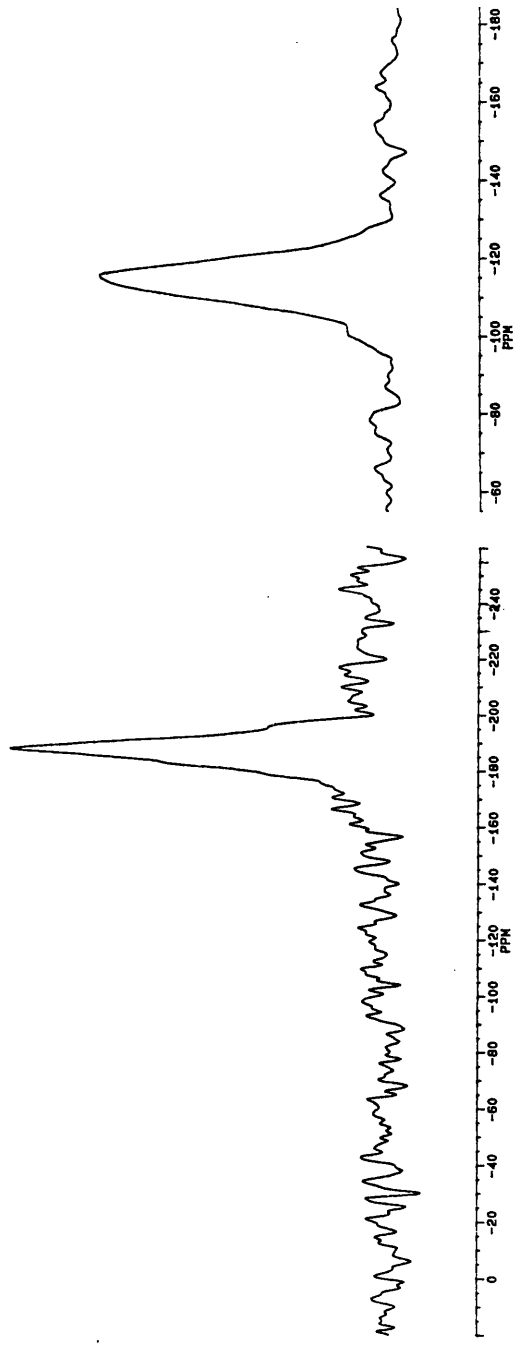


1b. ^{29}Si Magic-Angle-Spinning Nuclear Magnetic Resonance Spectroscopy (MAS-NMR).

The apparent heterogeneous nature of the passive layer material made study by MAS-NMR spectroscopy suitable, as chemical shifts are influenced only by the short-range environment of the nucleus in question, whereas diffraction techniques (see Results:C.2) require long-range order. The passive layer material isolated from etching experiments (see Results:B1.a5) displayed a single peak in several ^{29}Si MAS-NMR spectra recorded, at -186 to -188 ppm (Figure 44:a) relative to TMS, typical for octahedrally coordinated silicon (90). Spectra of silica (Spectrosil B) and silicic acid, $\text{Si}(\text{OH})_4$, were recorded under similar conditions to allow comparison with "passive layer" material (Figure 44: b and c). Only signals attributable to tetrahedrally coordinated silicon were observed.

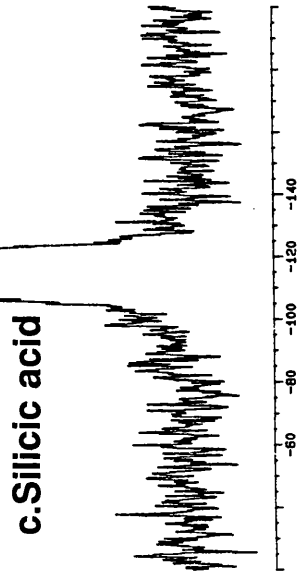
In an attempt to reduce line broadening caused by dipolar interactions (due to the presence of protons from water), the technique of High Power Proton Decoupling (HPPD) was used. HPPD provides high resolution spectra of dilute spins such as ^{29}Si where normal spinning speeds are inadequate. There appeared however to be little enhancement for any of the samples examined (Figure 44:d).

In order to circumvent the problem of long interpulse times for ^{29}Si (spin lattice relaxation time *ca.* 50 min) coupled with the condition that samples were left in the spectrometer for magnetisation many hours before the first pulse could be applied, the technique of cross-polarisation (CP) was employed. CP methods relate the experimental timescale to ^1H proton relaxation times which are much shorter than those for ^{29}Si . For all passive layer samples there was



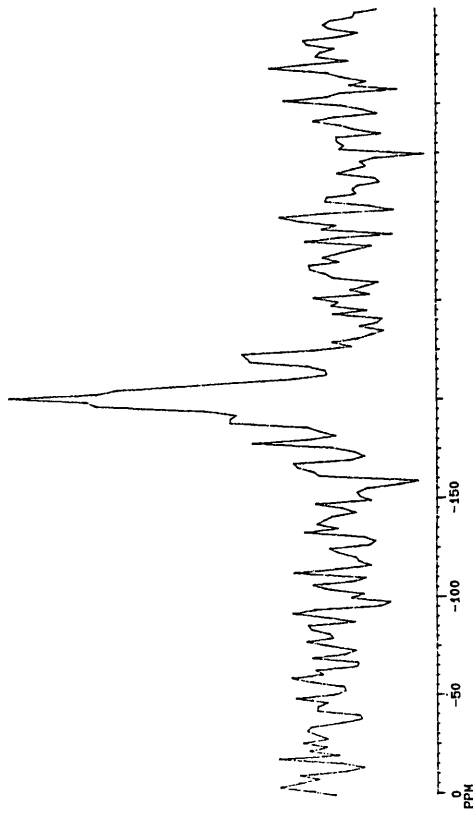
a. Material isolated from etching experiments

b. Spectrosil B powder



c. Silicic acid

d. HPPD of layer material



e. CP of silicic acid

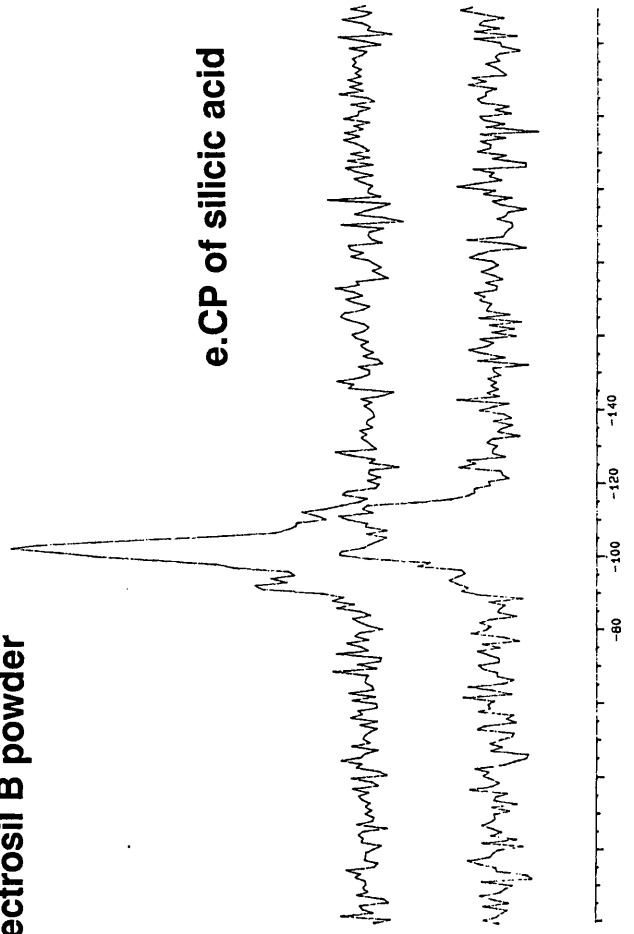


Figure 44: Silicon-29 MAS-NMR spectra

no evidence for signal enhancement using CP; in contrast the effect was observed clearly for silicic acid (Figure 44:e).

2. Powder X-ray diffraction.

Layer material isolated from polishing and etching experiments was examined by powder X-ray diffraction in order to substantiate results obtained by spectroscopic methods. Samples were prepared as an acetone slurry or as material mounted on sellotape. The former produced diffraction patterns consistent with a material amorphous in nature in contrast to the latter, which produced defined diffraction lines and was more informative. The pattern of results was consistent with a material composed of cubic and hexagonal modifications of K_2SiF_6 . As may be seen clearly from Table 10 the production of hexagonal K_2SiF_6 appeared to be dependent on solution pH, as material isolated from etching experiments at pH=3 (Table 10:B and F) contained less hexagonal K_2SiF_6 than material isolated from both polishing and etching experiments at pH=1. For all samples examined, cubic K_2SiF_6 was the predominant material. There was no firm evidence for the presence of silica in the material, although two diffraction lines could not be indexed ($2\theta=41^\circ$ and 47°).

3. Elemental analysis.

Material isolated from both polishing and etching experiments was analysed quantitatively for potassium and fluorine. Potassium analysis was accomplished by flame photometry and fluorine by titration. Fluorine was

Table 10

XRD analysis of layer material isolated from polishing and etching experiments

2θ/ degrees	Line intensities							
	A	B	C	D	E	F	G	H
22 ^c	100	100		80	100	100	100	100
24 ^b	20	5	40	20	20		20	15
31 ^b	25	5	40	20	20	5	30	20
36 ^a	50	80		45	65	30	80	60
37 ^b	10			5		5	5	5
39 ^b	5		20			5		
41	5		5				5	
43 ^c	5	10	20	10	20	5	5	5
45 ^c	30	60		35	50	25	60	60
46 ^b			10	5	5	5	15	10
47			5			5		
49 ^b	60	10	100	100	100	15	70	55
52 ^a	80	80	80	70	80	80	80	80
56 ^b	5		20	10	5	5	5	5
59 ^a	10			5	5	10		
65 ^a	5				5	5	5	10
70 ^a	5			5	5	5	5	5

^aLines attributed to cubic K₂SiF₆

^bLines attributed to hexagonal K₂SiF₆

^cLines common to both cubic and hexagonal K₂SiF₆

^{a,b,c} Joint Committee for Diffraction Standards, International Centre for Diffraction Data

A,C,G,H; material from etching experiments, pH=1 (see Results:B.1a.5)

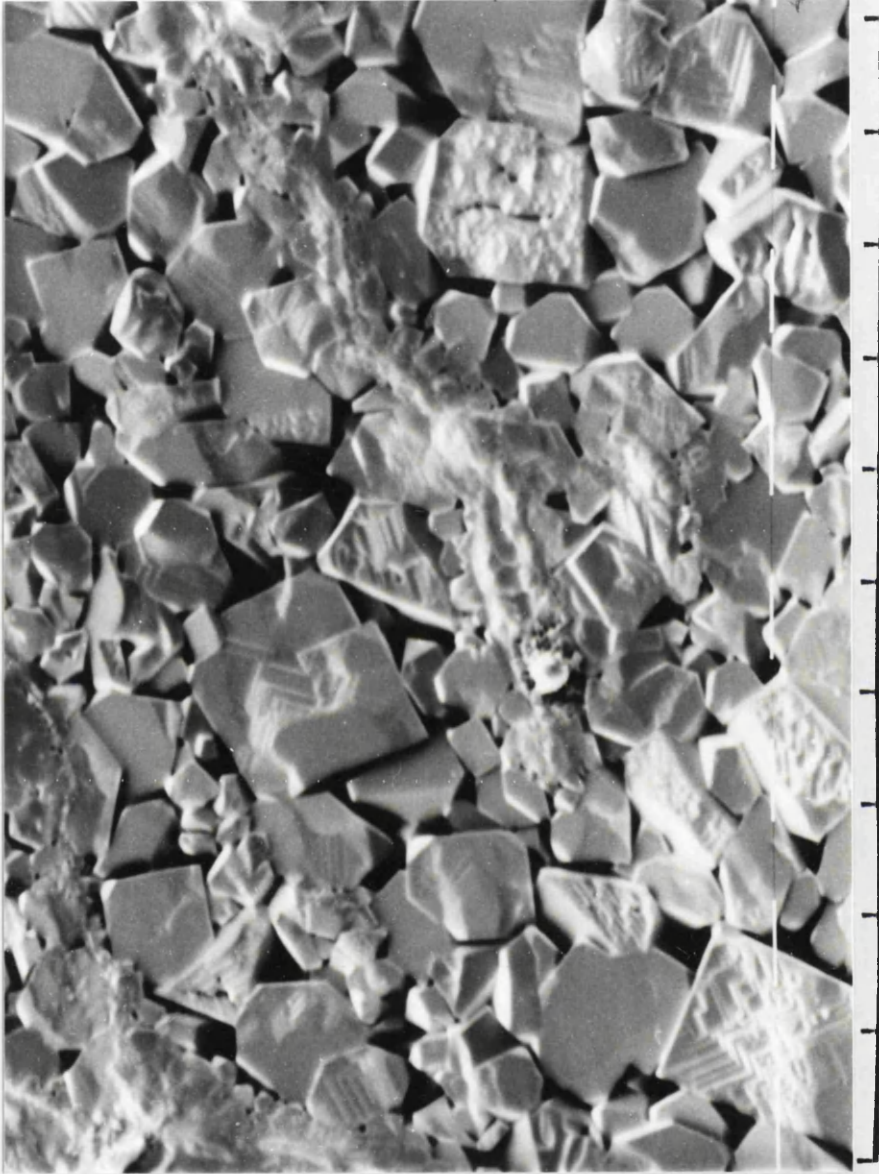
B,F; material from etching experiments, pH=3 (see Results:B.1a.5)

D,E: material from polishing experiments with Pilkington reagent (see Results:A.1a)

found to be present in the range 44-53% by weight (% F = 51.7 for K_2SiF_6) and potassium 11-14% by weight (% K = 35.5 for K_2SiF_6). Various explanations were proposed for the inconclusive nature of the results. Interference by fluorine or silicon in the flame photometry measurements for potassium and interference by silicon in the fluorine analysis were a possibility. An alternative explanation was for the presence of impurities in the material suspected as K_2SiF_6 . K:F ratios for each sample were determined and in each case were different. Levels of fluorine were lower than anticipated although consistent with material undergoing hydrolysis in contrast to the low levels of potassium, which could not be explained by a similar argument.

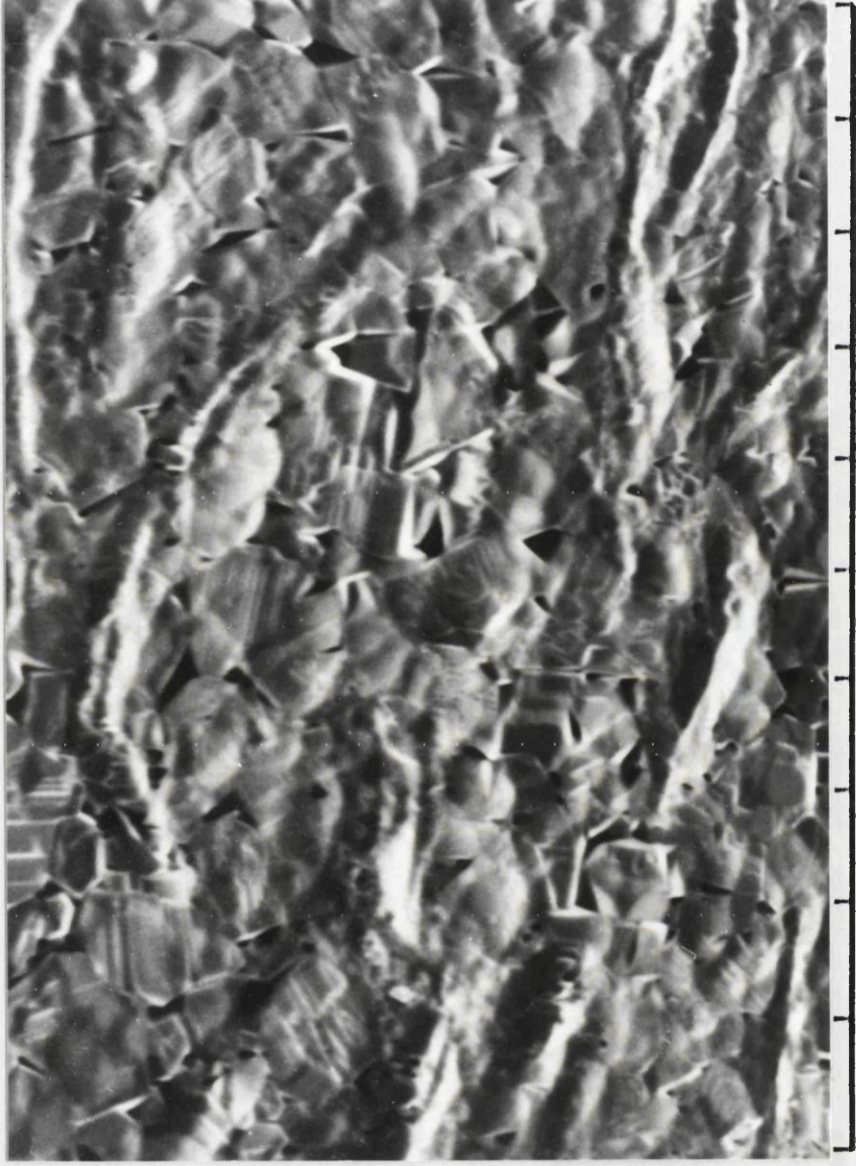
4. Scanning Electron Microscopy.

Layer material isolated from model etching experiments (see Results:B.1a) was examined by SEM in order to gain information on surface morphology. The material appeared to consist of two crystalline components in an irregular matted complex, with twinning between crystals (Figures 45, 48, 49, 50, 51, 53, 54 and 55). Washing with water removed the matrix from the surface of a silica wafer, dissolving one of the components in the process. For material prepared at pH=1, silica wafers and thick flakes of layer material remained after washing. These had a rippled surface (Figures 46, 47 and 55), while for material prepared at pH=3 this was not the case (Figure 45). The two crystalline components were accompanied often by a spongy material (Figures 45 and 54). The majority of the layer matrix was composed of euhedral octahedra displaying a perfect cleavage (typical of crystals belonging



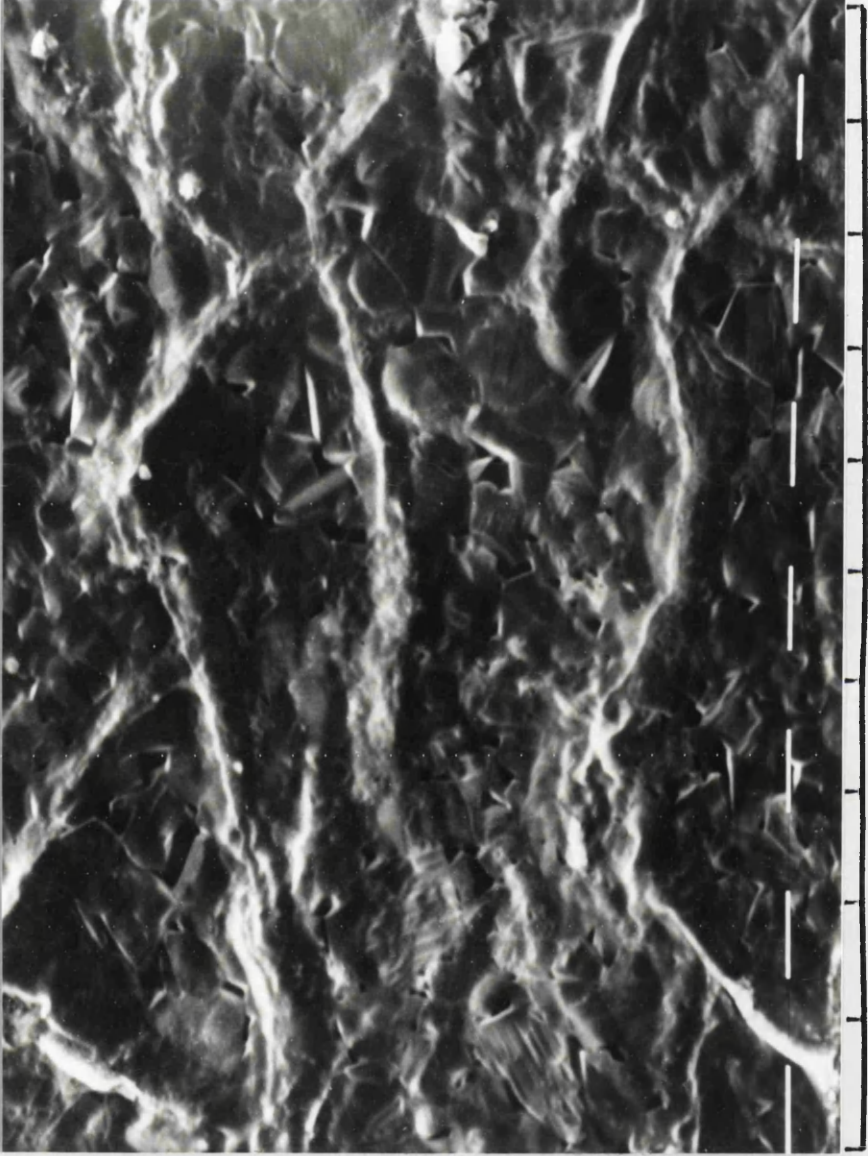
Magnification x800; 1 division=14 micron

Figure 45: SEM of passive layer material



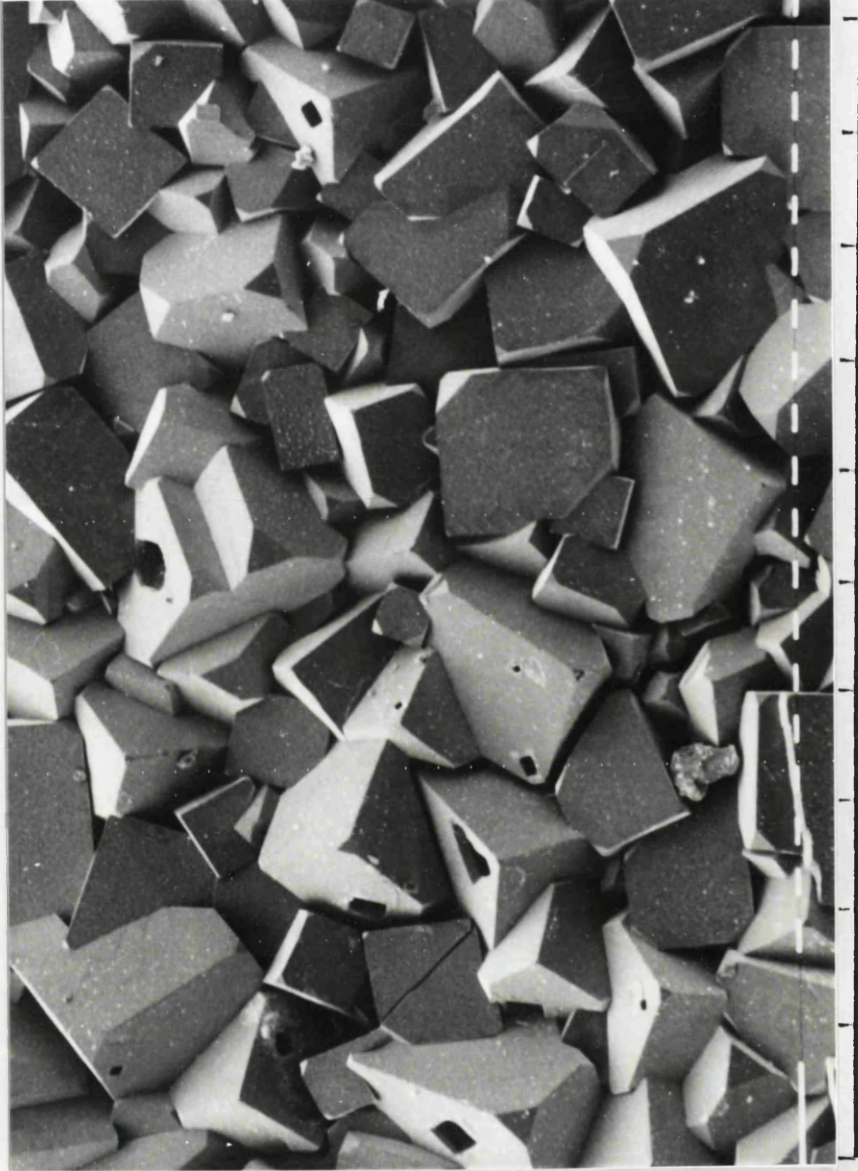
Magnification x800;1 division= 14 micron

Figure 46: SEM of passive layer material



Magnification x800; 1 division = 14 micron

Figure 47: SEM of passive layer material



Magnification x200; 1 division = 44 micron

Figure 48: SEM of passive layer material



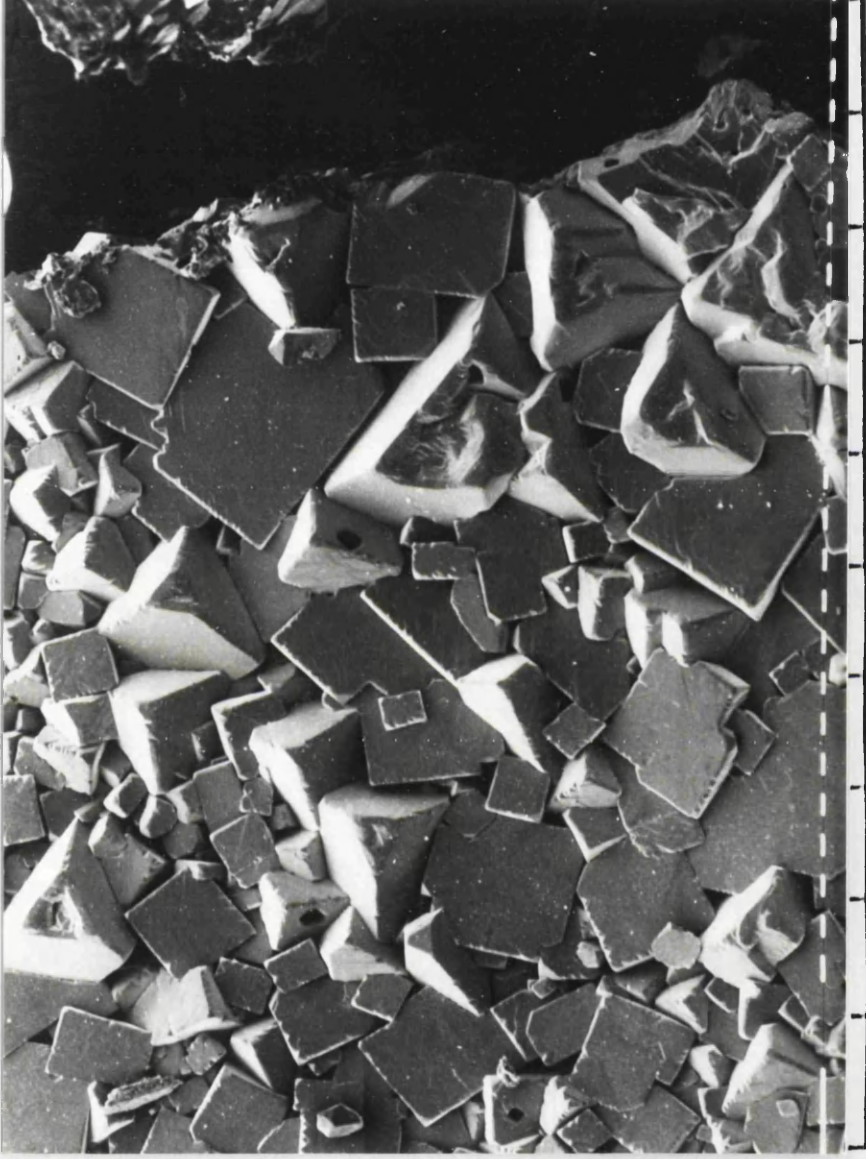
Magnification x200;1 division=54 micron

Figure 49: SEM of passive layer material



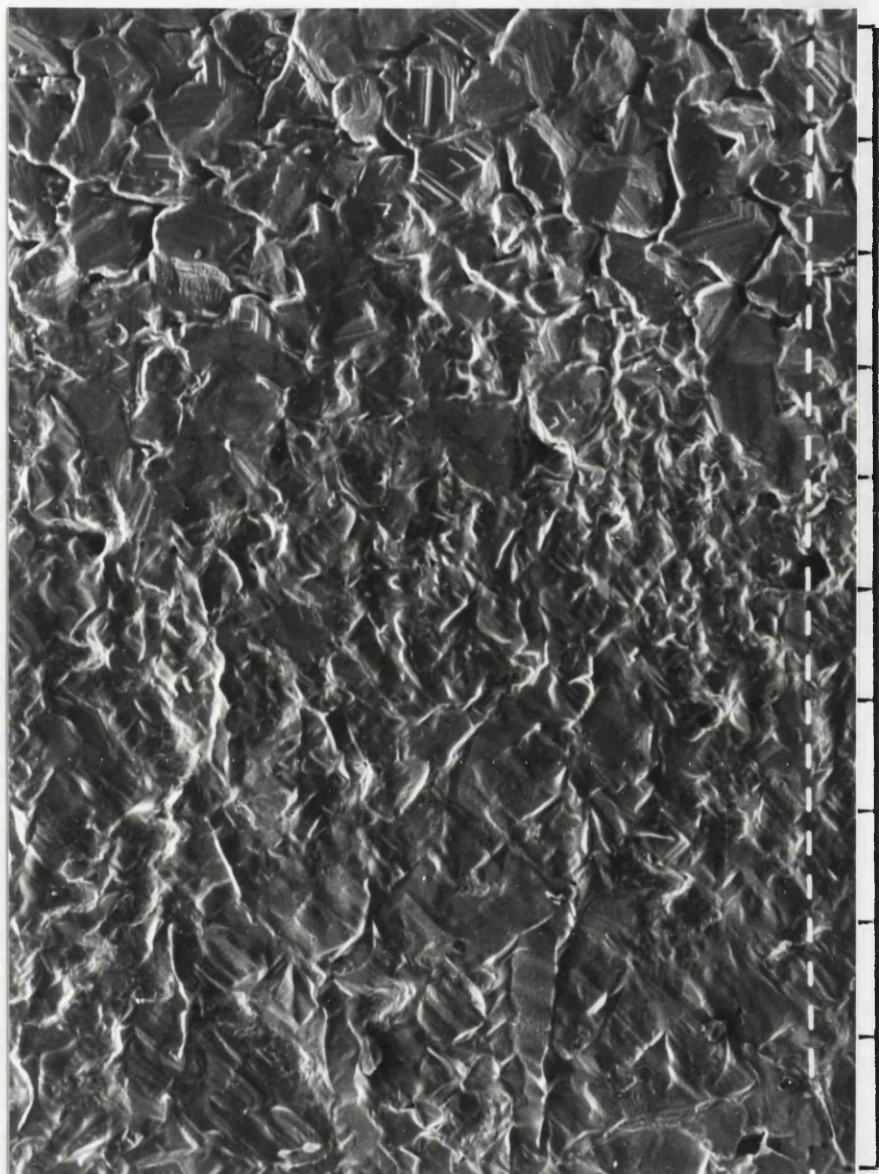
Magnification x200;1 division= 54 micron

Figure 50: SEM of passive layer material



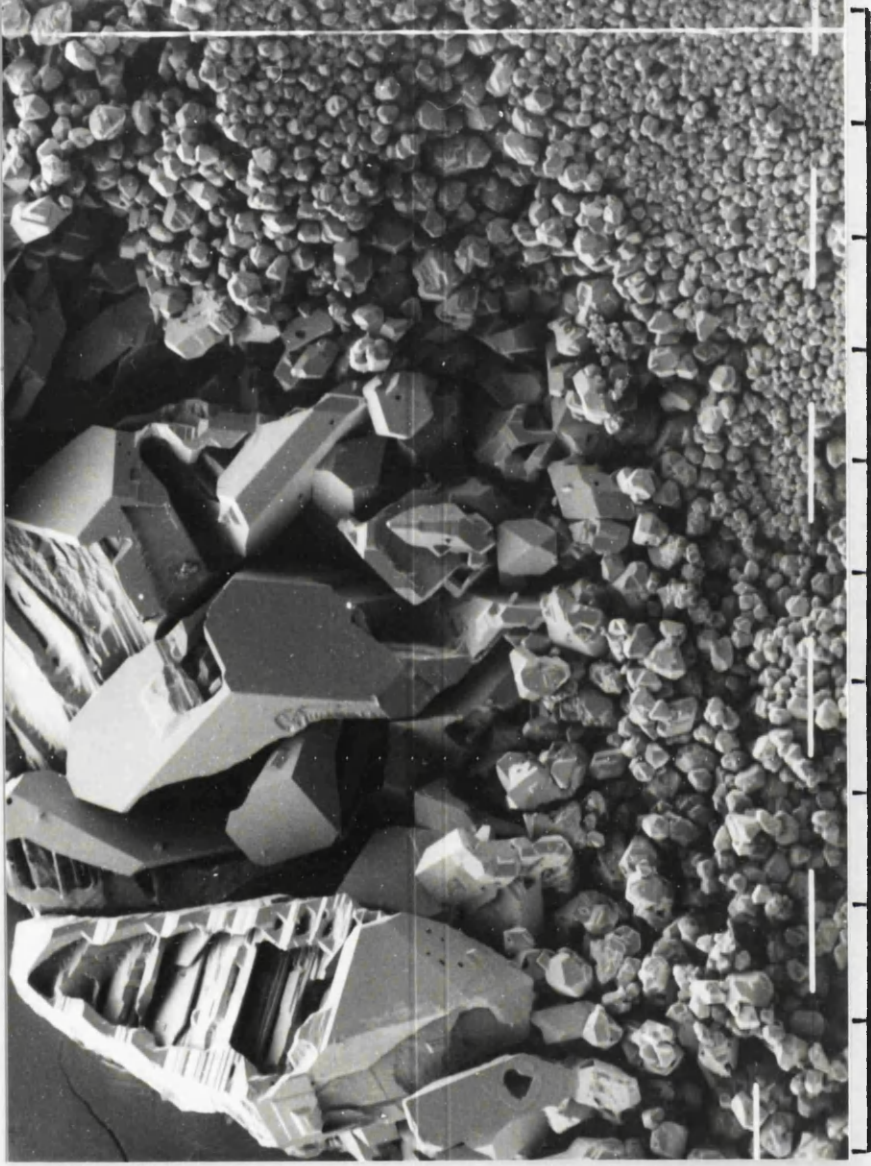
Magnification x200;1 division=54 micron

Figure 51: SEM of passive layer material



Magnification x200;1 division= 54 micron

Figure 52: SEM of passive layer material



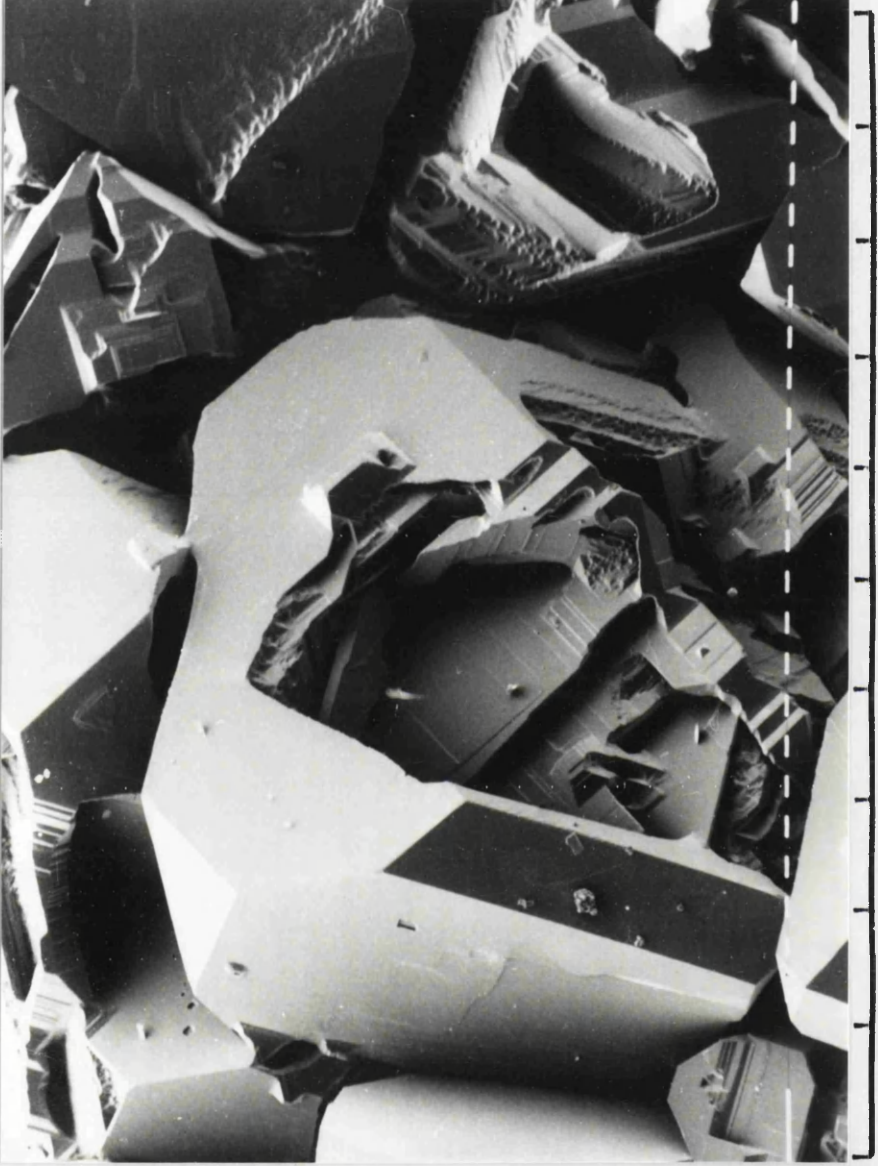
Magnification x100; 1 division=100 micron

Figure 53: SEM of passive layer material



Magnification x200; 1 division=54 micron

Figure 54: SEM of passive layer material



Magnification x200;1 division=54 micron

Figure 55: SEM of passive layer material

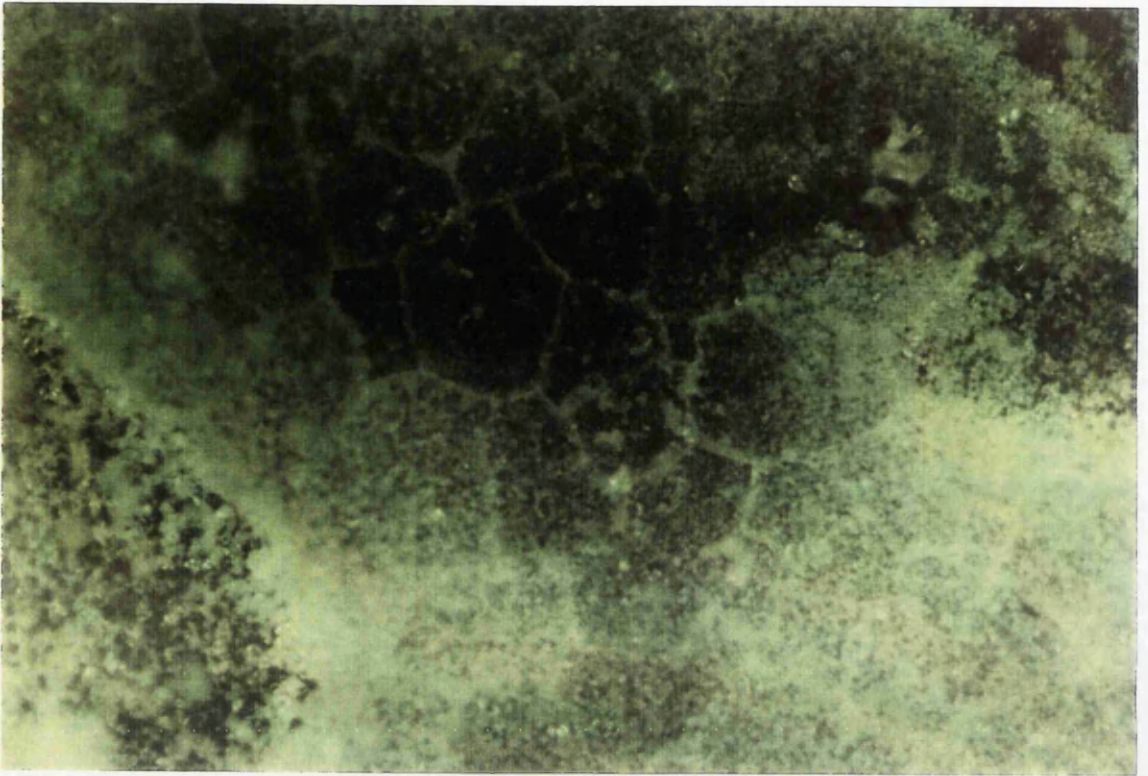
to the cubic system where uneven development of the faces mask the regular symmetry). Some of these crystals, from material formed at pH=1, displayed hexagonal etch pits where the edges of the pits were not parallel to the faces of the crystal (Figure 49). This feature would be consistent with a crystal belonging to the hexagonal system. The second type of crystals observed were composed of thin based platelets of poor cleavage, typical of crystals belonging to the trigonal system (Figures 45, 48, 49, 50, 51, 53, 54 and 55). Larger platelets displayed conchoidal fracture (Figure 55).

The above observations were consistent with a material composed of crystalline cubic K_2SiF_6 (with evidence for some hexagonal modification) and dense spongy K_2SiF_6 (found naturally in stactitic concretions (114)) with crystalline quartz. It was however not possible to conduct powder X-ray diffraction analysis of the material to make positive identifications.

5. Nomarski light microscopy.

Under plane polarised light the material appeared to consist of compact flakes with areas of crystalline and spongy aggregates, but under the low magnification employed (x80) it was difficult to examine discrete crystals (Figure 56:a). Edges of layer material appeared to show conchoidal fracture (Figure 56:b). Examination under cross polars indicated the material was largely isotropic (or amorphous) as it appeared dark, although rotation of the stage produced tinges of white/yellow in small areas. Edges of layer material were light under cross polars, consistent with a material exhibiting stress birefringence.

**Figure 56:Nomarski light microscopy
of passive layer material**



a.Layer material composed of crystalline and spongy aggregates



b.Conchoidal fracture at edge of layer material on silica wafer

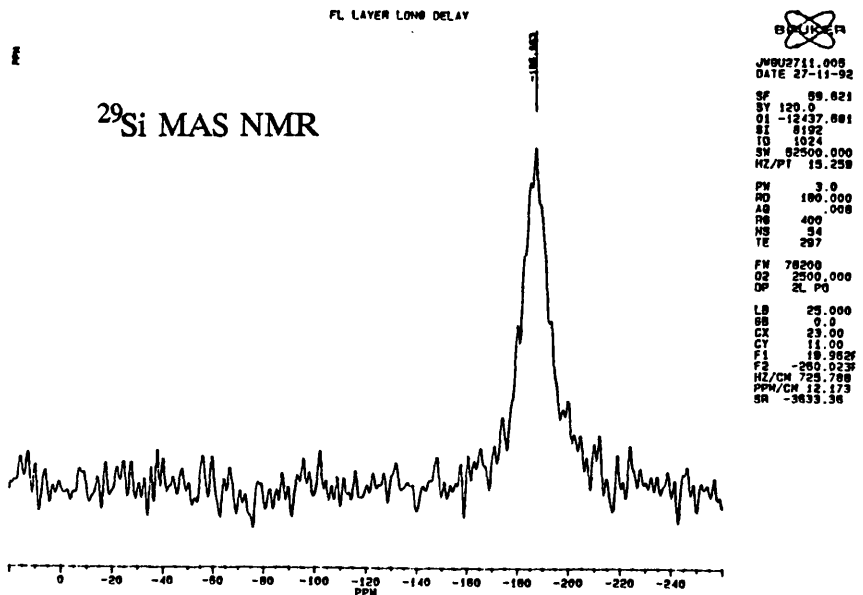
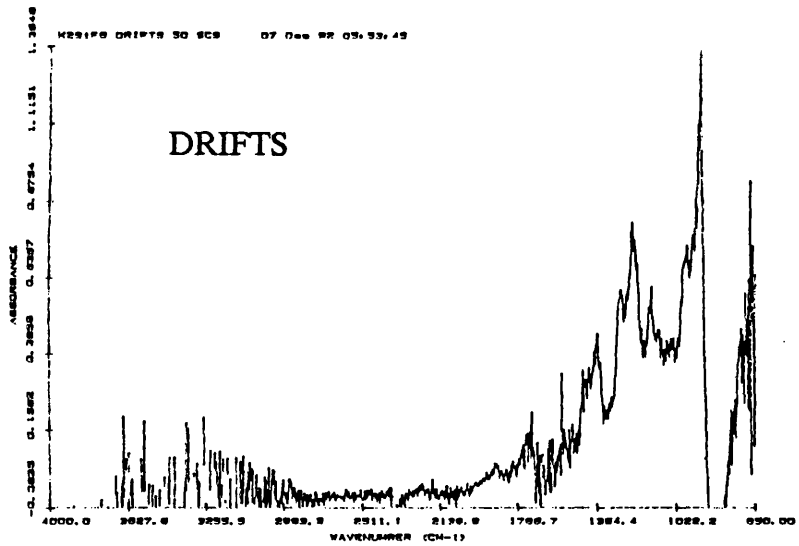
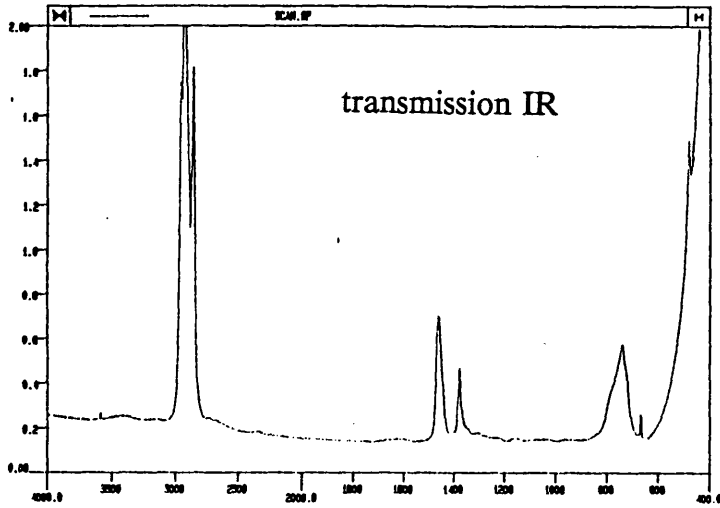
6. Comparison of authentic K_2SiF_6 with reaction intermediate.

A comparison of the spectroscopic characteristics of material isolated from polishing and etching experiments (see Results:B.1a) with synthetic K_2SiF_6 (115) was conducted. The compound K_2SiF_6 is found as cubic crystals, white to grey or colourless, of vitreous lustre. It exists naturally as stalactitic concretions (dense to spongy in texture) in areas of volcanic activity. A hexagonal modification is known only as an artificial compound. The transmission IR spectrum of K_2SiF_6 prepared as a KBr disc exhibits two intense bands assigned as $\nu_4(F_{1u})$ at 491 cm^{-1} and $\nu_3(F_{1u})$ at $745\text{-}780\text{ cm}^{-1}$ of $[SiF_6]^{2-}$ (112). K_2SiF_6 left in moist air for several hours produced reflectance (DRIFTS) and ^{29}Si MAS NMR spectra which resembled closely those of material isolated from polishing and etching experiments (Figure 57).

D. Electronic and infrared spectroscopic analysis of supported thin organic films prior to and after chemical modification.

Polycyclic aromatic hydrocarbons (PAHs) and phthalocyanines are good π -donors and an obvious way of modifying their electronic properties is via the formation of charge-transfer complexes (see Introduction:E) with electron acceptor moieties, such as volatile Lewis acid halides adsorbed on the surface of a film. Incomplete charge-transfer is expected for halides of relatively low electron affinity (such as PF_5) but complete transfer of an electron (or electron pair) is anticipated for stronger oxidizing agents (such as MoF_6 or AsF_5). In this work a number of PAHs were prepared as thin films on chemomechanically polished silica and silicon wafers (see Experimental:C) and examined by

Figure 57: Comparison of authentic K_2SiF_6 with passive material



electronic and infrared spectroscopies, prior to and in many cases after chemical modification with MoF_6 , WF_6 , AsF_5 , PF_5 and BF_3 and the solid organic electron acceptor 7,7,8,8-tetracyano-p-quinodimethane (TCNQ) (Figure 58).

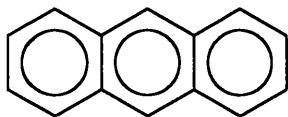
The presence of an aromatic system can in principle be detected readily by infrared spectroscopy, as aromatic compounds exhibit a characteristic C-H stretching absorption at 3030 cm^{-1} and a series of peaks in the $1450\text{-}1600\text{ cm}^{-1}$ region. It was anticipated that thin film reactions, employing silicon substrates as supports using the evacuable reaction gas cell fitted with silicon windows (transparent to IR radiation in the region of interest) would yield information, such as whether or not the interaction of the PAHs with electron acceptors would produce ionic compounds/radical cation salts. For weak interactions the infrared spectrum of a complex is the superposition of the spectra of the neutral donor and acceptor species, whereas with stronger interactions the spectra correspond closely to the sum of the spectra of the radical cation and the counter-anion. It was found however that films of PAHs on silicon substrates were intractable in the transmission mode. IR reflectance spectroscopy was employed therefore to examine thin films on silica substrates prior to chemical modification in order to investigate, for example, whether or not the process of preparing thin films produced changes in the chemical and physical nature of the compounds in question.

Electronic spectra were recorded and reported as peak positions $\lambda_{\text{max}}(\text{nm})$ with absorption coefficients $10^{-4}\alpha^*$ (where Absorbance = $\alpha^*(\text{cm}^{-1}) \times$ film thickness (cm)) prior to and after exposure to oxidants. Absorbance units on the axes of the electronic spectra are arbitrary. Results are summarised

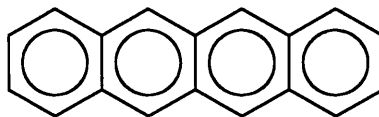
Figure 58: Compounds used to prepare thin films

Cata-condensed polycyclic aromatic hydrocarbons:

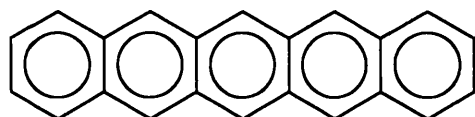
The acene series, linear planar alternate hydrocarbons.



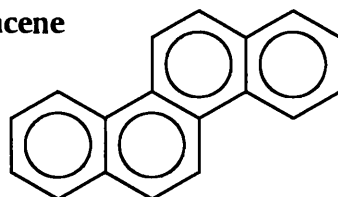
Anthracene



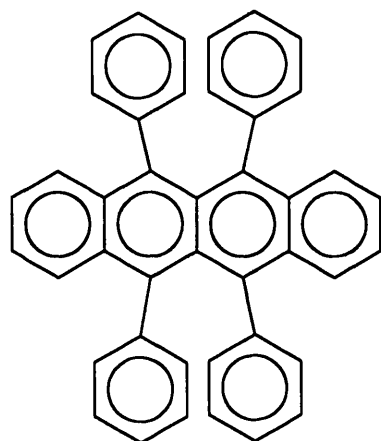
Tetracene



Pentacene

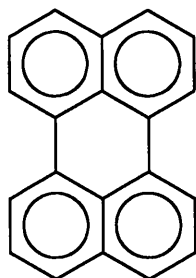


Chrysene, an angular cata-condensed hydrocarbon

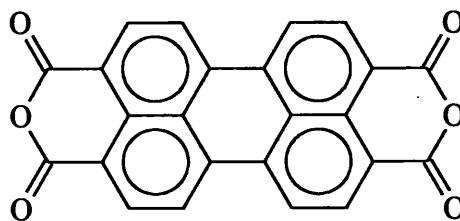


Rubrene, a non-planar hydrocarbon

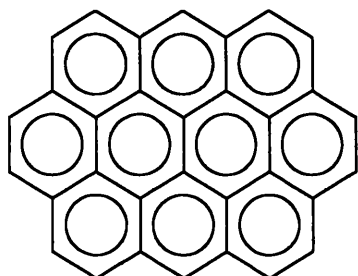
The peri-condensed hydrocarbons:



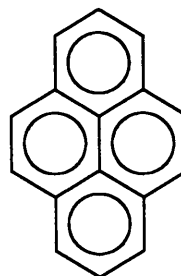
Perylene



Perylene tetracarboxylic dianhydride



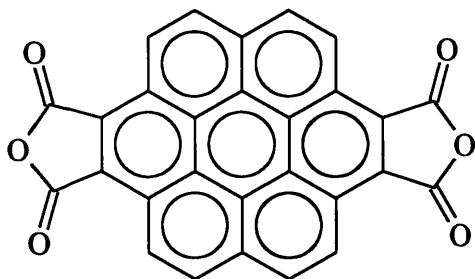
Ovalene



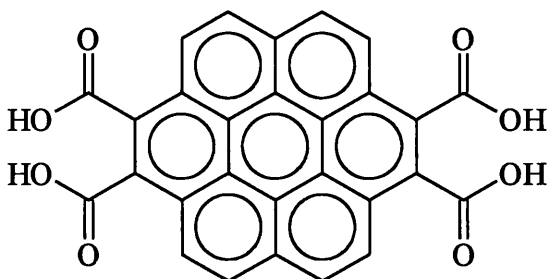
Pyrene

Figure 58: Compounds used to prepare thin films

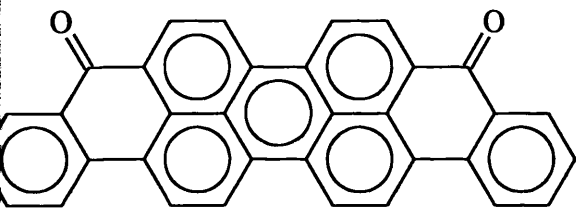
The peri-condensed hydrocarbons (cont.)



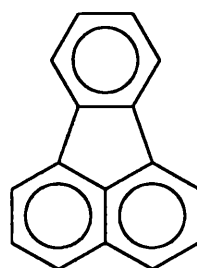
Coronene tetracarboxylic dianhydride
CTCDA



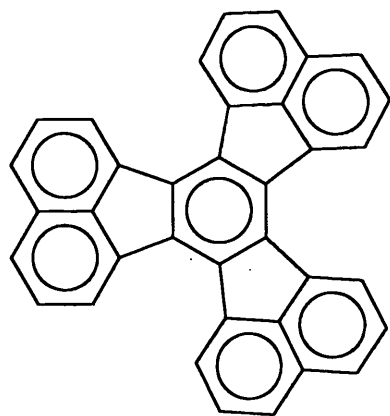
Coronene tetracarboxylic acid
CTA



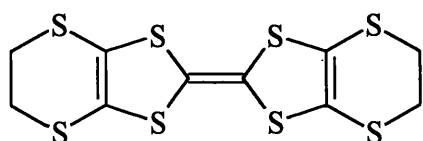
Violanthrone



Fluoranthene

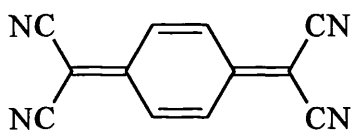


Decacycene, a non-planar non-alternate polycyclic aromatic hydrocarbon



Bis(ethylenedithio)tetrathiafulvalene (BEDT-TTF)

The building block for many organic molecular conductors



7,7,8,8-tetracyano-p-quinodimethane (TCNQ)

An organic electron-acceptor molecule

Table 11a: Electronic absorptions additional to those assigned to the components

DONOR	Effect of increasing film thickness (ca. 50-1000nm)	Acceptor species		
		^{a,b} MoF ₆	^{a,b} WF ₆	^{a,b} AsF ₅
Perylene	Little loss in resolution	1000(3.76), 660(4.40) and 495(5.60)	623(13.23), 479(13.24) and 407(17.70)	1230(5.46), 650(4.36) and 490(4.77)
BEDT-TTF	Loss in resolution	895(0.9), 775(3.69), 758sh (3.52) and 710sh (1.88)		
Violanthrone	Complete loss in resolution	920(12.44), 725(6.32)	No evidence for reaction	890(1.58) and 690(3.71)
Pentacene	Loss in resolution	975(0.82) and 785(4.92)	No evidence for reaction	No evidence for reaction
Ovalene	Loss in resolution	962(3.62), 850(2.87), 670(3.89) and 620(3.6)	1000(0.91), 750(2.57) and 550(5.5)	1000(9.07), 750(9.12) and 550(10.02)
Tetracene	No loss in resolution	775(4.11), 725sh (4.99), 670(25.04) and 610sh (8.81)	No evidence for reaction	1010(3.11), 765(1.8), 675(0.98) and 625(0.82)
Rubrene	Interference patterns formed. Loss in resolution.	780(4.59) and 615(10.01)	No evidence for reaction	No evidence for reaction

^aBand positions λ_{max} (nm)

^bNumbers in parentheses refer to the absorption coefficient $10^4\alpha^*$,

where Absorbance $=\alpha^*(\text{cm}^{-1})\times\text{film thickness}$

Table 11b: Electronic absorptions additional to those assigned to the components

DONOR	Effect of increasing film thickness (ca. 50-1000nm)	Acceptor species		
		^{a,b} MoF ₆	^{a,b} WF ₆	^{a,b} AsF ₅
PTCDA	Loss in resolution	770(4.42) and 620(4.59)	No evidence for reaction	
Coronene TCDA	Loss in resolution	500(14.51)	No evidence for reaction	No evidence for reaction
Coronene TC Acid	Loss in resolution	No evidence for reaction	No evidence for reaction	No evidence for reaction
Decacyclene	Complete loss in resolution	770(3.17)	No evidence for reaction	No evidence for reaction
Chrysene	Loss in resolution	925(1.2), 680(1.47), 533(2.0) and 455(2.82)	680(1.09) and 500(1.36)	560(0.68), 480(0.8) and 433(0.91)
Anthracene	Loss in resolution. Films unstable under vacuum.	920(0.52), 720sh (0.52), 510sh (0.67) and 405sh (0.88)	460(2.3)	430(2.48)
Fluoranthene	Loss in resolution. Films unstable under vacuum.	No evidence for reaction	No evidence for reaction	No evidence for reaction
Pyrene	All spectra dominated by interference patterns.			750

^aBand positions λ_{max} (nm)

^bNumbers in parentheses refer to the absorption coefficient $10^4\alpha^*$,

where Absorbance = α^* (cm⁻¹) × film thickness

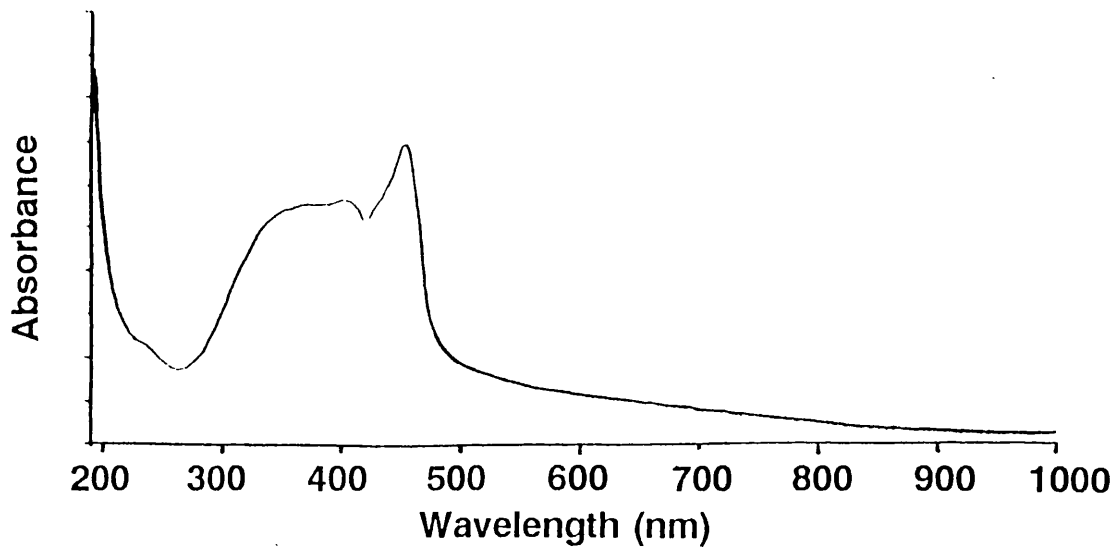
in Table 11. Representative examples of infrared spectra of thin films on silica are included later in the chapter.

1. Electronic spectra.

a. Perylene.

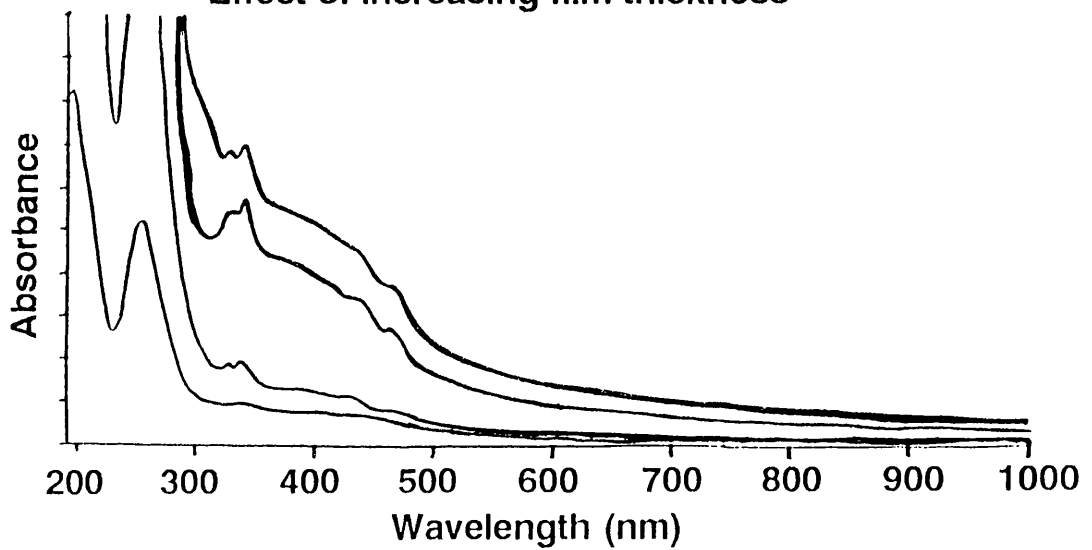
Perylene crystallizes in large golden yellow plates (m.p. 266-267°C) and its molecular compounds with many electron acceptors have been reported in the literature (116). Electronic spectra of thick films on silica (Electronic spectra:a:1.) appeared to differ little from those obtained for thin films (*ca.* 60nm) which resembled spectra obtained in solution (117). Films were formed on substrates whose temperatures were in the range 40-60°C. Thin films of perylene exposed to MoF₆, WF₆, and AsF₅ exhibited an immediate colour change. This was most pronounced for films exposed to MoF₆ where the golden-yellow film displayed a series of colour changes following the sequence red-crimson-violet-black over a period of 1 hr. As seen clearly in Table A the absorption coefficients of all bands observed in the electronic spectra increased for films exposed to oxidant. The effect was observed for many of the organic thin films examined. Electronic absorptions additional to those assigned to the absorption bands of the components were found for films exposed to MoF₆, WF₆ and AsF₅ (Electronic spectra:a:2 and a:3) and for films produced by the co-evaporation of perylene with TCNQ (Electronic spectra:a:4) (see this section, p). For all organic films examined, interpretation of the electronic spectra upon exposure to oxidant was difficult for reasons discussed in detail later in this chapter (eg. multiplicity or splitting of bands).

Electronic spectra of TCNQ



Electronic spectra: a.1

Effect of increasing film thickness



Electronic spectra: a.2

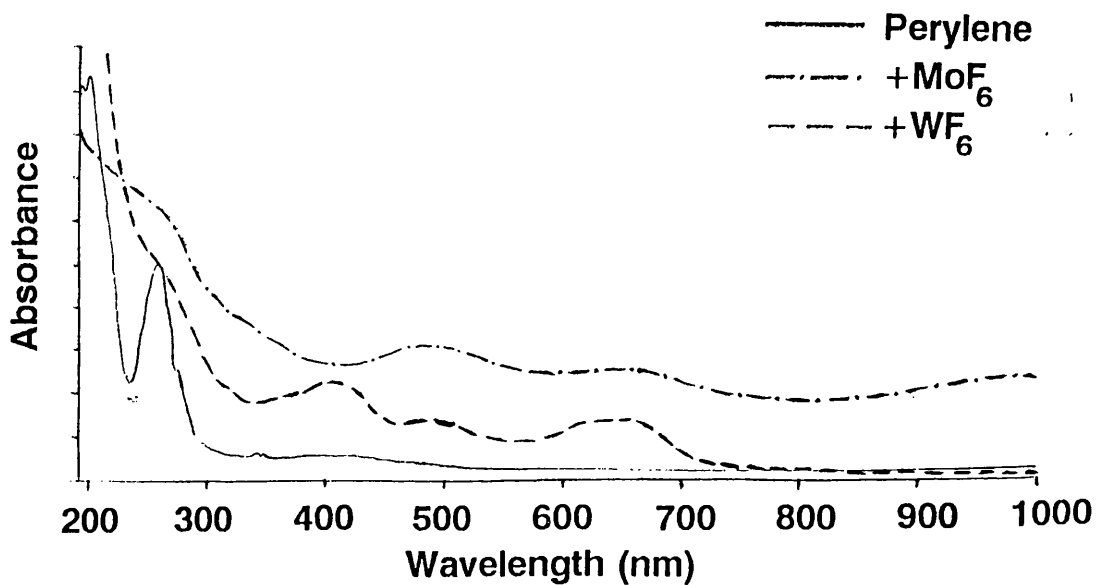


Table A: Electronic spectra of perylene on silica exposed to oxidant vapour

Perylene ^a	+WF ₆	Perylene ^b	+MoF ₆	+AsF ₅
λ_{\max} (nm)	λ_{\max} (nm)	λ_{\max} (max)	λ_{\max} (nm)	λ_{\max} (max)
$10^{-4}\alpha^*(\text{cm}^{-1})$	$10^{-4}\alpha^*(\text{cm}^{-1})$	$10^{-4}\alpha^*(\text{cm}^{-1})$	$10^{-4}\alpha^*(\text{cm}^{-1})$	$10^{-4}\alpha^*(\text{cm}^{-1})$
189 (29.28)	189 (81.97)	189 (14.90)	189 (22.11)	190 (35.37)
260 (13.77)	225sh	260sh (9.34)	270sh	365sh (7.54)
330 (8.85)	270 (24.59)	330sh (1.96)	330sh (7.25)	490 (4.77)
340 (8.36)	358sh	340sh (2.03)	360sh (5.96)	650 (4.36)
435sh (6.15)	407 (17.70)	435 (1.94)	495 (5.60)	1230 (5.46)
470sh (5.41)	479 (13.29)	470 (1.77)	660 (4.40)	
	505sh		1000 (3.76)	
	623 (13.28)			

^aFilm thickness ca. 60nm

^bFilm thickness ca. 110nm

sh=shoulder

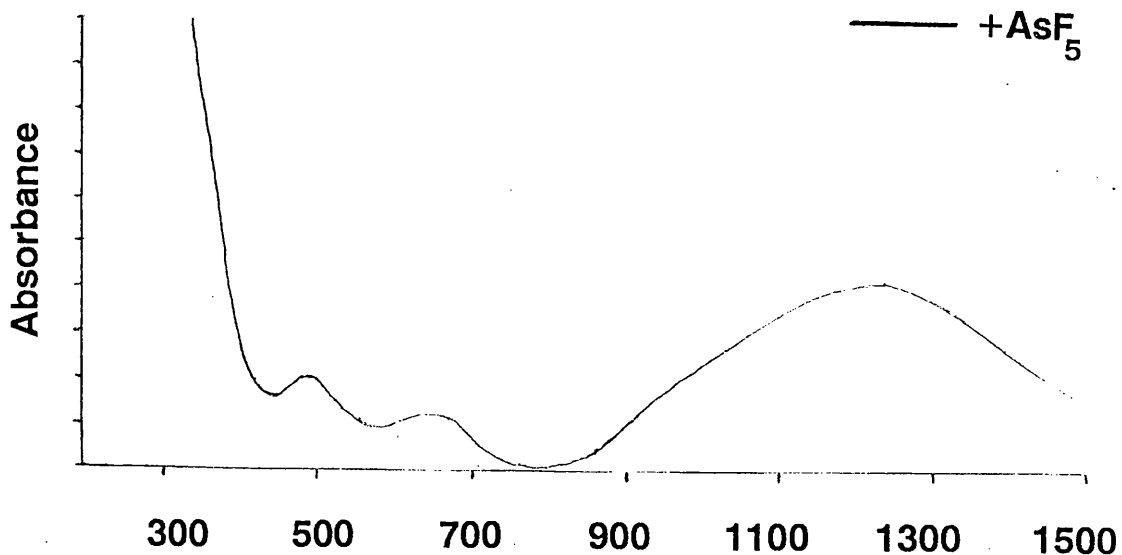
b. Bis(ethylenedithio)tetrathiafulvalene (BEDT-TTF)

BEDT-TTF is the basis of a number of organic conductors and fabrication of superconducting organic films of (BEDT-TTF)-iodide, by means of an evaporation method, has been achieved (118). In this work films of BEDT-TTF were prepared and stored in the absence of light as the material is sensitive to UV radiation. A low temperature for evaporation (*ca.* 80°C) was employed to avoid thermal degradation (decomposes > 244°C). Films were formed on substrates whose temperatures were in the range 20-40°C. Electronic absorptions additional to those assigned to the absorptions bands of the components were found for films exposed to MoF₆ and for films produced by the co-evaporation of BEDT-TTF with TCNQ (see this section, p). Films exposed to MoF₆ developed a blue colouration; as seen in Electronic spectra:b.1 two new features centred at 775 nm and 895 nm were prominent. Tabulation of the absorption bands (Table B) led to the conclusion that considerable modification of the electronic structure of the film had occurred, as all band positions appeared to have changed.

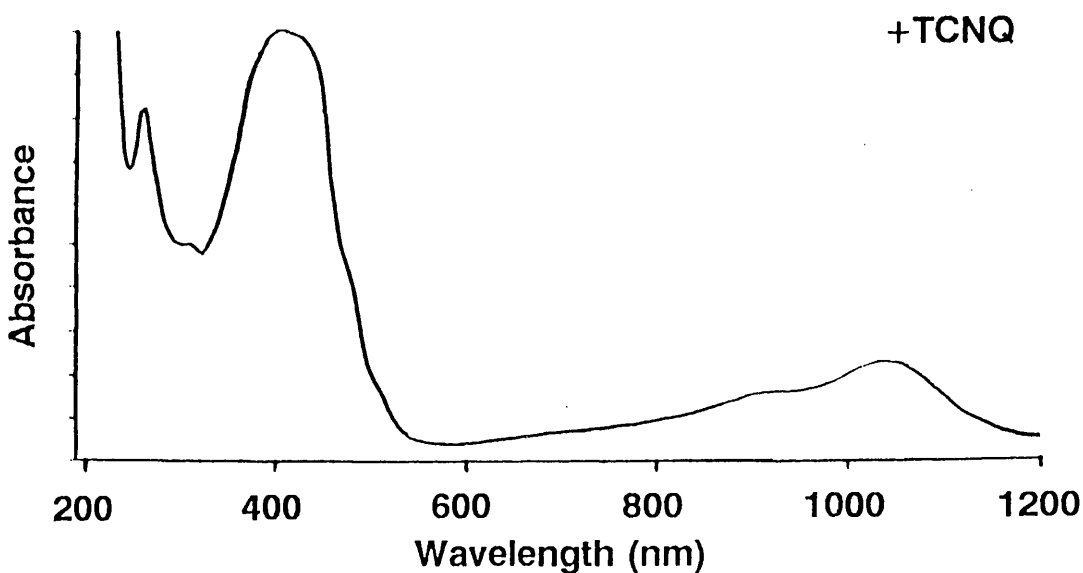
c. Violanthrone.

Violanthrone (m.p. = 425°C) is of great importance in industry as its derivatives form valuable vat dyes (119). The compound forms deep violet crystals from nitrobenzene. Films were formed on substrates whose temperatures were in the range 60-80°C and it was found that there was a total loss of definition in electronic spectra of thin films on silica with increasing film thickness (Electronic spectra:c.1). Electronic absorptions additional to those

Electronic spectra: a.3



Electronic spectra: a.4



Electronic spectra: b.1

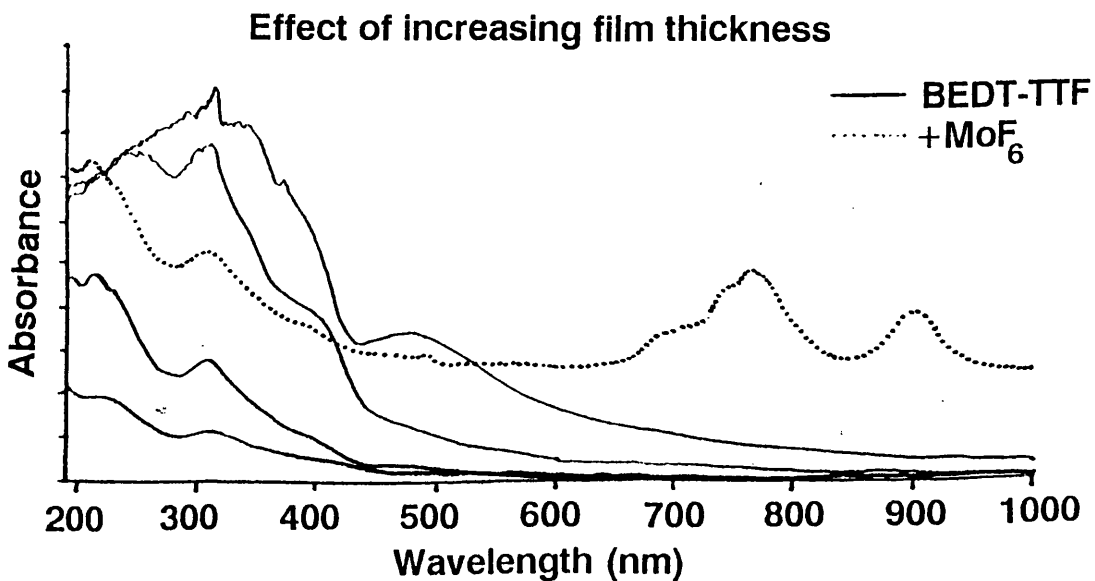


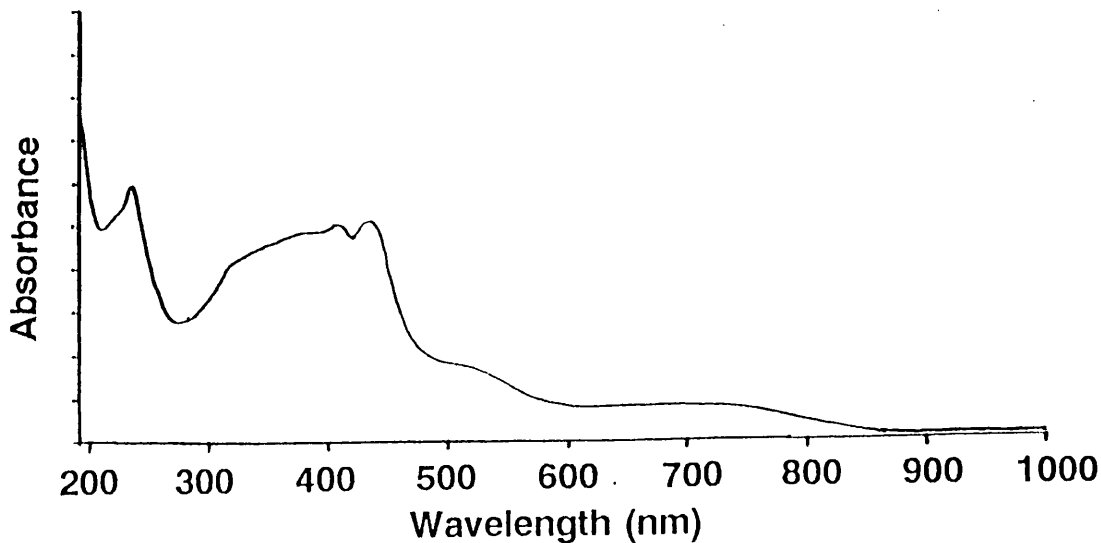
Table B: Electronic spectra of BEDT-TTF (bis(ethylenedithio)tetrathiafulvalene) on silica exposed to oxidant vapour

BEDT-TTF	+MoF ₆
λ_{\max} (nm)	λ_{\max} (nm)
$10^{-4} \alpha^*$ (cm ⁻¹)	$10^{-4} \alpha^*$ (cm ⁻¹)
194(15.24)	194(27.20)
220(12.95)	258sh(19.02)
235sh(11.48)	325(7.87)
315(8.03)	370sh(9.02)
390sh(3.28)	385(9.84)
480(2.46)	410sh(5.90)
	465(1.97)
	480(1.80)
	505(1.06)
	710sh(1.88)
	758sh(3.52)
	775(3.69)
	895(0.90)

sh=shoulder

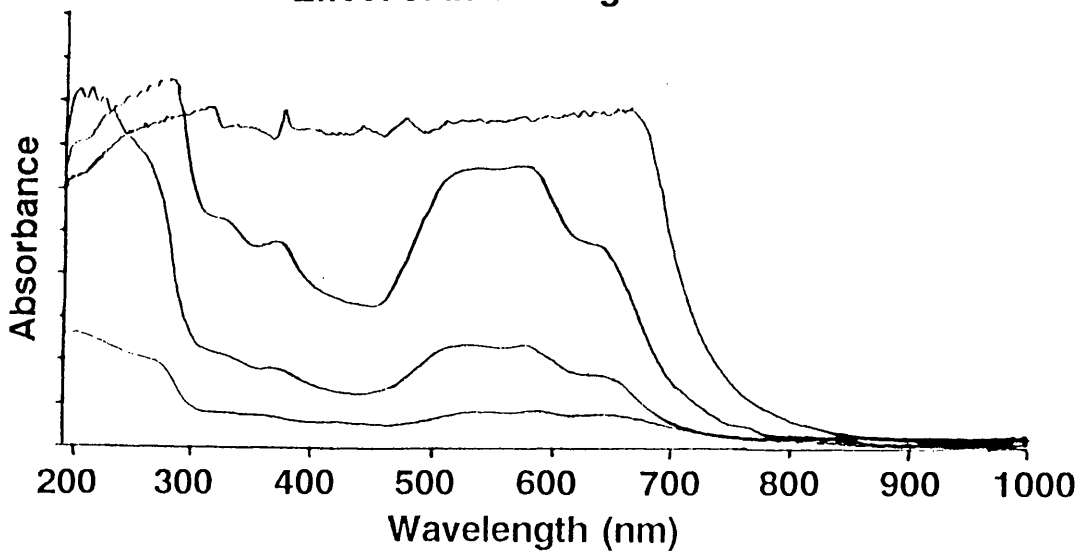
Electronic spectra: b.2

+TCNQ



Electronic spectra: c.1

Effect of increasing film thickness



Electronic spectra: c.2

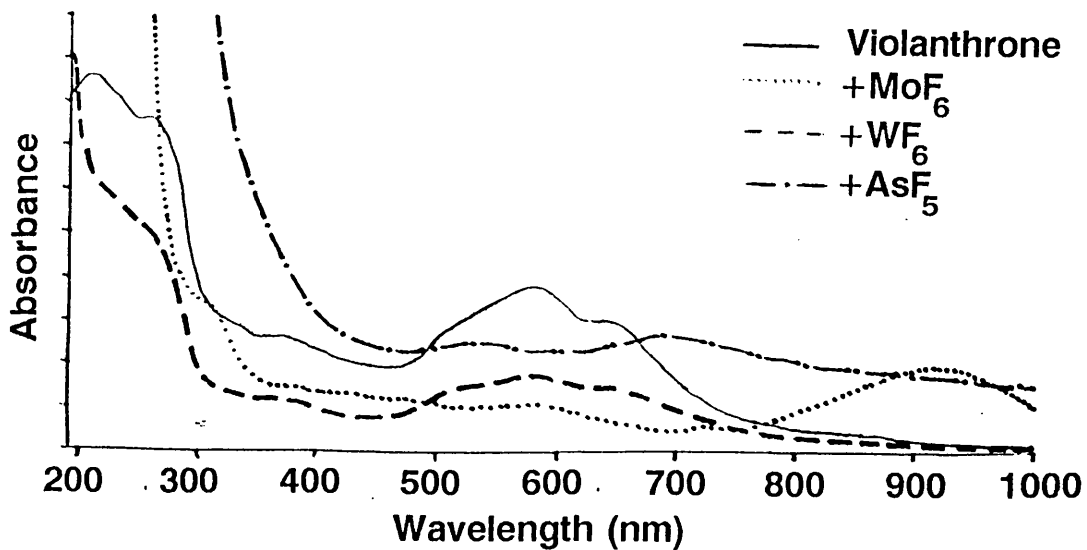


Table C: Electronic spectra of violanthrone on silica exposed to oxidant vapour

Violanthrone	+WF ₆	+MoF ₆	+AsF ₅
λ_{\max} (nm)	λ_{\max} (nm)	λ_{\max} (nm)	λ_{\max} (nm)
$10^{-4}\alpha^*$ (cm ⁻¹)			
215(12.44)	195(72.40)	250(121.95)	190(79.82)
235sh (11.71)	225sh (20.68)	310sh (64.63)	280sh (42.44)
257(11.16)	257(18.53)	375(40.24)	375sh (7.44)
280sh (9.70)	280sh (15.32)	480(36.34)	525(3.66)
330sh (4.02)	330sh (5.82)	580(9.08)	690(3.71)
375(3.66)	375(5.39)	725(6.32)	890(1.58)
505sh (3.70)	505sh (6.46)	920(12.44)	
580(5.49)	580(6.73)		
640sh (3.90)	640sh (6.46)		

sh=shoulder

assigned to the absorption bands of the components were found for films exposed to MoF₆ and AsF₅. In each case there was no obvious colour change. Considerable modification of the electronic spectrum was found for films exposed to AsF₅ (Table:C and Electronic spectra:c.2), although the additional absorption bands were less well defined than was the case for films exposed to MoF₆, where a broad feature centred at 920 nm was the most prominent feature.

d. Pentacene.

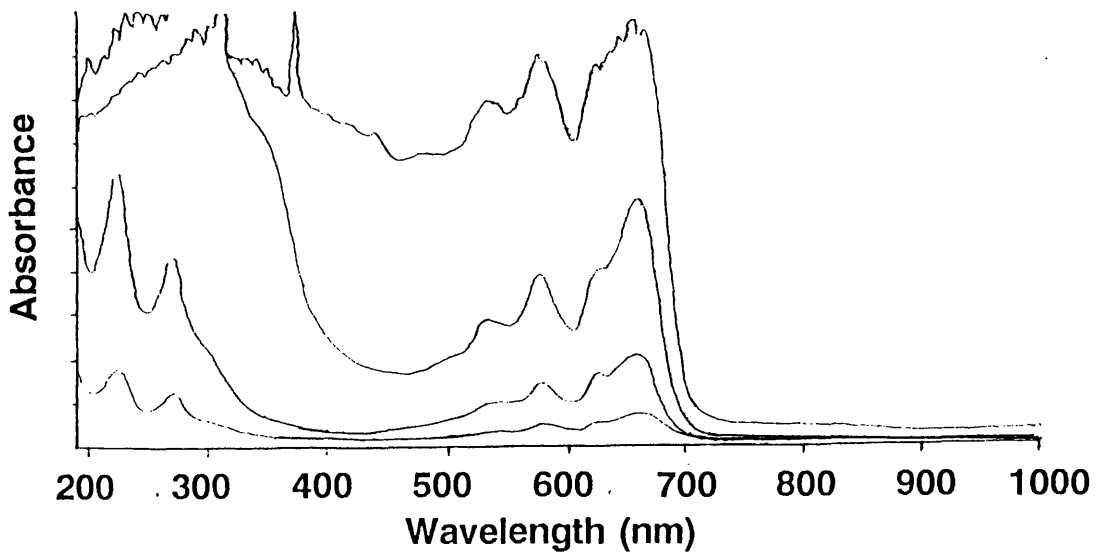
Pentacene is a deep violet-blue hydrocarbon of relatively high reactivity ascribed to its acene structure. It is sublimable *in vacuo* and decomposes at temperatures above 300°C to form dihydropentacene and a carbonaceous residue (120). Films were formed on substrates whose temperatures were in the range 60-80°C and in this work it was found that there was loss of definition in electronic spectra for thicker films (see Electronic spectra:d.1). Electronic absorptions additional to those assigned to the absorption bands of the components were found for films exposed to MoF₆ and films produced by the co-evaporation of pentacene with TCNQ (see this section, p). Films exposed to MoF₆ did not exhibit any obvious colour change but two new bands in the electronic spectrum (centred at 785 nm and 975 nm) were found (Table:D and Electronic spectra:d.2).

e. Ovalene.

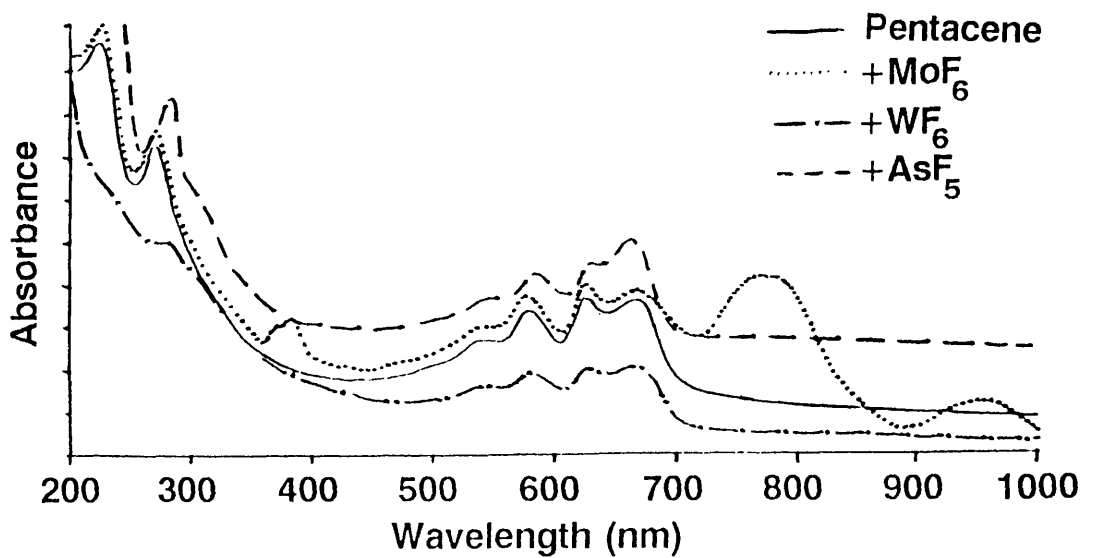
Ovalene crystallizes in long orange needles (m.p. = 473°C) and is a

Electronic spectra: d.1

Effect of increasing film thickness



Electronic spectra: d.2



Electronic spectra: d.3

+TCNQ

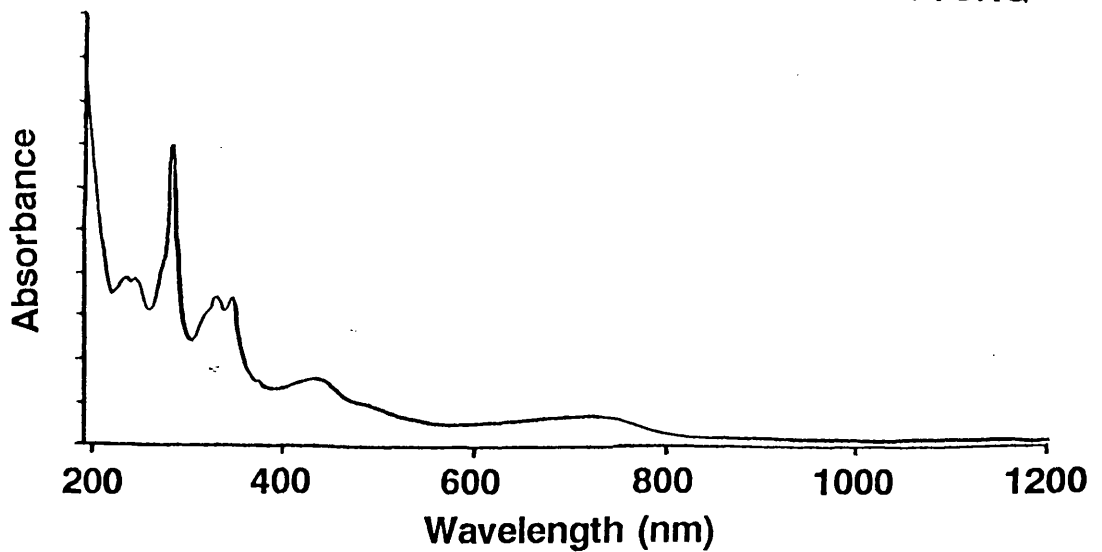


Table D: Electronic spectra of pentacene on silica exposed to oxidant vapour

Pentacene	+WF ₆	+AsF ₅	+MoF ₆
λ_{\max} (nm)	λ_{\max} (nm)	λ_{\max} (nm)	λ_{\max} (nm)
$10^{-4}\alpha^*$ (cm ⁻¹)			
190(42.62)	190(45.90)	190(44.01)	190(50.82)
225(6.56)	225sh (5.74)	225(40.56)	270sh (14.92)
270sh (4.84)	270sh (4.43)	270sh (31.26)	290(15.08)
290sh (3.61)	290sh (3.28)	300sh (21.97)	375sh (10.16)
320sh (3.28)	320sh (3.20)	320sh (20.59)	390(10.66)
530(1.64)	530sh (1.64)	385(11.66)	425(4.92)
580(1.80)	580(1.80)	425(11.30)	480(1.64)
630sh (2.46)	630sh (2.46)	490(11.09)	505(0.98)
665(2.22)	665(2.30)	530(13.02)	540(0.82)
		580(14.05)	585(1.64)
		630sh (14.39)	630sh (2.79)
		670(16.11)	670(4.43)
			785(4.92)
			975(0.82)

sh=shoulder

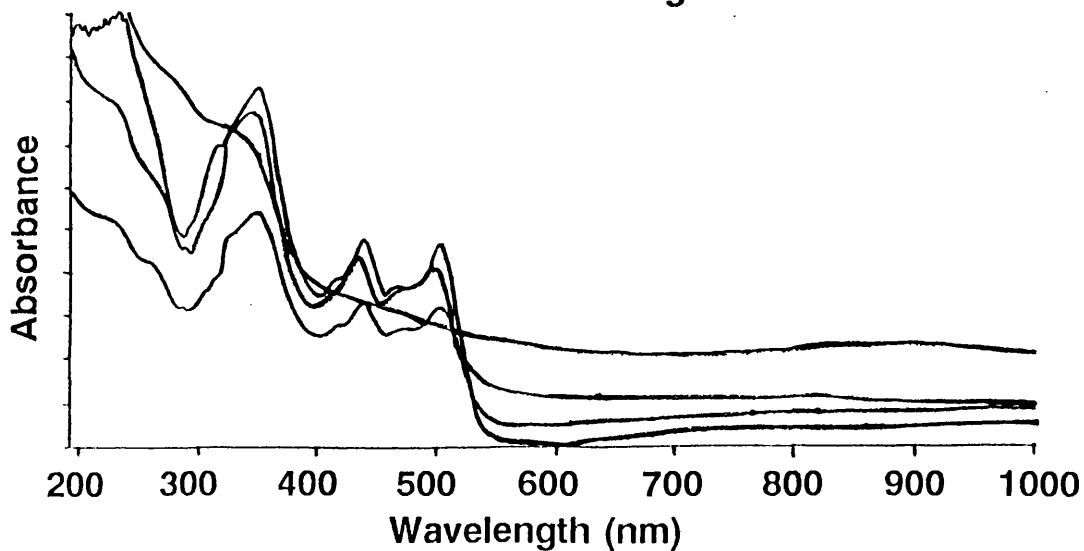
semiconductor with high magnetic anisotropy (121). Films of ovalene were formed on substrates whose temperatures were in the range 60-80°C and produced satisfactory electronic spectra with little loss in definition for films approaching *ca.* 900 nm thickness (Electronic spectra:e.1). Electronic absorptions additional to those assigned to the absorption bands of the components were found for films exposed to MoF₆, WF₆ and AsF₅. A blue-green colour developed immediately on the surface of films of ovalene when exposed to MoF₆ and AsF₅. No such colour change was observed for films exposed to WF₆. As seen clearly in Electronic spectra:e.2 and Table:E there was considerable modification of the electronic spectra in all cases, with many new bands at low energy and changes in position and intensities of existing bands.

f. Tetracene.

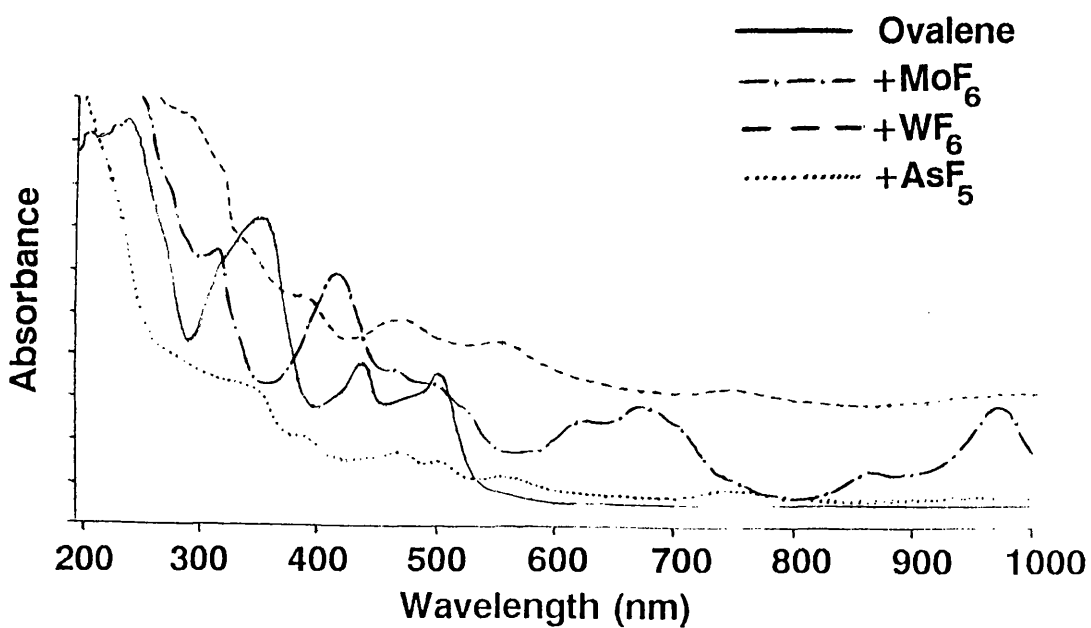
Tetracene crystallizes in orange-yellow leaflets (m.p. = 357°C) which are sublimable. It forms a number of molecular compounds with electron acceptor species (122) and is a semiconductor and photoconductor (123). In this work films of tetracene were formed on substrates whose temperatures were in the range 60-80°C. Definition in the electronic spectra appeared to be insensitive to effects due to increasing film thickness (*ca.* 30-800 nm) as seen in Electronic spectra:f.1. In common with thin films of perylene (*ca.* 40 nm thickness), films of tetracene produced electronic spectra that resembled closely those obtained in solution. Electronic absorptions additional to those assigned to the absorption bands of the components were found for films exposed to MoF₆ and

Electronic spectra: e.1

Effect of increasing film thickness



Electronic spectra: e.2



Electronic spectra: f.1

Effect of increasing film thickness

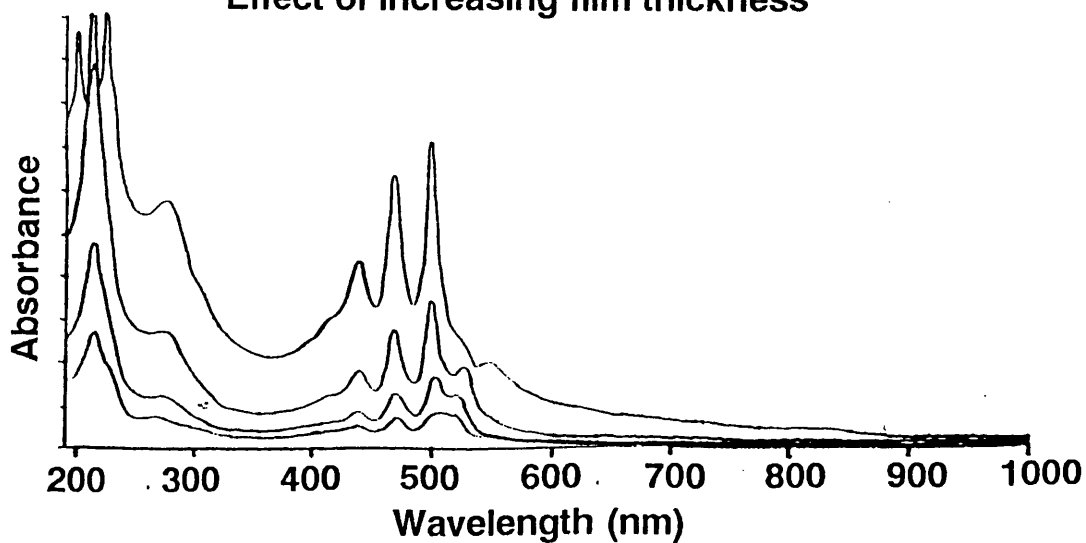
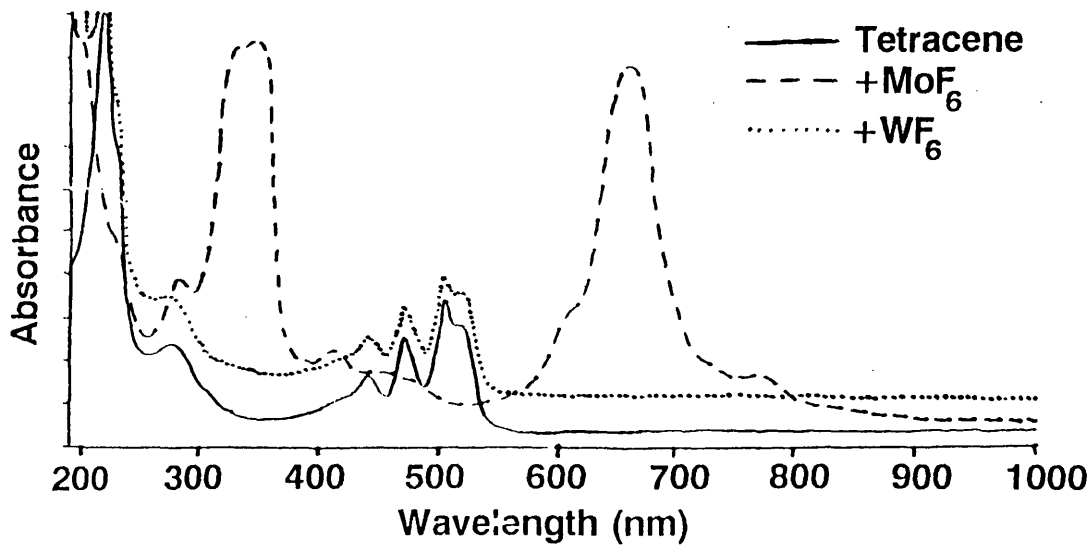


Table E: Electronic spectra of ovalene on silica exposed to oxidant vapour

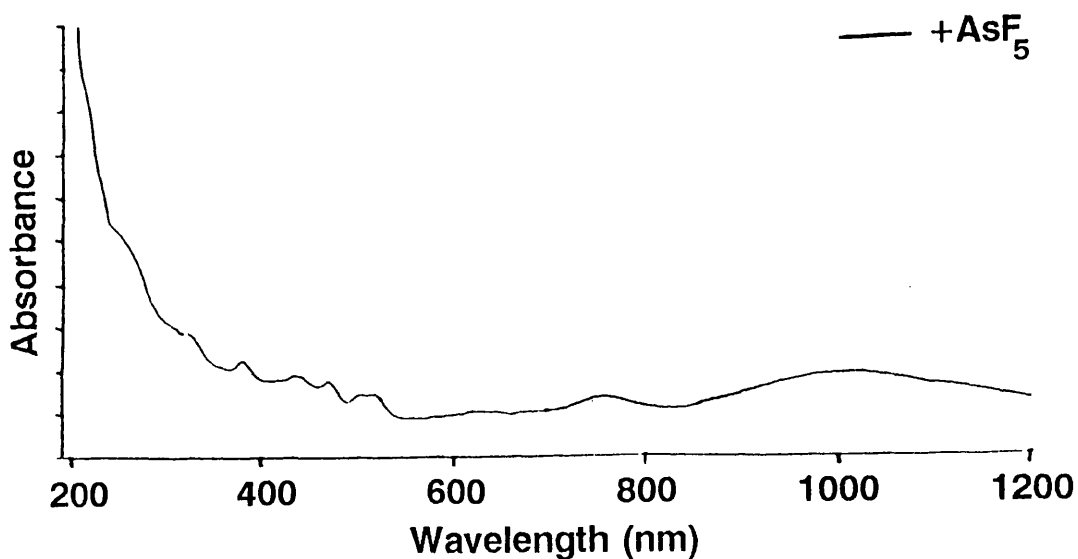
Ovalene	+WF ₆	+MoF ₆	+AsF ₅
λ_{\max} (nm)	λ_{\max} (nm)	λ_{\max} (nm)	λ_{\max} (nm)
$10^{-4}\alpha^*(\text{cm}^{-1})$	$10^{-4}\alpha(\text{cm}^{-1})$	$10^{-4}\alpha(\text{cm}^{-1})$	$10^{-4}\alpha(\text{cm}^{-1})$
190(54.98)	190(45.87)	190(45.87)	190(35.09)
225sh (48.62)	235sh (26.15)	260sh (7.63)	350sh (16.34)
255sh (39.45)	285sh (20.00)	310(6.53)	385 (13.17)
285sh (29.82)	337sh (11.01)	325sh (5.36)	437(11.71)
350(49.54)	385(8.26)	413(6.16)	465(12.00)
413sh (24.77)	465(6.88)	462sh (4.48)	500(11.71)
438sh (31.19)	550(5.50)	495sh (4.26)	530(10.49)
475sh (25.23)	750(2.57)	525sh (3.89)	550(10.24)
505(30.27)	1000(0.92)	620sh (3.50)	750(9.12)
		670(3.89)	1000(9.07)
		850(2.87)	
		962(3.62)	

sh=shoulder

Electronic spectra: f.2

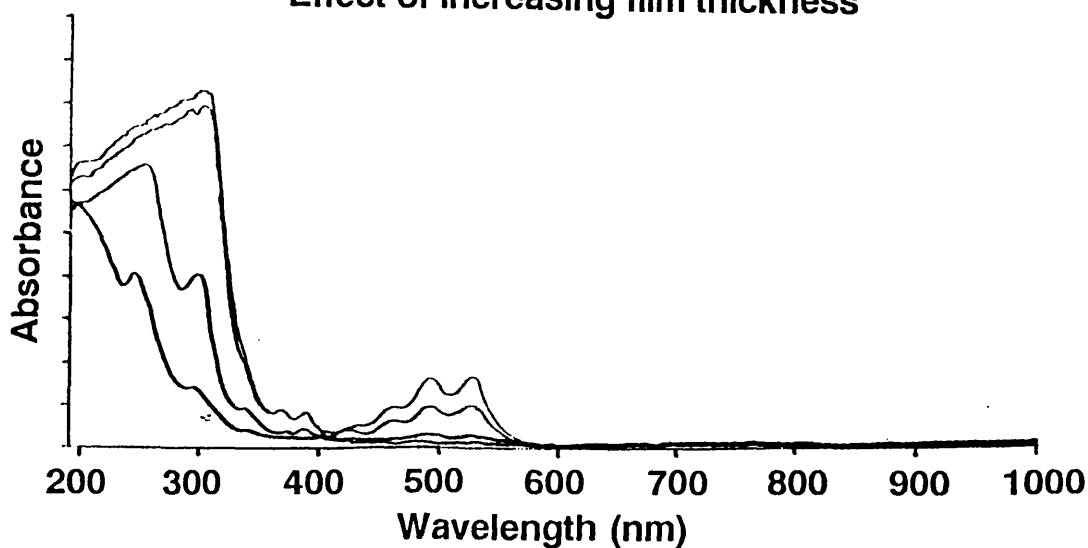


Electronic spectra: f.3



Electronic spectra: g.1

Effect of increasing film thickness



AsF₅ and in both cases a colour change was observed, blue-green with MoF₆ and emerald-green with AsF₅. As seen clearly in Electronic spectra:f.2 and Table:F, two bands centred at 670 nm and 340 nm were most prominent in the electronic spectrum of the tetracene thin film exposed to MoF₆. In contrast, films exposed to AsF₅ produced several absorption bands at low energy in the electronic spectrum of relatively low intensity, the most striking of which was a broad feature centred at 1010 nm (Electronic spectra:f.3).

g. Rubrene.

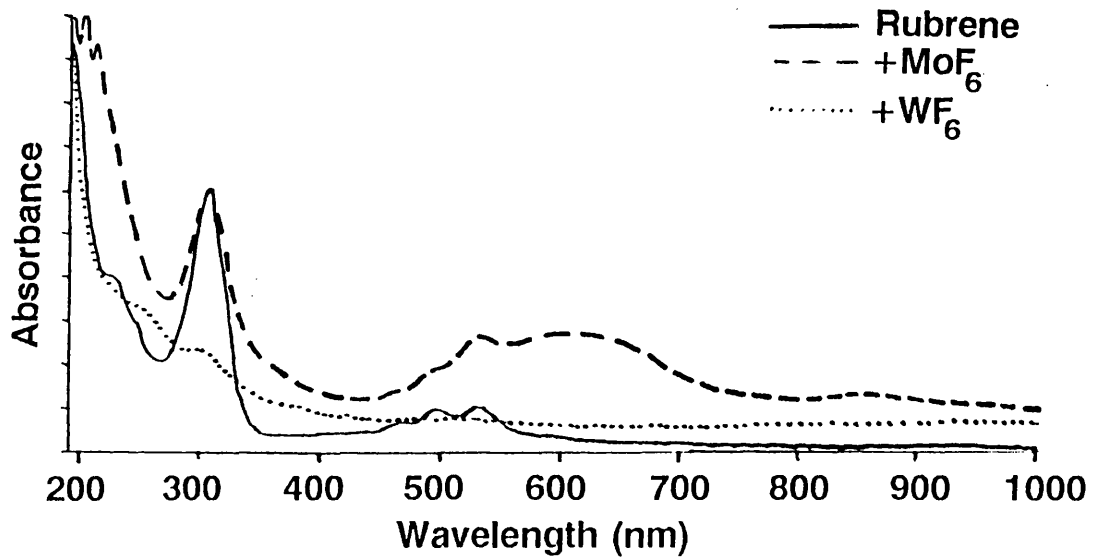
Rubrene is a bright orange hydrocarbon (m.p. = 334°C) of high reactivity ascribed to its acene structure. It undergoes a reversible photo-oxidation process (124). It is thermochromic and electronic spectra of solutions of rubrene exhibit a considerable red shift at low temperature (125). Films of rubrene were formed on substrates whose temperatures were in the range 20-30°C. There was loss of definition in electronic spectra obtained for thick films which were susceptible also to photo-oxidation. In many cases thick films were found to exhibit interference patterns in the electronic spectrum. Electronic absorptions additional to those assigned to the absorption bands of the components were found for films exposed to MoF₆ which exhibited a colour change from orange to blue. Films exposed to WF₆ did not appear to produce any change in colour or additional absorption bands in the electronic spectrum although there was a significant loss in resolution (Electronic spectra:g.2 and Table:G).

Table F: Electronic spectra of tetracene on silica exposed to oxidant vapour

Tetracene	+MoF ₆	+WF ₆	+AsF ₅
λ_{\max} (nm)	λ_{\max} (nm)	λ_{\max} (nm)	λ_{\max} (nm)
$10^{-4}\alpha^*(\text{cm}^{-1})$	$10^{-4}\alpha^*(\text{cm}^{-1})$	$10^{-4}\alpha(\text{cm}^{-1})$	$10^{-4}\alpha(\text{cm}^{-1})$
190(20.64)	190(29.10)	190(45.87)	190(81.97)
206(22.71)	205sh (27.01)	215(45.87)	225sh (27.87)
213(45.87)	225sh (13.21)	230sh (29.36)	275sh (14.75)
225sh (28.90)	280(10.57)	275(11.65)	305(10.24)
275(11.56)	338sh (26.42)	305sh (5.96)	385(5.74)
305sh (6.19)	345(26.60)	385sh (3.67)	438(3.82)
387(4.13)	350(26.79)	412sh (5.32)	472(3.36)
412sh (5.37)	387(4.70)	438(7.25)	505(2.46)
438(7.43)	412(5.87)	472(11.01)	525(2.44)
472(1.14)	460(4.40)	503(13.85)	625(0.82)
503(14.04)	478sh (3.82)	520(13.62)	675(0.98)
525(7.34)	605sh (8.81)		765(1.80)
	670(25.04)		1010(3.11)
	725sh (4.99)		
	775(4.11)		

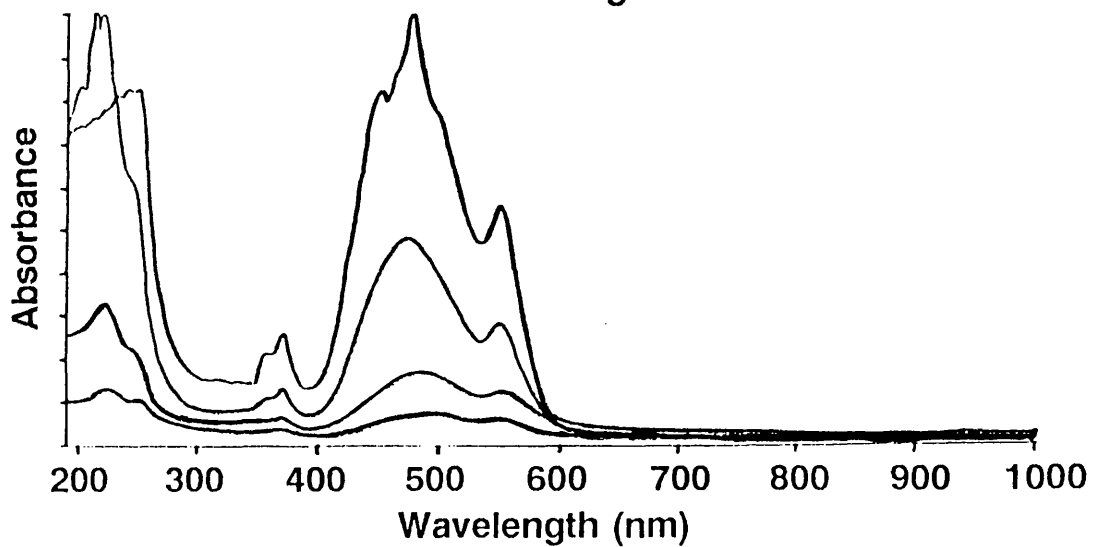
sh=shoulder

Electronic spectra: g.2



Electronic spectra: h.1

Effect of increasing film thickness



Electronic spectra: h.2

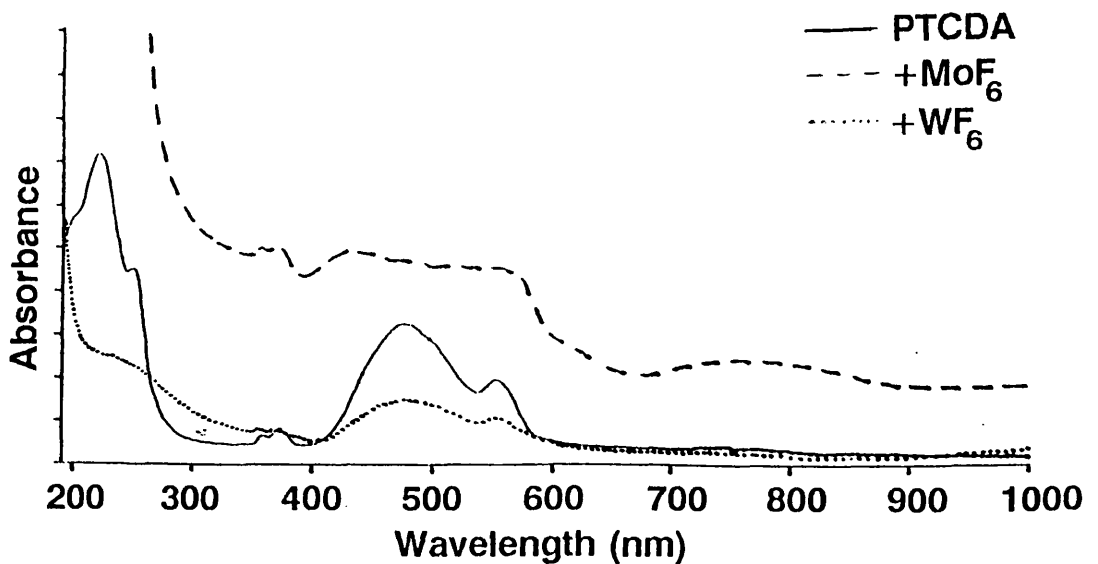


Table G: Electronic spectra of rubrene on silica exposed to oxidant vapour

Rubrene	+MoF ₆	+WF ₆
λ_{\max} (nm)	λ_{\max} (nm)	λ_{\max} (nm)
$10^{-4}\alpha^*(\text{cm}^{-1})$	$10^{-4}\alpha^*(\text{cm}^{-1})$	$10^{-4}\alpha^*(\text{cm}^{-1})$
190(20.18)	190(45.87)	190(25.91)
200(21.10)	305(22.02)	245sh (9.17)
245(15.14)	465sh (4.86)	305sh (6.41)
300(5.04)	490sh (7.34)	386sh (2.83)
337(1.38)	530(9.82)	430(2.20)
362(1.28)	615(10.09)	495(2.08)
386(1.38)	780(4.59)	530(2.06)
430sh (0.50)		
464(0.46)		
490(0.92)		
525(0.92)		

sh=shoulder

h. Perylene tetracarboxylic dianhydride (PTCDA).

PTCDA is a well known organic dye compound which has important applications as a photoconductor and photoreceptor in the form of submicron thin organic films. Materials formed by interfacing PTCDA and metal phthalocyanines are of interest as they absorb energy in complementary regions of the visible spectrum and form heterojunctions in combination with each other (126). Films of PTCDA were formed on substrates whose temperatures were in the range 40-60°C and it was found that there was relatively little loss of definition in electronic spectra for thicker films (Electronic spectra:h.1). Electronic absorptions additional to those assigned to the absorption bands of the components were found for films exposed to MoF₆. There was a slight deepening of colour of the pale red film of PTCDA upon exposure to MoF₆; the electronic spectrum displayed an additional broad absorption band centred at 770 nm (see Electronic spectra:h.2 and Table:H).

i. Coronene tetracarboxylic dianhydride (CTCDA)

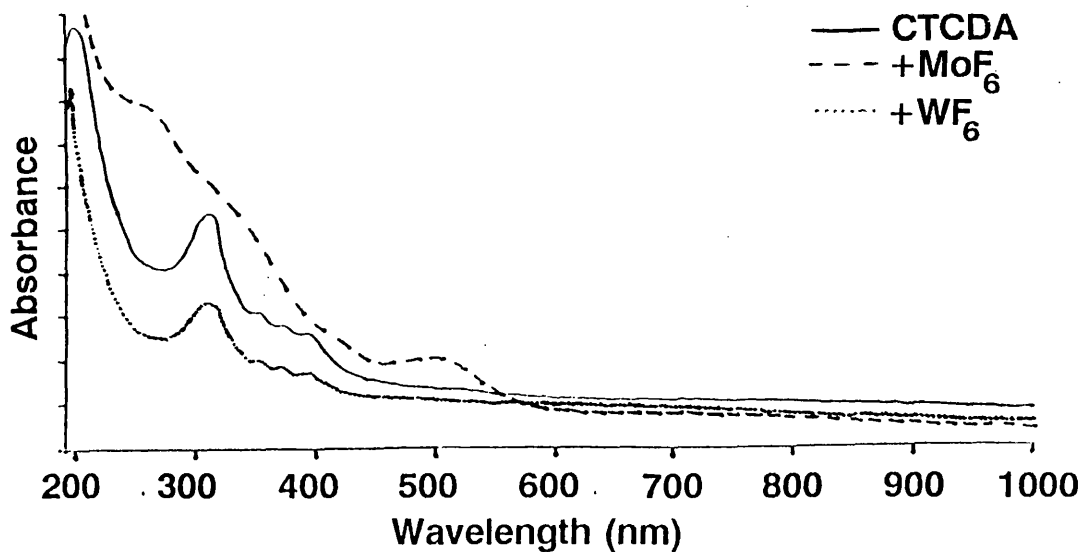
Large polycyclic aromatic compounds like coronene and its derivatives have become of interest to astrophysics recently because of their discovery in interstellar matter (127). Stimulus for study of such hydrocarbons, as their positive ions, is provided since a large fraction of these compounds are considered to be singly ionized (128). In this work films were formed on substrates whose temperatures were in the range 60-80°C and there was loss of definition in electronic spectra with thicker films. Electronic absorptions additional to those assigned to the absorption bands of the components were

Table H: Electronic spectra of PTCDA (perylene tetracarboxylic dianhydride) on silica exposed to oxidant vapour

PTCDA	+MoF ₆	+WF ₆
$\lambda_{\max}(\text{nm})$	$\lambda_{\max}(\text{nm})$	$\lambda_{\max}(\text{nm})$
$10^{-4}\alpha^*(\text{cm}^{-1})$	$10^{-4}\alpha^*(\text{cm}^{-1})$	$10^{-4}\alpha(\text{cm}^{-1})$
190(9.17)	190(45.87)	190(21.69)
205sh(9.79)	365sh (10.50)	205(20.64)
220(12.11)	375(10.59)	220(24.50)
245sh (8.26)	425(10.59)	250(15.69)
360sh (3.72)	475(9.91)	360sh (3.62)
380(4.59)	550(8.35)	375(4.13)
450sh (4.59)	620(4.59)	475(14.86)
475(5.87)	770(4.42)	550(8.53)
550(4.59)		

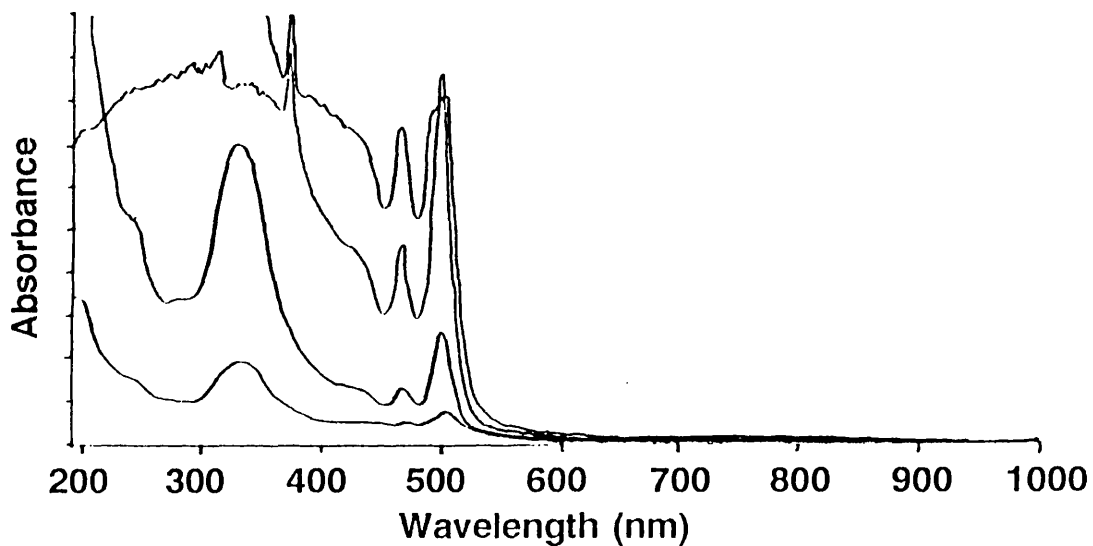
sh=shoulder

Electronic spectra: i.1



Electronic spectra: j.1

Effect of increasing film thickness



Electronic spectra: j.2

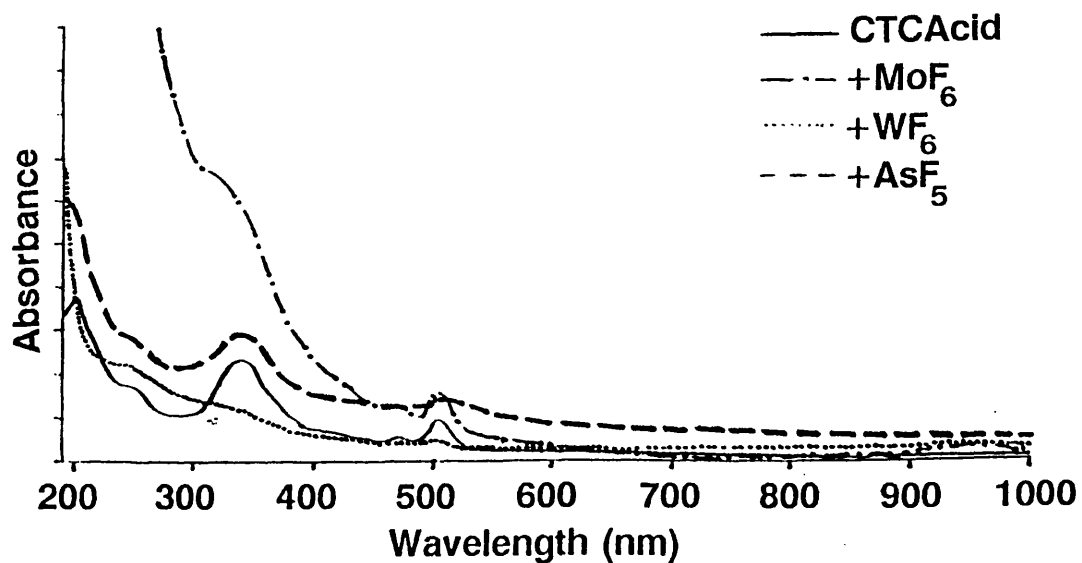


Table I: Electronic spectra of CTCDA (coronene tetracarboxylic dianhydride) on silica exposed to oxidant vapour

CTCDA	+MoF ₆	+WF ₆
$\lambda_{\max}(\text{nm})$	$\lambda_{\max}(\text{nm})$	$\lambda_{\max}(\text{nm})$
$10^{-4}\alpha^*(\text{cm}^{-1})$	$10^{-4}\alpha(\text{cm}^{-1})$	$10^{-4}\alpha(\text{cm}^{-1})$
200(6.41)	190(81.97)	190(3.73)
230sh (3.62)	250sh (52.70)	312(1.80)
312(3.52)	350sh (34.51)	350(1.06)
350(1.99)	425sh (19.79)	375(0.92)
375(1.80)	500(14.51)	400(0.84)
400(1.72)		

sh=shoulder

formed for films exposed to MoF_6 (see Electronic spectra:i.1 and Table:I). There was no observable change in the tan colour of the film upon exposure to MoF_6 although the electronic spectrum revealed an additional band centred at 500 nm and a loss of resolution of all other bands.

j. Coronene tetracarboxylic acid (CTA).

Films of CTA were formed on substrates whose temperatures were in the range 60-80°C and there was a significant loss of definition (Electronic spectra:j.1) in electronic spectra of thicker films (*ca.* > 150 nm). Under all conditions, no electronic absorptions additional to those assigned to the absorption bands of CTA were found for films exposed to MoF_6 , WF_6 , AsF_5 or films produced by the co-evaporation of CTA with TCNQ (see this section, p). Exposure to MoF_6 and WF_6 produced loss of definition in the electronic spectrum of CTA (see Electronic spectra:j.2).

1k. Decacyclene.

Decacyclene crystallizes in yellow needles (m.p. = 387°C) and is a non-planar hydrocarbon of recent interest (129). Films of decacyclene were formed on substrates whose temperatures were in the range 40-60°C and it was found that there was a complete loss of definition in electronic spectra of thicker films (*ca.* > 50 nm) (see Electronic spectra:k.1). Electronic absorptions additional to those assigned to the absorption bands of the components were found for films exposed to MoF_6 and for films produced by the co-evaporation of decacyclene with TCNQ (see this section, p). It was interesting to observe

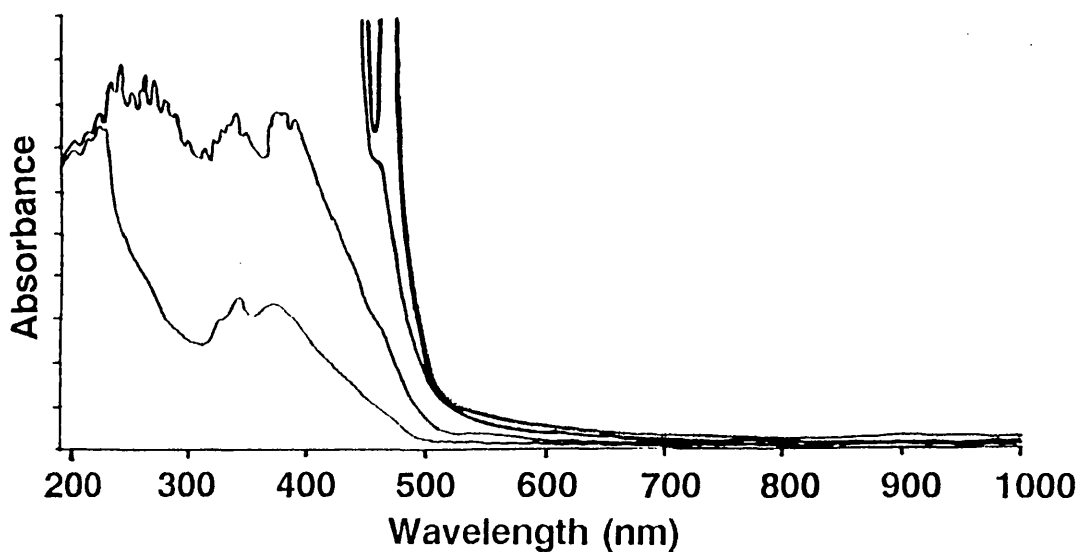
Table J: Electronic spectra of CTA
(coronene tetracarboxylic acid) on silica
exposed to oxidant vapour

CTA	+MoF ₆	+WF ₆	+AsF ₅
$\lambda_{\max}(\text{nm})$	$\lambda_{\max}(\text{nm})$	$\lambda_{\max}(\text{nm})$	$\lambda_{\max}(\text{nm})$
$10^{-4}\alpha^*(\text{cm}^{-1})$	$10^{-4}\alpha(\text{cm}^{-1})$	$10^{-4}\alpha(\text{cm}^{-1})$	$10^{-4}\alpha(\text{cm}^{-1})$
190(22.15)	190(9.34)	190(68.85)	190(54.92)
237sh (9.84)	200(9.84)	250sh (18.44)	200(64.92)
285sh (6.53)	237sh (4.75)	305sh (11.64)	250sh (29.50)
335(12.28)	285sh (3.52)	435sh (4.08)	290sh(20.26)
470(2.54)	335sh (5.08)	470sh (4.10)	335(39.18)
505(4.10)	470sh (2.29)	505(4.06)	430sh (11.80)
	505(2.62)		470(11.72)
	525(2.17)		505(16.26)

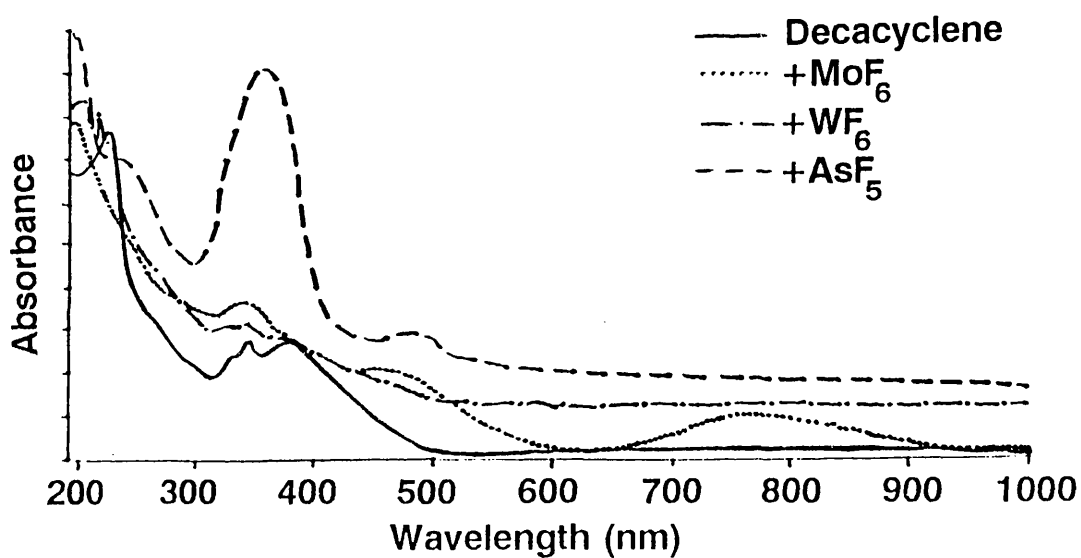
sh=shoulder

Electronic spectra: k.1

Effect of increasing film thickness



Electronic spectra: k.2



Electronic spectra: k.3

+TCNQ

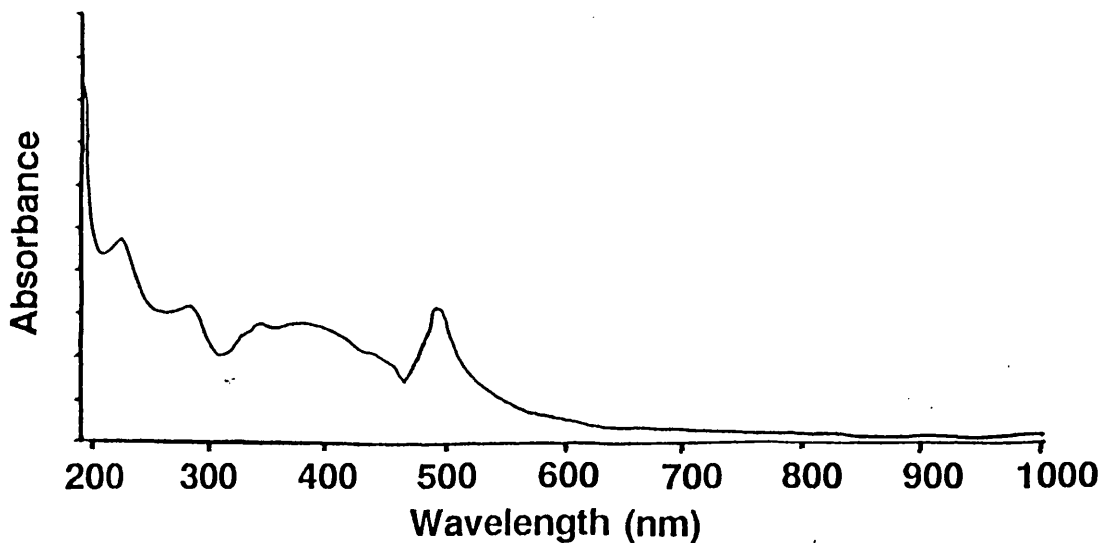


Table K: Electronic spectra of decacyclene on silica exposed to oxidant vapour

Decacyclene	+MoF ₆	+WF ₆	+AsF ₅
λ_{\max} (nm)	λ_{\max} (nm)	λ_{\max} (nm)	λ_{\max} (nm)
$10^{-4}\alpha^*(\text{cm}^{-1})$	$10^{-4}\alpha^*(\text{cm}^{-1})$	$10^{-4}\alpha(\text{cm}^{-1})$	$10^{-4}\alpha(\text{cm}^{-1})$
190(25.61)	190(7.72)	190(42.41)	190(8.59)
202sh (28.33)	200(7.89)	265sh (19.10)	235sh (6.67)
215sh (29.06)	230sh (5.28)	325sh (10.57)	365(7.90)
225(30.16)	300sh (4.47)	337(11.22)	485(0.40)
230sh (29.67)	350(4.06)	375sh(9.92)	
265sh (16.26)	450(3.66)	465sh (0.33)	
325sh (12.11)	475sh (3.58)		
337(13.82)	770(3.17)		
375(13.82)			
465sh (34.55)			

sh=shoulder

the similarity of the feature centred at 340 nm in the electronic spectrum of tetracene exposed to MoF_6 (see Electronic spectra:f.2) with the absorption centred at 365 nm in the electronic spectrum of decacyclene exposed to AsF_5 (see Electronic spectra:k.2 and Table:K). Films exposed to MoF_6 exhibited a broad absorption band centred at 770 nm.

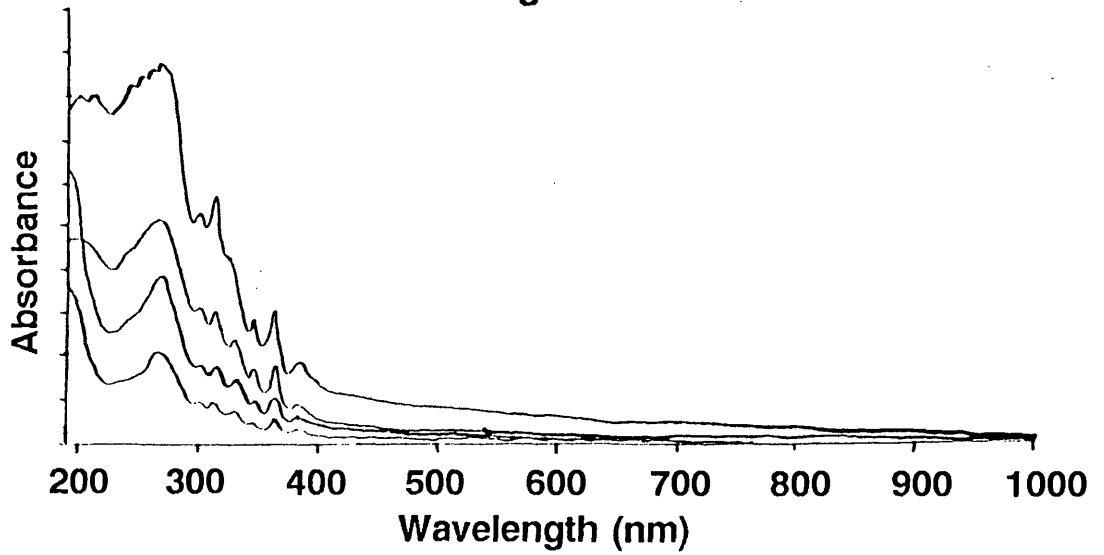
l. Chrysene.

Chrysene forms colourless plates (m.p. = 255-256°C) and is sublimable. Pure crystals of chrysene exhibit a blue fluorescence (130). Films of chrysene in this work were formed on substrates whose temperatures were in the range 20-30°C. There was little loss of definition in electronic spectra of chrysene with increasing film thickness (ca. 30-1000 nm) and electronic absorptions, additional to those assigned to the absorption bands of the components, were found for films exposed to MoF_6 , WF_6 and AsF_5 . There was no observable change in colour of the films in each case. As seen clearly in Electronic spectra:l.2 and Table:L the chemically modified films exhibited many additional absorption bands in the electronic spectra. In contrast to many of the other organic films examined after chemical modification, the additional absorption bands were of very low intensity.

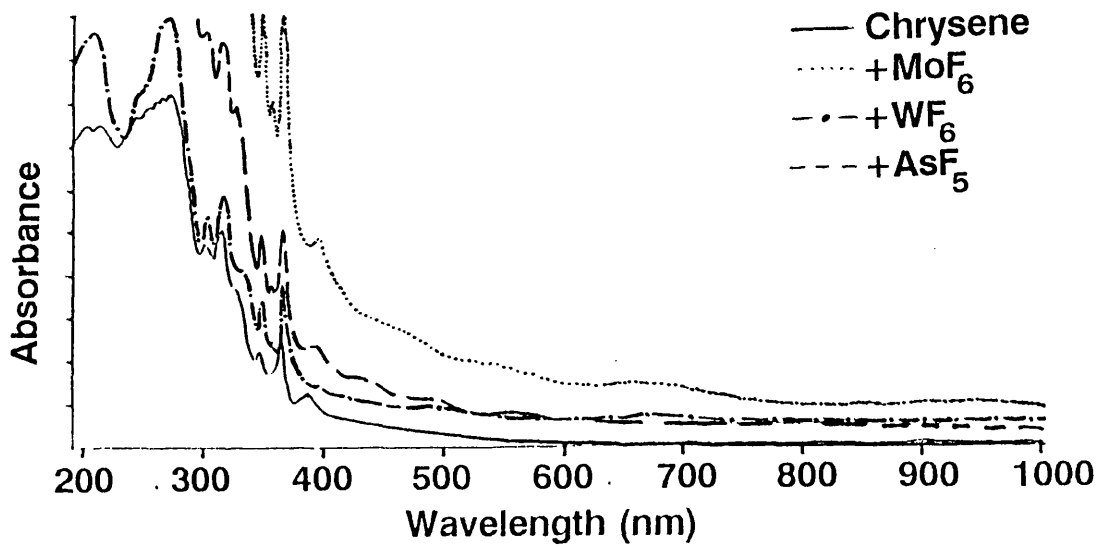
m. Anthracene.

Anthracene forms colourless, fluorescent (blue) monoclinic plates and is sublimed readily (m.p. = 218°C). Anthracene is a semiconductor (131) and becomes a conductor when irradiated at 366.3 - 400 nm (132). The photo-

Electronic spectra: l.1
Effect of increasing film thickness



Electronic spectra: l.2



Electronic spectra: m.1
Effect of increasing film thickness

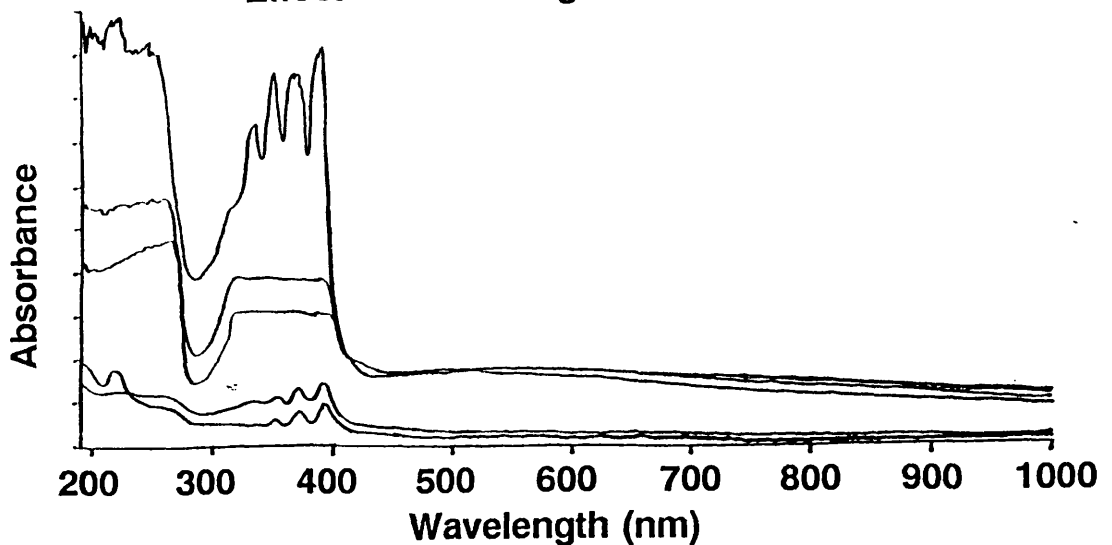


Table L: Electronic spectra of chrysene on silica exposed to oxidant vapour

Chrysene	+MoF ₆	+WF ₆	+AsF ₅
$\lambda_{\max}(\text{nm})$	$\lambda_{\max}(\text{nm})$	$\lambda_{\max}(\text{nm})$	$\lambda_{\max}(\text{nm})$
$10^{-4}\alpha^*(\text{cm}^{-1})$	$10^{-4}\alpha(\text{cm}^{-1})$	$10^{-4}\alpha(\text{cm}^{-1})$	$10^{-4}\alpha(\text{cm}^{-1})$
190(28.51)	190(28.09)	207(25.64)	190(4.57)
240sh (11.34)	205(27.18)	245sh (2.17)	305(3.11)
270(14.80)	240(25.09)	300(2.64)	317(3.17)
305(6.45)	275(25.63)	305sh (13.64)	330(2.73)
317(6.45)	305(18.82)	317(14.89)	348(1.86)
330(5.64)	317(21.27)	330sh (10.36)	355(1.56)
348(3.54)	328(15.16)	348(8.73)	368(1.92)
368(3.82)	350(10.91)	358(9.54)	400(1.13)
387(2.18)	355(8.18)	370(9.38)	433sh (0.91)
393(1.73)	368(12.82)	400(2.73)	480sh (0.80)
	395(5.09)	500(1.360)	560(0.68)
	455sh (2.82)	680(1.09)	
	533sh (2.00)		
	680(1.47)		
	925(1.20)		

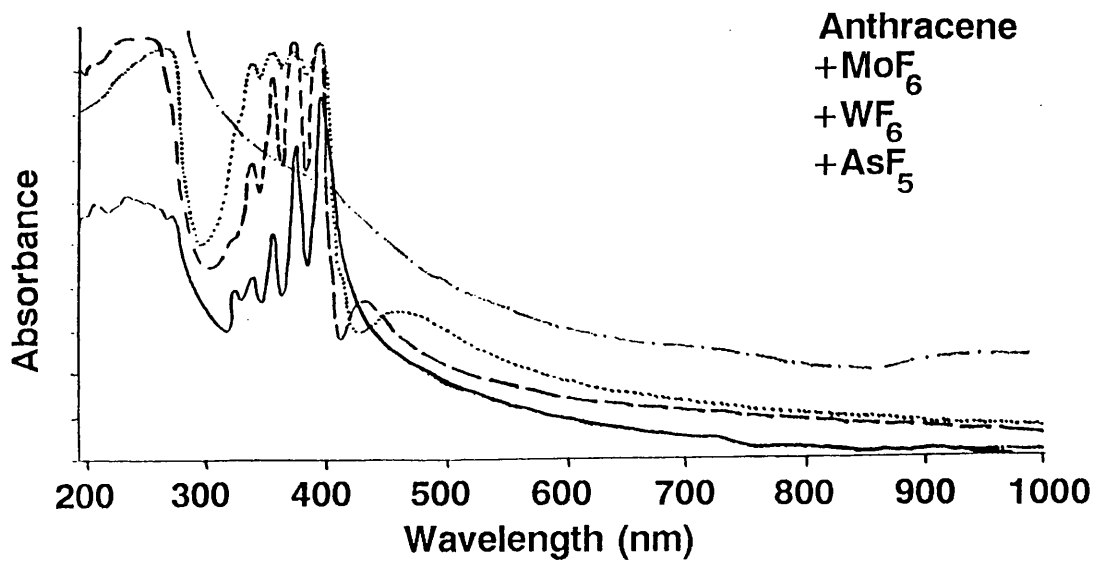
sh=shoulder

conductivity and electronic spectra are related closely (133). Anthracene forms many molecular compounds, the most well-known of which is with TCNQ (134). In this work it was found that thin films of anthracene could be prepared only on substrates allowed to cool to ambient temperature. Thick films of anthracene were removed rapidly from the surface of silica substrates under vacuum. There was a loss of definition in electronic spectra of thicker films (*ca.* > 100 nm) (see Electronic spectra:m.1). Electronic absorptions additional to those assigned to the absorption bands of the components were found for films exposed to MoF₆, WF₆, AsF₅ and for films produced by the co-evaporation of anthracene with TCNQ (see this section, p). As seen clearly in Electronic spectra:m.2 and Table:M films of anthracene exposed to MoF₆ produced electronic spectra of poor resolution, in contrast to spectra obtained for films exposed to both WF₆ and AsF₅. Films exposed to MoF₆ exhibited two additional electronic absorptions centred at 920 nm and 720 nm. Films exposed to WF₆ and AsF₅ produced similar spectra with additional absorption bands at 460 nm and 430 nm respectively.

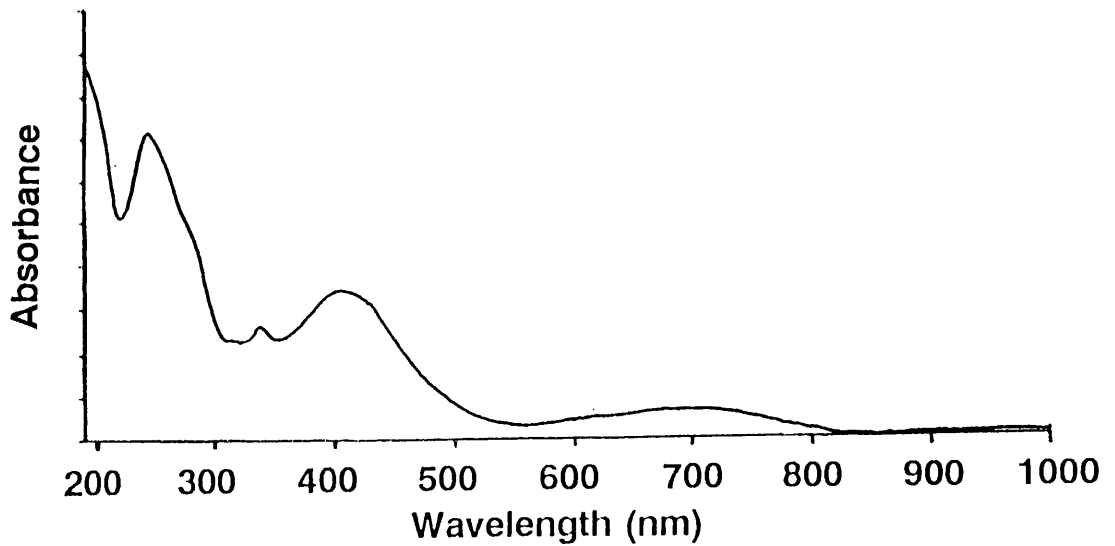
n. Fluoranthene.

Fluoranthene crystallizes in colourless needles or plates (m.p. = 110°C) and has been obtained by the destructive hydrogenation of coal (135). In this work it was found that thin films of fluoranthene could be prepared only on substrates allowed to cool to ambient temperature. There was a complete loss of definition in electronic spectra of fluoranthene with increasing film thickness (Electronic spectra:n.1). Under all conditions there were no electronic

Electronic spectra: m.2



Electronic spectra: m.3 +TCNQ



Electronic spectra: n.1

Effect of increasing film thickness

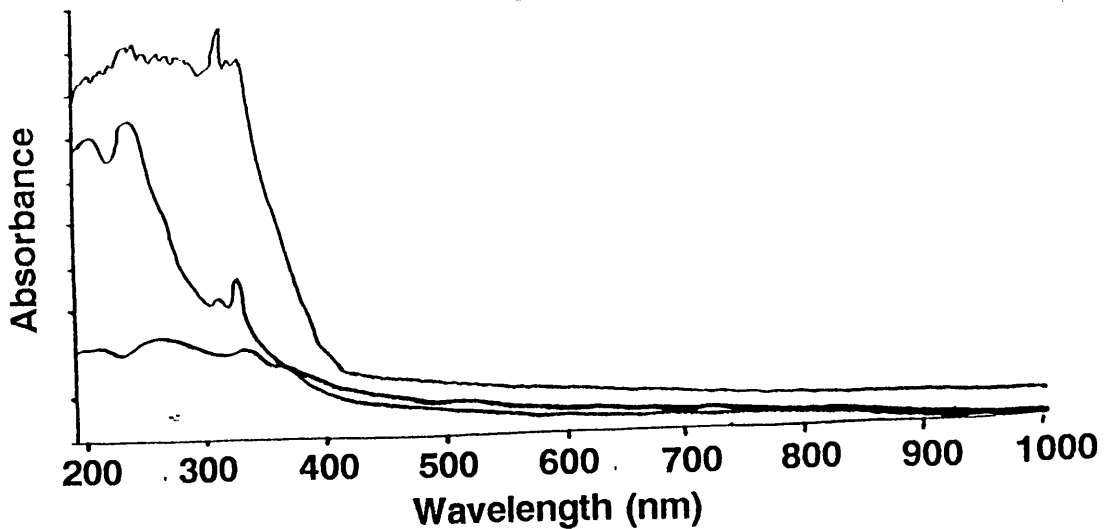
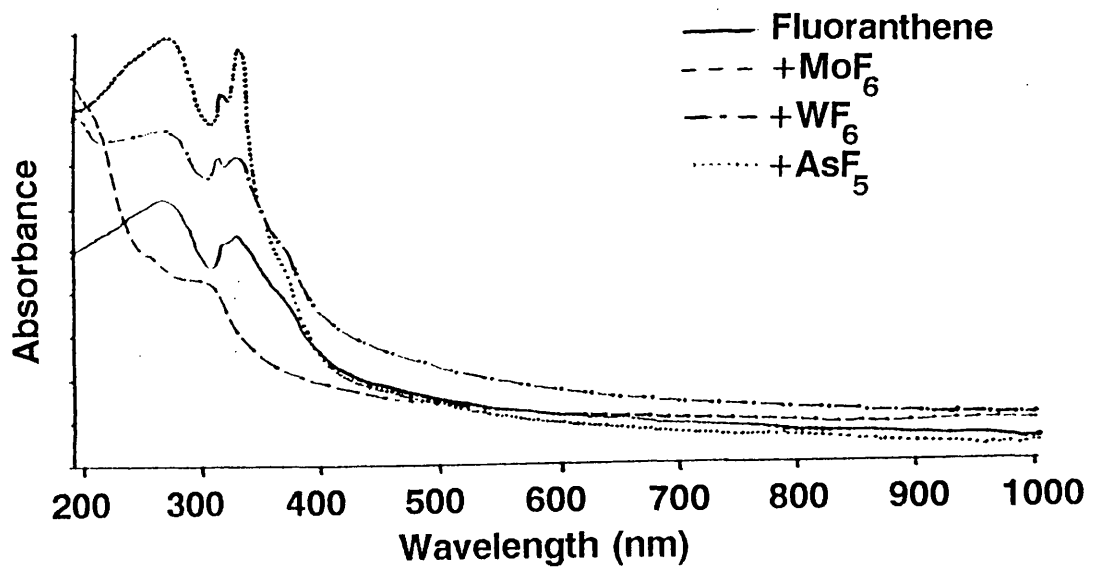


Table M: Electronic spectra of anthracene on silica exposed to oxidant vapour

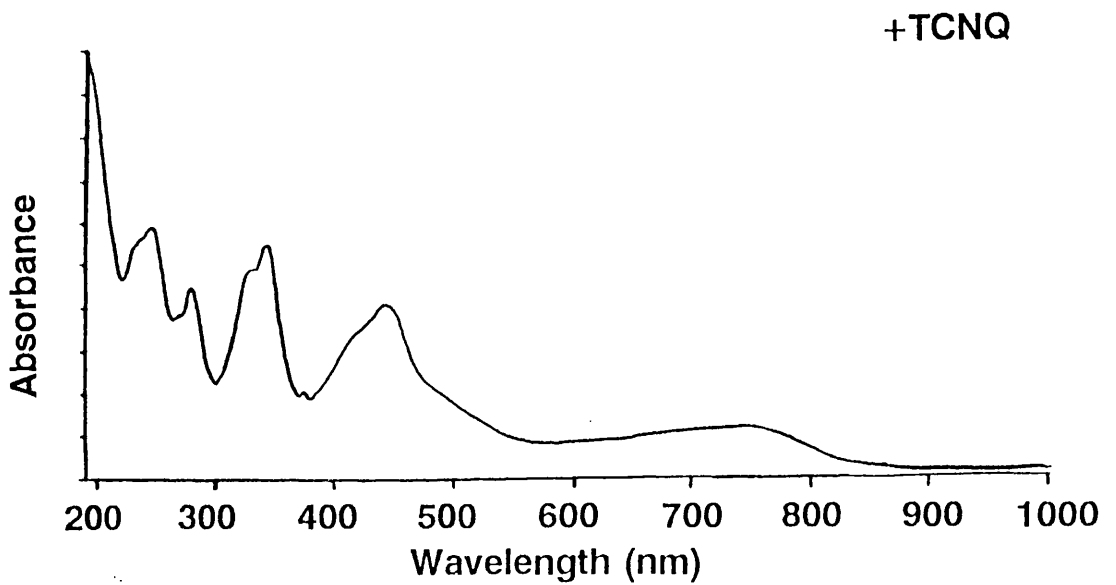
Anthracene	+WF ₆	+MoF ₆	+AsF ₅
$\lambda_{\max}(\text{nm})$	$\lambda_{\max}(\text{nm})$	$\lambda_{\max}(\text{nm})$	$\lambda_{\max}(\text{nm})$
$10^{-4}\alpha^*(\text{cm}^{-1})$	$10^{-4}\alpha(\text{cm}^{-1})$	$10^{-4}\alpha(\text{cm}^{-1})$	$10^{-4}\alpha(\text{cm}^{-1})$
190(5.52)	190(5.59)	190(34.48)	190(21.73)
225(4.41)	275(6.59)	405sh (0.88)	265(6.76)
265(3.03)	333sh (5.17)	510sh (0.67)	275sh (5.74)
314sh (2.10)	350(6.24)	720sh (0.52)	337(4.66)
337(2.86)	363(6.28)	920(0.52)	356(5.98)
356(3.52)	385(6.34)		375(6.70)
375(3.68)	395(6.38)		395(6.74)
395(3.97)	405sh (2.83)		430(2.48)
	460(2.30)		

sh=shoulder

Electronic spectra: n.2



Electronic spectra: o.1



Electronic spectra: o.2

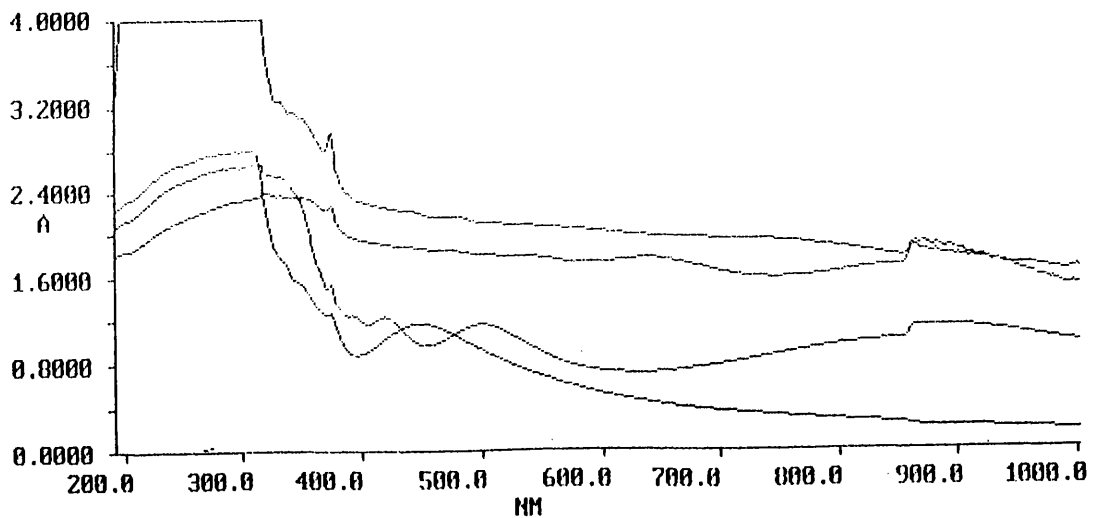


Table N: Electronic spectra of fluoranthene on silica exposed to oxidant vapour

Fluoranthene	+MoF ₆	+WF ₆	+AsF ₅
$\lambda_{\max}(\text{nm})$	$\lambda_{\max}(\text{nm})$	$\lambda_{\max}(\text{nm})$	$\lambda_{\max}(\text{nm})$
$10^{-4}\alpha^*(\text{cm}^{-1})$	$10^{-4}\alpha^*(\text{cm}^{-1})$	$10^{-4}\alpha^*(\text{cm}^{-1})$	$10^{-4}\alpha^*(\text{cm}^{-1})$
190(12.92)	190(16.14)	190(21.92)	190(19.23)
205sh (13.54)	262sh (9.85)	205sh (21.54)	268(23.00)
235sh (12.62)	312sh (8.83)	275(20.77)	320(19.62)
240(14.30)		335(20.08)	330(22.06)
262(14.30)		375sh (15.83)	367sh (11.31)
312(11.14)		400(11.31)	400sh (5.77)
327(12.92)			
362sh (10.79)			
387sh (8.20)			
400(6.17)			

sh=shoulder

absorptions additional to those assigned to the absorption bands of fluoranthene for films exposed to MoF_6 , WF_6 , AsF_5 (Electronic spectra:n.2 and Table:N) or for films produced by the co-evaporation of fluoranthene with TCNQ (see this section, p). There was an uncertainty in all reactions however as films were unstable and were removed rapidly under vacuum, to a greater extent than was the case for anthracene. As a consequence no firm conclusions could be drawn from the electronic spectra.

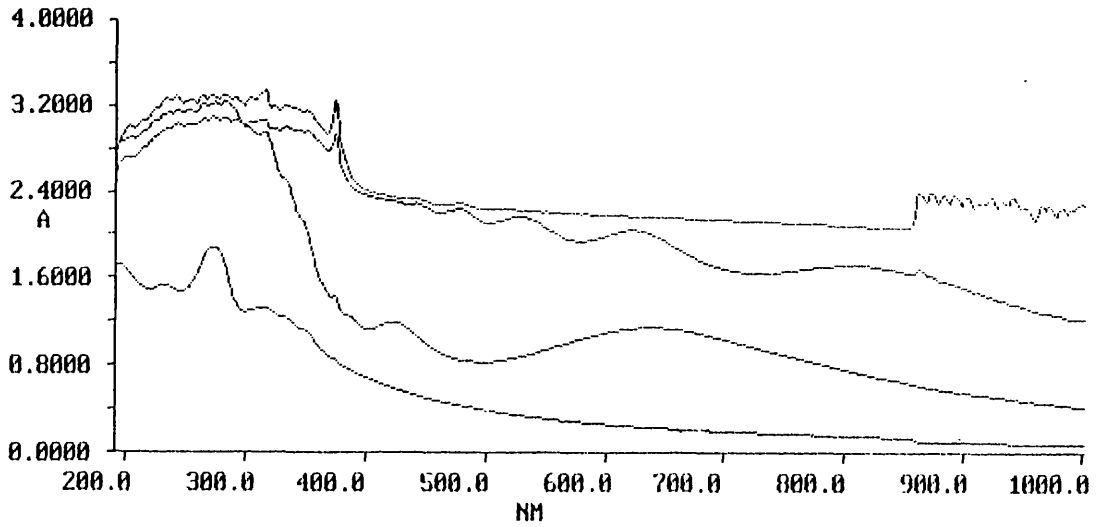
o. Pyrene.

Pyrene crystallizes in monoclinic plates (m.p. = 156°C). In this work it was found that thin films on silica could be produced only on a substrate allowed to cool to ambient temperature. Under all conditions electronic and vibrational spectra were dominated by interference patterns (Electronic spectra:o.2-5) and as a consequence no conclusions could be drawn from the electronic spectra of films exposed to MoF_6 , WF_6 and AsF_5 . Films produced by the co-evaporation of pyrene with TCNQ (see this section, p) were more satisfactory and exhibited an absorption band additional to those assigned to the absorption bands of the components (Electronic spectra:o.1).

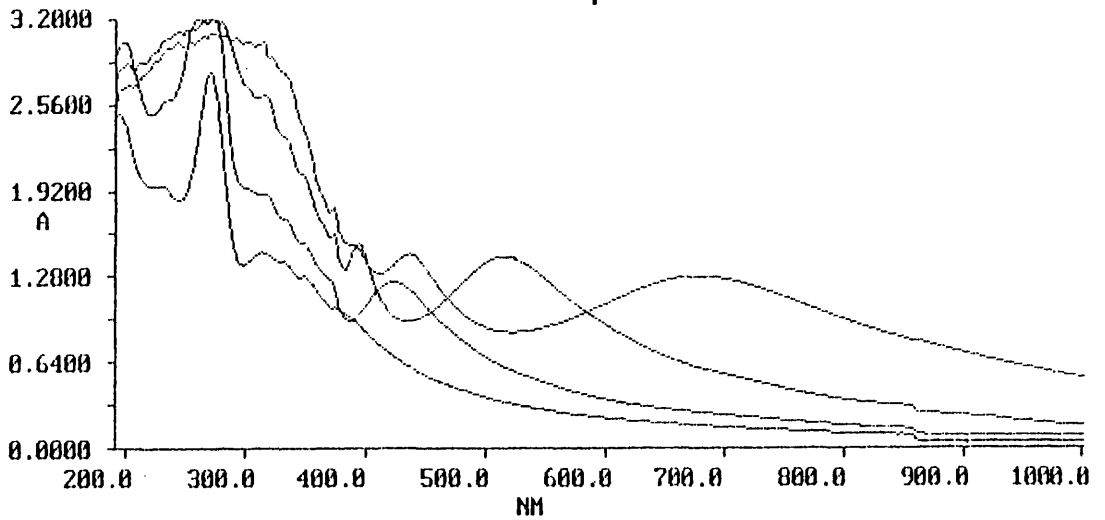
p. 7,7,8,8-tetracyano-p-quinodimethane (TCNQ)

The majority of organic solids are electrical insulators. There are however many interesting examples of salts formed from the organic electron acceptor TCNQ and donor hydrocarbon molecules, which were shown to be semiconductors primarily as a result of work at Du Pont during the 1960s

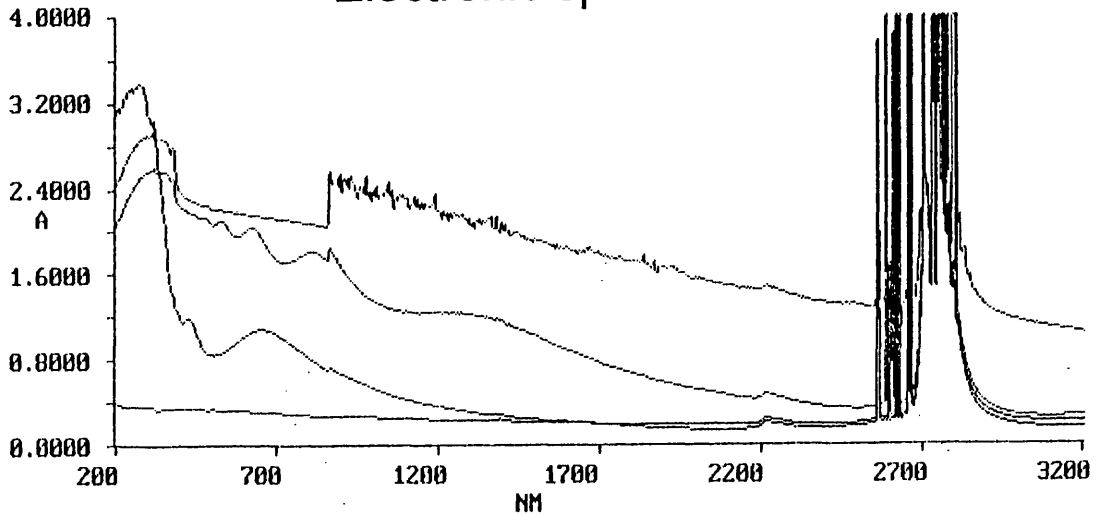
Electronic spectra: o.3



Electronic spectra: o.4



Electronic spectra: o.5



(136). This area was discussed earlier in Introduction:G.

In the present work attempts were made to produce charge-transfer complexes supported on silica by the co-evaporation of TCNQ with the compounds a. to o. discussed previously. Films were prepared as follows. A quantity of both TCNQ and the compound in question were ground in an agate mortar and pestle until a fine homogeneous powder was obtained and used subsequently to produce a thin film on silica (see Experimental:C). Films were formed on substrates whose temperatures were in the range 30-50°C. Electronic spectra were recorded for the chemically modified films and the results reported as peak positions λ_{max} (nm). Absorption coefficients could not be determined. Results are summarised in Table 11. Electronic absorptions additional to those assigned to the absorption bands of the components were found for films derived from perylene (Electronic spectra:a.4), BEDT-TTF (Electronic spectra:b.2), pentacene (Electronic spectra:d.3), decacyclene (Electronic spectra:k.3), anthracene (Electronic spectra:m.3) and pyrene (Electronic spectra:o.1). A broad symmetrical absorption band in the region 700-750 nm was observed in the electronic spectra of all films except those derived from perylene, which exhibited an electronic absorption of exceptional bandwidth centred at 1050 nm.

2. Attempted chemical modification using PF_5 or BF_3

Under all conditions no changes in the electronic spectra of perylene, BEDT-TTF, violanthrone, pentacene, ovalene, tetracene, rubrene, PTCDA, CTCDA, CTA, decacyclene, chrysene, anthracene, fluoranthene and pyrene were

observed for films exposed to PF_5 or BF_3 .

3. Classification of the spectroscopic data.

From the results obtained for organic thin films on silica, exposed to the oxidants MoF_6 , WF_6 and AsF_5 , the organic compounds could be placed into three categories.

A. Films which exhibited both electronic and physical perturbations, such as the loss of definition and new absorption bands at lower energies in the electronic spectra upon chemical modification. In all cases there was no conclusive evidence in the electronic spectra for the formation of radical cations (as reported in the literature (137)) derived from the donor PAHs (perylene, BEDT-TTF, violanthrone, pentacene, ovalene, tetracene, rubrene, PTCDA, CTCDA, decacyclene, chrysene and anthracene). Some absorption bands, additional to those assigned to the components, appeared to be characteristic of a particular PAH (perylene, violanthrone, ovalene, tetracene, chrysene and anthracene) and were not dependent greatly on the oxidant material (MoF_6 , WF_6 or AsF_5) in those cases where chemical modification of the film was found to occur for more than one oxidant (eg. absorption centred at 620-660 nm in chemically modified films of perylene). For those films where exposure to less powerful oxidizing agents (see Introduction:F) did not produce additional absorption bands, definition in the electronic spectra was lost completely and a broad featureless band was observed (violanthrone, pentacene, tetracene, rubrene, PTCDA, CTCDA and decacyclene). Films in category A were found to exhibit effects such as a loss of definition and changes in relative band

intensities in the electronic spectra with increasing film thickness. Electronic spectra of thin films (*ca.* 50 nm) in many cases approximated those of solution spectra.

B. Films which exhibited changes in definition and relative band intensities in the electronic spectra upon exposure to oxidants, with no additional absorption bands (CTA and fluoranthene). It was concluded tentatively that a physical perturbation of the film occurred, where the molecular order of the film on the surface of the silica was disrupted. Films were found to exhibit effects such as a loss of definition and changes in relative band intensities in the electronic spectra with increasing film thickness.

C. Films which were dominated by interference patterns in the electronic and vibrational spectra. These patterns were assumed to result from the interaction of radiation transmitted through the film and radiation reflected by the inner surfaces of the film layers then transmitted. In particular films of pyrene were susceptible to these effects and rubrene to a lesser extent. For such films no sensible conclusions could be established from experiments where films were exposed to oxidants.

4. Infrared spectra.

In order to ascertain whether or not the process of preparing thin films on silica (see Experimental:C) produced changes in the chemical and physical nature of the organic compounds employed, a number of FT-IR spectroscopic

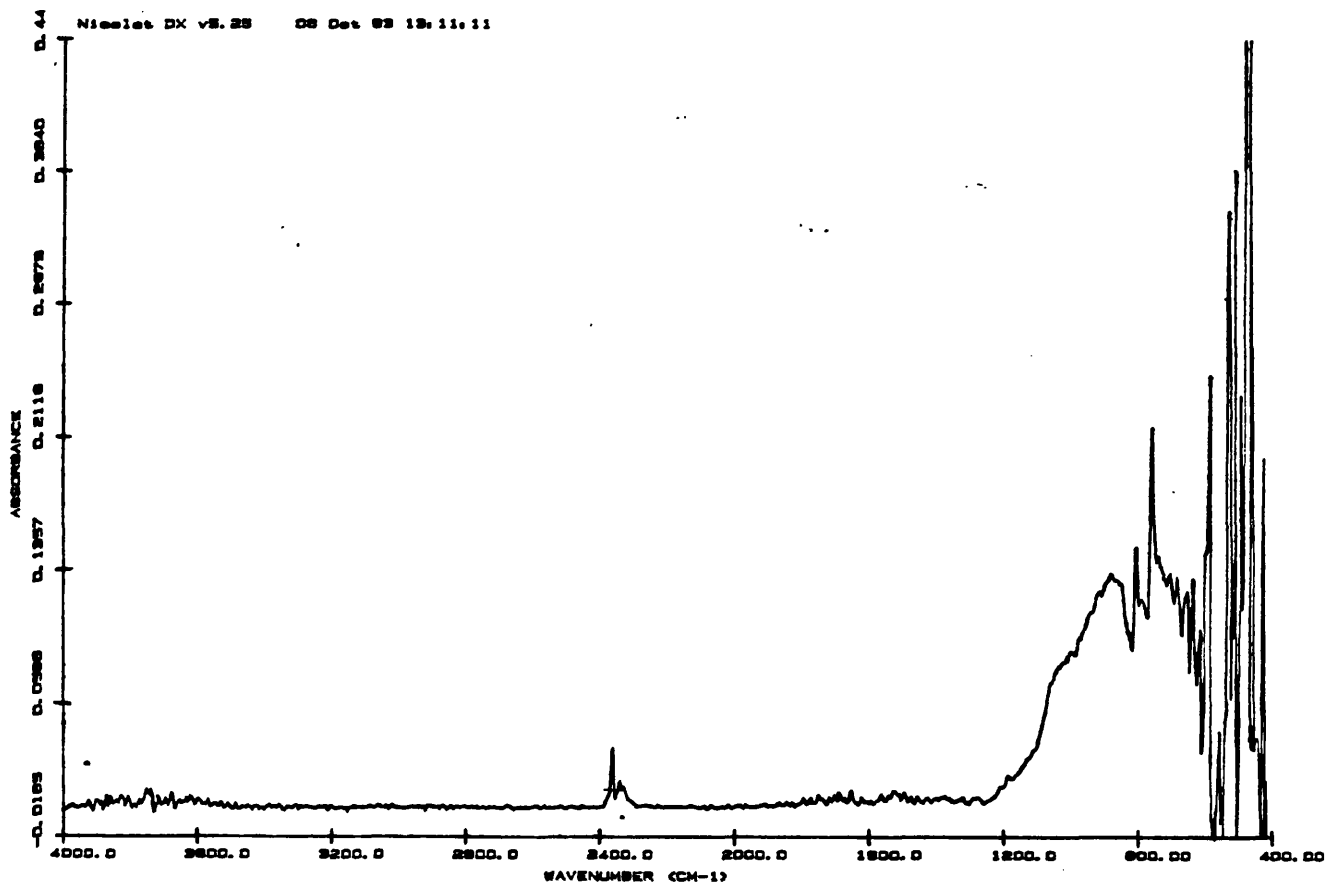
Infrared spectra of thin films of PAHs on silica

^a Chrysene	^a Perylene	^a Anthracene	^a Tetracene	^a Fluoranthene	^b PTCDA	^a Pyrene
640	760	700	740	760	680	687
688	800	760	790	780	720	728
760	840	880	875	840	760	817
820	880	900	920	880	795	910
876	900	960	940	1140	840	947
880	100	1160	1300	1160	876	1059
920	1180	1280	1390	1188	920	1078
940	1220	1320	1460	1220	960	1097
1140	1280	1400	1520	1264	1092	1134
1195	1324	1460	1540	1292	1120	1171
1240	1360	1480		1320	1240	1227
1260	1408	1540		1340	1312	1301
1300	1440			1368	1428	1424
1428	1460			1420	1600	1487
1480	1480			1440	1640	1506
1512	1500			1452	1756	1525
1560	1520			1480	1760	1562
1600	1560			1488	1764	1580
	1600			1540	1878	1655
				1560	1900	1748
				1575	1924	1796
				1600	1942	1860

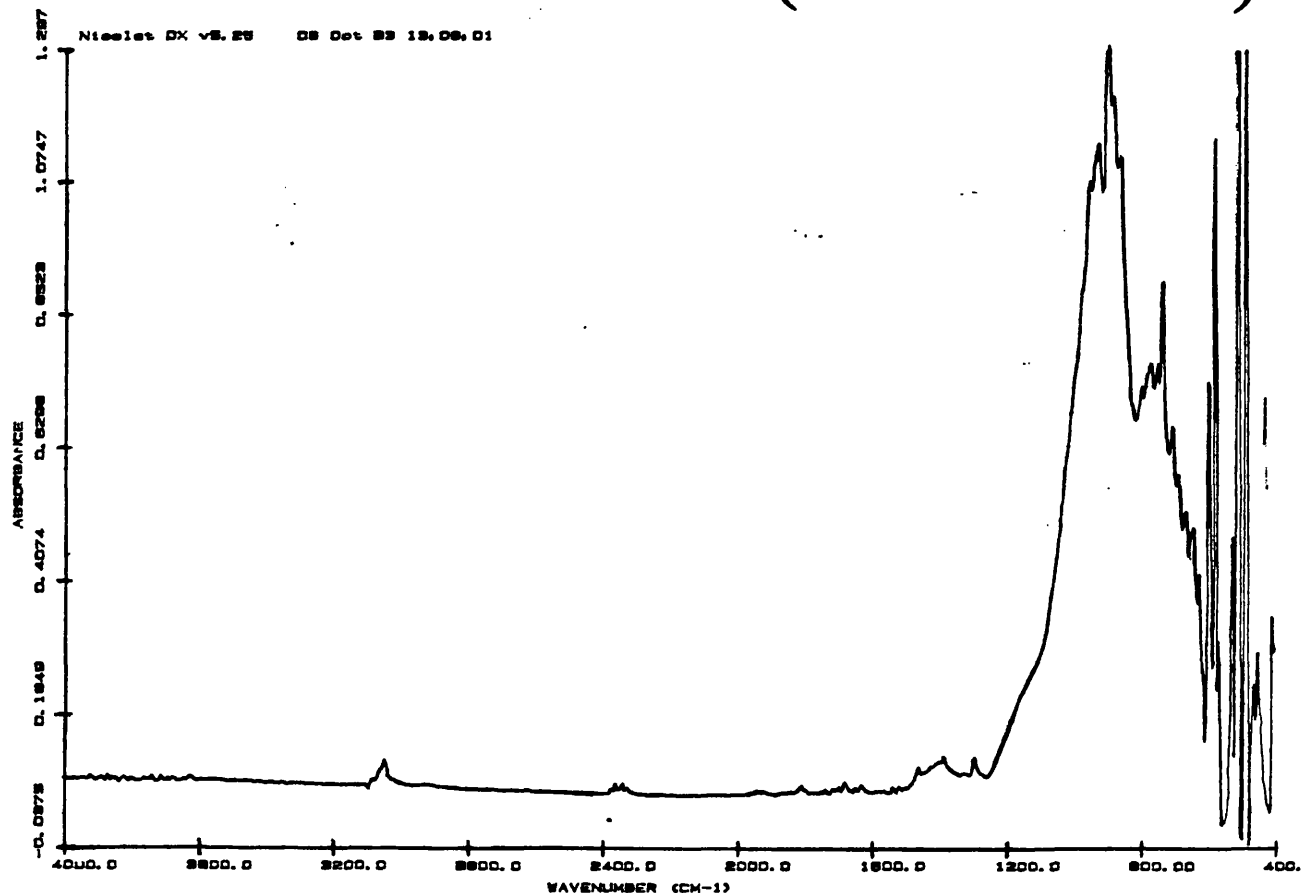
^aBands assigned to PAH (see Ref. 189) in bold type

^bBands assigned to PAH (K.Akers, R.Aroca, A-M. Hor and R.O.Loutfy, *J.Phys.Chem.*, 1987, **91**,2954) in bold type

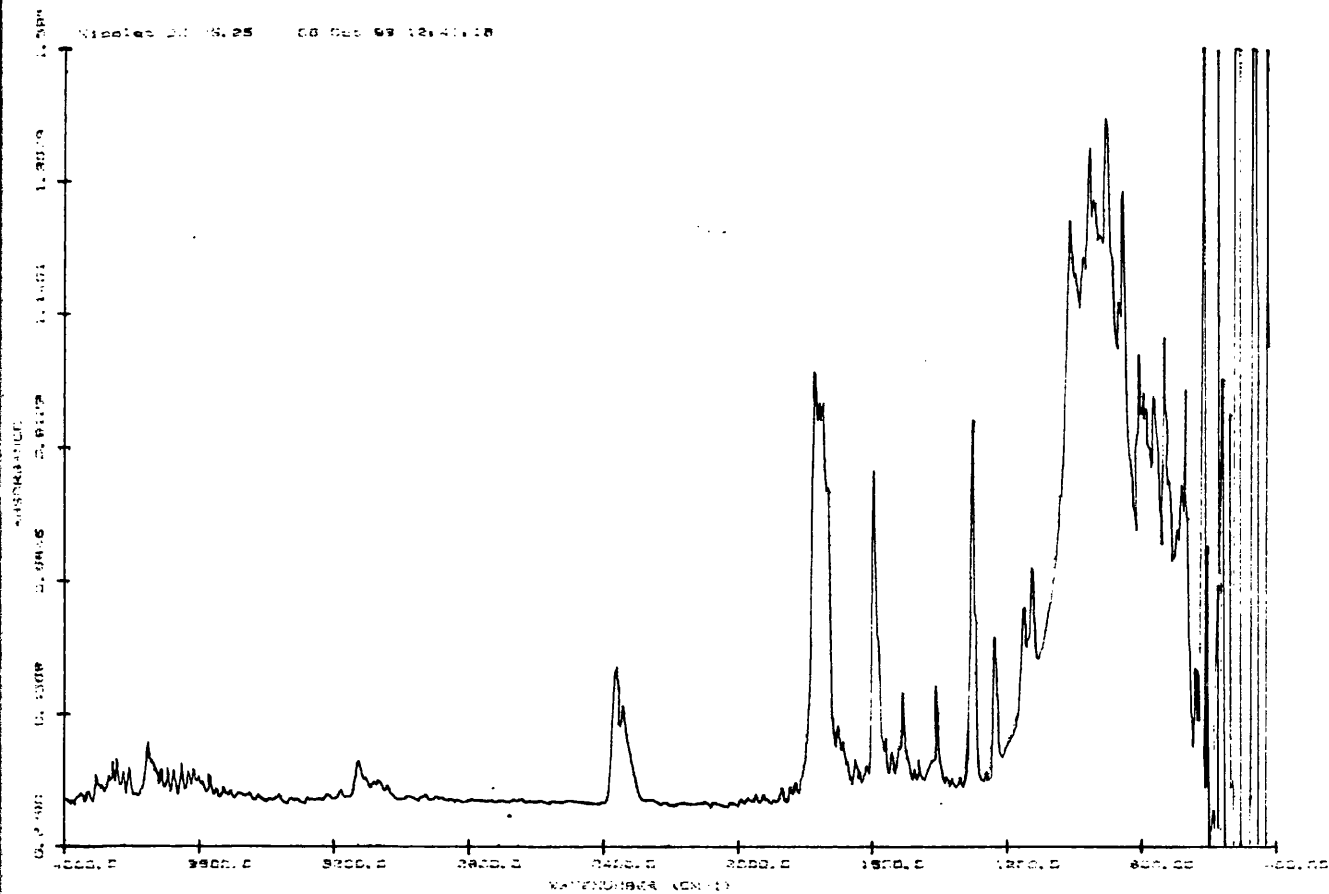
Perylene on silica (ATR-FT-IR)



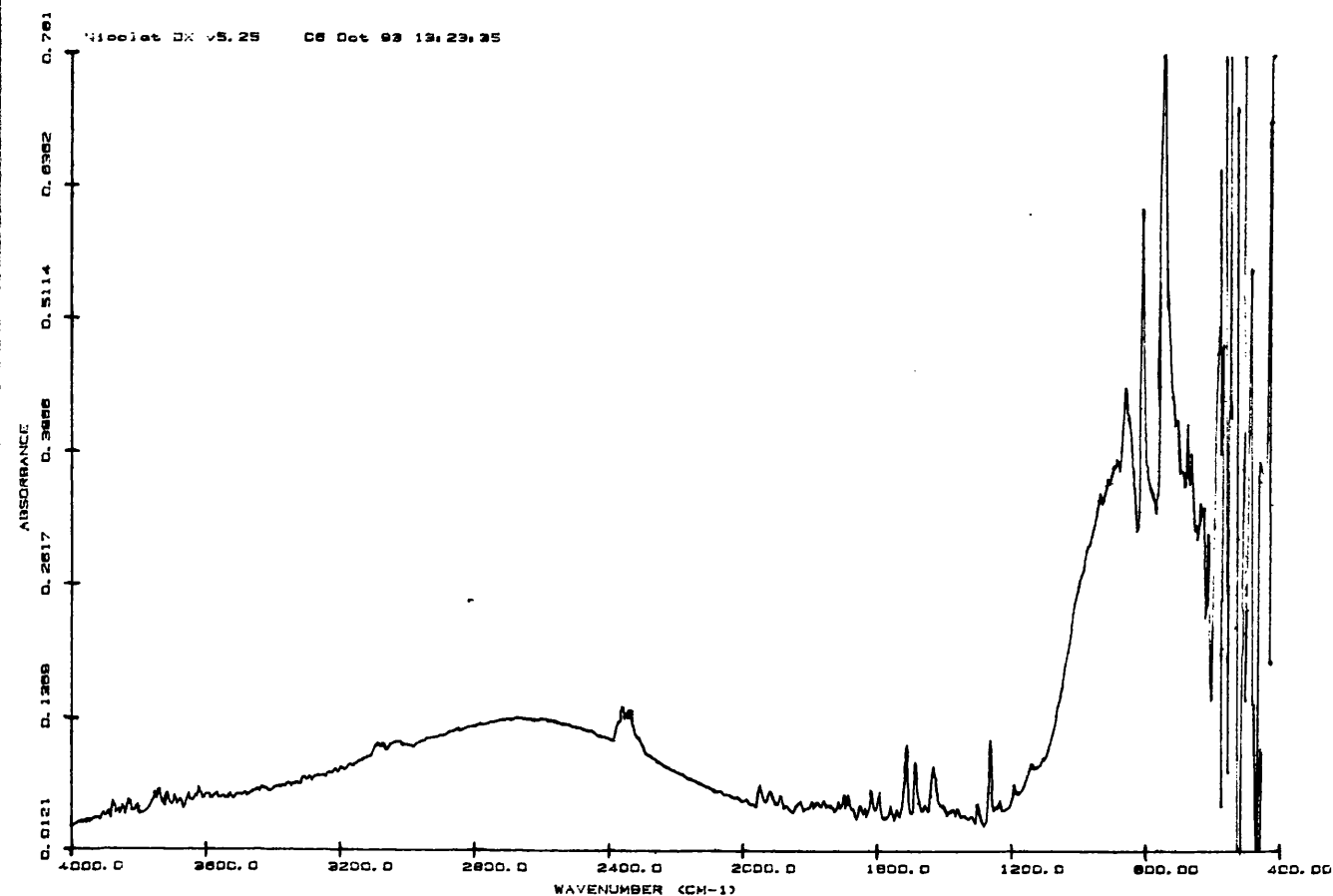
Tetracene on silica (ATR-FT-IR)



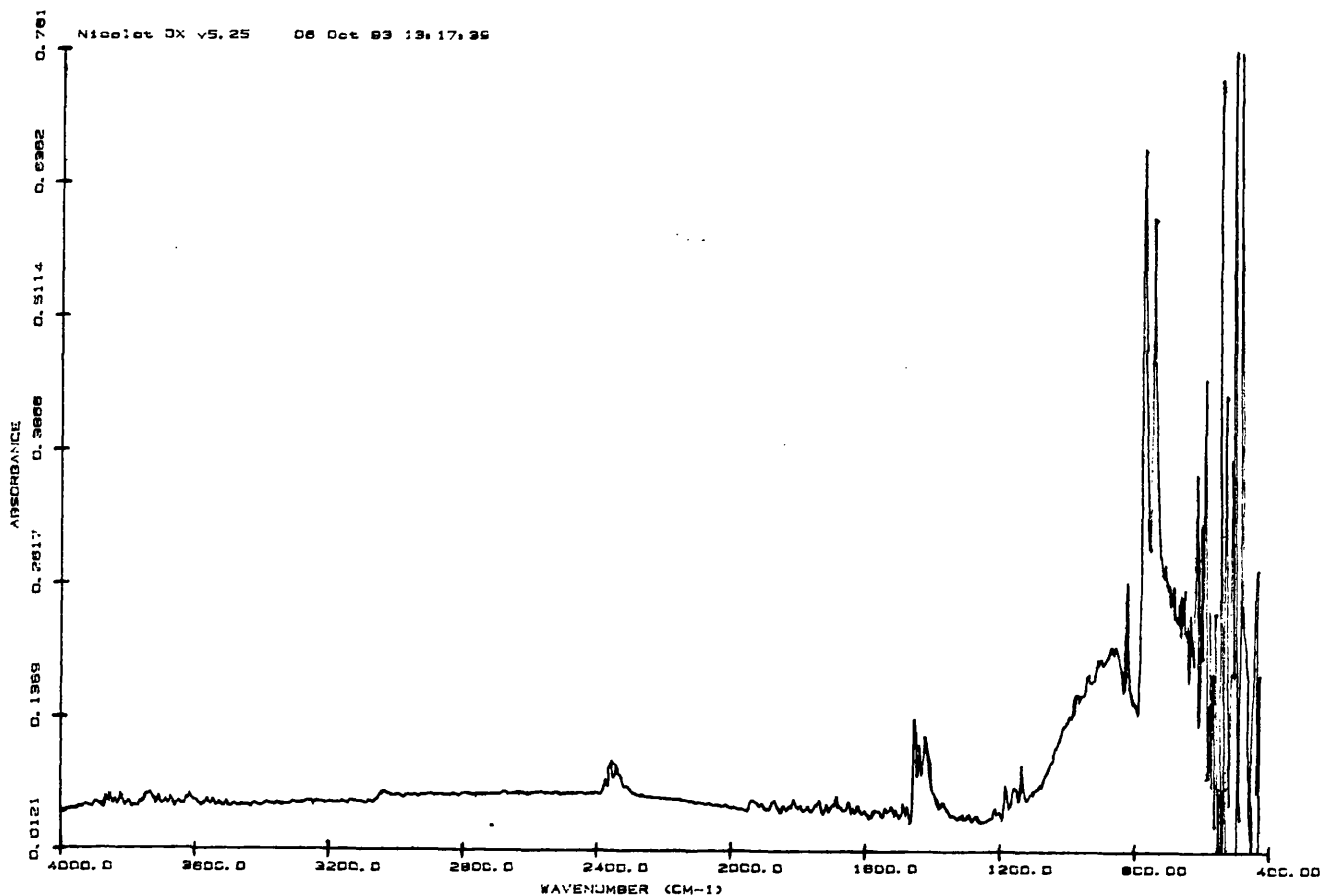
PTCDA on silica (ATR-FT-IR)



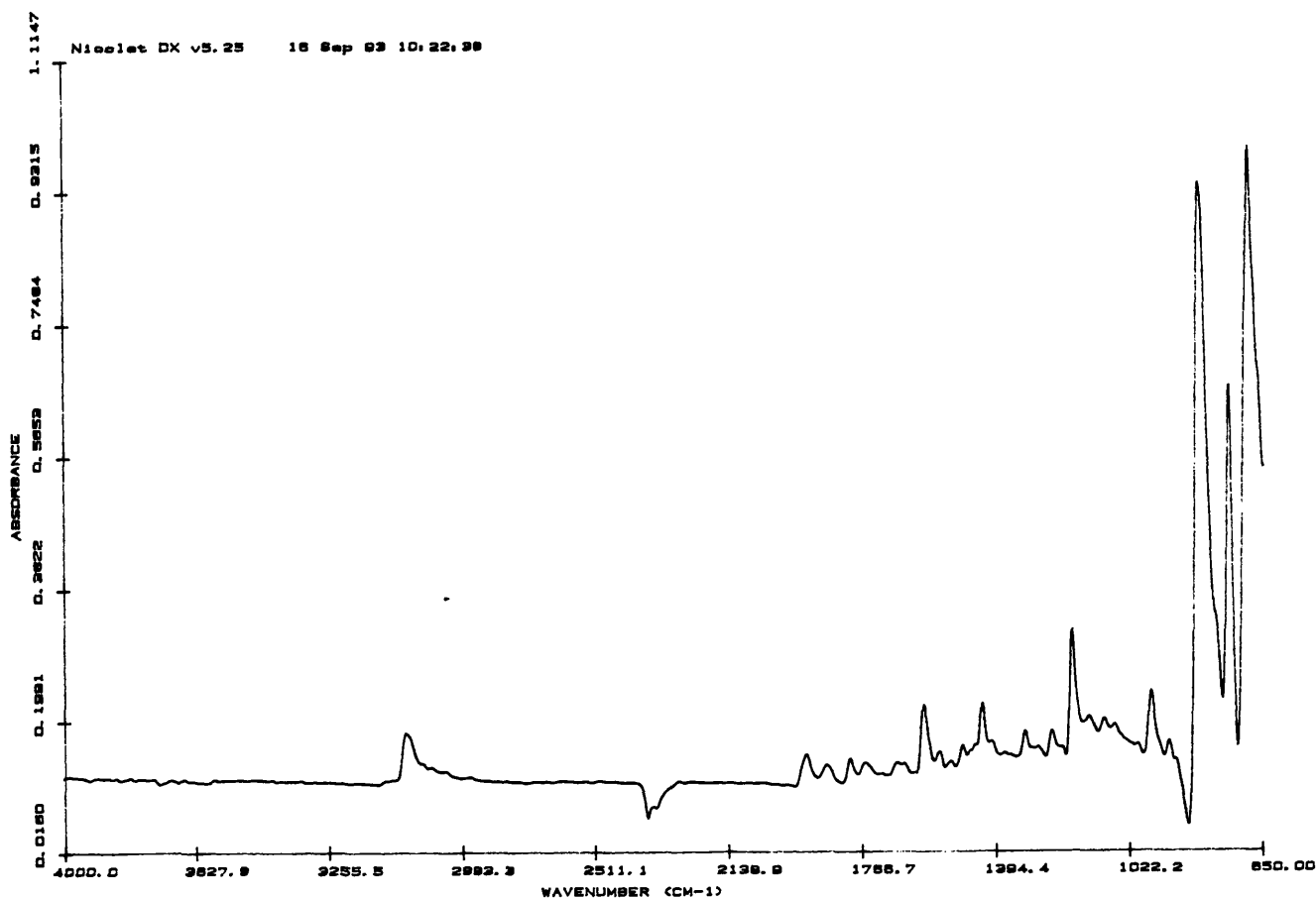
Chrysene on silica (ATR-FT-IR)



Fluoranthene on silica (ATR-FT-IR)

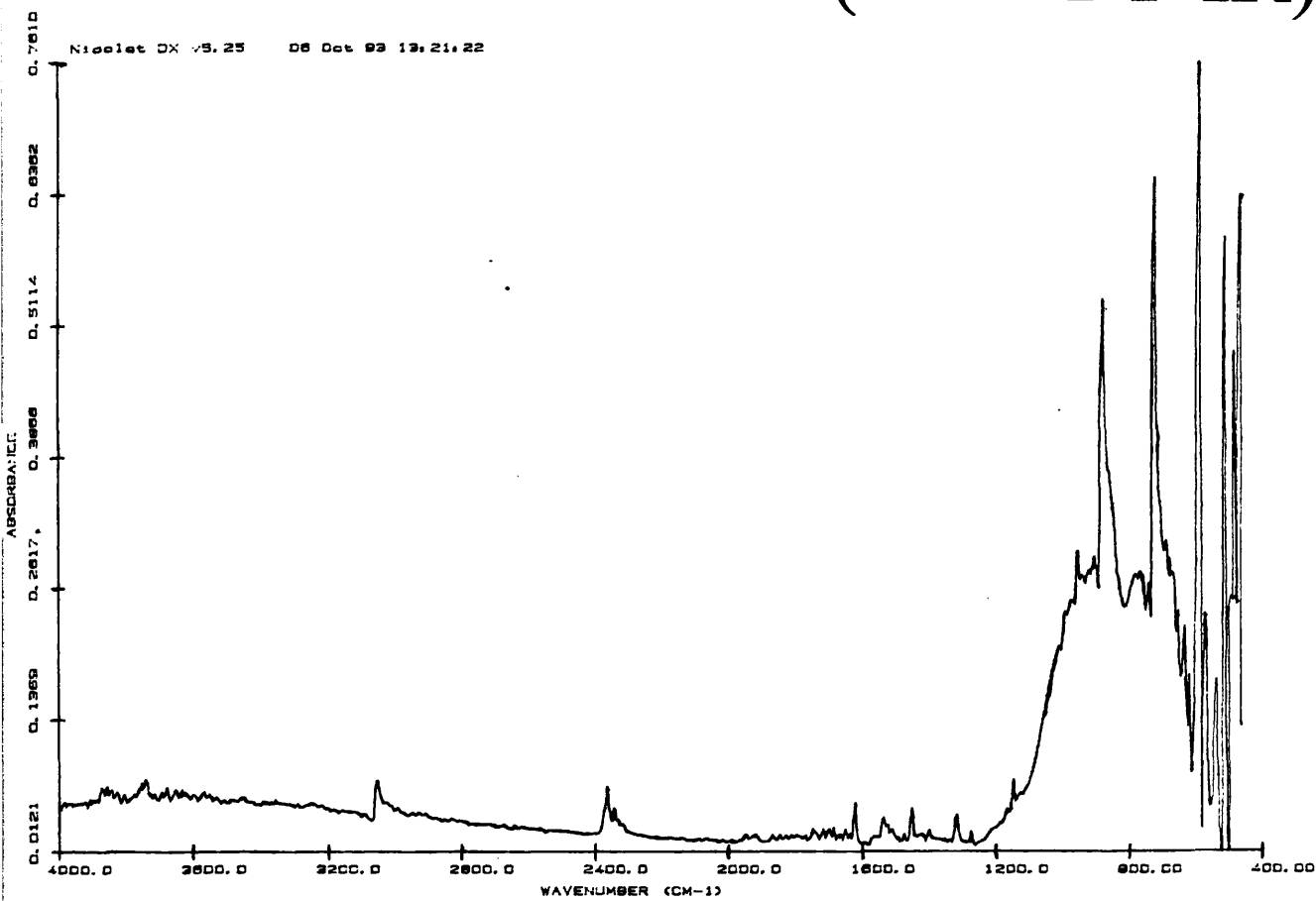


Pyrene on silica (ATR-FT-IR)



Anthracene on silica (ATR-FT-IR)

Nicolet DX v3.25 06 Oct 93 13:21:22



techniques were employed, namely Microspectroscopy, ATR and DRIFTS (see Experimental:F.1). Under all conditions DRIFTS proved unsuccessful. Microspectroscopy and ATR were found to be effective only for films of thickness *ca.* 200 nm (as calculated by the equation in Experimental:C) or greater. Microspectroscopy in reflectance mode produced spectra of variable quality. Many organic thin films on silica produced spectra which were dominated by bands ascribed to siloxane groups. Peaks due to CO₂ and H₂O were difficult to circumvent also. ATR proved more successful although due to the nature of the technique (penetration depth into samples increases with increasing wavelength of radiation) the siloxane bands dominated spectra below *ca.* 1100 cm⁻¹. Representative examples of spectra are given in: Infrared spectra of thin films on silica.

E. The Quartz Crystal Microbalance (QCM) technique *in vacuo* as applied to the reaction of [Al(Pc)F]_n with MoF₆ (see Experimental:E).

Piezoelectric devices have been used for many years in the communications field as frequency controllers, filters in electronic networks and as sensors to measure temperature accurately (44). They have been employed recently in analytical chemistry for the detection and determination of air pollutants at the ppm level (138). In this work the QCM technique *in vacuo* was exploited in order to monitor the doping of the polymeric fluoro-bridged phthalocyanine [Al(Pc)F]_n with MoF₆, through a series of simultaneous spectroscopic, conductivity and mass measurements.

The electrical conductivity of many polymeric phthalocyanine complexes

increases significantly when partially oxidised, resulting in segregated stacks of partially oxidised phthalocyanine with arrays of counter-ions or in simpler terms, electron donors and electron acceptors in different columns (56). The electrical conductivity is dependent necessarily on the electronic structure; changes in the electronic structure of phthalocyanine molecules upon doping depend on the size, shape, electron affinity and quantity of the doping molecules employed.

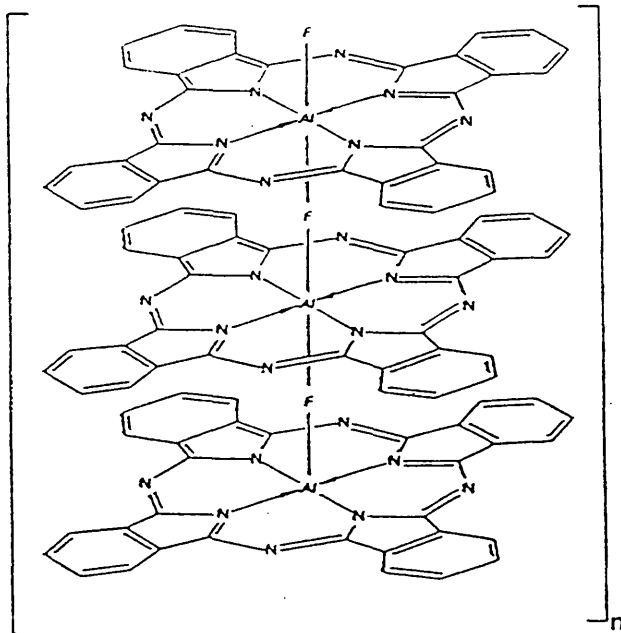
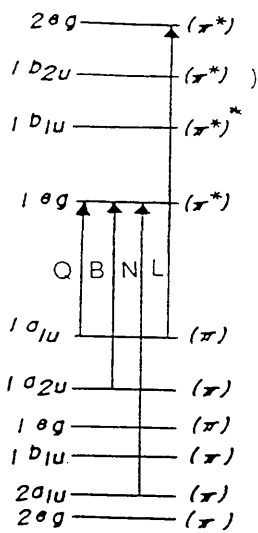
The study of the electronic spectra before and after doping can yield information such as the effect of doping on the state of polymerisation.

The electronic spectra of most metal-phthalocyanine (MPc) complexes consist of five absorption bands in the region 800 - 200 nm, labelled Q, B, N, L and C. The Q band appears in the visible part of the spectrum (the Q-region) near 600 - 700 nm while the remaining bands appear in the ultraviolet (the B-region) between 200 - 400 nm (139). A shoulder on the low energy side of the B band is observed in the electronic spectra of many MPc complexes and is assigned tentatively to the $n \rightarrow \pi$ transition from bridging aza links (140).

The electronic spectra of the $[\text{Al}(\text{Pc})\text{F}]_n$ polymer consists of four absorption bands in the Q and B regions, with a shoulder on the low energy side of the B band. Assignments of the bands were taken from a previous study (141) (Figure 59).

The electronic spectra of thin films on silica substrates (see Experimental:C) were recorded in the region 185 - 3200 nm and compared with those films exposed to MoF_6 . The comparison revealed that in all cases the Q band was broadened and split, producing bands at 600 nm and 720 nm of decreased intensity. In the initial stages of doping the B, N and L bands

Figure 59: Electronic spectra of metal phthalocyanines (MPc)



Structure of poly(fluoroaluminium-phthalocyanine), $[Al(Pc)F]_n$.

620 nm	Q	$1a_{1u}(\pi) \rightarrow 1e_g(\pi^*)$
330 nm	B	$1a_{2u}(\pi) \rightarrow 1e_g(\pi^*)$
285 nm	N	$2a_{1u}(\pi) \rightarrow 1e_g(\pi^*)$
235 nm	L	$1a_{1u}(\pi) \rightarrow 2e_g(\pi^*)$

moved to shorter wavelength and lower intensity. In contrast, at higher levels of doping all three bands increased in intensity, the N band increasing in intensity more rapidly than the B and L bands.

Experiment 1.

In order to establish the experimental parameters an experiment was conducted, as described in Experimental:E, without employing the external oscillator circuitry (i.e. with omission of any mass or conductivity measurements). Electronic spectra were recorded in the region 190 - 1000 nm for the film before and after addition of MoF₆ (Figure 60:a).

Experiment 2.

This and all subsequent experiments were conducted as described in Experimental:E. Electronic spectra were recorded in the region 190 - 3200 nm for the film before and after addition of MoF₆ (Figure 60:b). Although the initial addition of oxidant was far in excess of that which was desirable for the observation of the partial oxidation of the [Al(Pc)F]_n polymer, the experiment was useful as there appeared to be an irreversible adsorption or reaction of MoF₆ on the surface of the gold electrode of the quartz crystal. A subsequent experiment employing an uncoated gold electrode/quartz crystal confirmed this observation. It was estimated that *ca.* 33% of all mass increments of MoF₆ as detected by the QCM were due to an interaction with the gold electrode. In all subsequent experiments it was necessary to take this factor into account (i.e. each addition of MoF₆ was corrected by 33%).

Figure 60:a. QCM experiment 1

X: USER003; 1000.0 - 190.0 NM; pts 811; int 1.00; ord 0.2671 - 1.5070 A
Inf: 00:54:05 00/01/01

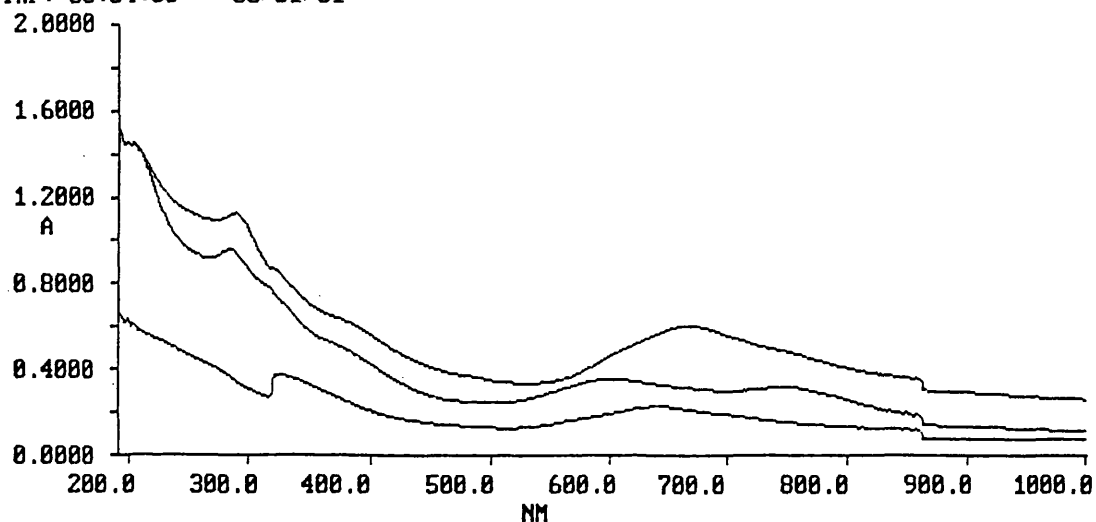
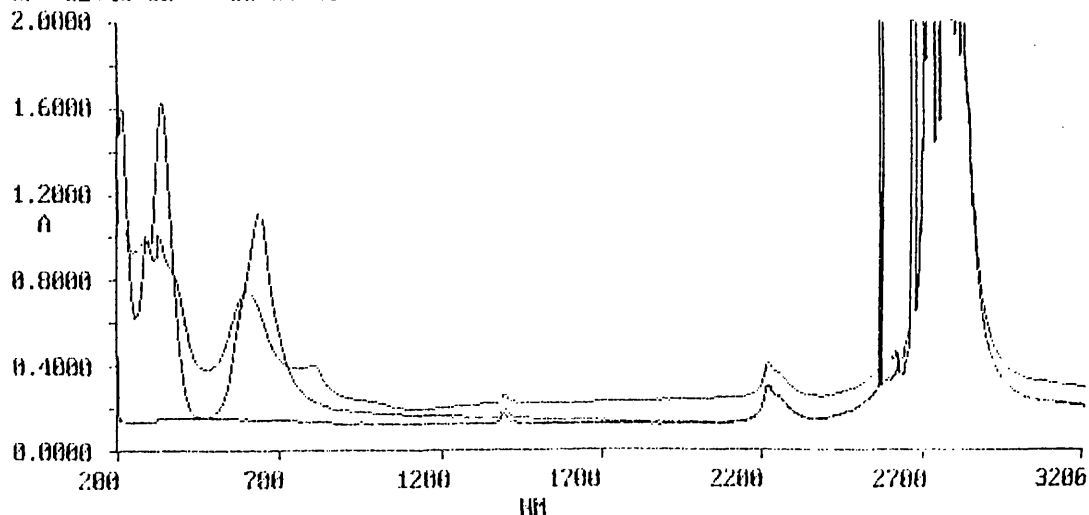


Figure 60:b. QCM experiment 2

X: dsbPfla01; absc 3200.0- 190.0; pts 3011; int 1.00; ord 0.1220-5.9904; a
Inf: 02:46:52 00/01/01



Experiment 3.

Electronic spectra were recorded in the region 190 - 3200 nm for the film before and after additions of MoF₆ (Figure 60:c). It was found that the electronic conductivity rose immediately with the initial addition of oxidant, though of an order of magnitude lower than that expected for a semiconductor (*ca.* 0.5 Ω⁻¹cm⁻¹) and remained constant throughout the experiment. The initial addition of oxidant was far in excess of that which was necessary for the partial oxidation of the polymer; oxidation was found to be complete for a mole ratio of [Al(Pc)F]_n to MoF₆ of 1:14.

Experiment 4.

Electronic spectra were recorded in the region 190 - 3200 nm for the film before and after additions of MoF₆ (Figure 60:d). Due to experimental difficulties encountered in the previous run, conductivity measurements were omitted. This experiment proved more satisfactory and a series of electronic spectra corresponding to different levels of doping were collected and the results tabulated (Table 12).

Experiment 5.

Electronic spectra were recorded in the region 190 - 3200 nm for the film before and after additions of MoF₆ (Figure 60:e). A series of electronic spectra corresponding to different levels of doping were collected and the results tabulated (Table 13).

Figure 60:c. QCM experiment 3

Z: dsbp0502; absc 3200.0- 190.0; pts 3011; int 1.00; ord 0.2911-5.9904; A
inf: 02:26:59 00/01/01

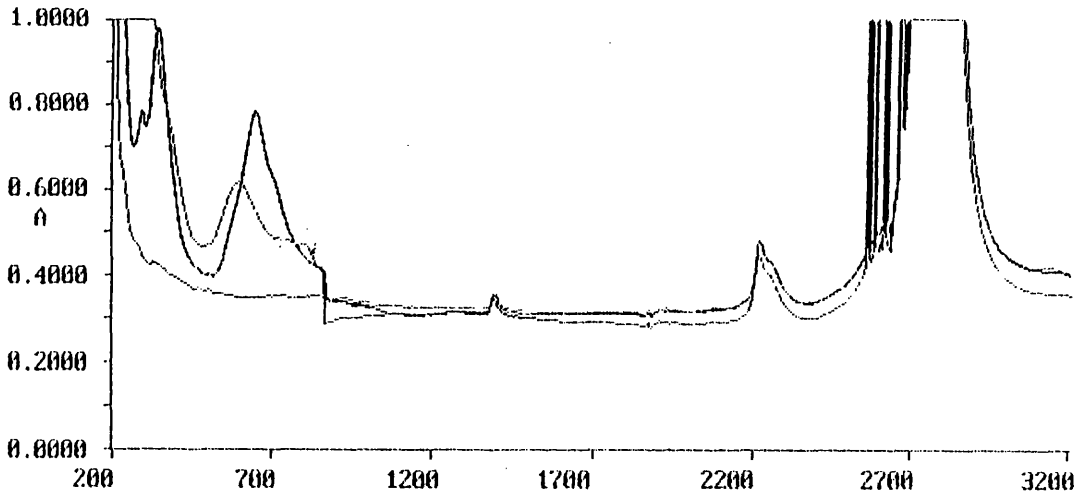


Figure 60:d. QCM experiment 4

X: dsbph014; 3200.0 - 190.0 NM; pts 3011; int 1.00; ord 0.2625 - 5.9904 A
Inf: 06:29:02 00/01/01

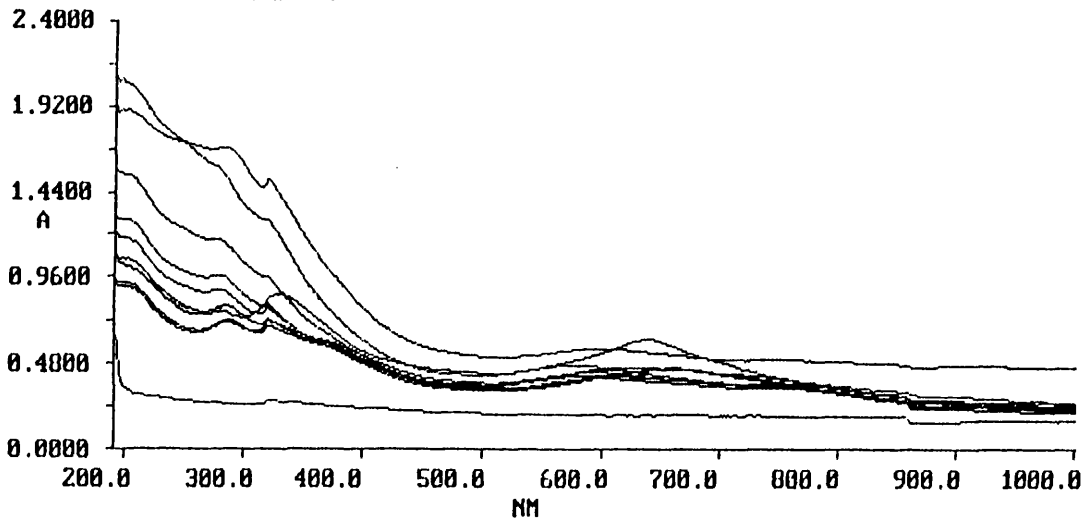
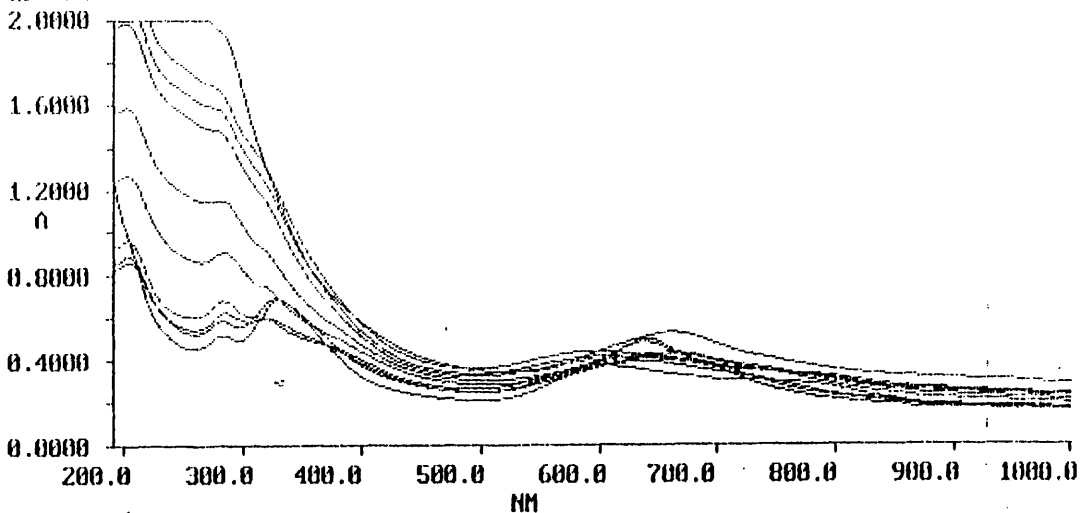


Figure 60:e. QCM experiment 5

X: dsbph915; absc 3200.0- 190.0; pts 3011; int 1.00; ord 0.1705-5.9904; A
inf: 04:26:59 00/01/01



Aliquot of MoF ₆ added	Spectroscopic observations made with each MoF ₆ addition Band positions (nm) / intensities (Absorption coefficient $10^4 \epsilon^*$ (cm ⁻¹))	Mole ratio [Al(Pc)] _n : MoF ₆
None	DSBPH803 640(2.6), 385sh (21.30), 330(28.70), 285(27.20) DSBPH805 750sh (14.00), 640(15.40), 385sh (19.10), 330(24.00), 285(24.60)	
First	New band at 750nm. Bands at 640,330 and 285nm lowered in intensity. Shoulder at 385nm.	1 : 1.8
Second	DSBPH806 750sh (14.00), 640(15.20), 385sh (19.10), 330(24.00), 285(24.60) DSBPH807 750sh (15.50), 640(18.40), 385sh (19.90), 330(25.00), 285(27.20) Band at 640nm increased in intensity relative to other bands.	1 : 3.5
Third	DSBPH808 760sh (12.20), 640(14.70), 600sh (14.00), 385sh (17.70), 330(23.80), 285(26.20) The 640nm band decreased in intensity and split into two new bands at 760nm and 600nm.	1 : 9.2
Fourth	DSBPH810 780(12.20), 600(14.00), 385sh (18.30), 330(26.20), 285(30.10) Bands at 780&600nm established; 640nm band gone. Bands at 385, 330 and 285nm increased in intensity.	1 : 15.7
Fifth	DSBPH811 780(13.60), 600(15.50), 385sh (19.80), 330(27.70), 285(32.30) Bands at 385, 330 and 285nm increase in intensity.	1 : 16.6
Sixth	DSBPH812 780(13.70), 600(15.60), 385sh (21.20), 330(31.20), 285(39.70) Bands at 385, 330 and 285nm increased in intensity.	1 : 19.6
Seventh	DSBPH813 780(13.60), 585(16.00), 385sh (25.00), 330(43.30), 285(52.10) 600nm band moves to 585nm and increases in intensity as do bands at 385, 330 and 285nm. DSBPH814 Cell opened to atmo. sphere. Loss in resolution of bands over 5min.	1 : 19.6

Table 12: Quartz Crystal Microbalance experiment 4

Aliquot of MoF ₆ added	Spectroscopic observations made with each MoF ₆ addition Band positions (nm) / intensities (Absorption coefficient 10 ⁴ α* (cm ⁻¹))	Mole ratio [Al(Pc)F] _n : MoF ₆
None	DSBPPH901 685sh (19.56), 640(23.20), 330(26.80), 285(20.00) DSBPPH902 685sh (19.40), 640(23.00), 325(27.00), 285(21.18)	
First	DSBPPH903 750sh (17.20), 640(19.80), 385sh (20.00), 310(23.60), 285(23.60) 640nm band decreases in intensity. Shoulder appears at 385nm. 330nm band moves to higher energy.	1 : 0.57
Second	DSBPPH904 760(17.04), 600(18.20), 385(20.00), 310sh (23.80), 285(25.40) 285&330nm bands increase in intensity; 285 overtakes 310sh. 640nm band splits into 600&760nm bands.	1 : 0.89
Third	DSBPPH905 760sh (17.20), 660(18.20), 600sh (18.00), 385(20.00), 310sh (24.40), 285(27.20) Band splitting diminishes; 660nm band with 760&600nm shoulders. 285nm band dominates at high energy.	1 : 1.41
Fourth	DSBPPH906 760sh (17.40), 660(20.00), 600(18.00), 385sh (20.54), 310sh (25.60), 285(29.00) 660nm band increased in intensity. 310sh almost gone. 285nm band increased in intensity.	1 : 2.47
Fifth	DSBPPH907 760sh (17.56), 660(20.80), 600sh (18.24), 310sh (27.40), 285(30.80) 660nm band increases in intensity; 760&600 shoulders minor features. 285nm band increases in intensity.	1 : 3.05
Sixth	DSBPPH908 760sh (17.60), 660(20.00), 600sh (18.29), 310sh (29.20), 285(32.60) 660nm band decreased/ 600nm shoulder increased in intensity. 310nm shoulder almost disappeared.	1 : 3.87
Seventh	DSBPPH909 760sh (17.60), 660(19.60), 600sh (18.40), 285sh (36.80) 760&600nm bands increased in intensity relative to 660nm band. 310nm shoulder has disappeared.	1 : 4.78
Eighth	DSBPPH910 760sh (17.40), 660(18.80), 600sh (19.20), 285sh (41.60) 660nm band decreases in intensity and broadens. 600sh overtakes the 660nm band.	1 : 6.08
Ninth	DSBPPH911 760sh (17.60), 660sh (18.40), 600(19.60), 285sh (50.40) 660nm band is now a shoulder on band centred at 600nm.	1 : 7.54
Tenth	DSBPPH912 760sh (17.40), 660sh (18.00), 600(20.00), 285sh (56.80) 600nm band increases in intensity with the shoulder at 660nm a minor feature.	1 : 8.86
Eleventh	DSBPPH913 760sh (17.40), 660sh (17.60), 600(20.80), 285sh (63.20) DSBPPH914 760sh (17.60), 660sh (17.20), 600(20.80), 285sh (73.60) DSBPPH915 660(23.60), 285sh (76.00) Gas cell opened to air; band at 600nm collapses	1 : 9.95

Table 13: Quartz Crystal Microbalance experiment 5

Chapter 4

Discussion

Discussion

1. Chemomechanical polishing of silica and silicon.

The objective of this part of the work was to prepare highly polished silica and silicon substrates as supports for organic films. Polishing reagents were assessed ultimately by their ability to produce a surface finish which approached the subnanometre level within 1 hr, in a reproducible manner.

The surface roughness of the substrates was determined by a Talystep mechanical profiler (see. Experimental:H.1) where a diamond stylus measures the vertical displacement as it translates the surface under examination. The absolute measurements were suspect, as stylus dimensions exceed greatly those of the variation between high and low points over a short distance on the surface, but relative comparisons were possible. The sensitivity of the instrument may be affected by the mechanical properties of the substrate (eg. a diamond stylus may "plough" through a soft material) and as silica glass and silicon have different hardness values (142) it was not possible to make a direct comparison of silica with silicon under similar polishing conditions. A comparison of reagents using a given substrate was possible however.

In this work a comparison of fluoride-based reagents with a conventional polishing reagent for optical glass, cerium(IV) oxide (CeO_2) was conducted. The incorporation of CeO_2 in polishing compositions for glasses is well documented (10). Mineral and organic materials have been polished also with similar reagents (143). Cerium(IV) oxide is most effective and employed almost exclusively in aqueous media, at neutral to alkaline solution pH, for the chemomechanical polishing of optical glass (10) although examples

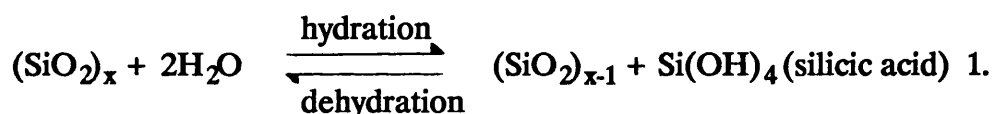
where acidic (144) or non-aqueous or dry (145) conditions are employed are known in the literature. Fluoride-based reagents are based often on buffered aqueous hydrogen fluoride (BHF) (146) although aqueous polishing suspensions containing fluoride in acidic (69) or basic (147) media are documented; the former is the subject of the present study.

The dissolution of glasses by acidic fluoride solutions has taken on new technological importance in recent years, through its use in the fabrication process for microelectronic devices (148). The chemical processes involved have been the subject of many studies. It has been reported that the rate of dissolution of silica is linearly dependent on the concentration of $[\text{HF}_2]^-$ and HF in dilute fluoride solutions, where the predominant species is the $\text{H}_3\text{O}^+\text{F}^-$ tight ion pair, the reaction with $[\text{HF}_2]^-$ occurring four to five times as fast as that with HF (104). It is accepted in the literature that the dominant etching species in fluoride-based reagents is $[\text{HF}_2]^-$ (149). In the present study the $[\text{HF}_2]^-$ anion was found to be effective at low pH for the chemomechanical polishing of silica, as in the Pilkington reagent. The pattern of results obtained for Syton (an aqueous alkaline silica sol, pH = 9-10) and fluoride-modified Syton (pH-7) suggested there was no obvious advantage in employing the latter over Syton alone. The spreads of results obtained with the Pilkington reagent was attributed to incomplete removal, by mechanical means or otherwise, of insoluble reaction products formed rapidly at the silica surface. The material is described in the "passivating layer" concept (17,34) which has been invoked in mechanistic explanations for chemomechanical polishing, particularly for silica (17). The work conducted in this study has enabled a positive

identification of a passivating layer to be made; in previous studies the presence of a layer has been inferred without being proven (150).

The unique nature of the silica-water system has been described by many researchers (151). There is much confusion in the literature concerning the silica-water interface as the hydration and solubility characteristics are poorly understood, for example the observation that silica sols are stable at $\text{pH} = 2$ (silica has an isoelectronic point of 2.8 (152)) and are increasingly sensitive to electrolytes at higher pH where the zeta potential is greatest is in direct contradiction to accepted double-layer theory (153).

The mechanism by which the dissolution of silica in water is understood to operate has been discussed in detail in the literature (154). The dissolution and deposition of silica in water may be simplified to



There are many factors that determine the overall process, but regardless of the phase of silica employed (eg. quartz, tridymite or amorphous) the reaction may be described as a depolymerisation through hydrolysis, involving a reaction species or "catalyst" that is chemisorbed and thus increases the coordination number of tetrahedrally coordinated silicon and facilitates the breakup of network bonds, such as hydroxide anion. The dissolution mechanism has been discussed in detail by Strelko (155) who considered analogous systems for the dissolution of silica with catechols, HF , H_3PO_4 and acidic acetyl acetone all of which are known to form compounds in which silicon is coordinated by six fluorine or oxygen ligands. The mechanism may explain the observation that

stishovite, the only form of silica known in which the silicon atoms are octahedrally coordinated with oxygen, is insoluble in HF (156). Catechol and related compounds dissolve silica in neutral solution, but it is not certain that a catalytic effect is involved and it is more likely that these materials adsorb strongly the silicic acid as it is liberated from the surface, thus preventing the solution becoming saturated.

Silicic acid is only partially ionised in water ($pK_A = 9.6$) so will dissolve appreciably only in solution pH values greater than 8, where the silicic acid ionises according to the process (157)



At pH greater than 12 the following complex will be formed by the detachment of two protons



This species has been detected by Raman spectroscopy (158). The diffusion of water in silica controls the rate of dissolution below the surface and there are two processes involved, one involving the rapid diffusion of molecular water into the silica structure and another slower process for the cleavage of siloxane linkages (Si-O-Si) to form network terminating silanol groups (Si-OH) (159).

The surface hydroxyl equilibrium is written



The relative concentrations of each species is dependent on the conditions. Silica has a $pK_A \sim 6.5$ (160) and an isoelectronic point (IEP) of 2.8 (the isoelectronic point of a hydrated oxide is the pH at which there is charge neutrality on the surface, due to very few but equal numbers of oppositely

charged species with the vast majority of surface hydroxyl groups remaining unionised) and will therefore have significant numbers of Brønsted base sites on the surface in water (10).

At low pH, below 3, traces of F^- have a marked catalytic effect on the polymerisation of silicic acid. Iler (161) found that whereas the polymerisation reaction is catalysed above $pH = 2$ by hydroxide anion, at lower pH that rate of polymerisation is proportional to the concentrations of hydrogen and fluoride ions. The stability of silicic acid in solution is dependent also on the presence or otherwise of trace impurities, such as aluminium(III) ions or to a lesser extent iron(III), thorium(IV) and beryllium(II) ions which form complex fluorides thus retarding polymerisation in the pH range below 3 (162). A concentration of fluorine of 1 ppm has a marked effect on the rate of polymerisation in acidic solution.

Many ions are strongly and often irreversibly adsorbed on the weakly acidic surface of silica. Simple ion exchange is involved in the case of monovalent cations of Na^+ , K^+ and NH_4^+ although different mechanisms are involved depending on the solution pH (163). Silica suspended in a solution of many polyvalent metal salts begins to adsorb metal ions when the pH is within 1-2 pH units below that required for precipitation of the polyvalent metal hydroxide (164). This would not be predicted on simple electrostatic grounds where adsorption would be expected to occur when the solution pH is high enough for ionisation of the silica surface with development of a negative charge. The number of charged sites is zero at $pH = 2.8$ (152) and yet metal cations in high oxidation states are generally adsorbed at $pH = 2$ or

lower, for example Fe^{3+} is adsorbed at $\text{pH} = 2$ (165) and Zr^{4+} at $\text{pH} = 0$ (166).

The effects of fluoride and hydroxide on silica are not identical as is obvious from the observation that silica is soluble in aqueous NaOH but not NaF. Fluoride ion is effective only at low solution pH for the dissolution of silica, in agreement with results obtained in the present study. The interaction of HF with any phase of silica (eg. quartz, tridymite or amorphous) will convert the surface Si-OH to Si-F groups. A silica surface covered with Si-OH groups is hydrophilic whereas a surface covered with Si-F groups is hydrophobic. This phenomenon has been used to explain the insolubility of stishovite in aqueous HF. Upon fluorination of all silanol groups on the surface of quartz, which has a relatively open structure in comparison to stishovite (which has the rutile structure, the silicon atoms are coordinated octahedrally to oxygen and is more dense than quartz), dissolution via depolymerisation through hydrolysis is possible as water molecules are not precluded from the surface in contrast to stishovite, where fluorination of the silanol groups results in a densely packed hydrophobic surface.

Stishovite is however soluble in weak base (156). It is not possible to rationalize a dissolution mechanism involving the expansion of the coordination number of silicon for stishovite and it has been suggested that this phase of silica is hydrolytically unstable and decomposes ultimately to amorphous silica (167).

The effect of solution pH on the rate of dissolution below $\text{pH} = 3$ has been investigated by a number of groups. Elmer and Nordberg (168) found

the initial rate of dissolution reaches a maximum at 0.8N HNO_3 (corresponding to $\text{pH} = 0.1$) and declines above this pH . Baumann has shown that from $\text{pH} = 3$ to 6 the rate of dissolution increases in proportion to the hydroxide ion concentration and concludes that a small minimum between 0.1 and 3.0 has gone unnoticed (169). Bergman conducted extensive measurements on the dissolution rates of particles of quartz and tridymite (in the submicron diameter range) in 0.1 and 1.0 mol dm^{-3} HF solution at 298 K (170). Tridymite dissolved in 0.1 mol dm^{-3} HF at a rate of around seven times that for quartz and vitreous silica about forty-five times that for quartz, but in 1.0 mol dm^{-3} HF there was little difference. On the basis of unit surface areas it was concluded that in 0.1 mol dm^{-3} HF, tridymite and cristobalite dissolve around ten times faster than quartz and vitreous silica about a hundred times faster. A fundamental study of the attack of HF on vitreous silica, preceded by a literature review, was published by Blumberg and Stavrinov (171).

It is apparent that silica glass polishing is dependent critically upon the presence of water. Polishing rates are extremely low in liquid hydrocarbons (172) or solvents without hydroxyl groups such as formamide (16). Cornish and Watt compared and contrasted polishing rates for silica with CeO_2 in aqueous media and a series of alcohols ranging from methanol to n-dodecanol. Polishing rates were found to increase with increasing hydroxyl activity and were greatest for water (11a). Studies of HF vapour phase etching of silica (173) have indicated residual water on the surface is necessary for the etching process to initiate. The role of water is to provide a condensed solvent

medium for HF adsorption on the surface. It has been reported that the differences between liquid and vapour phase etching of silica with HF-based reagents (174) are the presence of high concentrations of reaction products in the condensed phase, the need to desorb or remove by rinsing reaction products from the surface upon completion of the etching process and the initial adsorption of water in the vapour phase process. Results obtained in the present study indicate that during the course of both etching and chemomechanical polishing of silica (150), with reagents employing high concentrations of $[\text{HF}_2]^-$ at low solution pH, a high concentration of reaction products is formed at the solid:solution interface, described as a "passivating layer".

Conditions necessary for the production of passive layer material (identified as K_2SiF_6 coated with a thin silica layer) are in contrast to those reported in the literature for the preparation of K_2SiF_6 (175). A saturated solution of K_2SiF_6 at room temperature has a pH=4.3 as the $[\text{SiF}_6]^{2-}$ anion is subject to acidic hydrolysis to yield HF and SiF_4 (116). A potentiometric study of fluoride ion (117) has shown the $[\text{SiF}_6]^{2-}$ anion to be most stable in solution at pH \approx 3, the exact value dependent on ionic strength. The active species in fluoride-based reagents $[\text{HF}_2]^-$ exists in equilibrium with F^- and HF in aqueous solution and is the major species at pH = 3 (104). As optimum polishing and etching conditions in the present study were found to occur at pH = 1 it was concluded tentatively that $[\text{HF}_2]^-$ anion was not involved in any overall rate-determining step in the dissolution process. There was however a strong correlation between mass loss from silica wafers and the solution pH

in which the $[\text{HF}_2]^-$ species was employed. It is important to realise that as both polishing and etching processes are conducted under non-equilibrium conditions (i.e. material is lost constantly from the surface of the substrate) simple thermodynamic considerations of the relative stabilities of the reaction species are of limited relevance and kinetic factors are more likely to be important.

The solution etching of silicon is discussed in detail in the literature (22). The process may be conducted under isotropic or anisotropic conditions (27). Isotropic chemical etching is employed to remove damage produced by mechanical cutting or lapping, creating planar surfaces or patterns in single-crystal slices or polycrystalline substrates. Etchants containing HF, H_2O and HNO_3 are used most often and the principal reactions involve oxidation followed by dissolution of reaction products. For reagents employing a high concentration of HF relative to HNO_3 the rate-determining step is the oxidation step while for reagents employing a high concentration of HNO_3 relative to HF the dissolution step is rate-determining. In anisotropic (or orientation-dependent) solution etching the etch rate varies with the crystallographic plane of the silicon single crystal and the etchants employed are typically alkaline solutions at elevated temperatures (177). The principal reactions are oxidation of the silicon surface with subsequent dissolution of the reaction products with a complexing or chelating agent, such as pyrocatechol (178).

The pattern of results observed for the polishing and etching of silicon in the present study were similar to those found for silica. Dip-etch

experiments for silicon produced mass loss vs solution pH profiles that in the early stages resembled closely those obtained for silica under similar conditions. The observation was not surprising as the aim principally of any etching or polishing process for silicon is to remove the amorphous oxide layer on the surface. The oxide layer would be expected therefore to be removed rapidly by a reagent employing $[\text{HF}_2]^-$ anion at low pH, such as the Pilkington reagent (69). The reagent was unsuccessful for the chemomechanical polishing of silicon in the present study. This may be explained by a process where the rapid removal of surface oxide exposes the underlying silicon substrate to polishing debris and the corrosive reagent, leading to uncontrolled etching and pitting. The incorporation of $[\text{HF}_2]^-$ anion in Syton was found to be detrimental for the chemomechanical polishing of silicon. This observation was ascribed to the resulting change in solution pH upon addition of the $[\text{HF}_2]^-$ species, as colloidal silica sols are employed successfully for the chemomechanical polishing of silicon at alkaline pH (16). The binary combination of Syton and CeO_2 was successful and may be due in part to the ability of CeO_2 to form complexes with anionic species in the alkaline pH range employed (eg. complexation with H_3SiO_4^-) (10). It is likely also that the removal of the oxide layer is facilitated more readily by the incorporation of abrasive particles such as CeO_2 .

In the present study identification of the sparingly soluble material (the passive layer) formed during chemomechanical polishing and etching of silica with fluoride-based reagents was not straightforward. It was clear from analysis by spectroscopic and other methods that a mixture of species is

formed, as suggested by Judge (104). Elemental analysis of the solids indicated that they contained potassium and fluorine. The pattern of results obtained from examination by XRD, ^{29}Si MAS-NMR and transmission and reflectance IR spectroscopy indicated that while K_2SiF_6 was the major component of the bulk material, Si-OH and Si-O-Si groups were found to predominate at the surface. The difference was most apparent in the IR spectra. Diffuse reflectance, photoacoustic and microspectroscopic IR methods produced spectra which although differing in detail, were very similar to those observed for hydrated silica (113). Transmission spectra were however characteristic of $[\text{SiF}_6]^{2-}$ in K_2SiF_6 (112). Analysis by SEM and Nomarski light microscopy appeared to indicate that the material was composed of isotropic cubic and hexagonal crystalline material (in agreement with results obtained by XRD methods), some spongy modification and provided evidence for crystalline quartz.

Dip-etch reactions were followed using the radiotracer ^{18}F ($t_{1/2} = 110$ min, β^+) for silica and silicon substrates and in agreement with earlier dip-etch experiments the interaction of fluorine with the substrate was greatest at low pH. Count rates were greatest at low pH, undetectable above pH = 10 and greater for virgin wafers compared with those etched previously at a given solution pH. In all cases ^{18}F was removed completely by washing. The observations were consistent with replacement of surface Si-OH_2^+ by Si-F groups followed by hydrolysis of the latter.

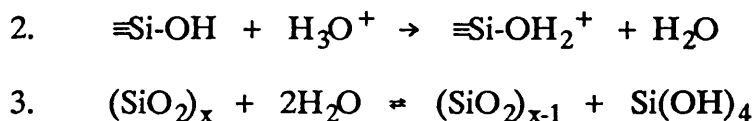
On the basis of the results obtained it was concluded that the intermediate produced in both polishing and etching reactions was K_2SiF_6

coated with a thin silica-like layer. The latter could be the result of surface hydrolysis, since the reflectance IR spectra of authentic K_2SiF_6 samples exposed to moist air for several hours were similar to those of passive layer material. Alternatively the data may reflect the incorporation of silica particles on K_2SiF_6 during the reactions.

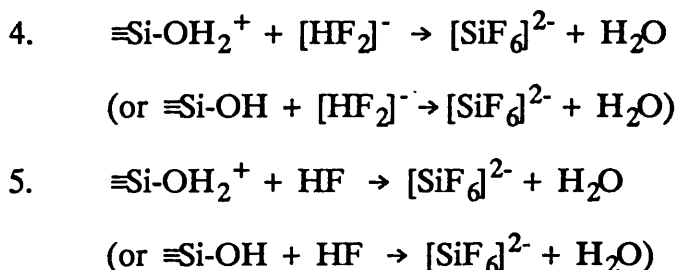
As outlined in Introduction:A.8 a model for chemomechanical polishing of silica may be described by a series of steps. Although operating by different mechanisms both CeO_2 and $[HF_2]^-$ species require the prior modification of the surface of the silica, as a consequence of the solution pH, for the successful chemomechanical polishing of the substrate. The surface reactions in both cases are acid-base in nature, where the terms acid and base are used both in the Lewis and Brønsted sense. The products of such reactions are acid-base complexes and expected to be a mixture of species whose composition is variable. The CeO_2 /silica system has been described elsewhere in detail (10) and operates via the interaction of basic sites on silica ($Si-O^-$) with acidic sites on ceria ($Ce-OH$ or $Ce-OH_2^+$), while in this study the $[HF_2]^-$ /silica system is found to operate via the interaction of acidic sites on silica ($Si-OH_2^+$) with the $[HF_2]^-$ anion.

A tentative mechanism for the dissolution of silica by fluoride-based reagents at low pH, with the production of passive layer material may now be described. 1. The adsorption of H_2O to produce surface silanol groups 2. Protonation of the silanol groups as a consequence of solution pH (ie. below the IEP of silica of 2.8 (152)) 3. Dissolution of silica by depolymerisation.



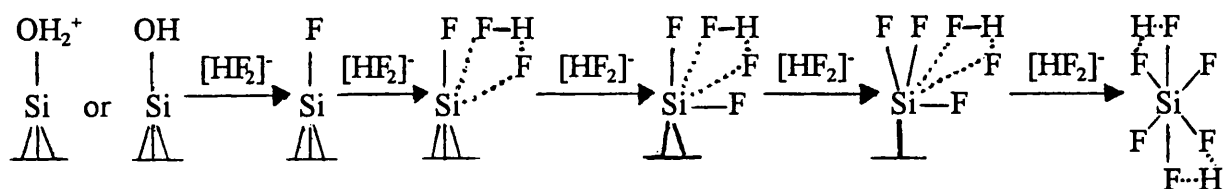


The latter reaction is likely to be of limited significance. Reactions occurring at the silica surface will involve $[\text{HF}_2]^-$ and to a lesser extent HF in acid-base interactions with silanol groups.

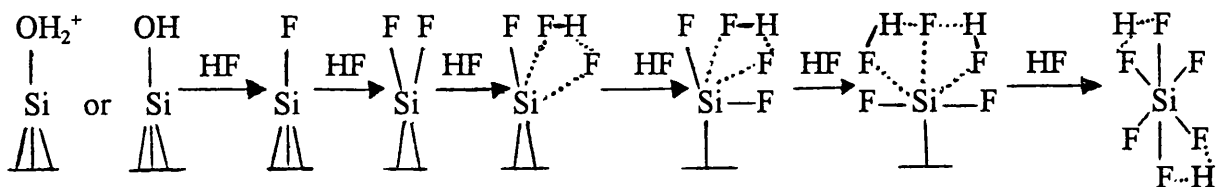


It is probable that the interaction between $[\text{HF}_2]^-$ and Si-OH_2^+ is the more significant reaction. The $[\text{HF}_2]^-$ and HF reaction pathways may be considered separately although the reactions are of course a simplification of the dissolution process as numerous combinations are possible.

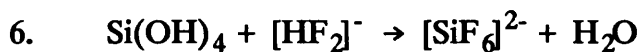
$[\text{HF}_2]^-$ reaction scheme



HF reaction scheme



The reverse reaction, although unlikely to occur, may account for the production of a thin silica layer on K_2SiF_6 which may be formed also by the reaction of $[HF_2]^-$ and HF with the products of depolymerisation of silica



2. Organic thin films.

The preparation of thin films of organic compounds by high vacuum sublimation is a well established technique (47,179) and often the objective is to prepare ordered films for electron microscopy, where the lateral extent of ordering and the crystal size are of less importance than the formation of well ordered domains. Current electronic devices are based almost exclusively on inorganic materials but there is considerable interest in the potential of organic-inorganic hybrid systems which promise enormous versatility. Of particular interest are epitaxial organic films on inorganic substrates where the production of a homogeneous single-crystal film is required (180).

Epitaxy may be defined as a matching of a substrate with an overlying crystal and may occur in many systems as diverse as metals on alkali halides, silicon on quartz, alkali halides on mica or other alkali halides (48) and polycyclic aromatic hydrocarbons on alkali halides (49). The epitaxial relationship of substrate and evaporated film is controlled by the surface structure of the substrate and the substrate temperature, which enables the organic molecules to migrate and adopt a preferred orientation on the substrate surface and with each other. The concept of lattice matching to

explain epitaxial growth (181) is of limited applicability to organic compounds as they are of lower symmetry generally and larger size than the lattice parameters of inorganic substrates. The match of an organic crystal on an inorganic support is usually limited to one dimension although studies of the epitaxial growth of perylene have indicated molecules may adopt a preferred orientation on a substrate at low temperatures, yet require a higher temperature to form a three-dimensionally orientated single-crystal film (182). Long range Coulombic interactions originating from the substrate may influence the weak dispersive forces responsible for the lattice energy of an organic crystal. Coincidence of a few atoms of the organic molecules with those of the substrate has been used to account for epitaxial relationships.

Factors that determine the temperature of the substrate T_S at which epitaxial growth may proceed have been investigated. Optimum epitaxy was found to occur in many systems for a substrate temperature corresponding to one third of the boiling point temperature of the evaporated material (49). Arguments based on bulk thermodynamics and re-evaporation as an explanation for the phenomenon of optimum temperature for epitaxy are not readily applicable to organic compounds as organic molecules exhibit a wide variation in sticking coefficients (182). The higher molecular mobility at higher temperatures may allow greater alignment with the substrate, where the effects of an ionic substrate are greater than the dispersive forces present in the crystalline organic film, which may often align with principal planes or steps associated with emergent dislocations in the substrate (49). A strongly polarizing substrate such as KCl may enforce a particular orientation on the

surface for a series of structurally related organic compounds (183). A less polarizing substrate such as mica or amorphous silica glass will not produce similar long-range Coulombic interactions. This has been demonstrated for phthalocyanines and quaterrylene (184).

In the present study films of polycyclic aromatic hydrocarbons (PAHs) were formed on highly polished silica glass and silicon substrates. The nature of the two substances is different as silica glass is an amorphous material in contrast to monocrystalline [100]-silicon employed in this work. Preliminary work with PAHs supported on silicon substrates in the present study appeared to suggest these systems were intractable to investigate by simple spectroscopic methods and hence no further investigations were conducted. Films formed on silica are not epitaxial by definition but it was envisaged that although the crystal lattice stabilization energy for molecular crystals is small, the planar PAH molecules would form ordered films on a flat, chemically well characterised surface of silica glass. No structural studies were conducted and the quality of the films was assessed by the definition or otherwise in electronic spectra of the films.

In this type of study heating of the substrate after sublimation is carried out in order to anneal evaporated films. The growth of organic crystals is not similar to metals however in that island annealing or isotropic growth are dominated by the shape of the molecules (49). An important observation of the annealing process is that it is significant only above a temperature of half the melting point of the evaporant material. In the present study a comparison of substrate temperature T_S required for optimum film deposition

and growth with the melting point of the organic compound was conducted. It was established that larger polycyclic aromatic systems formed satisfactory films, at a temperature near to or slightly above that of half the melting point of the organic compound, representing a temperature where the molecules have sufficient kinetic energy to migrate and orientate themselves on the surface of the substrate without re-evaporation becoming significant. At higher T_S the number of nucleation sites is diminished thus raising the average crystal size. However for greater T_S values the sticking coefficient is greatly reduced and hence the probability of re-evaporation is increased. In contrast smaller PAHs were found to deviate markedly from the relationship especially fluoroanthene and pyrene, where the ratio of deposition temperature (K) over melting point (K) was 0.76 and 0.7 respectively. Experiments below room temperature were not conducted however and therefore the poor quality of films of these compounds may reflect only the experimental limitations in the present study.

PAHs prepared as thin films on chemomechanically polished silica substrates were examined by electronic and infrared spectroscopy, prior to and in many cases after, chemical modification with MoF_6 , WF_6 , AsF_5 , PF_5 , BF_3 or the solid organic electron acceptor 7,7,8,8-tetracyano-p-quinodimethane (TCNQ). The visible and ultraviolet absorption spectra of aromatic hydrocarbons are characterised by four main regions of absorption. A low energy transition of complex vibrational structure and very low oscillator strength (termed α by Clar (185) and 1L_b by Platt (186) is the first band in *ca.* 50% of all aromatics and in acenes (in the present study anthracene, tetracene and

pentacene) has longitudinal polarisation. Another low energy transition with an oscillator strength about ten times greater (termed p by Clar (185) and 1L_a by Platt (186) occurs as either the first or second band in the spectra and in acenes has transverse polarization. It is accompanied by a strong excitation of a 1400 cm^{-1} vibrational mode. At higher energies, a transition with oscillator strength again ten times greater (termed β by Clar (185) and 1B_b by Platt (186)) with longitudinal polarization in the acenes is appended by the highest energy transitions (termed β^1 by Clar (185) and 1B_a by Platt (186)) with an oscillator strength intermediate between those of the β and p bands, exhibiting a transverse polarization in the acenes.

Classifications such as those described have however many limitations. The assignments in electronic spectra for large PAHs (whose occupied π -orbital levels converge so that a large density of excited singlet states exist) is often a problem. Owing to large changes in geometry that follow electronic transitions, overlap of bands is common. The spectra of overcrowded hydrocarbons (such as decacyclene in the present study) are diffuse, consisting in extreme cases of a single broad band. Comparison of intensities of bands may be helpful in assignments for catacondensed hydrocarbons (in which all the carbon atoms are part of a conjugated system). There are no general rules regarding the intensities of the α , p , β and β^1 bands in pericondensed hydrocarbons (ie. not all the carbon atoms participate in a conjugated system). The p and β^1 bands correlate linearly with the first and second ionisation potentials respectively while the α and β band energies correlate linearly with the mean of the first and second ionisation potentials (Fig.61) (187).

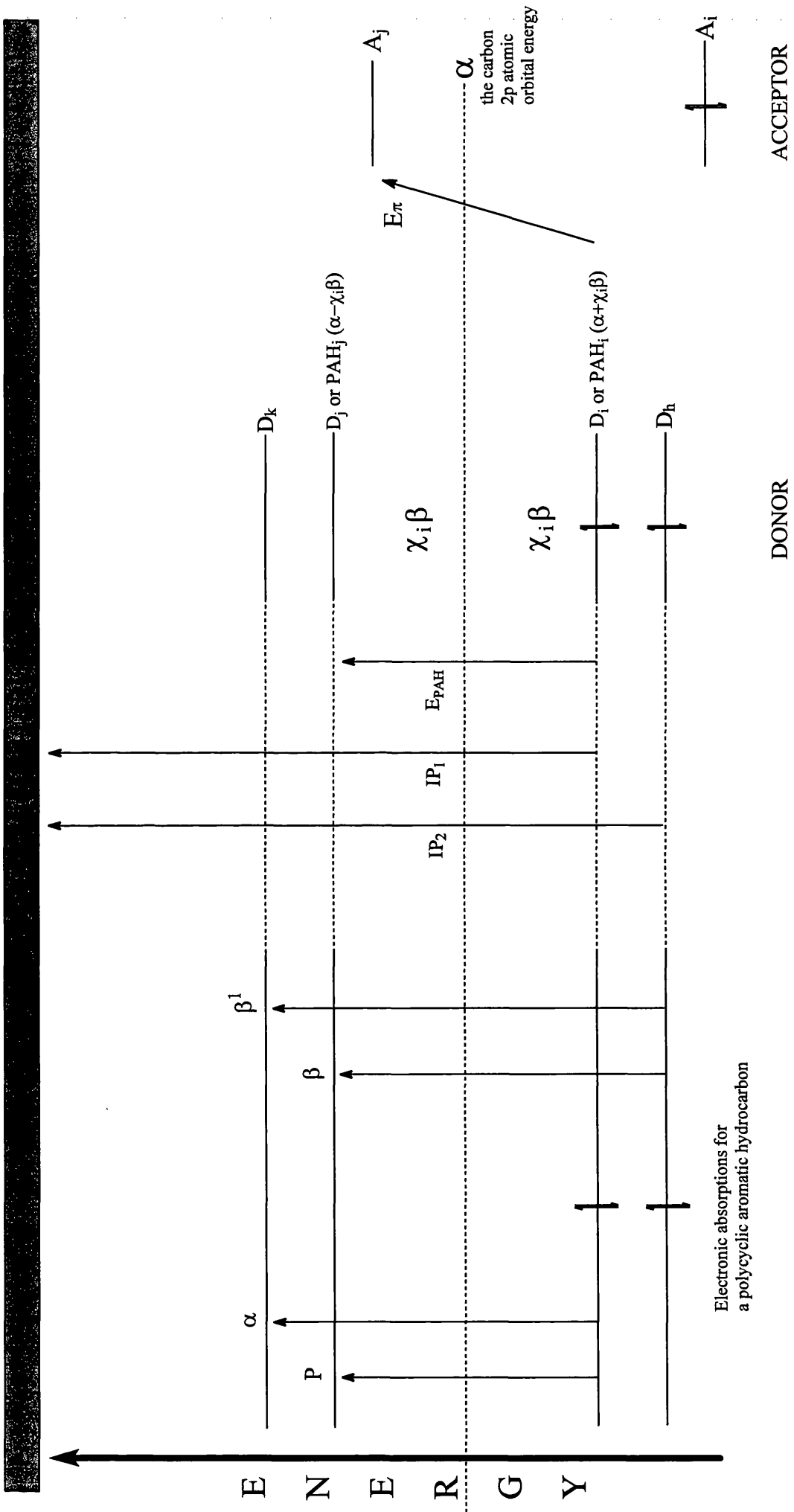
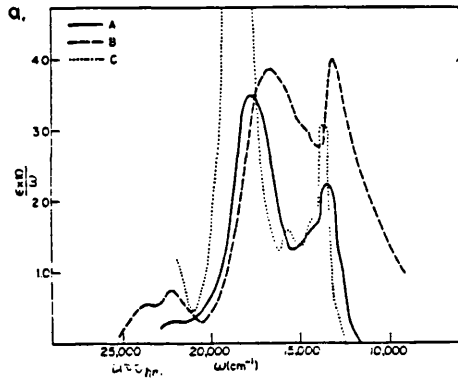


Figure 61: Diagrammatical representation of important electronic transitions

The IR spectra of PAHs consist generally of absorptions (188) arising from C-H stretching vibrations near $3000\text{-}3100\text{ cm}^{-1}$, C-C skeletal vibrations at $1500\text{-}1600\text{ cm}^{-1}$ and out-of-plane C-H vibrations between 650 and 900 cm^{-1} . The latter are most characteristic since from one to four adjacent hydrogen atoms on the same ring may yield strong absorptions in different regions and in favourable cases the out-of-plane C-H vibrations may be used to locate the position of substitution. In the present study, IR reflectance spectroscopy was employed to examine thin films of PAHs on silica substrates prior to chemical modification, as films on silicon substrates were intractable in the transmission mode. The chief disadvantages of conventional dispersive IR have precluded its use as a method of analysis for PAHs in the environment. The introduction of matrix-isolation FT-IR for the qualitative and quantitative analysis of PAHs (189) has enabled problems due to lack of unique features in the spectra and lack of proportionality between band strengths and concentration to be addressed. MI-FT-IR circumvents problems originating from interference of solute molecules with each other and the solvent, allowing the recording of spectra at cryogenic temperatures. Under such conditions the spectra consist of very sharp vibrational lines (190). The results from similar work (189) were compared and contrasted with those obtained in the present study and for all systems examined there was no evidence for chemical modification of the organic compounds upon thin film formation on silica.

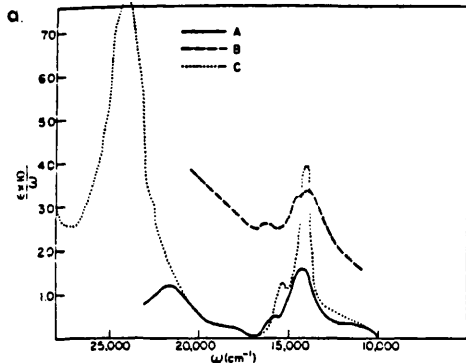
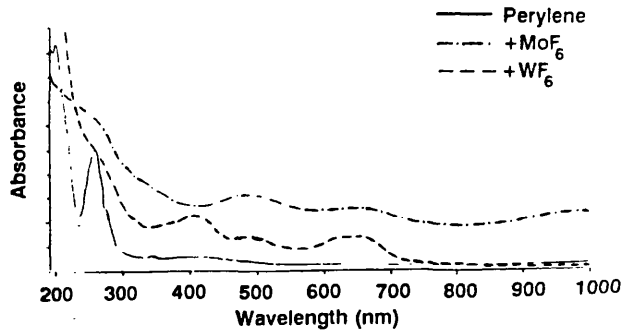
From the results obtained for organic thin films on silica exposed to MoF_6 , WF_6 and AsF_5 it was apparent that there was no firm evidence in the electronic spectra for the formation of radical cations derived from the donor

Figure 62: Comparison of electronic spectra of PAH films exposed to oxidant with those of their radical cations



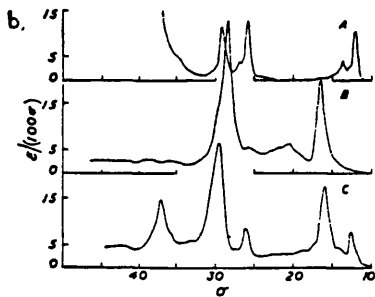
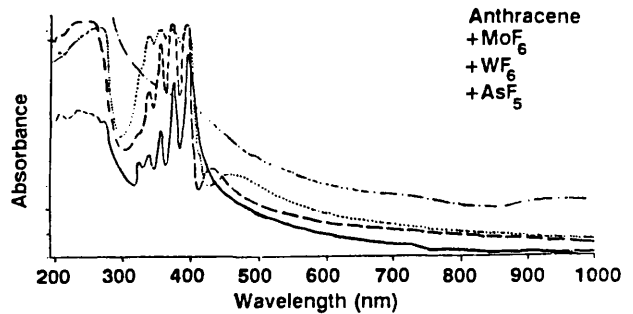
Spectrum of the perylene⁻ ion. A. Perylene-SbCl₅ in colloidal solution (—). B. Solid Perylene-SbCl₅ in KBr pellet (---). C. Perylene in H₂SO₄ (.....).
 Note: In (A), the absorption peaks of the neutral perylene show at 22,000 and 23,000 cm⁻¹. In (B), the intensity is an arbitrary scale.

Electronic spectra: a.2



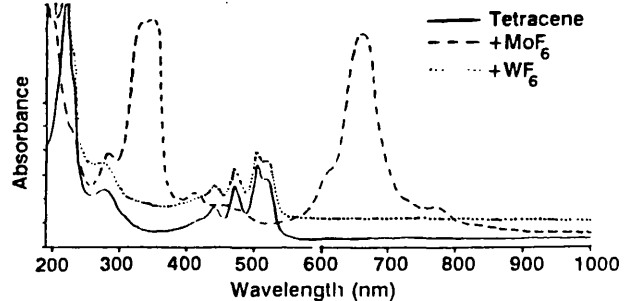
Spectrum of the anthracene⁻ ion. A. Anthracene-SbCl₅ in colloidal solution (—). B. Solid Anthracene-SbCl₅ in KBr pellet (---). C. Anthracene in H₂SO₄ (.....) (anthracene⁻ and anthracene-H⁺).
 Note: The spectrum of the solid is on an arbitrary intensity scale.

Electronic spectra: m.2



A. Monopositive ion of tetracene (solvent CF₃-CO₂H-BF₃-H₂O in contact with air); B. Tetracene²⁺ 2(Na⁺) in tetrahydrofuran; C. Tetracene + SO₂ in dimethyl sulphate.

Electronic spectra: f.2



PAHs (Fig.62). The pattern of results were consistent however with the formation of charge-transfer complexes (56) where the interactions between the electron donor PAH and electron acceptor high oxidation state binary fluoride produces an electronic absorption (or absorptions) additional to those of the components. The origin of the electronic absorption lies in the excitation from the ground state of the complex ψ_N to the excited state ψ_E (55). The ground state is composed such that

$$\text{Ground State } \psi_N(A,D) = a\psi_0(A,D) + b\psi_1(A^-D^+)$$

where ψ_0 is the no-bond function (binding due only to physical forces like van der Waals)

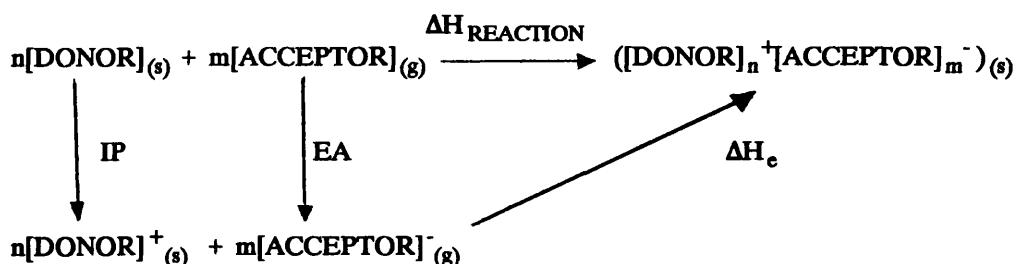
ψ_1 is the dative function where the structure has one electron removed completely from donor D to acceptor A

a and b are coefficients

The electronic absorption is due therefore to a one-electron transfer from ψ_0 to ψ_1 and termed an intermolecular charge transfer. It is important to realise however that ψ_1 contributes little to the ground state for weak interactions. For strong interactions there is considerable ionic character in the complex and the electronic spectrum resembles more closely that of the radical cation (formed from the donor) and counter-anion (formed from the acceptor) superimposed on each other.

The reactions in the present work may be discussed in a similar manner as those conducted by Bartlett (191) in his studies of the oxidising properties of third row transition series hexafluorides. The reaction between an electron donor and electron acceptor species with complete transfer of an electron may

be represented by a Born-Haber cycle where IP, EA and ΔH_e are the ionization potential (of the PAH), electron affinity (of the MF_6 species) and enthalpy term reflecting the electrostatic interaction between cations (derived from the PAH) and anions (derived from MF_6) in the adduct respectively.

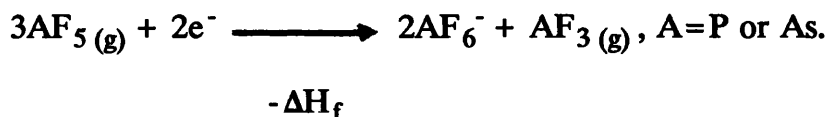


The ionisation potential (IP) refers to the process



The electron affinity (EA) is defined as the difference in energy between the neutral molecule or atom in its ground state and ion in its ground state (64).

A similar scheme may be drawn for the reaction involving the pentafluorides of arsenic and phosphorus where the process denoted by the term EA is replaced by $-\Delta H_f$ for the process



The measurement of electron affinities is experimentally difficult due to the complexity of molecular negative ions and as a result the EA for relatively few molecules is known with accuracy. The most recent values for gaseous molybdenum and tungsten hexafluorides are 492 kJ mol^{-1} and 338 kJ mol^{-1} respectively (192). It has been established that in the absence of a solvent, the oxidising abilities of the d-block hexafluorides increase from left

to right across the row in the Periodic Table (193), the hexafluorides of 4d elements being stronger oxidizing agents than their 5d analogues. In the gas phase it has been shown that nitric oxide is oxidised by MoF₆ to give products which contain the [NO]⁺ cation (194). It has been demonstrated that the electron affinity of WF₆ is less than that of MoF₆ as the former does not intercalate into graphite spontaneously and oxidatively in contrast to MoF₆ (66).

The oxidising properties of AsF₅ and PF₅ are widely documented (195). The available evidence indicates that AsF₅ is significantly stronger as an oxidising agent than is PF₅. A similar order is believed to be the case for their Lewis acidities (eg. F⁻ affinities). In liquid HF it is reported that AsF₅ is a stronger Lewis acid than PF₅ (196). Values for the enthalpy term $-\Delta H_f$ in the Born-Haber cycle outlined previously have been reported as -686 kJ mol⁻¹ and -1012 kJ mol⁻¹ for phosphorus pentafluoride and arsenic pentafluoride respectively (66).

For the complete transfer of an electron from PAH to MF₆ (M = Mo or W) it is necessary (in a homogeneous gas phase reaction) for the EA (or $-\Delta H_f$ in systems where PF₅ or AsF₅ are employed) value to be numerically greater than the IP of the PAH. As illustrated clearly in the Born-Haber cycle the term ΔH_e is important also, as the lattice energy of the products formed and the electrostatic interaction between the cations and anions of the products have roles in driving the reactions to occur.

Upon examination of the IPs of the PAHs in the present study (187,197) the formation of radical cations, derived from PAHs exposed to MoF₆ or WF₆

would not be expected. In contrast exposure to AsF_5 and in many cases PF_5 would be expected to produce radical cations derived from the PAH. For all PAHs examined however there was no observable reaction with PF_5 and in many cases AsF_5 whereas under comparable conditions exposure to MoF_6 often produced considerable modification of the electronic spectrum (eg. thin films of pentacene). The pattern of results obtained in the present study suggest that factors other than the IP and EA are important, such as the ability of the oxidant to interact with or adsorb on the PAH prior to oxidation, the size of the oxidant used and the size of the anion formed in relation to the layers of the films on the silica substrate. The lack of positive evidence for radical cation formation in the electronic spectra (137) does not discount the possibility of the process taking place, but does suggest that the electron donor:electron acceptor interactions for all systems examined in this work are relatively weak and described more satisfactorily as molecular or charge-transfer complexes (55,56).

The interpretation of electronic spectra is often difficult for systems assigned tentatively as charge-transfer complexes (56). Multiplicity of bands is common and in the present study multiple charge-transfer bands were observed (see Table 11) for ten of the fifteen polycyclic aromatic systems examined (ie. perylene + $\text{MoF}_6/\text{WF}_6/\text{AsF}_5$ BEDT-TTF + MoF_6 violanthrone + $\text{MoF}_6/\text{AsF}_5$ pentacene + MoF_6 ovalene + $\text{MoF}_6/\text{WF}_6/\text{AsF}_5$ tetracene + $\text{MoF}_6/\text{AsF}_5$ rubrene + MoF_6 PTCDA + MoF_6 chrysene + $\text{MoF}_6/\text{WF}_6/\text{AsF}_5$ and anthracene + MoF_6). An asymmetric band of exceptional bandwidths is often observed in the electronic spectra of charge-

transfer complexes and was so in the present study for thin films of perylene exposed to AsF₅ (see Electronic spectra:a.3). Multiplicity may arise as a result of electron donation from more than one level in the donor. Alternatively the process of electron donation to more than one level in the acceptor, differences in the interaction energies or a mixture of all or some of the above may explain the complexity in many electronic spectra of charge-transfer complexes. It follows that where multiplicity arises as a result of more than one electronic level in the donor participating, the energy difference between the charge-transfer bands should be constant for a given donor with different acceptors (198). Conversely if the energy difference between the charge-transfer bands is constant for a given acceptor with different donors, the transitions may occur from a single electronic level in the donor to two vacant levels in the acceptor (199).

Simple molecular orbital (MO) treatment states the energy ΔE_{ij} for an electronic transition (51) from the i^{th} orbital of the donor (the Highest Occupied Molecular Orbital, HOMO) to the j^{th} orbital of the acceptor (the Lowest Unoccupied Molecular Orbital, LUMO) may be written

$$\Delta E_{ij} = m_j - m_i \quad (\text{Equation:1})$$

For a charge-transfer complex involving a donor D and acceptor A the energy of the charge-transfer band which occurs on excitation of the π -complex is described similarly by

$$E_{\pi} = A_j - D_i \quad (\text{Equation:2})$$

The energy of a filled molecular orbital of a polycyclic aromatic hydrocarbon

as given by Hückel MO theory (51) is

$$E = \alpha_0 + \chi_i \beta_0 \quad (\text{Equation:3})$$

where α_0 is the coulomb integral and is a measure of the coulombic energy of an electron in a $2p_z$ orbital in C_6H_6 β_0 is the bond integral and is a measure of the interaction between $2p_z$ orbitals on adjacent atoms in C_6H_6 and depends on the carbon-carbon distance and χ_i is the molecular orbital coefficient calculated for the i^{th} orbital (the HOMO) where χ_i is numerically equal but negative in sign for unfilled orbitals compared to filled orbitals. Both α_0 and β_0 are negative quantities.

For χ_i corresponding to the HOMO of a donor hydrocarbon, the transition energy $E\pi$ for the first π -complex charge-transfer band may be described by (see Fig.61)

$$E\pi = A_j \alpha_0 - \chi_i \beta_0 \quad (\text{Equation:4})$$

Internal transitions occur between filled and unfilled orbitals in a single molecule and for a polycyclic aromatic hydrocarbon PAH the $\pi \rightarrow \pi^*$ transition energy can be given as

$$\Delta E_{PAH} = PAH_j - PAH_i \quad (\text{Equation:5})$$

where i and j are filled (HOMO) and unfilled (LUMO) orbitals respectively.

The energy of a LUMO is therefore, using Equation:3

$$PAH_j = \alpha_0 - \chi_j \beta_0 \quad (\text{Equation:6})$$

The internal transition energy from the HOMO to LUMO is now

$$E_{PAH} = 2\chi_j \beta_0 \quad (\text{Equation:7})$$

As $\chi_j \beta_0$ is common to Equation:4 and Equation:7 a simple relationship should exist between the lowest energy charge-transfer band of a π -complex and the

lowest energy internal transition of the donor. The charge-transfer band energy E_{π} and the internal transition band energy E_{PAH} are related by the expression

$$E_{\pi} = A_j - \alpha_o + (E_{\text{PAH}}/2) \quad (\text{Equation:8})$$

The relationship assumes perturbation of the energy levels in the donor and acceptor are negligible upon charge-transfer complex formation. Numerous studies have been conducted employing similar MO treatment and in each case the agreement between theoretical calculations and experimental results has been close, for example the π -complexes of trinitrobenzene with aromatic hydrocarbons (200).

There have been many studies of charge-transfer complexes in which attempts have been made to correlate the energy of the charge-transfer band or bands with some property of the donor or acceptor, for example, the ionisation potential of the donor with a common acceptor species (201), molecular orbital coefficients χ_i of the donor (202) and internal transitions ($\pi \rightarrow \pi^*$) in the donor (203). Similar strategies were employed in the analysis of results obtained in the present study but failed to establish relationships such as those outlined. This may reflect the diversity of PAHs employed in this study (Fig.58) such as peri- and cata-condensed, planar and non-planar, alternate and non-alternate and substituted PAHs. The differences in chemical behaviour and spectroscopic characteristics between series of structurally related PAHs are reported widely (50-54); correlations within any given series are expected and often found (137).

In contrast a relationship between, for example, the lowest energy

charge-transfer band observed in the electronic spectra for the acene series anthracene-tetracene-pentacene upon exposure to MoF₆ with the MO coefficient χ_i or IP of the donor PAH was not found in the present study. There was also no simple correlation between the appearance of additional electronic absorption bands and the thermodynamic oxidising ability of the oxidant employed, suggesting that for many of the systems examined perturbation of the energy levels in the donor and acceptor may be significant and lead to a breakdown in the simple MO treatment of the results. The strength of the perturbational influence is demonstrated most clearly for thin films of perylene + MoF₆/WF₆/AsF₅, BEDT-TTF + MoF₆, violanthrone + MoF₆/AsF₅, ovalene + MoF₆/WF₆/AsF₅, PTCDA + MoF₆, CTCDA + MoF₆ and anthracene + MoF₆ (Table.14). For these systems the term "charge-transfer complexes" does not reflect the strong interactions between donor and acceptor species. Systems to whom the description was more appropriate were perylene + TCNQ, BEDT-TTF + TCNQ, pentacene + MoF₆/TCNQ, tetracene + MoF₆/AsF₅, rubrene + MoF₆, decacyclene + MoF₆/TCNQ, chrysene + MoF₆/WF₆/AsF₅, anthracene + WF₆/AsF₅/TCNQ and pyrene + TCNQ (Table.15).

Complexes of TCNQ with a variety of donor PAHs have been reported in the literature (204). Studies of solid crystalline complexes are of special interest as in these systems it has been possible to observe multiple charge-transitions which cannot be observed in vapour phase or solution (205). For many solid crystalline complexes formed between strong electron donors and electron acceptors there are indications of ionic character in the ground state

DONOR	ACCEPTOR		
	^{a,b} MoF ₆	^{a,b} WF ₆	^{a,b} AsF ₅
Perylene	1000(3.76), 660(4.40) and 495(5.90)	623(13.23), 479(13.24) and 407(17.70)	1230(5.46), 650(4.36) and 490(4.77)
BEDT-TTF	895(0.9), 775(3.69), 758sh (3.52) and 710sh (1.88)		
Violanthrone	920(12.44), 725(6.32)		890(1.58) and 690(3.71)
Ovalene	962(3.62), 850(2.87), 670(3.89) and 620(3.6)	1000(0.91), 750(2.57) and 550(5.5)	1000(9.07), 750(9.12) and 550(10.02)
PTCDA	770(4.42) and 620(4.59)		
Coronene TCDA	500(14.51)		
Anthracene	920(0.52)		

^aBand positions λ_{max} (nm) ; ^bNumbers in parentheses refer to the absorption coefficient $10^4 \alpha^*$, where Absorbance = $\alpha^* (\text{cm}^{-1}) \times \text{film thickness}$. All bands additional to those of the PAH.

Table 14: Donor:acceptor complexes exhibiting strong perturbations in the electronic spectra

DONOR	ACCEPTOR			SPECIES
	^{a,b} MoF ₆	^{a,b} WF ₆	^{a,b} AsF ₅	
Perylene				^a TCNQ 1050 and 910sh
BEDT-TTF				700
Pentacene	975(0.82) and 785(4.92)			730
Tetracene	775(4.11), 725sh (4.99), 670(25.04) and 610sh (8.81)		1010(3.11), 765(1.8), 675(0.98) and 626(0.82)	
Rubrene	780(4.59) and 615(10.01)			
Decacyclene	770(3.17)			700
Chrysene	925(1.2), 680(1.47), 533(2.0) and 455(2.82)	680(1.09) and 500(1.36)	560(0.68), 480(0.8) and 433(0.91)	
Anthracene		460(2.3)	430(2.48)	700
Pyrene				750

^aBand positions λ_{\max} (nm) ; ^bNumbers in parentheses refer to the absorption coefficient $10^4 \alpha^*$, where Absorbance = $\alpha^* (\text{cm}^{-1}) \times \text{film thickness}$. All bands additional to those of the PAH.

Table 15: Donor:acceptor systems described as charge transfer complexes

(56). The crystal structure of perylene-TCNQ (1:1) is known and is composed of linear stacks of alternating donor and acceptor molecules (206). The complex perylene-TCNQ (3:1) is known also in which the donor-acceptor interaction is more significant (207). It is reported that in the complex anthracene-TCNQ the first two charge-transfer transitions originate from the penultimately occupied molecular orbital of anthracene to the two lowest unoccupied molecular orbitals of TCNQ (205). In the present study there was evidence for charge-transfer complex formation with TCNQ for pyrene, anthracene, decacyclene, pentacene and BEDT-TTF in which additional electronic absorption centred around 700-750 nm was common to all complexes. In contrast a broad asymmetric band centred at 1050 nm with a shoulder at 910 nm was observed in the electronic spectrum of perylene-TCNQ.

In the present work the Quartz Crystal Microbalance (QCM) technique was employed for the reaction of the polymeric fluoro-bridged phthalocyanine $[\text{Al}(\text{Pc})\text{F}]_n$ with MoF_6 in order to determine the reaction stoichiometry. The pattern of results was in good agreement with those obtained in a previous study (141). It was established that there was considerable uptake of MoF_6 by the $[\text{Al}(\text{Pc})\text{F}]_n$ film. The observations were not consistent with a process such as simple adsorption, intercalation or stoichiometric oxidation of the polymer leading to radical cation formation. The results were consistent however with a process involving depolymerisation of $[\text{Al}(\text{Pc})\text{F}]_n$. MoF_6 has an effective diameter (6.320\AA) greater than the separation distances (3.66\AA) between the phthalocyanine rings in the $[\text{Al}(\text{Pc})\text{F}]_n$ polymer and therefore

intercalation between the rings must involve distortion of the eclipsed structure of the rings with subsequent breakup of the polymer backbone.

Chapter 5

Conclusions and Future Work

Conclusions and Future Work.

In the present study a comparison of fluoride-based reagents with conventional polishing reagents for silica and silicon was made. The fluoride-based reagents chosen were a $[\text{HF}_2]^-$ /cerium(IV) oxide/sucrose mixture at low pH described by Pilkington (69) and an alkaline silica sol (Syton) modified by the addition of $[\text{HF}_2]^-$. The conventional polishing reagents employed in the study were Syton and Opaline (a commercial cerium(IV) oxide polishing abrasive).

All four reagents were capable of producing surfaces on silica substrates which approached the subnanometre level, as determined by a Talystep stylus instrument, within 1 hr of polishing. The Pilkington and Opaline reagents achieved satisfactory finishes most rapidly. Neither sucrose nor cerium(IV) oxide appeared to be involved directly in the chemical processes for silica polishing with the Pilkington reagent. Under experimental conditions sucrose would be expected to undergo acid hydrolysis to yield fructose and glucose. Hydroxyl groups on carbohydrate molecules are available for hydrogen-bonding with silica species (154). Silica particles may undergo chelation with carbohydrate molecules, a process well known with catechols (10). Replacement of hydroxyl groups by fluorine may occur which would have consequences for the process of chelation of silica particles by carbohydrate molecules. All these factors warrant further investigation.

The pattern of results obtained appeared to suggest there was no obvious advantage in the addition of $[\text{HF}_2]^-$ to Syton for the chemomechanical polishing of silica and silicon. Under polishing conditions $[\text{HF}_2]^-$ was effective

only at low pH, near to the isoelectronic point of silica (152). The greatest mass loss in dip-etch experiments employing aqueous KHF_2/HCl mixtures occurred at $\text{pH} = 1.0$ and $[\text{HF}_2^-] = 2.5 \text{ mol dm}^{-3}$ for silica. A similar relationship was established in the early stages of etching for silicon substrates. The breakdown of the relationship over longer periods should be investigated further.

Etching reactions were followed using the radiotracer ^{18}F ($t_{1/2} = 110 \text{ min}$, β^+). Dip-etching silica and silicon in aqueous $[\text{F}^-]-[\text{HF}_2^-]$ for 60 min produced measurable ^{18}F activity from the wafers. Count rates were greatest at low pH, undetectable above $\text{pH} = 10$ for silica and $\text{pH} = 3$ for silicon and, at a given pH, were greater for virgin wafers compared with those which had been etched prior. Under similar experimental conditions the levels of incorporation of ^{18}F for silicon were of an order of magnitude less than those for silica substrates. In all cases ^{18}F was removed completely by washing. For all experiments, in order to minimise effects due to physical differences in each substrate (e.g. surface areas), samples of silica and silicon of similar mass and geometry were employed. However the sensitivity of the radiotracer technique has the effect of amplifying small discrepancies due to, for example, variations in surface area between samples. Therefore it would be sensible to repeat this part of the work, employing silicon and silica substrates whose effective surface areas are known accurately. This may be achieved by employing Kryton as the adsorbate gas in the BET method of surface area determination. The observations made in the etching and radiotracer studies were consistent with replacement of surface Si-OH_2^+ by Si-F groups followed

by hydrolysis of the latter.

During the course of both polishing and etching experiments with aqueous KHF_2/HCl mixtures, a surface layer developed on the silica which fractured and so was removed easily after washing and drying. Work conducted in this part of the study has enabled the positive identification of a "passivating layer" to be made for the first time; in previous studies the presence of a layer has been inferred without being proven. Elemental analysis of the layer material indicated that it contained potassium and fluorine. Examination by XRD, ^{29}Si MAS NMR and IR spectroscopy indicated that K_2SiF_6 was the major component in the bulk material. Reflectance IR methods revealed that Si-OH and Si-O-Si groups dominated the surface of the material, in contrast to transmission IR spectra which were characteristic of $[\text{SiF}_6]^{2-}$ in K_2SiF_6 . Passive material examined by ^{29}Si MAS NMR spectroscopy displayed a signal in the region characteristic for octahedrally coordinated Si(VI). Under all pulsing conditions there was no evidence for signals arising from amorphous silica. Analysis by SEM and Nomarski light microscopy was consistent also with a material composed mainly of K_2SiF_6 with evidence for crystalline quartz.

On the basis of all the available evidence it was concluded that the reaction intermediate produced in both polishing and etching reactions is K_2SiF_6 coated with a thin silica-like layer. The latter could be the result either of surface hydrolysis or incorporation of silica particles during the reactions.

By employing highly polished silica and silicon wafers, it was anticipated that the production of ordered organic films derived from polycyclic aromatic

hydrocarbons (PAHs) would be achieved. Large polycyclic aromatic hydrocarbons formed satisfactory films on silica substrates, as determined by the definition or otherwise in electronic spectra of the films, at a substrate temperature T_S near to or slightly greater than that of half the melting point of the particular PAH. Smaller PAHs, in particular pyrene and fluoranthene, were found to deviate markedly from the relationship.

From the results obtained for organic thin films on silica exposed to the oxidants MoF_6 , WF_6 , AsF_5 and TCNQ the PAHs could be placed into three categories; in all cases there was no conclusive evidence in the electronic spectra for the formation of radical cations derived from donor PAHs. The first group produced films which exhibited both electronic and physical perturbations, such as the loss of definition and new bands at lower energies in the electronic spectra upon chemical modification. Films in this group were found to exhibit effects such as loss of definition and changes in relative band intensities in the electronic spectra with increasing film thickness. Films could be subdivided further within this group; those for which the term "charge-transfer complexes" did not reflect the strong interactions between donor PAHs and acceptor species and those for which the description was more appropriate. Films derived from perylene, BEDT-TTF, violanthrone, pentacene, ovalene, tetracene, rubrene, PTCDA, CTCDA, dedacyclene, chrysene and anthracene were included in this category.

The second category of films exhibited changes in definition and relative band intensities in the electronic spectra upon exposure to oxidants, with no additional absorption bands. In common with the previous category,

increasing film thickness produced changes in relative band intensities in the electronic spectra. Films derived from coronene tetracarboxylic acid (CTA) and fluoroanthene formed this group.

The final category of films were defined as those for which the electronic and vibrational spectra were dominated by interference patterns and so no sensible conclusions could be established, from experiments where films were exposed to oxidants. Pyrene and to a lesser extent rubrene produced films in this group.

In future work, structural studies by TEM should be conducted in order to obtain information on lattice structures of the thin films prior to and after chemical modification. Although the pattern of results obtained in this study did suggest there was no simple correlation for the appearance of additional electronic absorption bands with the thermodynamic oxidising power of the oxidant employed, it would be interesting to use stronger oxidising agents such as UF_6 under similar experimental conditions. Experimental difficulties encountered in this study concerning IR vibrational spectroscopy of organic thin films on silica and silicon should be addressed in future work, in order to obtain positive evidence or otherwise for the formation of ionic compounds/radical cation salts (i.e. radical cations of PAHs and counter-anions of MoF_6^- , WF_6^- , or AsF_6^-) in reactions of thin films with MoF_6 , WF_6 or AsF_5 , as the counter-anions are readily identified by their characteristic absorption bands in the IR vibrational spectrum.

In the present study the Quartz Crystal Microbalance (QCM) technique was employed to determine the reaction stoichiometry for the interaction of

MoF₆ with the polymeric fluoro-bridged phthalocyanine [Al(Pc)F]_r. It was established that there was considerable uptake of MoF₆ by the [Al(Pc)F]_n film that could not be explained by a process such as simple adsorption, intercalation or stoichiometric oxidation of the polymer. The results were consistent however with a process involving depolymerisation of [Al(Pc)F]_r. It would be beneficial to repeat this work and amplify the results with conductivity studies (which due to experimental difficulties were omitted for many of the reactions) and extend the QCM technique to the PAHs thin film reactions investigated in this study.

References.

1. F. Twyman, *Prism and Lens Making*, Adam Hilger, London, 1957.
2. I.V. Grebenshikov, *Keramika i Steklo*, 1931, 7, 36-41; I.V. Grebenshikov, *Sotsialisticheskaya Reconstructsiya i Nauka.*, 1935, 2, 22-23.
3. W.A. Bourne, *A Treatise on the Properties and Qualities of Glasses for Optical Purposes*, 1585; I. Newton, *Opticks*, 1721.
4. E. Ruska, *Z. Phys.*, 1934, 87, 580; J. Hillier and E.G. Ramberg, *J. Appl. Phys.*, 1947, 18, 48.
5. J.M. Bennett and L. Mattsson, *Introduction to Surface Roughness and Scattering*, Optical Society of America, Washington DC, 1989.
6. E.J. Abbott and F.A. Firestone, *Mech. Eng.*, 1993, 55, 569-72.
7. D.C. Cornish, *The Mechanism of Glass Polishing*, Taylor & Francis Ltd, London, 1961; L. Holland, *The Properties of Glass Surfaces*, Chapman and Hall, London, 1964; N.J. Brown, *Precision Engineering*, 1987, 9, 129; L.M. Cook, *J. Non-Cryst. Solids.*, 1990, 120, 152-171 and references therein.
8. J.M. Bennett, *Meas. Sci. Technol.*, 1992, 3, 1119-1127.
9. D.F. Horne, *Optical Production Technology*, Adam Hilger, Bristol, 1972.
10. L.M. Cook, *J. Non-Cryst. Solids.*, 1990, 120, 152-171.
11. a) D. Cornish and L. Watt, *Br. Sci. Instr. Res. Assoc. Rep.*, 1963, R295.
b) T. Izumitani, Topical Meeting on the Science of Polishing, Paper TuB-A1, Tech. Digest, Optical Society of America, April 1984.
12. T. Izumitani, *Glass Technology.*, 1971, 12, 131.

13. L. McGhee and J.M. Winfield, *Chemical Polishing to Subnanometre Levels*, Post-LINK Report No. 1, University of Glasgow, 1991.
14. R. Ridgeway, A. Ballard and B. Bailey, 63rd General Meeting of the Electrochemical Society, Montreal, 1993; Abstract, p. 369.
15. F.P. Bowden and K.E.W. Ridler, *Proc. R. Soc.*, 1936, **A154**, 640.
16. R.J. Walsh and A.H. Herzog, *U.S. Pat.*, 1965, 3, 170, 273; Monsanto Chemical Co. (*Chem. Abstr.*, **62**, 11293a; **66**, 12527c).
17. N.J. Brown, *Precision Engineering*, 1987, **9**, 129.
18. J.E. Lawrence and L.L. Barnes, Topical Meeting on the Science of Polishing, Paper TuB-B5-1, Tech. Digest, Optical Society of America, April 1984; D.F. Weirrauch, *J. Electrochem. Soc.*, 1985, **132**, 250.
19. F.A. Cotton and G. Wilkinson, *Basic Inorganic Chemistry*, John Wiley & Sons Inc, New York, 1976.
20. F. Preston, *J. Soc. Glass. Tech.*, 1927, **11**, 214.
21. T. Izumitani, Topical Meeting on Optical Fabrication and Technology, Paper MA1, Tech. Digest, Optical Society of America, 1982.
22. B. Tuck, *J. Mater. Sci.*, 1975, **10**, 321-339.
23. P.J. Holmes, *The Electrochemistry of Semiconductors*, Academic Press, London, 1962, and references therein.
24. R.P. Tijburg, *Physics in Technology*, 1976 (Sept), 202-207; R.P. Tijburg and T. van Dongen, *J. Electrochem. Soc.*, 1976, **123**, 687.
25. P. Rai-Choudhurg, *J. Electrochem. Soc.*, 1971, **118**, 266.
26. J.L. Vossen and W. Kern, *Thin Film Processes*, Academic Press, New York, 1978.

27. W. Kern, *RCA Review*, 1978, **39**, 279-308.
28. M. Beveridge, D.S. Boyle, L. McGhee, S. McMeekin, M.I. Robertson and J.M. Winfield, 9th International Fluorine Conference, Bochum, Germany, 1991, Abstract : The Role of Inorganic Fluoride in Chemomechanical Polishing.
29. R.K. Iler, *Colloid Chemistry of Silica and Silicates*, Cornell University Press, Ithaca, New York, 1955.
30. L.D. Belyakova, O.M. Dzhigit, A.V. Kiselev, G.G. Muttk and K.D. Shcherbakova, *Russ. J. Phys. Chem. Engl. trans.*, 1959, **33**, 551.
31. H. Itoh, Y. Ohmori and N. Nakahara, *J. Lightwave Technol.*, 1985, **LT-3**, 43.
32. E.M. Rabinovich, *Phys. Chem. Glasses.*, 1983, **24**, 56; K. Noguchi et al, *Appl. Phys. Lett.*, 1984, **44**, 491.
33. R. William and M.H. Woods, *J. Appl. Phys.*, 1975, **46**, 695.
34. M. Beveridge, L. McGhee, S.G. McMeekin, M.I. Robertson, A. Ross and J.M. Winfield, *J. Mater. Chem.*, 1994, **4**, 119.
35. D.E. Polk, *J. Non-Cryst. Solids.*, 1971, **5**, 365.
36. S.R. Elliott, C.N.R. Rao and J.M. Thomas, *Angew. Chem. Int. Ed. Engl.*, 1986, **25**, 31.
37. R. Parthasarathy, K.J. Rao and C.N.R. Rao, *Chem. Soc. Rev.*, 1983, **12**, 361.
38. S. Bhattachanya, S.R. Nagel, L. Fleishman and S. Susman, *Phys. Rev. Lett.*, 1984, **46**, 1266.

39. A. Paul, *Chemistry of Glasses*, Chapman and Hall, 1982; R.H. Doremus, *Glass Science*, John Wiley & Sons, 1973; W.A. Weyl and E.C. Marboe, *The Constitution of Glasses*, Wiley-Interscience, 1962.
40. A.F. Wells, *Structural Inorganic Chemistry*, Clarendon Press, Oxford, 4th edn. 1975.
41. F.W. Maarsen, M.C. Smit and J. Matze, *Rev. Trav. Chim. Pays-Bas.*, 1957, **76**, 713.
42. R.A. Heising, *Quartz Crystals for Electrical Circuits*, Van Nostrand, New York, 1946.
43. G.Z. Sauerbrey, *Z. Phys.*, 1959, **155**, 206; 1964, **178**, 457.
44. J. Hlavay and G.G. Guilbault, *Anal. Chem.*, 1977, **49**, 1890.
45. I. Langmuir, *J. Chem. Phys.*, 1933, **1**, 756; *J. Franklin. Inst.*, 1934, **218**, 143. K.B. Blodgett, *J. Am. Chem. Soc.*, 1936, **56**, 495; 1935, **57**, 1007; *J. Opt. Soc. Am.*, 1934, **24**, 313; I. Langmuir and K.B. Blodgett, *Kolloid-Z.*, 1935, **73**, 257.
46. A. Ulman, *An Introduction to Ultrathin Organic Films*, Academic Press, Boston, 1991 and references therein.
47. L. Holland, *Vacuum Deposition of Thin Films*, Chapman & Hall Ltd, London, 1956;. M. Ashida, *Bull. Chem. Soc. Jpn.*, 1966, **39**, 2632.
48. L.I. Maissel and R. Glang, *Handbook of Thin Film Technology*, McGraw-Hill Inc, 1970; R.W. Berry, P.M. Hall and M.T. Harris, *Thin Film Technology*, D. Van Nostrand Company Inc, 1968; B. Lewis and J.C. Anderson, *Nucleation and Growth of Thin Films*, Academic Press Inc, London, 1978.

49. J.R. Fryer, *Mol. Cryst. Liq. Cryst.*, 1983, **96**, 275.
50. E. Hückel, *Zeit. Physik.*, 1932, **76**, 628.
51. C.A. Coulson, B.O'Leary and R.B. Mallion, *Hückel Theory for Organic Chemists*, Academic Press, London, 1978.
52. R. Scholl, *Ber. Dtsch. Chem. Ges.*, 1911, **44**, 1662; R. Stelzner, *Lit. Reg. Org. Chem.*, 1921, **3**, 21; E. Clar, *Ber. Dtsch. Chem. Ges.*, 1939, **72**, 2137; J. Patterson, *J. Am. Chem. Soc.*, 1925, **47**, 543.
53. E. Clar, *Aromatische Kohlenwasserstoffe*, Springer-Verlag, Berlin, 1952.
54. E. Clar, *Tetrahedron*, 1959, **5**, 98; **6**, 355; 1960, **9**, 202.
55. R.S. Mulliken, *J. Am. Chem. Soc.*, 1950, **72**, 600; 4493; R.S. Mulliken, *J. Chem. Phys.*, 1951, **19**, 514.
56. R. Foster, *Organic Charge Transfer Complexes*, Academic Press, London 1969.
57. G.N. Lewis, *Valence and the Structure of Atoms and Molecules*, The Chemical Catalogue Co., New York, 1923.
58. R. S. Mulliken, *J. Phys. Chem., Ithaca.*, 1952, **56**, 801.
59. P.R. Hammond, *Nature*, London, 1965, **206**, 891.
60. P.R. Hammond and R.H. Knipe, *J. Am. Chem. Soc.*, 1967, **89**, 6063.
61. B. Weinstock, H.H. Claasgen and J.G. Malm, *J. Am. Chem. Soc.*, 1957, **79**, 5832.
62. T.A. O'Donnell and D.F. Stewart, *Inorg. Chem.*, 1966, **5**, 1434.
63. N. Bartlett, *Angew. Chem. Int. Ed. Engl.*, 1968, **7**, 433.
64. R.N. Compton, P.W. Reinhardt and C.D. Copper, *J. Chem. Phys.*, 1978, **68**, 2028.

65. N. Bartlett, E.M. McCarron and B.W. McQuillan, *Synth. Met.*, 1980, **1**, 221; J. Burgess, I.H. Haigh, R.D. Peacock and D. Taylor, *J. Chem. Soc., Dalton Trans.*, 1974, **2**, 1064.
66. N. Bartlett and D.W. McQuillan, in *Intercalation Chemistry*, eds. M.S. Whittingham and A.J. Jacobson, Academic Press, New York, 1982, p.19.
67. D.R. Kearns and M. Calvin, *J. Am. Chem. Soc.*, 1961, **83**, 2110; M.M. Labes, O.N. Rudyj and P.L. Kronick, *J. Am. Chem. Soc.*, 1962, **84**, 499; M.M. Labes and O.N. Rudyj, *J. Am. Chem. Soc.*, 1963, **85**, 2055.
68. L.B. Coleman, M.J. Cohen, D.J. Sandman, F.G. Yamagishi, A.F. Garito and A.J. Ferraris, *Solid State. Commun.*, 1973, **12**, 1125; J.P. Ferraris, D.O. Cowan, V. Valetka and J.H. Perlstein, *J. Am. Chem. Soc.*, 1973, **95**, 948.
69. N.A. Murphy, J.G. Banner, E. Fletcher and A. Brown, *UK Pat. Appl.*, 1980, 2055792A; *US Pat.*, 1980, 4 343116.
70. F. Fairbrother and J.F. Nixon, *J. Chem. Soc.*, 1958, 322A.
71. P.M.A. Sherwood, *Vibrational Spectroscopy of Solids*, Cambridge University Press, 1972; A.J. Barnes and W.J. Orville-Thomas, *Vibrational Spectroscopy-Modern Trends*, Elsevier, 1977, and references therein.
72. C.V. Raman and K.S. Krishnan, *Nature*, 1928, **121**, 501; G. Landsberg and L. Mandelstam, *Naturwiss.*, 1928, **16**, 577.
73. C.N. Banwell, *Fundamentals of Molecular Spectroscopy*, McGraw-Hill, 3rd edn. 1983.

74. *Fourier Transform Infrared Spectroscopy - Applications to Chemical Systems*, ed. J.R. Ferraro and L.J. Basile, Academic Press; vol. 1, 1978; vol.2, 1979; vol.3, 1983; vol.4, 1985 and references therein.
75. M.P. Fuller and P.R. Griffiths, *Appl. Spectrosc.*, 1980, **34**, 533; *Anal. Chem.*, 1978, **50**, 1906.
76. K. Krishnan and J.R. Ferraro, in *Fourier Transform Infrared Spectroscopy - Techniques Using Fourier Transform Interferometry*, ed. J.R. Ferraro and L.J. Basile, Academic Press, vol. 3, 1983, p. 149. A. Rosenswaig, *Chemical Analysis Vol. 57 : Photoacoustics and Photoacoustic Spectroscopy*, John Wiley & Sons, New York, 1980.
77. N.J. Harrick, *Internal Reflection Spectroscopy*, Wiley Interscience, New York, 1967.
78. *Infrared Microspectroscopy : Theory and Application*, ed. R.G. Messerschmidt and M.A. Harthcock, Marcel Dekker, New York, 1988 and references therein.
79. P. Kubelka, *J. Opt. Soc. Am.*, 1948, **38**, 448; P. Kubelka and F. Munk, *Z. Tech. Phys.*, 1931, **12**, 593.
80. D.W. Vindrine, *Appl. Spectrosc.*, 1980, **34**, 314.
81. J.P. Deely, R.J. Gigi and A.J. Liotti, *J. Tech. Assoc. Paper Pulp Ind.*, 1966, **49**, 57A.
82. H.H. Jaffé and M. Orchin, *Theory and Applications of Ultraviolet Spectroscopy*, John Wiley & Sons, New York, 1962; C.N.R. Rao, *Ultraviolet and Visible Spectroscopy*, Butterworths, London, 1975.
83. A.B.P. Lever, *Inorganic Electronic Spectroscopy*, Elsevier, 1968.

84. G. Engelhardt and D. Michel, *High Resolution Solid-State NMR of Silicates and Zeolites*, John Wiley & Sons, New York, 1987; C.A. Fyfe, *Solid State NMR for Chemists*, Guelph, Ontario:CFC, 1984.
85. E.R. Andrew, *Int. Rev. Phys. Chem.*, 1981, **1**, 195.
86. J. Shaefer and E.O. Stejskal, *J. Am. Chem. Soc.*, 1976, **98**, 1031.
87. E. Lippmaa, A. Samoson, M. Mägi, R. Teeäär, J. Schraml, J. Götz, *J. Non-Cryst. Solids.*, 1982, **50**, 214; J.M. Thomas, J. Klinowski, P.A. Wright, R. Roy, *Angew. Chem. Int. Ed. Engl.*, 1983, **22**, 614.
88. C.N. Rao, J.M. Thomas, J. Klinowski, U. Selvaraj, K.J. Rao, G.R. Millward and S. Ramdas, *Angew. Chem. Int. Ed. Engl.*, 1985, **24**, 61.
89. E. Lippmaa, M. Mägi, A. Samoson, G. Engelhardt and A.R. Grimmer, *J. Am. Chem. Soc.*, 1980, **102**, 4889.
90. J.F. Stebbins and M. Kanzaki, *Science*, 1991, **251**, 294.
91. M. von Laue, *Sitzungsberichte. K. Bayer. Akad., München.*, 1912, 303.
92. E.W. Nuffield, *X-Ray Diffraction Methods*, John Wiley & Sons, New York, 1966.
93. J.M. Bennett and J.H. Dancy, *Appl. Opt.*, 1981, **20**, 1785.
94. G. Nomarski, *J. Phys. Radiat.*, 1955, **16**, 95.
95. J.W.S. Hearle, J.T. Sparrow and P.M. Cross, *The Use of the Scanning Electron Microscope*, Pergamon Press, Oxford, 1972; P.R. Thornton, *Scanning Electron Microscopy*, Chapman & Hall Ltd, London, 1968.
96. W.D. Ehmann and D.E. Vance, *Radiochemistry and Nuclear Methods of Analysis*, John Wiley & Sons, New York, 1991.

97. Nuclear Data Sheets, ed. by the Nuclear Data Group of the National Academy of Sciences National Research Council, Washington DC., vol. 5, No. 3.
98. *Tables of Isotopes*, ed. C.M. Lederer and V. Shirley, Wiley-Interscience, 7th edn., 1978.
99. A.S. Al-Ammar and G. Webb, *J. Chem. Soc., Faraday Trans. 1*, 1978, **74**, 194.
100. K.W. Dixon, Ph.D. thesis, University of Glasgow, 1986.
101. K.Z. Morgan, in Radiation Hazards associated with Tritium, Seminaire sur la Protection Contre les Dangers du Tritium, Service Central de Protection Contre les Rayonnements Ionisants, le Vesinet, April 16-18, 1964; CONF-640413, p.1.
102. J. Thomson, Ph.D. thesis, University of Glasgow, 1988.
103. A.J. Dalladay, *Trans. Optical Society of London*, 1921, **23**, 170. E.G. Nikolova, *J. Mater. Sci.*, 1985, **20**, 1.
104. J.S. Judge, *J. Electrochem. Soc.*, 1971, **118**, 1772.
105. O. Podzimek, NASA report No. WB-85-16; B8664575, University of Twente, April 1986.
106. S.J. Patwe, B.N. Wani, U.R.K. Rao and K.S. Venkateswarlo, *Can. J. Chem.*, 1989, **67**, 1815.
107. I. Langmuir, *J. Am. Chem. Soc.*, 1918, **40**, 1361.
108. V.Y. Davydov, A.V. Kiselev and L.T. Zhuravlev, *Trans. Faraday. Soc.*, 1964, **60**, 2254.
109. H.P. Boehm, *Adv. Catal.*, 1966, **16**, 226.

110. S. Brunauer, P. H. Emmett and E. Teller, *J. Am. Chem. Soc.*, 1938, **60**, 309.
111. W. Kern, *J. Electrochem. Soc.*, 1990, **137**, 1887.
112. R.B. Badachhape, G. Hunter, L.D. McCorry and J.L. Margrave, *Inorg. Chem.*, 1966, **5**, 929.
113. N.L. Rockley, M.K. Woodard and M.G. Rockley, *Appl. Spectrosc.*, 1984, **38**, 329; R.L. White and A. Nair, *Appl. Spectrosc.*, 1990, **44**, 69.
114. C. Palanche, H. Berman and C. Frondel, *Dana's System of Mineralogy*, John Wiley & Sons Inc, New York, 7th edn., 1951, vol. 2.
115. F. Ulmann, *Enzyklopädia der technischen Chemie.*, Urban & Schwarzenberg, Vienna, 1929, vol. 4, p.47.
116. Y. Yokozawa and I. Miyoshita, *J. Chem. Phys.*, 1956, **25**, 796.
117. E. Clar, *Spectrochim. Acta.*, 1950, **4**, 116.
118. K. Kawabata, T. Tanaka and M. Mizutani, *Adv. Mater.*, 1991, **3**, 157.
119. Bad. Anilin-und Soda-Fabrik, *German Patent*, 226215, 1909; Scottish Dyes Ltd, *German Patent* 417068, 1921; Farbwerke Höchst, *German Patent* 420147, 1923.
120. E. Clar, *Polycyclic Hydrocarbons*, Academic Press, London, 1964; vol. 1, p. 425.
121. H. Akamatu, H. Inokuchi and H. Honda, *Nature, London*, 1951, **168**, 520; H. Inokuchi, *Bull. Chem. Soc. Jpn.*, 1951, **24**, 222.
122. K. Brass and K. Fanta, *Ber. Dtsch. Chem. Ges.*, 1936, **69**, 1.
123. D.J. Carswell and J.E. Lyons, *J. Chem. Soc.*, 1955, 1728.

124. G. Wittig and D. Naldi, *J. Prack. Chem.*, 1942, **160**, 242; C. Moureu, C. Dufraisse and G.L. Butler, *C.R. Acad. Sci. Paris.*, 1926, **183**, 101.
125. K.H. Kim, L. Smith, T. Beinecke and J.H. Day, *J. Org. Chem.*, 1963, **28**, 1890.
126. K. Akers, R. Aroca, A.M. Hor and R.O. Loutfy, *J. Phys. Chem.*, 1987, **91**, 2954.
127. A. Léger and J.L. Puget, *Astron. Astrophys.*, 1984, **137**, L5; J.L. Puget, A. Léger and F. Boulanger, *Astron. Astrophys.*, 1985, **142**, L19; L.B. d'Hendecourt, A. Léger, G. Olafsson and W. Schmidt, *Astron. Astrophys.*, 1986, **170**, 91.
128. A. Léger and L.B. d'Hendecourt, *Astron. Astrophys.*, 1985, **146**, 81.
129. E. Keinan, S. Kumer, R. Moschenberg, R. Ghirlando and E.J. Wachtel, *Adv. Mater.*, 1991, **251**, 254.
130. Ref. 120, p. 249.
131. H. Inokuchi, *Bull. Chem. Soc. Jpn.*, 1951, **24**, 222; D.M.J. Compton and T.C. Waddington, *J. Chem. Phys.*, 1957, **27**, 160; D.J. Carswell, J. Ferguson and L.E. Lyons, *Nature, London*, 1954, **173**, 736.
132. A.T. Vartanjan, *Dockl. Akad. Nauk S.S.S.R.*, 1950, **71**, 641.
133. A. Bree, D.J. Carswell and L.E. Lyons, *J. Chem. Soc.*, 1955, 1728; 1754.
134. R.M. Williams and S.C. Wallwork, *Acta. Crystallogr. Sect. B.*, 1968, **24**, 168.
135. I.G. Farbenindustrie AG, *Brit. Patent 435254*, 1934; *French Patent 781543, 45561.*, 1934.
136. D.O. Cowan and F.M. Wiygel, *C & EN* (July 21), 1986, p. 28.

137. Z.H. Khan and B.N. Khanna, *J. Chem. Phys.*, 1969, **50**, 3291; 1973, **59**, 3015; E. Clar and W. Schmidt, *Tetrahedron*, 1975, **31**, 2263; W. Schmidt, *J. Chem. Phys.*, 1977, **66**, 824; Z.H. Khan, *Can. J. Spectrosc.*, 1978, **23**, 8; 1984, **29**, 63; *Z. Naturforsch.*, 1984, **39a**, 668; 1987, **42a**, 91; *Spectrochim. Acta.*, 1988, **44A**, 313; 1125.
138. M.W. Frechette and J.L. Fasching, *Environ. Sci. Technol.*, 1973, **7**, 1135.
139. M. Gouterman, G.H. Wagner and L.C. Snyder, Jr., *J. Mol. Spectrosc.*, 1963, **11**, 2; C. Weiss, H. Kobayashi and M. Gouterman, *J. Mol. Spectrosc.*, 1965, **16**, 415; A.J. McHugh, M. Gouterman and C. Weiss, *Theor. Chem. Acta.*, 1972, **24**, 346.
140. P.C. Minor, M. Gouterman and A.B. Lever, *Inorg. Chem.*, 1985, **24**, 1994.
141. A.H. Fzea, Ph.D. thesis, University of Glasgow, 1992.
142. J.F. Shackelford and W. Alexander, *CRC Materials Science and Engineering Handbook*, CRC Press, Boca Raton, FL, 1991.
143. J.P.H. Williamson and J.L. Moilliet, *Eur. Pat. Appl.* 1981, 31,204(C1.C09K3/14).
144. G. Fehlau and D. Achilles, *Ger.(East)DD.*, 1987, 242,401 (C1.CO3C15/02).
145. T. Izumitani and S. Harada, *Glass Technol.*, 1971, **12**, 131.
146. J. Dey, M. Lundgren and S. Harrell, *Proc. Kodak Photoresist Seminar*, 1968, **2**, 4.
147. T.P. Yakovleva, L.V. Chunyaeva, A.A. Grizik and L.G. Nekhamkin, *U.S.S.R. SU*, 1986, 1,208,055 (C1.C09G1/02).

148. H. Neilson and D. Hackleman, *J. Electrochem. Soc.*, 1983, **130**, 708.
149. H. Kikuyama et al, *J. Electrochem. Soc.*, 1992, **139**, 2239; C.R. Helms and B.E. Deal, *J. Vac. Sci. Technol., A*, 1992, **10**, 806.
150. D.S. Boyle, J.A. Chudek, G. Hunter, D. James, M.I. Littlewood, L. McGhee, M.I. Robertson and J.M. Winfield, *J. Mater. Chem.*, 1993, **3**, 903.
151. W.A. Weyl and E.C. Marboe, *The Constitution of Glasses*, John Wiley & Sons, New York, 1967, vol. 2, p. 1480; E. W. Washburn, *J. Am. Ceram. Soc.*, 1933, **29**, 1049. F. Ephraim, *Inorganic Chemistry*, Nordemann, New York, 4th edn., 1943.
152. C.D. Fung, P.W. Cheung and W.H. Ko, *IEEE Trans., Electron. Devices*, 1986, **33**, 8.
153. J.A. Kitchener, *Faraday Disc. Chem. Soc.*, 1972, **52**, 379.
154. R.K. Iler, *The Chemistry of Silica*, John Wiley & Sons New York, 1979, p. 62.
155. V.V. Strelko, *Teor. Eksp. Khim.*, 1973, **10**, 359.
156. W. Stöber, *Beitr. Silikose-Forsch. Sonderb.*, 1964, **6**, 35.
157. R.H. Doremus, Topical Meeting on the Science of Polishing, Paper TuB-C3-1, Tech. Digest, Optical Society of America, April 1984.
158. E.D. Palik, H.F. Gray and P.B. Klein, *J. Electrochem. Soc.*, 1983, **130**, 956.
159. W. Lanford, C. Burman and R. Doremus, in *Advances in Materials Characterisation 2*, ed. R. Snyder, R. Condrate and P. Johnson, Plenum, New York, 1985, p. 203.

160. Ref. 154, p. 660.
161. R.K. Iler, *J. Phys. Chem.*, 1952, **56**, 680.
162. Ref. 154, p. 221.
163. A.P. Dushina et al, *Ionnyi Obmen*, 1970, **132** (Chem. Abstr., **74**, 116290b); T. Wakatsuki, H. Furukawa and K. Kawaguchi, *Soil. Sci. Plant. Nutr. Tokyo.*, 1974, **20**, 353 (Chem. Abstr., **82**, 160671r).
164. S. Ahrland et al, *Acta. Chem. Scand.*, 1960, **14**, 1059; J.H. Stanton and R.W. Maatman, *J. Colloid. Sci.*, 1963, **18**, 132.
165. T.W. Healy, R. Cooper and R.O. James, *Am. Chem. Soc. Sect. Div. Water Air Waste Chem., Prepr.*, 1967, **7**, 91.
166. E. Akatsu et al, *J. Nucl. Sci. Technol. Tokyo.*, 1965, **2**, 141.
167. W. Stöber, *Beitr. Silikose-Forsch.*, **1.**, 1966, **89**, 1.
168. T.H. Elmer and M.E. Nordberg, *J. Am. Ceram. Soc.*, 1958, **41**, 517.
169. H. Baumann, *Beitr. Silikose-Forsch.*, 1955, **37**, 47.
170. I. Bergmann, *J. Appl. Chem.*, 1963, **13**, 356.
171. A.A. Blumberg and S.C. Stavrinou, *J. Phys. Chem.*, 1960, **64**, 1438.
172. T. Izumitani, in *Treatise on Material Science and Technology*, ed. M. Tomozawa and R. Doremus, Academic Press, New York, vol. 17, 1979, p. 115.
173. N. Miki, H. Kikuhama, I. Kawanabe, M. Miyashita and T. Ohmi, *IEEE Trans. Electron. Devices.*, 1990, **37**, 107; M. Monta, T. Ohmi, E. Hasegawa, M. Kawakami and M. Ohwada, *J. Appl. Phys.*, 1990, **68**, 1272; N. Miki, M. Maeno, K. Maruhashi and T. Ohmi, *J. Electrochem. Soc.*, 1990, **137**, 787.

174. C.R. Helms and B.E. Deal, *J. Vac. Sci. Technol., A*, 1992, **10**, 806.
175. W. Lange, in *Fluorine Chemistry*, Academic Press Inc., New York, 1950, vol. 1, p. 126.
176. N.N. Golovnev, *Russ. J. Inorg. Chem.*, 1986, **31**, 367.
177. H.A. Waggener and J.V. Dalton, *Electrochem. Soc. Ext. Abstr.*, 1972, **72-2**, 587; J.B. Price, in *Semiconductor Silicon 1973*, ed. H.R. Huff and R.R. Burgess, The Electrochemical Society, Princeton, N.J., 1973, p. 339.
178. R.M. Finne and D.L. Klein, *J. Electrochem. Soc.*, 1967, **114**, 965.
179. N. Ulyeda, M. Ashida and E. Suito, *J. Appl. Phys.*, 1965, **36**, 1453; Y. Murato, J.R. Fryer and T. Baird, *J. Microsc.*, 1976, **108**, 261.
180. D. Dudde, K.H. Frank and E.E. Koch, *J. Electron Spectrosc. Related Phenom.*, 1988, **47**, 245. P. Yannoulis, R. Dudde, K.H. Frank and E.E. Koch, *Surf. Sci.*, 1987, **189-190**, 519.
181. D.W. Pashley, *Adv. Phys.*, 1965, **14**, 327; L. Royer, *Bull. Soc. Franc. Min.*, 1928, **51**, 7.
182. J.R. Fryer and C. Ewins, *Philosophical Magazine A*, 1992, **66**, 889.
183. J.R. Fryer, *Acta Crystallogr. A*, 1979, **35**, 327.
184. J.R. Fryer and D.J. Smith, *Proc. R. Soc. A*, 1982, **381**, 225.
185. E. Clar, *Ber. Dtsch. Chem. Ges.*, 1936, **69**, 607.
186. H.B. Klevens and J.R. Platt, *J. Chem. Phys.*, 1949, **17**, 470.
187. W. Schmidt, *J. Chem. Phys.*, 1977, **66**, 828.
188. C.G. Cannon and G.B.M. Sutherland, *Spectrochim. Acta.*, 1951, **4**, 373.

189. M.L. Lee, *Analytical Chemistry of Polycyclic Aromatic Hydrocarbons*, Academic Press Inc., New York, 1981, p. 346.
190. H.E. Hallam and G.F. Scrimshaw, in *Vibrational Spectroscopy of Trapped Species*, ed. H.E. Hallam, John Wiley & Sons, New York, 1973, p. 11.
191. N. Bartlett, *Angew. Chem. Int. Ed. Engl.*, 1968, 7, 433.
192. B.K. Annis and S. Datz, *J. Chem. Phys.*, 1977, 66, 4468; P.M. George and J.L. Beauchamp, *Chem. Phys.*, 1979, 36, 345.
193. J.M. Winfield, *J. Fluorine Chem.*, 1986, 33, 159.
194. J.R. Geichman, E.A. Smith, S.S. Trond and R.R. Ogle, *Inorg. Chem.*, 1962, 1, 661; N. Bartlett, S.P. Beaton and N.K. Jha, *J. Chem. Soc. Chem. Commun.*, 1966, 168.
195. J. Emsley and D. Hall, *The Chemistry of Phosphorus*, Harpe & Row Ltd, London, 1976, p. 49; S. Brownstein, *Can. J. Chem.*, 1969, 47, 605; T.C. Rhyne and J.G. Dillard, *Inorg. Chem.*, 1971, 10, 730.
196. F.M. Page and G.C. Goode, *Negative Ions and the Magnetron*, Wiley Interscience, New York, 1969.
197. E. Clar and W. Schmidt, *Tetrahedron*, 1975, 31, 2263.
198. G. Breigleb, J. Czekalla and G. Reuss, *Z. Phys. Chem. Frankf. Ausg.*, 1961, 30, 316.
199. S. Iwata, J. Tanaka and S. Nagakura, *J. Am. Chem. Soc.*, 1966, 88, 894.
200. M.J.S. Dewar and A.R. Lepley, *J. Am. Chem. Soc.*, 1961, 83, 4560.
201. R.S. Mulliken and W.B. Person, *A. Rev. Phys. Chem.*, 1962, 13, 107.
202. M.J.S. Dewar and H. Rogers, *J. Am. Chem. Soc.*, 1962, 84, 395; A.R. Lepley and C.C. Thompson, Jr., *J. Am. Chem. Soc.*, 1967, 89, 5523.

203. A. Streitwieser, Jr., *Molecular Orbital Theory for Organic Chemists*, John Wiley & Sons, New York, 1961, Chapter 8.
204. G.R. Anderson, *J. Am. Chem. Soc.*, 1970, **92**, 3552; V. Kuban and J. Janak, *Scr. Fac. Sci. Nat. Univ. Purkyniana Brun.*, 1973, **3**, 123 (Chem. Abstr. **83**, 66356r).
205. C.J. Eckhardt and R.R. Pennelly, *J. Am. Chem. Soc.*, 1976, **98**, 2034.
206. I.J. Tickle and C.K. Prout, *J. Chem. Soc. Perkin Trans. II.*, 1973, 726.
207. K.D. Truong and A.D. Bandrauk, *Chem. Phys. Lett.*, 1976, **44**, 232.